

DOE/TIC--11223

DOE/TIC-11223
(DE82002045)

DE82 002045

Handbook on ATMOSPHERIC DIFFUSION

Steven R. Hanna
Gary A. Briggs
Rayford P. Hosker, Jr.

Atmospheric Turbulence and Diffusion Laboratory
National Oceanic and Atmospheric Administration

Prepared for the
Office of Health and Environmental Research
Office of Energy Research
U. S. Department of Energy

1982

Jean S. Smith, Publication Editor
Editing, composition, proofreading, book design,
illustrations, and page makeup for this publication
were performed by staff members of the Technical
Information Center.

Published by
TECHNICAL INFORMATION CENTER
U. S. DEPARTMENT OF ENERGY

This document is
PUBLICLY RELEASABLE

Barry Steele
Authorizing Official
Date: 5/18/04

DISCLAIMER

This report was prepared as an account of work sponsored by an agency of the United States Government. Neither the United States Government nor any agency Thereof, nor any of their employees, makes any warranty, express or implied, or assumes any legal liability or responsibility for the accuracy, completeness, or usefulness of any information, apparatus, product, or process disclosed, or represents that its use would not infringe privately owned rights. Reference herein to any specific commercial product, process, or service by trade name, trademark, manufacturer, or otherwise does not necessarily constitute or imply its endorsement, recommendation, or favoring by the United States Government or any agency thereof. The views and opinions of authors expressed herein do not necessarily state or reflect those of the United States Government or any agency thereof.

DISCLAIMER

Portions of this document may be illegible in electronic image products. Images are produced from the best available original document.

NOTICE

International Copyright. © U. S. Department of Energy, 1982, under the provisions of the Universal Copyright Convention. United States copyright is not asserted under the United States Copyright Law, Title 17, United States Code.

Library of Congress Cataloging in Publication Data

Hanna, Steven R.

Handbook on atmospheric diffusion.

Includes bibliographical references and index.

"DOE/TIC-11223."

1. Atmospheric diffusion—Handbooks, manuals, etc. 2. Smoke plumes—Handbooks, manuals, etc. 3. Cooling towers—Climatic factors—Handbooks, manuals, etc. I. Briggs, Gary A. II. Hosker, Rayford P. III. United States. Dept. of Energy. Office of Energy Research. IV. United States. Dept. of Energy. Office of Health and Environmental Research. V. Title. QC880.4.D44H36 551.5'153 81-15149 ISBN 0-87079-127-3 AACR2

Available as DE82002045 (DOE/TIC-11223) for \$10.75 from

National Technical Information Service
U. S. Department of Commerce
Springfield, Virginia 22161

DOE Distribution Category UC-11

Printed in the United States of America

1982

Preface

With the Clean Air Acts and increased environmental consciousness, many engineers, consulting companies, planners, and meteorologists find themselves propelled into the work of calculating atmospheric diffusion. Many of these people are not interested in knowing the detailed theoretical derivation of a formula and its complete set of references. All they want to know are the best current formulas for their problems plus a simple physical description of the principles of analysis. This book should be helpful to those who must make such problem-solving calculations of atmospheric diffusion.

The book can be used also as a textbook for a one-quarter course at either the upper undergraduate or the graduate level. In fact, the basic outline evolved from a graduate course on atmospheric diffusion taught in the Environmental Engineering Department at the University of Tennessee.

The number of pages was purposely limited to make the book more usable. A detailed index permits quick location of subject areas, and a few problems are provided after each chapter.

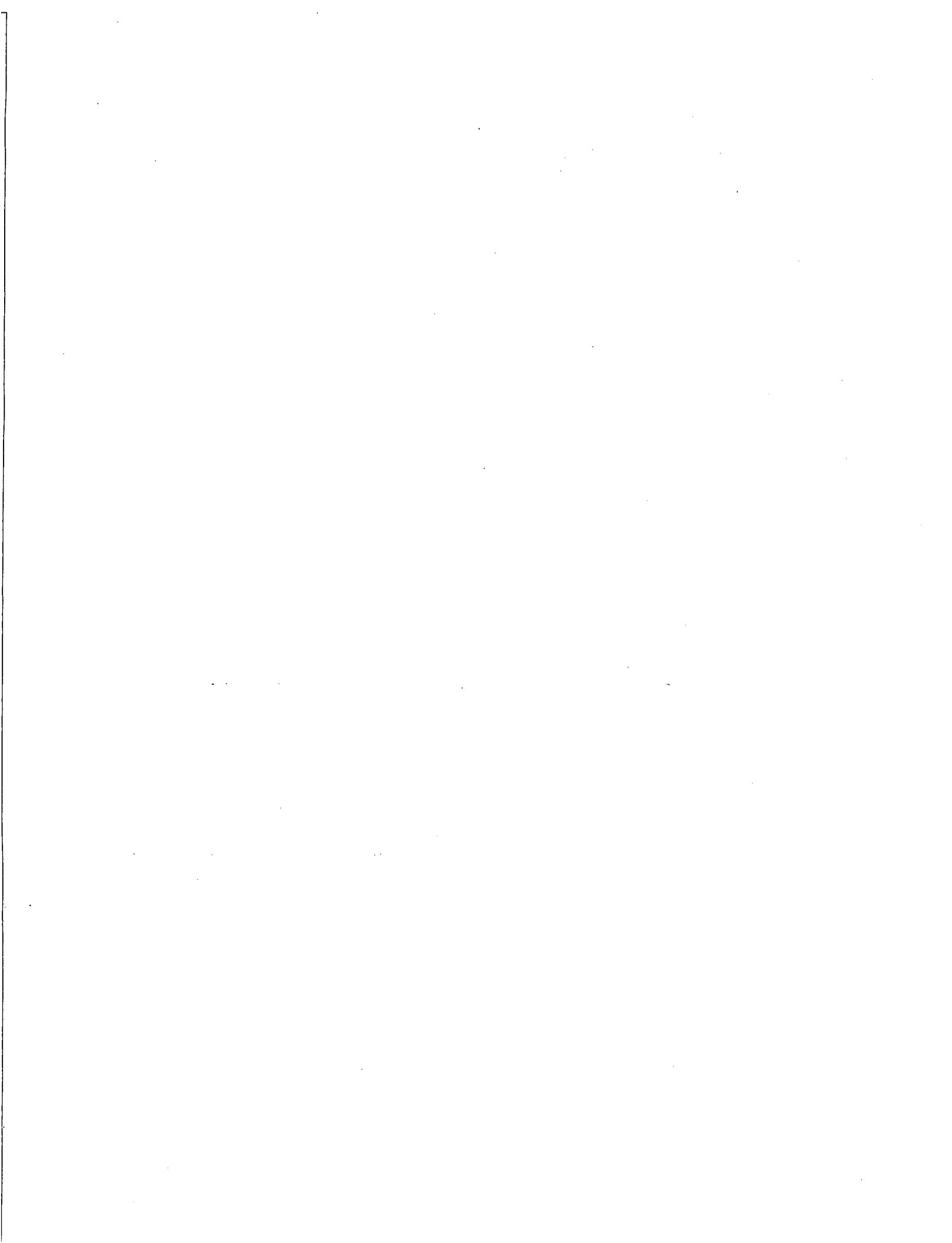
Basic meteorological concepts are covered first and then plume rise, source effects, and diffusion models. Chapters on cooling tower plumes and urban diffusion are included. Suggestions are made for calculating diffusion in special situations, such as for instantaneous releases (puffs), over complex terrain, over long distances (10 km to global scales), and during times when chemical reactions or dry or wet deposition are important.

This work was performed under an agreement between the U. S. Department of Energy and the National Oceanic and Atmospheric Administration.

[Editor's Note: Dr. Steven Hanna and Dr. Gary Briggs were with National Oceanic and Atmospheric Administration, Atmospheric Turbulence and Diffusion Laboratory, Oak Ridge, Tenn., during the preparation of this book; at present Dr. Hanna is with Environmental Research and Technology, Lexington, Mass., and Dr. Briggs is with Environmental Protection Agency, Research Triangle Park, N.C.]

Steven R. Hanna
Atmospheric Turbulence and Diffusion Laboratory

September 1981



Contents

Preface	iii	2-8 Multiple Sources	17
1 Meteorology	1	Problems	17
1-1 Introduction	1	3 Source Effects	19
1-2 General Circulation	1	3-1 Overview	19
1-3 Vertical Temperature Structure and Stability	2	3-2 Stack Aerodynamic Effect	19
1-3.1 Adiabatic Temperature Gradient	2	3-3 Structure of Flow Around Buildings	19
1-3.2 Stability	3	3-4 Diffusion Calculations Around Buildings	21
1-4 Structure of the Planetary Boundary Layer	4	3-4.1 Isolated Sources Upwind of Buildings	22
1-4.1 Turbulence Fluxes	4	3-4.2 Sources Close to Buildings	22
1-4.2 Ekman Spiral	5	Problems	24
1-4.3 Similarity Theory Gives Wind and Temperature Profiles in Surface Layer	6	4 Gaussian Plume Model for Continuous Sources	25
1-4.4 Turbulence Parameters	7	4-1 Why Use the Gaussian Model?	25
1-5 Use of Spectra to Estimate Turbulence Parameters	8	4-2 Form of the Gaussian Model	25
1-6 Lagrangian Turbulence	9	4-3 Stability Classification Schemes	27
Problems	10	4-4 Choice of σ_y and σ_z	27
2 Plume Rise	11	4-4.1 Stability Class Method	27
2-1 Introduction	11	4-4.2 The σ_θ and σ_e Method	30
2-2 Top-Hat-Model Equations	11	4-5 Wind-Speed Variation with Height	31
2-2.1 Definitions	11	4-6 Maximum Ground Concentration and Fumigation	32
2-2.2 Set of Equations for Vertical Plume	12	4-7 Averaging Times and Peak-to-Mean Concentration Ratios	33
2-2.3 Set of Equations for Bent-Over Plume	13	4-8 Sector Model for Long Sampling Times	34
2-3 Plume Trajectory Near Source	13	Problems	35
2-3.1 Vertical Plumes	13	5 Statistical Models of Diffusion from Continuous-Point Sources	36
2-3.2 Bent-Over Plumes	13	5-1 Introduction	36
2-4 Plume Rise Limited by Ambient Stability	14	5-2 Taylor's Theorem	36
2-4.1 Vertical Plumes	14	5-3 Influence of Eddy Size on σ	38
2-4.2 Bent-Over Plumes	14	5-4 Lagrangian—Eulerian Relations	39
2-5 Plume Penetration of Elevated Inversion	14	5-5 Monte Carlo Particle Trajectory Models of Diffusion	40
2-6 Plume Rise Determined by Ambient Turbulence	15	Problems	40
2-6.1 Nearly Neutral Conditions	16	6 Puff Diffusion	41
2-6.2 Convective Conditions	16	6-1 Introduction	41
2-7 Maximum Ground Concentration with Breakup Model	17	6-2 Statistical Approach	41

6-3	Similarity Approach	42	9-5.2	Trajectory Models	62
6-4	Applications	44	9-5.3	Grid Models with Winds Prescribed	62
	Problems	44	9-6	Environmental Protection Agency Models	62
7	Similarity Models of Diffusion	46	9-7	Model Evaluation	63
7-1	Introduction	46		Problems	66
7-2	Diffusion of Continuous Plumes in the Surface Layer	46	10	Removal Mechanisms	67
7-2.1	Neutral Conditions	46	10-1	Introduction	67
7-2.2	Nonneutral or Adiabatic Conditions	47	10-2	Dry Deposition	67
7-3	Diffusion in the Full Depth of the Daytime Planetary Boundary Layer	48	10-2.1	Gravitational Settling	67
	Problems	49	10-2.2	Deposition of Gases and of Particles with Radii Less Than About $10\ \mu\text{m}$	68
8	Gradient Transport (K) Models	50	10-3	Wet Deposition	71
8-1	The Basic Gradient Transport Model	50	10-4	Chemical Removal	72
8-2	Analytical Solutions	50	10-5	Removal Processes in the Box Model	73
8-2.1	One-Dimensional Equation, Time-Dependent, Constant K, No Wind, Instantaneous Area Source	50		Problems	73
8-2.2	Three Dimensions, Time- Dependent, Constant K, No Wind, Instantaneous Point Source	51	11	Cooling Tower Plumes and Drift Deposition	74
8-2.3	Two-Dimensional, Time- Independent, Variable u and K , Continuous Ground-Level Line Source	51	11-1	Introduction	74
8-2.4	Three-Dimensional, Time- Independent, Constant u and K , Continuous-Point Source at Ground Level	52	11-2	Plume Rise from Cooling Towers	74
8-3	Numerical Solutions of the Diffusion Equation	53	11-2.1	Visible Plume Dimensions	76
8-3.1	Numerical Instabilities	53	11-2.2	Numerical Approach for Deep Visible Plumes	77
8-3.2	Specifying the Vertical Diffusivity	54	11-3	Drift Deposition	78
8-4	Higher Order Closure	55		Problems	80
	Problems	56	12	Air-Pollution Meteorology in Complex Terrain	81
9	Urban Diffusion Models	57	12-1	Introduction	81
9-1	Importance of Emissions	57	12-2	Meteorology	81
9-2	Box Model	57	12-3	Diffusion Calculations	84
9-3	The Atmospheric Turbulence and Diffusion Laboratory Model	59		Problems	86
9-4	Street Canyon and Highway Submodels	61	13	Long-Range Transport and Diffusion	87
9-5	Computerized K Models for Urban Diffusion	62	13-1	Introduction	87
9-5.1	An Urban Diffusion Model That Also Predicts Winds and Temperatures	62	13-2	Modeling Concepts	87
			13-3	Application to an Inert Tracer	89
				Problems	90
				References	91
				Author Index	98
				Subject Index	100

Meteorology

1-1 INTRODUCTION

To set the stage for the remainder of the handbook, in this chapter we must briefly review several aspects of meteorology, including the general circulation, vertical stability, and surface-layer structure. Most students are eager to begin immediately the study of applications of the Gaussian plume model; however, even the application of the Gaussian plume model requires a knowledge of wind roses and stability and an appreciation of the influence of wind shear on the range of usefulness of the model. Also, the latest developments in plume-rise theories require the ability to understand and estimate vertical profiles of eddy dissipation rate. Therefore this chapter will be a useful reference for the remainder of this handbook.

1-2 GENERAL CIRCULATION

The sun is the source of nearly all energy received by the earth's atmosphere, and the spherical shape of the earth is responsible for the unequal absorption of this energy by the earth's surface and the atmosphere. Without the transport of heat by the atmosphere and the oceans from the equator to the poles, temperatures would be several tens of degrees colder at the poles and warmer at the equator. However, the fact is that there is a strong poleward transport of heat that is accomplished by direct Hadley cells, traveling high and low pressure systems, and major perturbations, such as hurricanes. In the northern hemisphere Hadley cell, air rises over the equator (causing much rainfall), moves at high elevations toward the north, descends at about 30° N latitude (causing dry desert regions), and then moves as the Northeast (NE) trade winds near the surface from 30° N toward the equator. The NE trades are known as the most persistent general wind system on earth.

North of 30° N latitude, the direct Hadley cell breaks down, and energy is transported by traveling high and low pressure systems moving from west to east. Warm southerly winds and cold northerly winds help accomplish the energy transport. Even more energy is transported by latent heat processes, where, for example, Gulf of Mexico water is evaporated, transported northeastward, and condensed again as precipitation. For each gram of water involved in this process, 540 cal is transported toward the north. Between 60° N and the pole is another wind belt with an easterly component at the surface, but this circulation is not well defined.

Upper-level winds strongly influence winds near the surface, where most diffusion problems occur. In general, the speed of the upper-level winds is proportional to the slope of surface of constant pressure. The atmospheric pressure (p) typically varies by no more than about 5% at sea level over the earth's surface. However, the temperature (T) could be 300°K at the equator and 240°K at the poles. The equation of state for the atmosphere,

$$p = \rho RT \quad (1.1)$$

where R is the gas constant (0.287×10^7 ergs g^{-1} °K $^{-1}$), tells us that the density (ρ) must be less at the equator than at the poles. The hydrostatic equation,

$$\frac{\partial p}{\partial z} = -\rho g \quad (1.2)$$

where z is the height and g is the acceleration of gravity (980 cm/sec 2), then suggests that the pressure decreases with height faster at the poles than at the equator. It follows that, if pressure p is constant (say 1000 mb, or 10^6 dynes/cm 2) at sea level, then any other constant pressure surface aloft (say 500 mb, or 0.5×10^6 dynes/cm 2) will slope downward from the equator to the pole, as in Fig. 1.1.

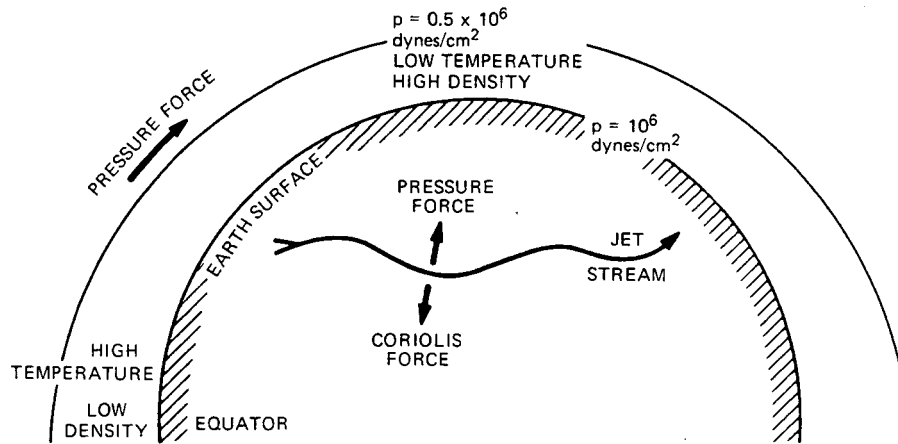


Fig. 1.1 Cross section of the earth's atmosphere, showing how sloping pressure surfaces result at mid-atmosphere. Westerly winds are caused by a balance between pressure forces and Coriolis forces.

The equation of motion says that air will first be accelerated toward the poles along the upper constant pressure surface in the figure:

$$\frac{dv}{dt} = -g \frac{\partial z}{\partial y} \Big|_p - fu \quad (1.3)$$

where u = easterly component of wind speed
 v = northerly component of wind speed
 y = northerly coordinate axis
 subscript p = constant pressure surface
 f = Coriolis parameter, which is equal to two times the earth's rotation rate times the sine of the latitude

The parameter f is of the order of 10^{-4} sec^{-1} . The apparent Coriolis force arises as a result of the earth's rotation, which constantly displaces a cartesian coordinate system fixed to the surface. An analogy is given by rolling a marble from the edge of a rotating record turntable toward the center. The marble will encounter regions with less angular momentum than it has. To an observer fixed to the turntable, the marble will always curve toward the right if the turntable is rotating counterclockwise. Similarly, in the northern hemisphere the Coriolis force is to the right, and in the southern hemisphere it is to the left. The poleward pressure force is thus balanced by a Coriolis force toward the equator in both hemispheres, which causes general westerly flow at mid-levels in the atmosphere at mid-latitudes. The magnitude of the resulting "geostrophic" wind speed is given by setting $du/dt = 0$ in Eq. 1.3, which yields the formula

$$u = -\frac{g}{f} \frac{\partial z}{\partial y} \Big|_p \quad (1.4)$$

Other hydrodynamic forces, which are beyond the scope of this chapter, frequently cause the westerly flow to be compressed into narrow belts, called jet streams, with speeds up to 200 km/hr.

Meteorological data are gathered from many stations across the globe and are stored at the National Climatic Center, National Oceanic and Atmospheric Administration (NOAA), Asheville, N.C. Many statistical operations (e.g., annual wind roses or frequency distributions of wind direction and speed) have already been carried out and can be obtained from the National Climatic Center at very reasonable prices. Surface weather summaries at larger National Weather Service stations are collected into reports called "Local Climatological Data," which are mailed to subscribers monthly. The *Climate Atlas of the United States* (U. S. Department of Commerce, 1968) contains many data useful for diffusion calculations.

1-3 VERTICAL TEMPERATURE STRUCTURE AND STABILITY

1-3.1 Adiabatic Temperature Gradient

If a parcel of dry air is moved vertically without exchanging heat with its environment (i.e., adiabatically), the first law of thermodynamics becomes

$$0 = c_p dT - \frac{1}{\rho} dp \quad (1.5)$$

where c_p is the specific heat of air at constant pressure ($10^7 \text{ ergs g}^{-1} \text{ }^\circ\text{K}^{-1}$) and T must be in degrees Kelvin (or absolute). Substituting from the

hydrostatic equation (Eq. 1.2) yields the formula for the adiabatic temperature gradient:

$$\left(\frac{dT}{dz}\right)_{ad} = -\frac{g}{c_p} = -\frac{0.98^\circ\text{C}}{100\text{ m}} \quad (1.6)$$

or a temperature decrease of about 1°C for each elevation increase of 100 m. The potential temperature (θ) is an important parameter defined from Eq. 1.5 by substituting for $(1/\rho)$ with the use of the equation of state (Eq. 1.1) and by integrating from sea-level pressure (10^6 dynes/cm²) to the pressure p at any level.

$$\theta = T \left(\frac{10^6 \text{ dynes/cm}^2}{p} \right)^{R/c_p} \quad (1.7)$$

where the ratio R/c_p equals 0.286. In other words, the potential temperature of a parcel of air at temperature (T) and pressure (p) is the temperature that would result if the parcel were brought adiabatically from a pressure p to a pressure of 10^6 dynes/cm². It follows that

$$\frac{d\theta}{dz} = \frac{dT}{dz} + \frac{g}{c_p} \quad (1.8)$$

and

$$\theta \approx T + \frac{g}{c_p} z \quad (1.9)$$

where z is the height above mean sea level. The adiabatic potential temperature gradient ($d\theta/dz$) is zero. A wide range of temperature gradients is observed in the atmosphere, but the average value in the troposphere (lowest 10 km) is $-0.65^\circ\text{C}/100\text{ m}$. This represents a balance between vertical mixing processes and radiative heat exchanges.

When air is saturated with water vapor and is rising vertically, the adiabatic temperature decrease is less than that given by Eq. 1.6. As air cools, its capacity for water vapor decreases, and liquid water is condensed. This process releases heat to the air at a rate of about 540 cal/g (latent heat of vaporization, L) of condensed water. Thus part of the internal energy used in expansion is recovered from latent heat release, and the moist adiabatic temperature gradient $(dT/dz)_m$ is given by

$$\left(\frac{dT}{dz}\right)_m = -\frac{g}{c_p} - \frac{L}{c_p} \frac{dm_s}{dz} \quad (1.10)$$

where m_s is the saturated mixing ratio (mass of water vapor per mass of air at saturation). The wet adiabatic

temperature gradient is a function of temperature ranging from about $-0.9^\circ\text{C}/100\text{ m}$ in cold polar climates to about $-0.4^\circ\text{C}/100\text{ m}$ in warm tropical climates. The saturated water-vapor mixing ratio (m_s) is a function of temperature and is presented graphically in Fig. 11.4 of Chap. 11. With each 10°C rise in temperature, m_s roughly doubles.

1-3.2 Stability

Meteorologists distinguish three states of the atmospheric surface layer: unstable, neutral, and stable. These adjectives refer to the reaction of a parcel of air displaced adiabatically in the vertical direction. Figure 1.2 shows the environmental lapse rates that give rise to these stability classes. In each example the parcel originates at the height indicated by the circle in the figure; at this height the temperature of the parcel is the same as that of its environment. If the density of the parcel is less than that of its environment ($\rho_p < \rho_e$ or $T_p > T_e$), then the parcel is accelerated upward. If the density of the parcel is more than that of its environment ($\rho_p > \rho_e$ or $T_p < T_e$), then the parcel is accelerated downward. If the density of the parcel is the same as that of its environment ($T_p = T_e$), then the parcel continues at its original speed. For the example of the unstable layer, the parcel is continually accelerated away from its origin. The example of the neutral layer shows that the temperature of the parcel is always the same as that of its environment, and there is no force on it. The sketches above the temperature profiles illustrate the gravitational analogy for a ball on top of a hill (unstable), on a flat plain (neutral), and in a valley (stable).

We can formalize these stability criteria:

$$\begin{aligned} \text{Unstable: } \frac{\partial T_e}{\partial z} &< -0.98^\circ\text{C}/100\text{ m} \\ \text{Neutral: } \frac{\partial T_e}{\partial z} &= -0.98^\circ\text{C}/100\text{ m} \\ \text{Stable: } \frac{\partial T_e}{\partial z} &> -0.98^\circ\text{C}/100\text{ m} \quad (\text{inversion condition}) \end{aligned} \quad (1.11)$$

Typically, the criterion for instability is satisfied only within about 100 m of the surface on a sunny day. The atmosphere is neutral on a windy and cloudy day or night and is stable near the surface at night or at any time in an elevated inversion layer. During stable conditions a parcel displaced from an equilibrium

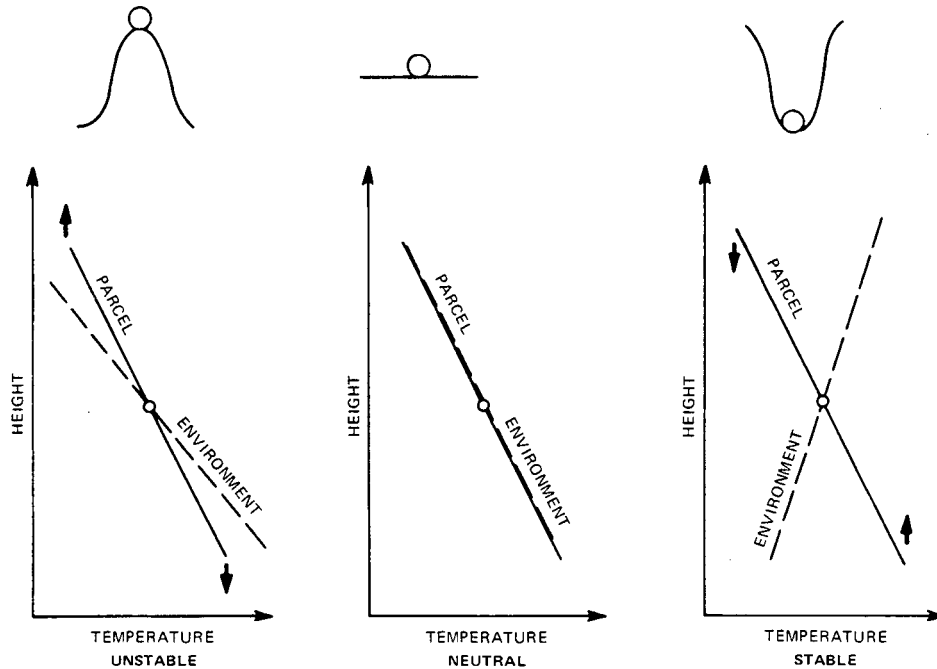


Fig. 1.2 Illustration of unstable, neutral, and stable environmental temperature profiles (---). An air parcel moved adiabatically cools as it rises vertically (—).

level, as in Fig. 1.2, will oscillate about the equilibrium level with the Brunt-Väisälä frequency n_{BV} (radians/sec):

$$n_{BV} = \left[\frac{g}{T_e} \left(\frac{\partial T_e}{\partial z} + \frac{0.98^\circ\text{C}}{100 \text{ m}} \right) \right]^{1/2}$$

$$= \left(\frac{g}{T_e} \frac{\partial \theta_e}{\partial z} \right)^{1/2} = s^{1/2} \quad (1.12)$$

where θ_e is the potential temperature. The stability parameter (s) in Eq. 1.12 will be important in the calculation of plume rise in Chap. 2. For typical stable temperature gradients ($0^\circ\text{C}/100 \text{ m}$ and $2^\circ\text{C}/100 \text{ m}$), the Brunt-Väisälä period ($2\pi/n_{BV}$) is 355 sec and 200 sec, respectively.

The parameter s may also be thought of as being proportional to the rate at which stability suppresses the generation of turbulence. On the other hand, turbulence is being generated by mechanical shear forces at a rate proportional to $(\partial u/\partial z)^2$. The ratio of these two processes is called the Richardson number (Ri):

$$Ri = \frac{g}{T} \frac{\partial \theta/\partial z}{(\partial u/\partial z)^2} = \frac{s}{(\partial u/\partial z)^2} \quad (1.13)$$

Clearly the stability parameter Ri gives us more information than s about the state of turbulence in

the atmosphere, which is, in turn, directly related to diffusion.

1-4 STRUCTURE OF THE PLANETARY BOUNDARY LAYER

The earth's surface exerts a drag on the atmosphere which influences wind speed up to a height of about 1 km. Diurnal variations in temperature and mixing ratio are also noticed up to the top of this layer, which is called the "planetary boundary layer" (PBL). Since most diffusion problems, with the exception of such problems as aircraft emissions and high level bomb blasts, occur in this layer, it is important to know the variations of winds, temperatures, and turbulence parameters in the PBL.

1-4.1 Turbulence Fluxes

The so-called eddy diffusivity (K), eddy viscosity (K_m), and eddy conductivity (K_h) coefficients are derived by assuming that any variable A is the sum of an average \bar{A} and a turbulent fluctuation A' :

$$A = \bar{A} + A' \quad (1.14)$$

where A could represent such variables as temperature, absolute humidity, or pollutant concentration.

The average is usually over a time period of about 1 hr. Further, the Reynolds averaging procedure is used:

$$\overline{A'} = 0 \quad \text{and} \quad \overline{\overline{A}} = \overline{A} \quad (1.15)$$

Next, consider the continuity equation for A:

$$\frac{dA}{dt} = \frac{\partial A}{\partial t} + u \frac{\partial A}{\partial x} + v \frac{\partial A}{\partial y} + w \frac{\partial A}{\partial z} = B + S \quad (1.16)$$

where B includes all external effects, S includes all internal sources, and w is vertical speed. Also, assume that the atmosphere is incompressible:

$$\frac{\partial u}{\partial x} + \frac{\partial v}{\partial y} + \frac{\partial w}{\partial z} = 0 \quad (1.17)$$

By substituting Eq. 1.14 into Eq. 1.16, using Eq. 1.17 (multiplied by A), and averaging according to Eq. 1.15, we obtain

$$\begin{aligned} \frac{d\overline{A}}{dt} &= \frac{\partial \overline{A}}{\partial t} + \overline{u} \frac{\partial \overline{A}}{\partial x} + \overline{v} \frac{\partial \overline{A}}{\partial y} + \overline{w} \frac{\partial \overline{A}}{\partial z} \\ &= \overline{B} + \overline{S} - \frac{\partial}{\partial x} (\overline{u'A'}) \\ &\quad - \frac{\partial}{\partial y} (\overline{v'A'}) - \frac{\partial}{\partial z} (\overline{w'A'}) \end{aligned} \quad (1.18)$$

The term $\overline{u'A'}$ is the flux of A in the x direction due to turbulent fluctuations.

Since such turbulent fluxes as $\overline{u'A'}$ can be measured only with fast-response instruments and are difficult to treat theoretically by analogy with the molecular case, the turbulent flux is commonly assumed to be proportional to the mean gradient:

$$\overline{w'A'} = -K \frac{\partial \overline{A}}{\partial z} \quad (1.19)$$

where K is a diffusivity coefficient (in units of m^2/sec). The negative sign is included so that the flux is down the gradient (i.e., from high values of A to low values). This technique is also called first-order closure. Second-order closure (e.g., Donaldson, 1973) is a more recent scheme that goes one step further and approximates such terms as $\overline{u'w'A'}$ with mean gradients of $(\overline{u'A'})$. Closure can be extended to any order, but the technique soon becomes unbearably complex.

If A is the concentration of a pollutant, then Eq. 1.18 yields the "diffusion equation:"

$$\begin{aligned} \frac{\partial \overline{A}}{\partial t} + u \frac{\partial \overline{A}}{\partial x} + v \frac{\partial \overline{A}}{\partial y} + w \frac{\partial \overline{A}}{\partial z} &= S + \frac{\partial}{\partial x} \left(K_x \frac{\partial \overline{A}}{\partial x} \right) \\ &+ \frac{\partial}{\partial y} \left(K_y \frac{\partial \overline{A}}{\partial y} \right) + \frac{\partial}{\partial z} \left(K_z \frac{\partial \overline{A}}{\partial z} \right) \end{aligned} \quad (1.20)$$

where S can represent internal processes, such as chemical reactions. If A is the wind-speed component u or v in the x or y direction, then Eq. 1.20 yields the equations of motion. For unaccelerated flow homogeneous in the x and y directions, these equations become

$$0 = -g \frac{\partial z}{\partial x} \Big|_p + fv + \frac{\partial}{\partial z} \left(K_{mz} \frac{\partial u}{\partial z} \right) \quad (1.21)$$

$$0 = -g \frac{\partial z}{\partial y} \Big|_p - fu + \frac{\partial}{\partial z} \left(K_{mz} \frac{\partial v}{\partial z} \right) \quad (1.22)$$

where K_{mz} refers to the vertical component of the diffusivity coefficient for momentum, or the eddy viscosity. There is a balance among pressure, Coriolis, and frictional forces in Eqs. 1.21 and 1.22. From this point on, the bar notation for averages has been removed.

1.4.2 Ekman Spiral

A simple expression for the variation of the wind velocity through the whole depth of the PBL was developed by Ekman in 1902. He assumed that the eddy viscosity coefficient for momentum in the vertical (K_{mz}) was constant and that the geostrophic wind-speed approximation was valid:

$$u_g = -\frac{g}{f} \frac{\partial z}{\partial y} \Big|_p \quad (1.23)$$

$$v_g = \frac{g}{f} \frac{\partial z}{\partial x} \Big|_p \quad (1.24)$$

The substitution of these equations into Eqs. 1.21 and 1.22 yields the following forms of the equations of motion:

$$0 = f(v - v_g) + K_{mz} \frac{\partial^2 u}{\partial z^2} \quad (1.25)$$

$$0 = -f(u - u_g) + K_{mz} \frac{\partial^2 v}{\partial z^2} \quad (1.26)$$

If we orient the x axis parallel to the geostrophic wind vector and assume that u_g and v_g are constant with height, the solution to these equations is

$$u(z) = u_g(1 - e^{-az} \cos az) \quad (1.27)$$

$$v(z) = u_g e^{-az} \sin az \quad (1.28)$$

where $a = (f/2K_{mz})^{1/2}$.

This solution is shown in Fig. 1.3, which shows that the predicted angle between the surface wind and the geostrophic wind is 45° . The predicted angle is higher than is usually observed because of the restricting assumptions made to get a solution. Typical observed angles between the surface wind and the geostrophic or free stream wind are 5 to 10° in unstable conditions, 15 to 20° in neutral conditions, and 30 to 50° in stable conditions. Wind-direction shear is very important for diffusion at large distances, where the bottom and top of the plume can move in directions differing as much as 40 or 50° and thus yield a much larger plume spread than that possible as a result of turbulent diffusion alone.

The real atmosphere usually does not agree with the Ekman spiral at the top of the mixed layer (z_i) because of the development of an inversion at that height. On most days this "capping inversion" at z_i results in strong discontinuities in such parameters as water vapor mixing ratio and eddy dissipation rate. Holzworth (1972) has analyzed observed temperature profiles and published maps and tables of z_i for most regions of the United States. Typical afternoon mixing depths (z_i) are about 1000 to 2000 m.

1-4.3 Similarity Theory Gives Wind and Temperature Profiles in Surface Layer

The momentum flux [$-u'w'$ or $K_{mz}(\partial u/\partial z)$] is used to define the quantity u_*^2 , where u_* is called the friction velocity:

$$u_*^2 = -\overline{u'w'} = K_{mz} \frac{\partial u}{\partial z} \quad (1.29)$$

The equation of motion (Eq. 1.25) can be used to show that u_*^2 usually varies by less than 20% in the surface layer, or the lowest 50 m of the atmosphere. During neutral or adiabatic conditions, the hypothesis $K_m \propto (\text{scaling speed}) \times (\text{scaling length})$ can be used, where the surface value of friction velocity (u_*) is the scaling speed and the height (z) is the scaling length, i.e.,

$$K = k u_* z \quad (1.30)$$

von Kármán's constant (k) is measured to be 0.35 over very smooth terrain and 0.4 over most other terrain.

If k is assumed to equal 0.4 , then Eq. 1.29 becomes

$$K \frac{\partial u}{\partial z} = 0.4 u_* z \frac{\partial u}{\partial z} = u_*^2$$

$$\frac{\partial u}{\partial z} = \frac{u_*}{0.4 z} \quad (1.31)$$

$$u = \frac{u_*}{0.4} \ln \left(\frac{z}{z_0} \right)$$

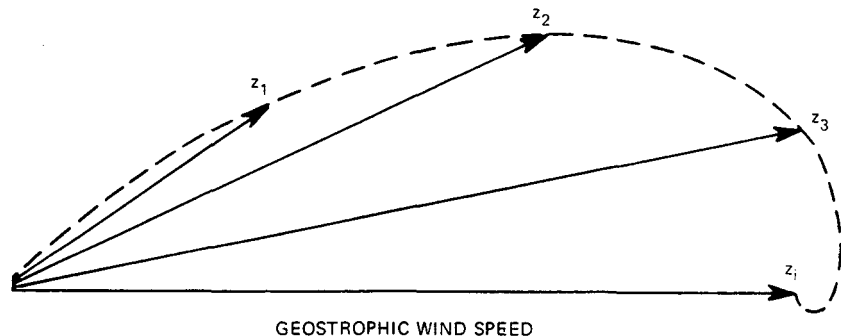
This is the well-known logarithmic wind profile, where the integration constant (z_0) is called the roughness length. In general, $z_0 \sim h/10$, where h is the height of the roughness elements, such as buildings or plant cover.

During diabatic conditions [$(\partial\theta/\partial z) \neq 0$] we define a scaling temperature [$T_* = (w'T'/u_*)$] and another scaling length

$$L = \frac{u_*^3}{0.4 (g/T) (-w'T')} \quad (1.32)$$

This is called the Monin-Obukhov length, after its founders (Monin and Obukhov, 1953). L is positive for stable conditions (usually at night), negative for unstable conditions (usually daytime), and approaches infinity for neutral conditions (dawn and dusk transition periods and cloudy, windy condi-

Fig. 1.3 Ekman wind spiral. The wind-velocity vectors at increasing heights (z_1 , z_2 , and z_3) approach the geostrophic wind-velocity vector at the top of the mixed layer (z_i).



tions). The absolute value of L can be thought of as the depth of the mechanically mixed layer near the surface. The ratio z/L is another stability parameter that has been found to approximate the Richardson number (Ri) during unstable conditions and equal $Ri/(1 - 5 Ri)$ during stable conditions. We can now make the similarity predictions:

$$\frac{u}{u_*} = fn \left(\frac{z}{z_0}, \frac{z}{L} \right) \quad (1.33)$$

$$\frac{T - T_0}{T_*} = fn' \left(\frac{z}{z_0}, \frac{z}{L} \right) \quad (1.34)$$

where subscript "0" refers to a surface value and fn and fn' are universal functions.

Consistent with the above, observations (Businger et al., 1971) show that

$$\begin{aligned} \frac{0.4 z}{u_*} \frac{\partial u}{\partial z} &= \phi_m \left(\frac{z}{L} \right) = \left(1 - 15 \frac{z}{L} \right)^{-1/4} \quad (\text{unstable}) \\ &= 1 + 5 \frac{z}{L} \quad (\text{stable}) \end{aligned} \quad (1.35)$$

$$\begin{aligned} \frac{0.4 z}{T_*} \frac{\partial \theta}{\partial z} &= \phi_h \left(\frac{z}{L} \right) = 0.74 \left(1 - 9 \frac{z}{L} \right)^{-1/2} \quad (\text{unstable}) \\ &= 0.74 + 5 \frac{z}{L} \quad (\text{stable}) \end{aligned} \quad (1.36)$$

where ϕ_m and ϕ_h are the dimensionless wind and temperature gradients, respectively. Paulson (1970) has integrated Eq. 1.35 for unstable conditions to give the solution

$$\begin{aligned} u &= \frac{u_*}{4} \left\{ \ln \frac{z}{z_0} - 2 \ln \left[\frac{1}{2} \left(1 + \frac{1}{\phi_m} \right) \right] \right. \\ &\quad \left. - \ln \left[\frac{1}{2} \left(1 + \frac{1}{\phi_m^2} \right) \right] + 2 \tan^{-1} \frac{1}{\phi_m} - \frac{\pi}{2} \right\} \end{aligned} \quad (1.37)$$

In stable conditions the following solution is easily derived:

$$u = \frac{u_*}{0.4} \left(\ln \frac{z}{z_0} + 5 \frac{z}{L} \right) \quad (1.38)$$

The eddy diffusivity for momentum (K_m) and for heat (K_h) can be defined by Eq. 1.9 by using $A = u$ and $A = \theta$, respectively:

$$K_m = 0.4 u_* \frac{z}{\phi_m(z/L)} \quad (1.39)$$

$$K_h = 0.4 u_* \frac{z}{\phi_h(z/L)} \quad (1.40)$$

The eddy diffusivity coefficient (K) for pollutants is usually assumed to equal K_h , and experimental evidence tends to support this.

1.4.4 Turbulence Parameters

In convective conditions, i.e., when the surface is warmer than the air above it, the important scaling parameters are the mixing-layer height (z_i) and the scaling velocity (w_*), which is defined by

$$w_* = \left(\frac{g}{T} \overline{w'T'} z_i \right)^{1/2} \quad (1.41)$$

Deardorff (1970) first made use of this parameter, and Kaimal et al. (1977) applied it in their analysis of a field experiment. The quantity $(g/T) \overline{w'T'}$ is called the surface buoyancy flux (H); it is proportional to the surface heat flux. The surface layer extends to a height of about $0.1 z_i$, and above that height, during unstable conditions, wind speed is nearly constant and wind direction turns slightly (5 to 10°) to the right (in the northern hemisphere). Wind profiles above the surface layer in neutral and stable conditions are more complicated; the interested reader should consult the basic references (Wyngaard, Cote, and Rao, 1974; Wyngaard, 1975).

The parameters σ_u , σ_v , and σ_w are the standard deviations of turbulent velocity fluctuations in the x , y , and z directions, respectively. Panofsky et al. (1977) have recently studied data from several different sites and have determined formulas 1.42, 1.48, and 1.51 for σ_w , σ_v , and σ_u , respectively, for unstable conditions. Irwin (1979b) developed the power-law formulas given in Eqs. 1.43 to 1.45 for the variation of σ_w/w_* above the surface layer. Formulas for neutral and stable conditions were obtained by fitting analytical formulas to curves presented by Wyngaard et al. (1975) and Wyngaard (1974).

$$\frac{\sigma_w}{w_*} = 0.96 \left(\frac{3z}{z_i} + \frac{L}{z_i} \right)^{1/2} \quad \left(0 < \frac{z}{z_i} < \frac{z_t}{z_i} \right) \quad (1.42)$$

$$= 0.763 \left(\frac{z}{z_i} \right)^{0.175} \quad \left(\frac{z_t}{z_i} < \frac{z}{z_i} < 0.4 \right) \quad (1.43)$$

$$= 0.722 \left(1 - \frac{z}{z_i} \right)^{0.207} \quad \left(0.40 < \frac{z}{z_i} < 0.96 \right) \quad (1.44)$$

$$= 0.37 \quad \left(0.96 < \frac{z}{z_i} < 1 \right) \quad (1.45)$$

where z_t/z_i is the height at which the first and second formulas give equal values of σ_w/w_* .

$$\frac{\sigma_w}{u_*} = 1.3 \exp\left(-2 \frac{fz}{u_*}\right) \quad (\text{neutral}) \quad (1.46)$$

$$= 1.3 \left(1 - \frac{z}{z_i}\right) \quad (\text{stable}) \quad (1.47)$$

$$\frac{\sigma_v}{u_*} = \left(12 - 0.5 \frac{z_i}{L}\right)^{1/2} \quad (\text{unstable}) \quad (1.48)$$

$$= 1.3 \exp\left(-2 \frac{fz}{u_*}\right) \quad (\text{neutral}) \quad (1.49)$$

$$= 1.3 \left(1 - \frac{z}{z_i}\right) \quad (\text{stable}) \quad (1.50)$$

$$\frac{\sigma_u}{u_*} = \left(12 - 0.5 \frac{z_i}{L}\right)^{1/2} \quad (\text{unstable}) \quad (1.51)$$

$$= 2.0 \exp\left(-3 \frac{fz}{u_*}\right) \quad (\text{neutral}) \quad (1.52)$$

$$= 2.0 \left(1 - \frac{z}{z_i}\right) \quad (\text{stable}) \quad (1.53)$$

In the daytime z_i is usually marked by an inversion capping the unstable well-mixed layer above the ground surface. At night an inversion is present to some degree at all levels, and z_i marks the height at which surface-induced mechanical turbulence dies off to zero. Turbulent intensity in the surface layer can be estimated by dividing the appropriate values in the set of Eqs. 1.42 to 1.53 by the appropriate values in the set of Eqs. 1.37 and 1.38. The turbulence intensities σ_v/u and σ_u/u decrease with height for all stabilities, whereas σ_w/u increases with height in unstable conditions and decreases with height in neutral and stable conditions.

The eddy dissipation rate (ϵ) gives the rate at which turbulence is being dissipated into heat at small scales. This rate will be important in the calculation of plume rise. In the surface layer, ϵ is given by the formula (from the energy equation).

$$\begin{aligned} \epsilon &= u_*^2 \frac{du}{dz} + \frac{g}{T} \overline{w'T'} \\ &= \frac{u_*^3}{kz} \left(\phi_m - \frac{z}{L}\right) \end{aligned} \quad (1.54)$$

Experiments indicate that $\epsilon \approx 0.5 H$ at heights above the surface layer at midday. During neutral

conditions, however, the data show that $\epsilon = u_*^3/0.4 z$ up to heights of several hundred meters.

1-5 USE OF SPECTRA TO ESTIMATE TURBULENCE PARAMETERS

The eddy energy spectrum [$S(n)$] gives information on the amount of energy carried by eddies of different sizes; it involves a Fourier transform of the correlation coefficient $R(\tau)$:

$$R_u(\tau) = \frac{\overline{u'(t)u'(t+\tau)}}{\sigma_u^2} \quad (1.55)$$

where τ is the time lag. The turbulence time scale is defined by

$$T = \int_0^\infty R(\tau) d\tau \quad (1.56)$$

The larger the "eddies," the slower R drops off with time and the larger the time scale T .

Energy spectra have been found to follow similarity theory also, and universal equations for their form can be written. (These equations will not be reproduced here but can be found in Kaimal et al., 1977). One important scaling parameter is the wavelength (λ_m) at which the eddies are carrying the maximum energy. Kaimal et al. (1977) deduce the following form for λ_m during convective daytime conditions:

$$\begin{aligned} w : \lambda_{mw} &= \frac{z}{(0.55 + 0.38 z/L)} \quad (z < -L) \\ &= 5.9 z \quad (-L < z < 0.1 z_i) \\ &= 1.5 z_i (1 - e^{-5z/z_i}) \quad (0.1 z_i < z < z_i) \end{aligned} \quad (1.57)$$

$$u, v : \lambda_{mu} = \lambda_{mv} = 1.5 z_i \quad (1.58)$$

For neutral conditions, the wavelength λ_m of peak energy is assumed to be equal for all three components of turbulence. Several researchers have proved the validity of the assumption that λ_m is proportional to height in the surface layer but asymptotically approaches a constant at great heights:

$$\lambda_m = 5 \frac{z}{(1 + 15 fz/u_*)} \quad (\text{neutral}) \quad (1.59)$$

Caughey, Wyngaard, and Kaimal (1979) give observations of the variation with height of the wavelength

λ_m for the three turbulence components during stable conditions. The observed points can be fit by the following simple power laws:

$$\frac{\lambda_{mu}}{z_i} = 1.5 \left(\frac{z}{z_i}\right)^{0.5} \quad (1.60)$$

$$\frac{\lambda_{mv}}{z_i} = 0.7 \left(\frac{z}{z_i}\right)^{0.5} \quad (1.61)$$

$$\frac{\lambda_{mw}}{z_i} = 1.0 \left(\frac{z}{z_i}\right)^{0.8} \quad (1.62)$$

The values of λ_{mw} given above can be used to estimate K_m by using the formula suggested by Hanna (1968):

$$K_m = A \sigma_w \lambda_{mw} \quad (1.63)$$

where Pasquill (1974) has determined that the best value for the constant A is 0.15. The parameter σ_w can be estimated by using the suggestions in Sec. 1-4.4.

1-6 LAGRANGIAN TURBULENCE

So far we have been discussing Eulerian turbulence, which is traditionally measured at a fixed point

on a meteorological tower (see Fig. 1.4). The wind and turbulence are measured by an anemometer as the air flows past. Another type of Eulerian measurement is made by an aircraft, which flies through the turbulence along a nearly straight line. Also, the measurement made by an anemometer moving with the mean wind speed through the flow is called a Eulerian measurement. In none of these cases does the measuring instrument move with the air.

Measurements of an air molecule (1 or 2 in Fig. 1.4) that has been tagged and followed as it moves through the turbulent field are called Lagrangian measurements. Clearly the diffusion of pollutants is a Lagrangian process, which unfortunately must usually be estimated by using Eulerian measurements, and some relationship between the two systems should be established.

An air molecule will generally think a given turbulent eddy has a lower frequency than that measured by a fixed anemometer. This is crudely illustrated by Fig. 1.5, in which a circular eddy with tangential speed (w) is immersed in a mean wind (\bar{u}). The molecule travels once around the eddy in time $2\pi R/w$, whereas the fixed anemometer sees the eddy pass in time $2R/\bar{u}$. Therefore the ratio of Lagrangian to Eulerian time scales (β) in this figure is given by

$$\beta = \frac{T_L}{T_E} = \frac{\pi}{w/\bar{u}} = \frac{\pi}{i} \quad (1.64)$$

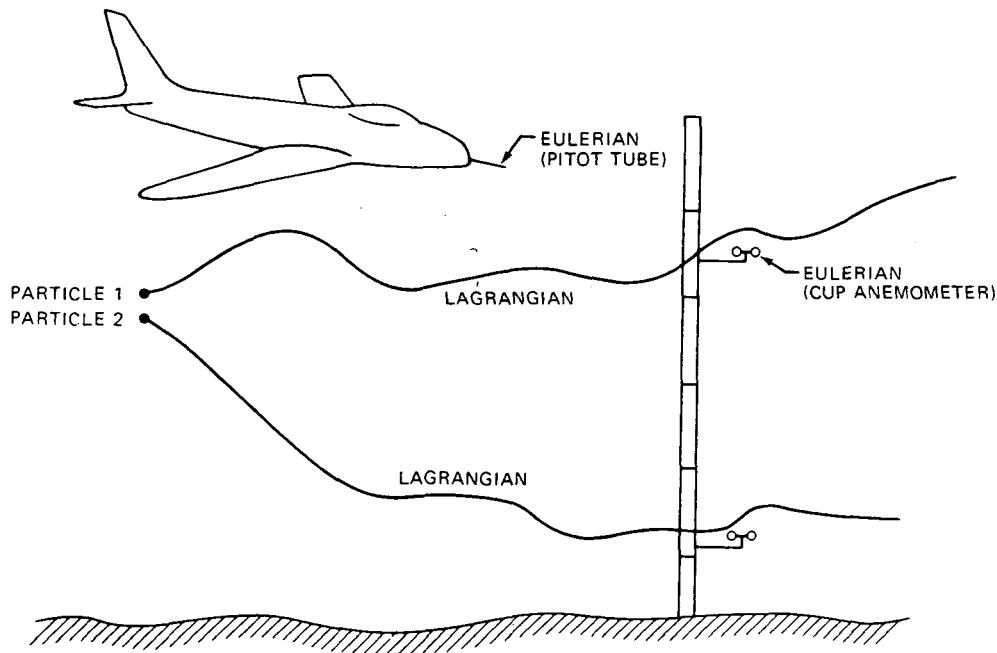


Fig. 1.4 Eulerian and Lagrangian wind-measuring systems. True Lagrangian wind measurements are given by tagged air particles 1 and 2.

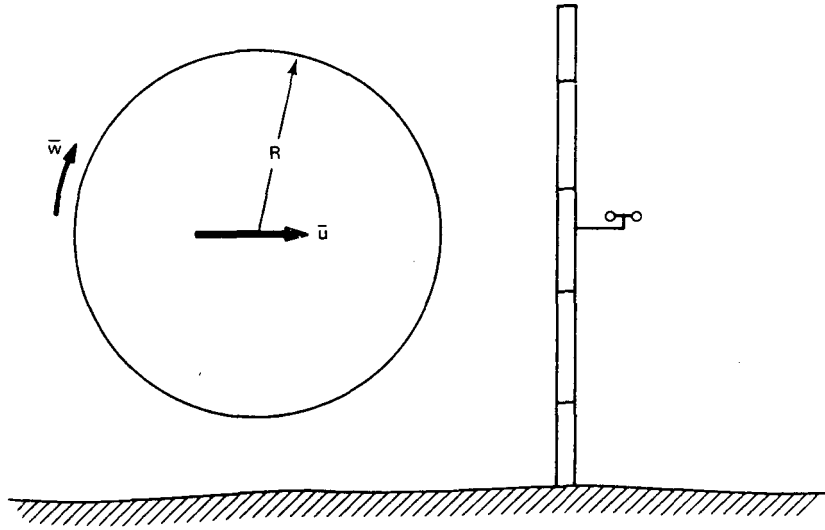


Fig. 1.5 Large eddy of radius R approaches an anemometer on a tower. The eddy moves with mean speed (\bar{u}) and has a mean tangential velocity (\bar{w}).

where i is the turbulence intensity, usually called σ_w/u . As turbulence intensity increases (stability decreases), the ratio β decreases. Pasquill (1974) suggests that a good average value for β is 4. Reid (1979) finds that more accurate diffusion calculations can be made if

$$\beta = \frac{0.5}{i} \quad (1.65)$$

which indicates that the relation $\beta \propto 1/i$ is correct but that the crude model in Fig. 1.5 overestimates the proportionality constant.

Problems

1. Calculate the mass of the atmosphere. (The easiest derivation will take less than one-half page.)

2. Suppose that the 500-mb surface is 1000 m higher over New Orleans, La., than it is over Chicago, Ill. What is the eastward component of the geostrophic wind at that level?

3. On a windy day the following wind observations are made:

$z, \text{ m}$	0.5	1.0	2.0	4.0	8.0
$u, \text{ m/sec}$	1.6	2.3	3.0	3.7	4.4

Estimate the roughness length (z_0) and the friction velocity (u_*).

4. Assume that $z_i = 1000 \text{ m}$, $L = -50 \text{ m}$, and $u_* = 0.3 \text{ m/sec}$. At what height does σ_w reach a maximum? What is its value? What is the value of σ_v at that height? If $u = 5 \text{ m/sec}$ at that height, what is the ratio of Lagrangian to Eulerian time scales (β) for the y and z components?


Plume Rise

2-1 INTRODUCTION

Plume rise is a very important factor in determining maximum ground-level concentrations from most sources since it typically increases the effective stack height by a factor of 2 to 10 times the actual release height. Because maximum ground-level concentration is roughly proportional to the inverse square of the effective stack height, it is clear that plume rise can reduce ground-level concentration by a factor of as much as 100. Most industrial pollutants are emitted with high velocity or temperature, and plume rise must be calculated. However, pollutants released from some building vents or motor vehicles have very little plume rise.

A few areas of plume rise are well understood, such as the trajectory before final rise is reached and final rise in stable conditions. In both of these cases, the effect of ambient turbulence in the air outside the plume is negligible. When ambient turbulence affects the plume, such as during final rise in neutral conditions and during the last half of rise in convective conditions, the models are less certain, and more research is needed.

2-2 TOP-HAT-MODEL EQUATIONS

The review article by Briggs (1975) provides background material on available plume-rise models. Most models are based on fundamental laws of fluid mechanics: conservation of mass, potential density, and momentum. The distribution of temperature, speed, or other quantities across the plume is assumed to have "top-hat" form (); that is, a variable has a certain value inside the plume, another value outside the plume, and a discontinuity at the plume radius (R). Basically we are looking at integrated averages of variables in a plume cross section.

2-2.1 Definitions

Figure 2.1 is a schematic drawing of a vertical plume and a bent-over plume which illustrates many of the variables and parameters important in calculating plume rise. A plume is usually more or less "vertical" if wind speed is less than about 1 m/sec. Note the difference on the figure in definitions of the plume volume flux:

$$\begin{aligned} V &= wR^2 && \text{(vertical)} \\ V &= uR^2 && \text{(bent over)} \end{aligned} \quad (2.1)$$

where w is plume vertical speed, u is ambient wind speed, and R is plume radius in a plane perpendicular to the plume axis. In Eqs. 2.1 as well as in other equations in this chapter, the factor π is left out. The initial volume flux is defined by using the initial plume vertical speed at stack exit:

$$V_0 = w_0 R_0^2 \quad (2.2)$$

Initial buoyancy flux (F_0) and momentum flux (M_0) are defined by the following equations:

$$F_0 = \frac{g}{T_{p0}} (T_{p0} - T_{e0}) V_0 \quad (2.3)$$

$$M_0 = \frac{\rho_{p0}}{\rho_{e0}} w_0 V_0 \quad (2.4)$$

where subscripts p , e , and 0 indicate plume, environment, and initial values, respectively. For plumes whose molecular weight (m) differs much from that of air, Eq. 2.3 should be rewritten by replacing all temperatures (T) with the ratio T/m_0 (m_{e0} can be assumed to equal 28.9). The values of the buoyancy

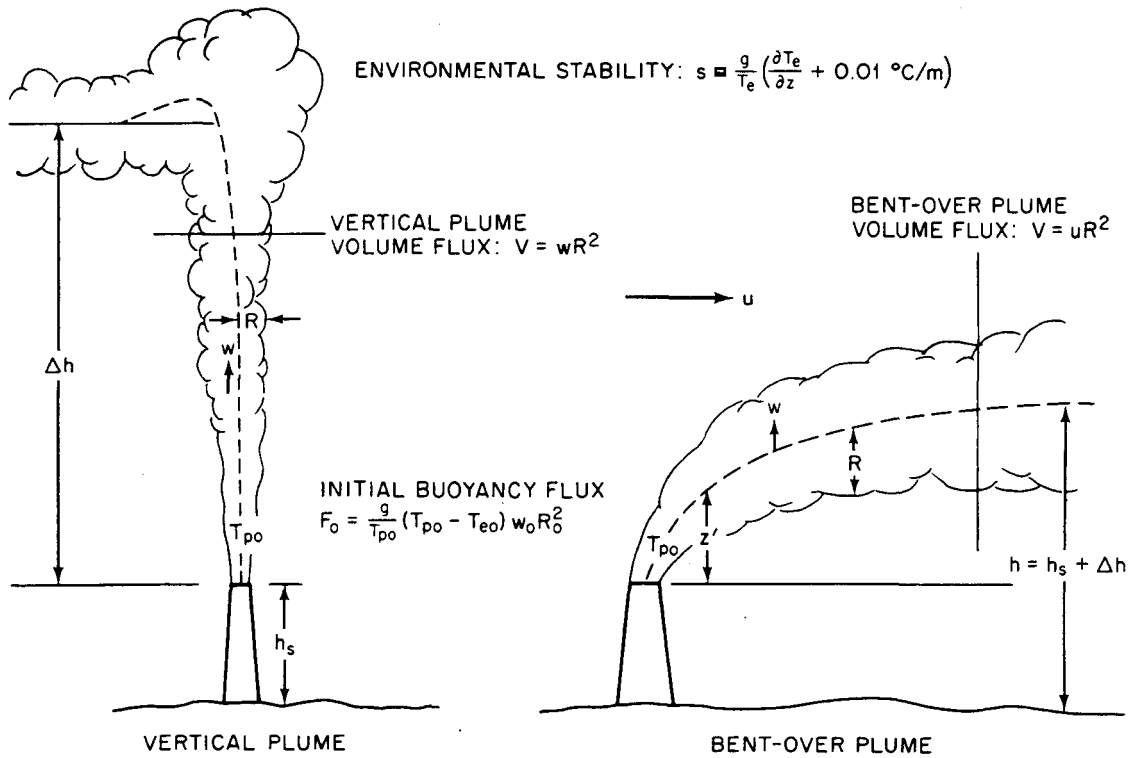


Fig. 2.1 Schematic diagram of vertical and bent-over plumes which illustrates some of the parameters and variables important for plume-rise calculations.

flux (F) and momentum flux (M) can change with height, where they are defined by the relations:

$$F = \frac{g}{T_p} (T_p - T_e) V \quad (2.5)$$

$$M = w V \quad (2.6)$$

Environmental stability (s) plays a prime role in slowing the plume's vertical motion:

$$s = \frac{g}{T_e} \left(\frac{\partial T_e}{\partial z} + 0.01 \text{ °C/m} \right) \quad (2.7)$$

The last factor is the adiabatic lapse rate, which is simplified to 0.01°C/m from its value of 0.0098°C/m in Eq. 1.6. Thus the last two terms could be replaced by $\partial \theta_e / \partial z$. From Eq. 1.12 we see that s is the square of the Brunt-Väisälä frequency n_{BV} .

The ratio (S) of the effective area influenced by the plume momentum to the cross-sectional area of the so-called thermal plume (Briggs, 1975) has now been recognized to be about 2.3 for bent-over plumes. This factor permits the accurate assessment of both plume trajectory and final plume rise.

Because we neglect the details of turbulence, we have one less conservation equation than we have

independent variables. An additional relationship, called the "closure assumption," is needed to solve the equations. The closure used most often is the Taylor entrainment assumption

$$\frac{dV}{dz} = 2 R v_e$$

$$v_e = \alpha w \quad (\text{vertical plumes})$$

$$v_e = \beta w \quad (\text{bent-over plumes})$$

The entrainment velocity (v_e) is the effective speed at which environmental air is drawn into the plume through its boundaries. Taylor (1948) proposed that v_e is proportional to plume vertical speed. The constants α and β are functionally similar, but β is much larger than α .

2-2.2 Set of Equations for Vertical Plume (from Briggs, 1975)

Buoyancy conservation

$$\frac{dF}{dz} = -sV \quad (2.8)$$

Momentum conservation

$$\frac{dM}{dz} = \frac{F}{w} \quad (2.9)$$

Closure

$$\frac{dV}{dz} = 2 \alpha R w = 2 \alpha M^{1/2} \quad (2.10)$$

where α equals 0.08.

2-2.3 Set of Equations for Bent-Over Plume (from Briggs, 1975)

Buoyancy conservation

$$\frac{dF}{dz} = -\frac{sV}{S} \quad (2.11)$$

where S equals 2.3.

Momentum conservation

$$\frac{dM}{dz} = \frac{F}{w} \quad (2.12)$$

Closure

$$\frac{dV}{dz} = 2 \beta R u$$

or, if u equals a constant,

$$R = \beta z \quad (2.13)$$

where β is equal to 0.6 for a buoyant plume and $\beta = 0.4 + 1.2 (u/w_0)$ for a jet.

2-3 PLUME TRAJECTORY NEAR SOURCE

Sometimes the plume trajectory near the source must be calculated before ambient stability or ambient turbulence has much effect. Stability has little influence at time periods less than $s^{-1/2}$, which varies between about 10 and 100 sec, and ambient turbulence is not important at distances less than about ten stack heights at typical power plants.

2-3.1 Vertical Plumes

For most plumes, early rise is dominated by momentum. In this stage radius (R) = 0.16 z and average vertical velocity (w) = 6.25 $M^{1/2}/z$. Transition to buoyancy domination occurs at $t = M/F_0$ (typically less than 10 sec), after which radius (R) = 0.15 z and average vertical velocity (w) = 2.3 $(F_0/z)^{1/2}$.

2-3.2 Bent-Over Plumes

For short times, the buoyancy flux can be assumed to be constant. The transition to buoyancy domination occurs at $t = M/F_0$, the same as for a vertical plume. This time has been found to be typically about 5 sec, which corresponds to a travel distance of only about 50 m. The plume trajectory in this region is given by the equation

$$z = \left(\frac{3}{\beta^2} \frac{M}{u^2} x + \frac{3}{2\beta^2} \frac{F_0}{u^3} x^2 \right)^{1/2} \quad (2.14)$$

This equation is compared with observations in Fig. 2.2, where plume rise and downwind distance

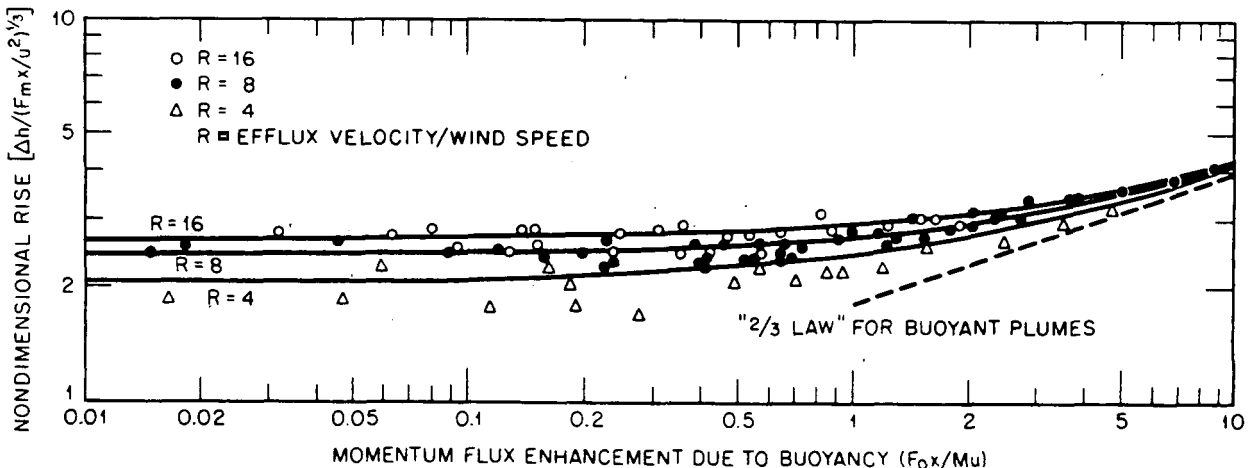


Fig. 2.2 Observed plume trajectories as a function of downwind distance (both nondimensionalized), showing transition from jet "1/3 law" to buoyant plume "2/3 law."

have been suitably nondimensionalized, and different curves are plotted for values of w_0/u equal to 4, 8, and 16. Consistent with the recommendations, $\beta = 0.6$ is used with the F_0 term in Eq. 2.14 and $\beta = 0.4 + 1.2 (u/w_0)$ is used with the M term.

For buoyancy-dominated plumes, Eq. 2.14 becomes

$$z = 1.6 F_0^{1/4} u^{-1} x^{3/8} \quad (2.15)$$

This is the famous " $z^{3/8}$ law," which has been shown to agree with a great bulk of field and laboratory data. The coefficient 1.6 can be expected to be accurate within $\pm 40\%$ with variations due to downwash or local terrain effects (Fay, Escudier, and Hoult, 1969; Briggs, 1981).

2-4 PLUME RISE LIMITED BY AMBIENT STABILITY

At night a deep (100 to 200 m) stable layer usually forms near the ground with other layers of varying stability above it. In the daytime there is usually a well-mixed convective boundary layer of depth 500 to 2000 m with a stably stratified "capping inversion" at the top. Plumes will nearly always have to contend with stable air at some point in their trajectory.

By recognizing that $w = dz/dt$, differentiating Eq. 2.9 or 2.12 with respect to t , and substituting from Eq. 2.8 or 2.11, we obtain

$$\frac{d^2 M}{dt^2} = -sM \quad (2.16)$$

This is the equation of a harmonic oscillator with period equal to the Brunt-Väisälä period $2\pi s^{-1/2}$. The vertical velocity (w) must act like a damped harmonic oscillator since the volume flux (V) always increases with time as a result of entrainment. Where vertical velocity first drops to zero, maximum plume rise is achieved. Plumes do reach a maximum rise and then drop down to an equilibrium height. As a result of wave drag, no more than one or two of the oscillations predicted by Eq. 2.16 are visible.

2-4.1 Vertical Plumes

Harmonic oscillator solutions and field and laboratory experiments suggest that the equilibrium height (z_{eq}) of a vertical jet in a stable environment is

$$z_{eq} = 2.44 \left(\frac{M}{s}\right)^{1/4} \quad (2.17)$$

For buoyant plumes, Briggs (1981) finds that

$$z_{eq} = 5.3 F_0^{1/4} s^{-3/8} - 6 R_0 \quad (2.18)$$

The correction term $6 R_0$ says that a virtual source exists a distance of six stack radii below the actual stack height.

2-4.2 Bent-Over Plumes

When the plume is bent over, the ratio of maximum plume height to equilibrium plume height is predicted to be 1.5 and 1.2 for a jet and a strongly buoyant plume, respectively. Formulas for the final rise of bent-over jets in a stable environment are not satisfactorily developed because of the lack of data. However, the formula for the final rise of a buoyant plume is well known:

$$\Delta h = 2.6 \left(\frac{F_0}{us}\right)^{1/2} \quad (2.19)$$

The coefficient in this formula was developed from comparisons with many observations, including the TVA power-plant plume-rise data reproduced in Fig. 2.3. For these data, the coefficient 2.6 is slightly conservative (underestimated plume rise). The wind speed (u) in this formula is an average value between the heights h_s and $h_s + \Delta h$.

2-5 PLUME PENETRATION OF ELEVATED INVERSION

If a plume can penetrate an elevated inversion, ground-level concentrations may be dramatically reduced because the inversion then is a strong inhibitor of downward diffusion. This situation is depicted in Fig. 2.4. If the plume does not penetrate the inversion, the plume is trapped below it, and high ground-level concentrations may result.

Let us arbitrarily define an elevated inversion to be a jump ($\Delta\theta_i$) in potential temperature at a height (z_{ei}) above the stack. Define an inversion strength $(g/\theta_a) \Delta\theta_i$. If a plume penetrates the inversion, its buoyancy flux is reduced by $(g/\theta_a) \Delta\theta_i V_i$, where V_i is the plume volume flux at height z_{ei} . We can conclude that the plume will penetrate this inversion if $F > (g/\theta_a) \Delta\theta_i V_i$. Remember that the plume volume flux (V) has been defined as being equal to the true volume flux divided by π .

The volume flux for vertical buoyant plumes and vertical jets is given by $0.07 F_0^{1/4} z^{3/8}$ and $0.16 M^{1/2} z$,

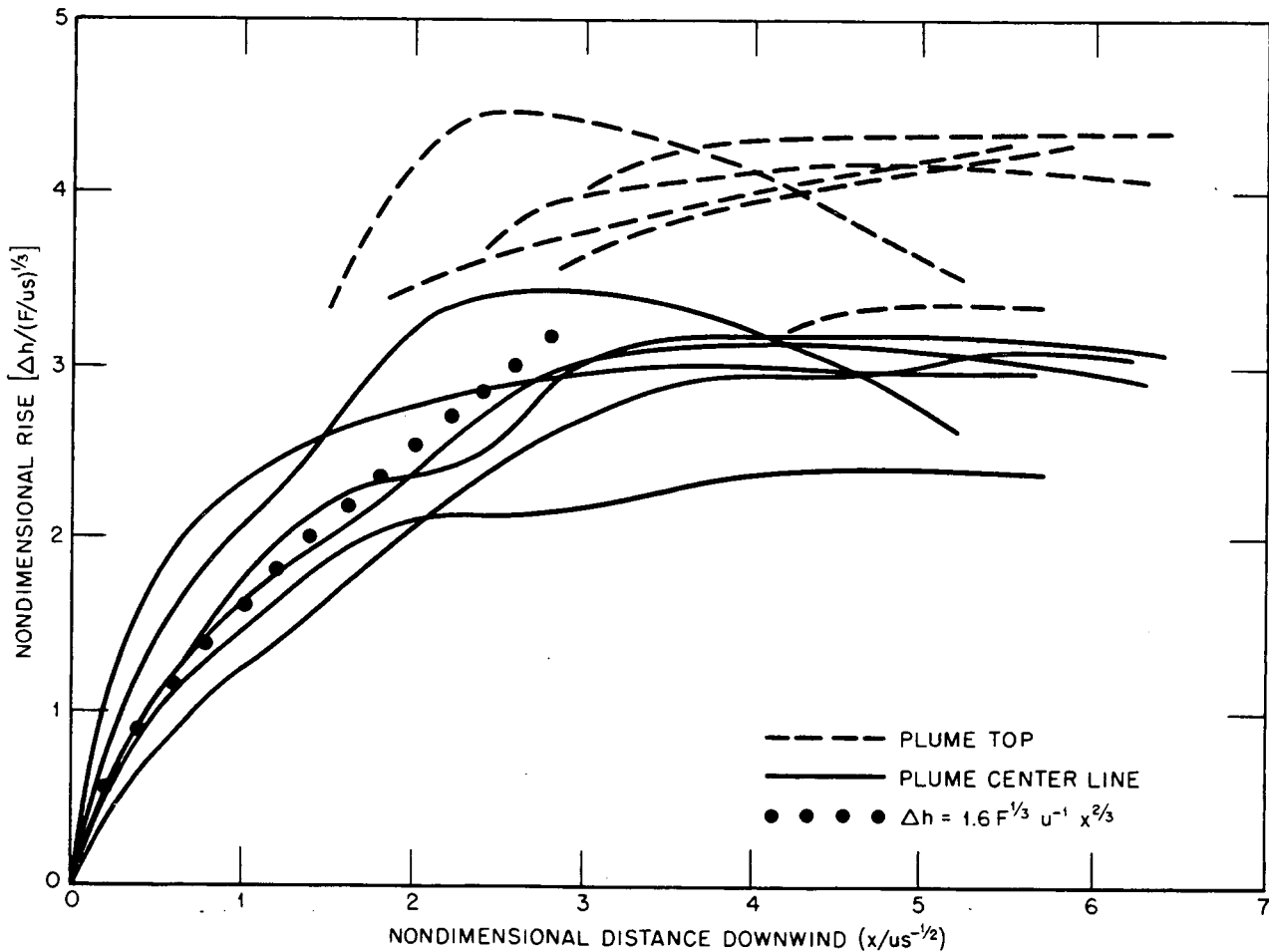


Fig. 2.3 Observed plume trajectories as a function of downwind distance (both nondimensionalized), showing maximum rise achieved by buoyant plumes.

respectively. Thus penetration of the inversion is forecast if the following conditions are met:

Vertical buoyant plume

$$z_{el} < 4.9 F_0^{2/5} \left(\frac{g}{\theta_a} \Delta\theta_i \right)^{-3/5} \quad (2.20)$$

Vertical jet

$$z_{el} < 6.2 \frac{F_0/M^{1/2}}{(g/\theta_a) \Delta\theta_i} \quad (2.21)$$

Bent-over jets will not be covered here because they have little ability to penetrate inversions. The volume flux (divided by π) of buoyant bent-over plumes is given by $V = 0.16 uz^2$, and penetration will occur if

$$z_i < 2.5 \left\{ \frac{F_0}{[u(g/\theta_a) \Delta\theta_i]} \right\}^{1/2} \quad (2.22)$$

This formula provided fair agreement with data from the Ravenswood power plant in New York City reported by Simon and Proudfit (1967). If the final plume rise (Δh) is within a factor of 2 of the inversion height (z_{el}) above the stack, only a fraction (P) of the plume can penetrate the inversion. In this case Briggs (1975) suggests the (untested) formula

$$P = 1.5 - \frac{z_{el}}{\Delta h} \quad (2.23)$$

A fraction $(1 - P)$ of the plume reflects off the bottom of the inversion and diffuses downward.

2-6 PLUME RISE DETERMINED BY AMBIENT TURBULENCE

On cloudy, windy days or typical sunny summer afternoons, the stability can be neutral or adiabatic in

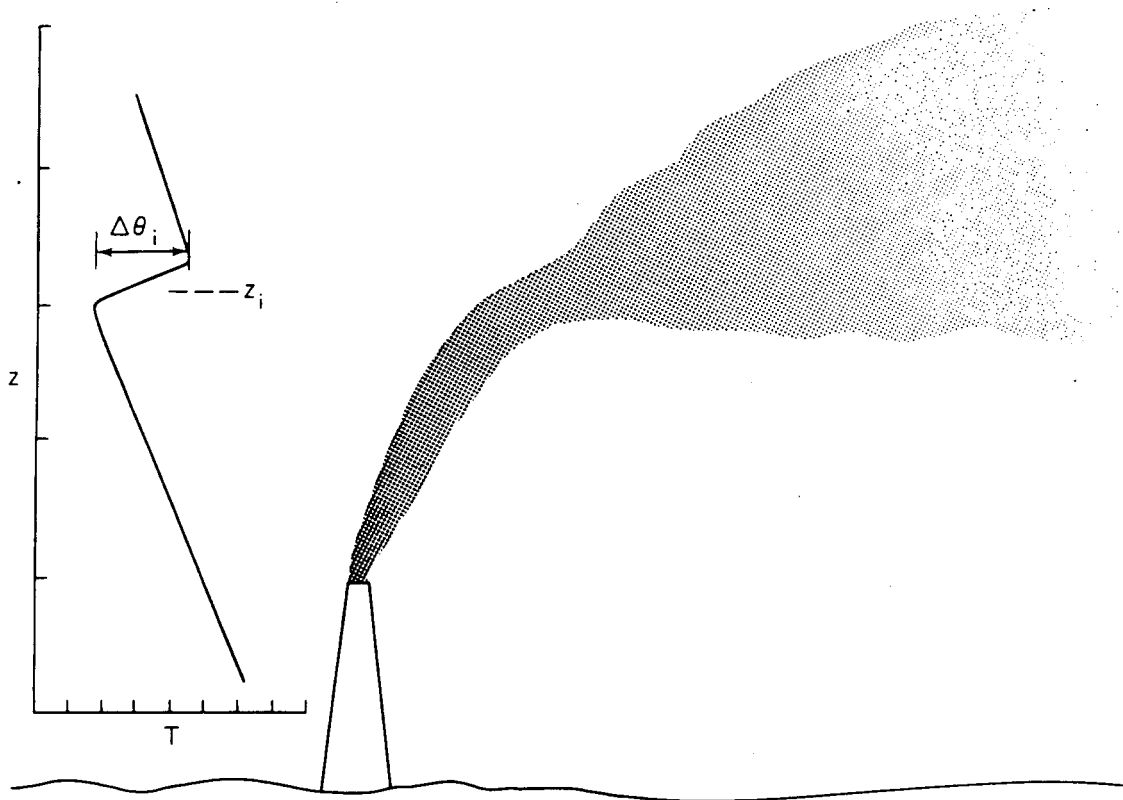


Fig. 2.4 Diagram of buoyant plume penetrating an elevated inversion.

the lowest 500 to 2000 m. If the plume reaches no stable layers, it may find its rise limited by ambient turbulence, which eventually dilutes the remaining plume buoyancy. Prior to that time the internal turbulence of the plume is significantly greater than the ambient turbulence. Briggs (1981) has developed the "breakup" model for the cases when rise is limited by ambient turbulence. In the "breakup" model the plume rise is assumed to terminate when the internal plume eddy dissipation rate just equals the ambient eddy dissipation rate.

The results in this section are highly dependent on Chap. 1, which gives methods of estimating boundary-layer profiles of eddy dissipation rate, turbulent energy, and wind speed.

2-6.1 Nearly Neutral Conditions

Final plume rise in the "breakup" model rise is assumed to occur when the following condition is met:

$$1.5 \frac{w^3}{z} = \epsilon \quad (2.24)$$

The left-hand ratio is the internal eddy dissipation rate of the plume, and ϵ is the ambient eddy

dissipation rate. For a buoyant, bent-over plume, $z = h_s + 1.6 F_0^{1/2} u^{-1} x^{3/2}$ (Eq. 2.15), and, by definition, $w = dz/dt$. With the use of $dx = u dt$ and $\epsilon = u_*^3 / 0.4 z$ evaluated at $z = h_s + \Delta h$ (valid during nearly neutral conditions), it is possible to arrive at the following simplified formula for plume rise Δh :

$$\Delta h = 1.54 \left(\frac{F_0}{uu_*^2} \right)^{2/3} h_s^{1/2} \quad (2.25)$$

For a jet, no verifying data exist, but a theoretical estimate of plume rise at "breakup" in neutral conditions is

$$\Delta h = 3D \left(\frac{w_0}{u} - 1 \right) \quad (2.26)$$

where D is the stack diameter and w_0 is the initial plume speed.

2-6.2 Convective Conditions

During convective conditions the neutral value for the eddy dissipation rate, $\epsilon = u_*^3 / 0.4 z$, must be replaced by an estimate made by Briggs for convec-

tive downdrafts, $\epsilon = 0.25H$, where H is the surface buoyancy flux (see Chap. 1, Sec. 1-4.4). The resulting prediction for buoyant plume rise is

$$\Delta h = 3 \left(\frac{F_0}{u} \right)^{3/5} H^{-2/5} \quad (2.27)$$

Please note that this is a *tentative* formula. Plume-rise observations in unstable conditions are the least satisfactory owing to rapid dilution.

2-7 MAXIMUM GROUND CONCENTRATION WITH BREAKUP MODEL

So that the dependence of maximum ground concentration (MGC) on effective plume rise $h_e = h_s + \Delta h$ can quickly be seen, suppose concentration in the plume was uniform. Thus MGC would be inversely proportional to the volume flux $\pi u h_e^2$ at the moment the plume first strikes the ground. This result is consistent with that obtained from the model that assumes a Gaussian distribution of material across the plume (see Chap. 4, Sec. 4-4) with standard deviation σ_y and σ_z in the crosswind horizontal and vertical directions, respectively. For σ_z/σ_y constant, the resulting MGC prediction is

$$\text{MGC} = 0.234 \frac{\sigma_z}{\sigma_y} \frac{Q}{u h_e^2} \quad (2.28)$$

Maximum ground concentration is low at low wind speeds because of high plume rise and is low at high wind speeds because of high dilution. As the wind speed increases, plume rise decreases but dilution increases. At a critical wind speed (u_c), MGC reaches a maximum. This occurs at a downwind distance x_c . For the neutral "breakup" model, if we assume that $\sigma_z/\sigma_y = 0.7$, the critical wind speed occurs at $\Delta h/h_s = 1/3$:

$$u_c = 2.15 \left(\frac{u}{u_*} \right)^{3/5} \left(\frac{F_0}{h_s} \right)^{1/5} \quad (2.29)$$

$$x_c = 0.043 \left(\frac{u_*}{u} \right)^{3/5} \frac{Q}{F_0^{1/5} h_s^{3/5}} \quad (2.30)$$

For the unstable model, the critical wind speed occurs at $\Delta h/h_s = 5$:

$$u_c = 0.43 F_0 H^{-2/5} h_s^{-3/5} \quad (2.31)$$

$$x_c = 0.015 \frac{QH^{2/5}}{F_0 h_s^{3/5}} \quad (2.32)$$

If there is some question about whether to use the neutral or unstable formulas, use those which give the highest (most conservative) MGC. In quantitative comparisons of MGC data measured near power plants by Moore (1974), Briggs (1974) finds that the dividing line for the neutral and unstable formulas is $u = 7$ m/sec.

2-8 MULTIPLE SOURCES

Many sites have several stacks that are close enough to each other that visual observations prove that the plumes indeed merge. The reduced entrainment and increased buoyancy of the merged plumes may increase plume rise significantly. Examples of multiple sources are mechanical-draft cooling towers or lines of power-plant stacks.

Briggs (1974) developed the following empirical method, which is based on TVA plume-rise data (Carpenter, Thomas, and Gartrell, 1968). The enhancement factor (E_N) is defined as the ratio of the plume rise from N stacks to that from one stack. The buoyant, bent-over plume rise from one stack (Δh_1) is assumed to be given by Eq. 2.19 [$\Delta h_1 = 2.6 (F_0/us)^{3/5}$]. The spacing between the stacks is Δx . Then a formula for E_N that has the proper asymptotic behavior is:

$$E_N = \left(\frac{N+S}{1+S} \right)^{1/2} \quad (2.33)$$

where

$$S = 6 \left[\frac{(N-1) \Delta x}{N^{1/2} \Delta h_1} \right]^{3/2} \quad (2.34)$$

There was no dependence of E_N on wind direction relative to the line of stacks for these data, although Hanna (1974) has found that the plume rise from lines of mechanical-draft cooling towers is greater for wind directions parallel to the line of sources.

For vertical plumes, merger is assumed at a height (z_m) where the radius (R) equals one-half the stack spacing ($0.5 \Delta x$). The plumes are then treated as if all buoyancy combines but comes from a virtual source a distance $(1 - N^{1/2})z_m$ below the actual stack heights. There are no data to test this model.

Problems

1. A stack has an inside diameter of 3 m. The plume has an initial speed of 10 m/sec and a temperature of 473°K. Ambient wind speed is 5 m/sec, temperature is 295°K, and vertical tempera-

ture gradient is 0.01°K/m . Calculate V_0 , M_0 , F_0 , and s . Calculate final plume rise Δh .

2. For the plume in Problem 1: (1) At what downwind distance does the buoyant rise term equal the momentum rise term? (2) At what downwind distance does the " $\frac{2}{3}$ law" give a plume rise equal to that calculated in problem 1?

3. A cooling-tower plume with an initial height of 100 m, $R_0 = 10$ m, $w_0 = 5$ m/sec, and $T_{p0} = 300^\circ\text{K}$

rises into a calm, dry atmosphere with $T_{e0} = 280^\circ\text{K}$ and $\partial T/\partial z = 0$. How high will the plume rise above the ground?

4. Surface friction velocity (u_*) is 0.3 m/sec, ambient temperature is 270°K , $\partial T/\partial z = 0$, and wind speed at stack height is 3 m/sec. Initial plume parameters are $T_{p0} = 400^\circ\text{K}$, $w_0 = 10$ m/sec, $R_0 = 0.5$ m, and the stack is 50 m tall. Calculate the final plume rise Δh .

Source Effects

3-1 OVERVIEW

Diffusion calculations would be greatly simplified if stacks and buildings did not obstruct the airflow. Most stacks are built near other industrial buildings. On the positive side, however, some utilities build huge 300-m stacks at fossil-fired power plants to ensure that pollutants from the stacks will be emitted high enough above the ground so that there will be no possibility of pollutant interaction with their other buildings. Other industries use short vents constructed on building roofs to release toxic materials to the atmosphere. Stacks on most residential dwellings and commercial structures are usually short and unobtrusive because of "aesthetic" considerations. The purpose of this chapter is to provide guidance on:

1. Calculation of concentrations in building complexes due to emissions from existing sources.
2. Design of stack placement for minimizing air-pollution effects.

The reviews by Hosker (1980, 1981) provide background information on the relevant phenomena and methods of calculation.

3-2 STACK AERODYNAMIC EFFECT

Low pressure in the wake of the stack may cause the plume to be drawn downward behind the stack. Downwash can be effectively prevented by maintaining the efflux velocity (w_0) at a magnitude greater than the crosswind velocity (u). The fact that downwash will not occur for w_0/u greater than 1.5 has been generally recognized. For w_0/u less than 1.5, Briggs (1973) suggests that the distance (h_d) that the plume downwashes below the top of the stack can be obtained by the following formula:

$$h_d = 2 \left(\frac{w_0}{u} - 1.5 \right) D \quad (3.1)$$

where D is the internal stack diameter, as illustrated in Fig. 3.1.

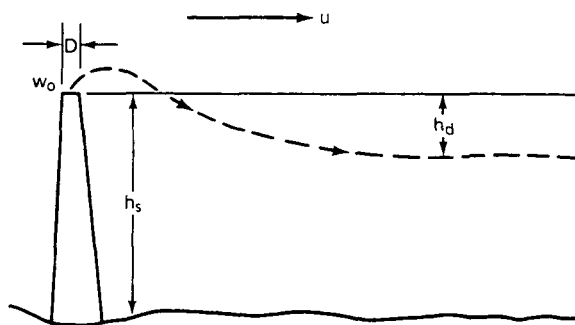


Fig. 3.1 Schematic diagram of stack and important physical parameters: w_0 , efflux velocity; u , wind speed; D , internal stack diameter; h_s , stack height; and h_d , downwash distance.

3-3 STRUCTURE OF FLOW AROUND BUILDINGS

We have a fairly good idea of the flow around a simple building, as drawn schematically in Fig. 3.2, as a result of many wind-tunnel and field experiments that have been done. The upstream boundary layer is assumed to be a turbulent shear flow. The face of the upstream building is not shown in this figure, but we know that there is a stagnation point about two-thirds the way up the face; downward-moving air is beneath this point. The important features of this diagram are the separated recirculation zones on the roof and sides, the turbulent wake cavity zone, and the turbulent wake.

Let the building height be H , the crosswind width W , and the alongwind length L . The wind is assumed

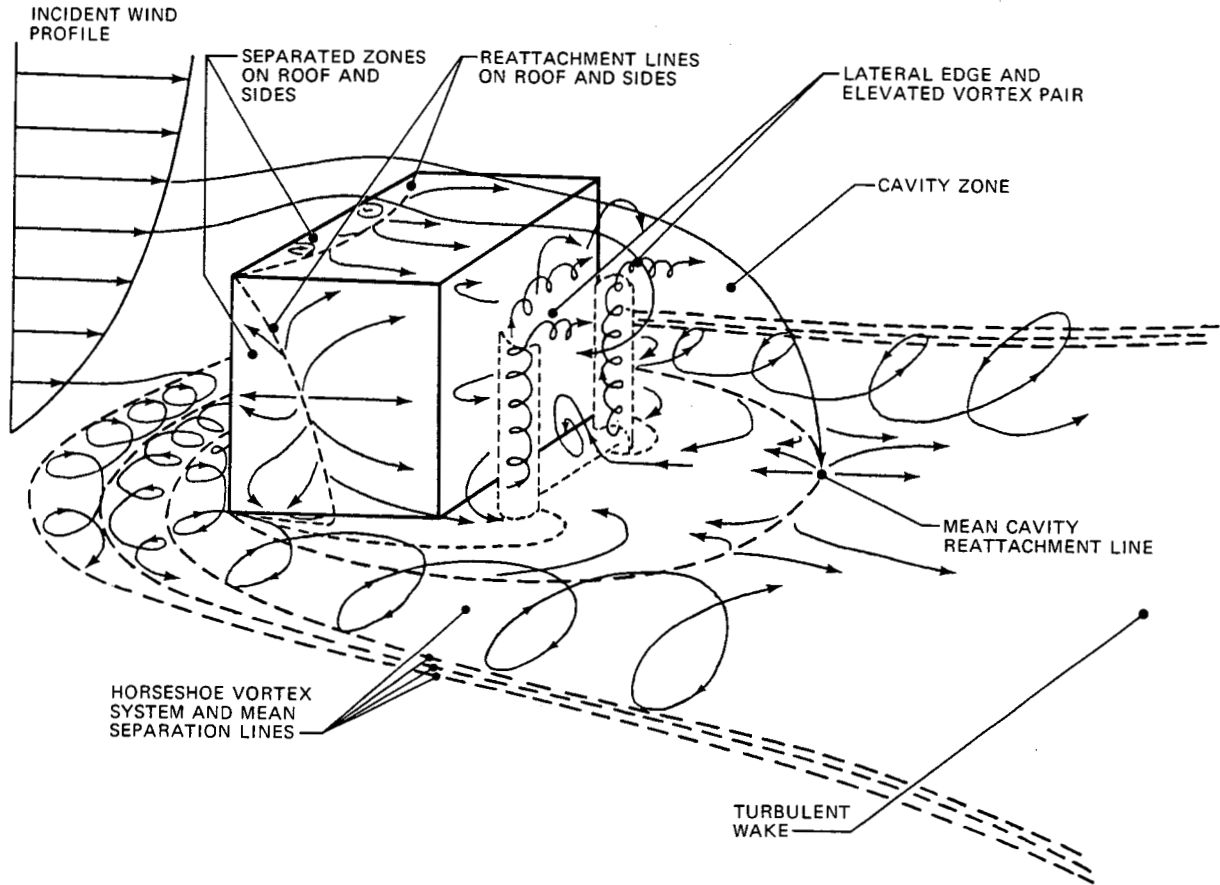


Fig. 3.2 Model of flow near a sharp-edged building in a deep boundary layer (Hosker, 1979).

to be perpendicular to the building face; if it is not, the flow is drastically changed, and the following techniques do not apply. For ratios L/H greater than about one, reattachment of the streamlines to the roof and sides can be expected unless W/H is very large. Between the upwind roof edge and the line of flow reattachment is a zone of recirculation (see Fig. 3.3). Pollutants released into the region by low velocity roof vents or short stacks may produce very high concentrations within this zone. Let ζ be the smaller of H and W and ξ the larger; define the characteristic length $\tilde{R} \equiv \zeta^{2/3} \xi^{1/3}$. Wilson (1979) finds that the roof cavity extends a distance

$$L_c \approx 0.9 \tilde{R} \quad (3.2)$$

from the upwind edge and reaches a maximum height

$$H_c \approx 0.22 \tilde{R} \quad (3.3a)$$

at a distance from the upwind edge of

$$x_c \approx \frac{\tilde{R}}{2} \quad (3.3b)$$

This cavity is bounded above by a turbulent shear layer (zone II in Fig. 3.3) and above that by the turbulent roof wake (zone III). The upper edge of the shear layer, which begins near the maximum cavity height, is given approximately by

$$\frac{Z_{II}}{\tilde{R}} \approx 0.27 - 0.1 \frac{x}{\tilde{R}} \quad (3.4a)$$

and the roof wake boundary is approximated by

$$\frac{Z_{III}}{\tilde{R}} \approx 0.28 \left(\frac{x}{\tilde{R}} \right)^{1/2} \quad (3.4b)$$

In Eqs. 3.4, x is measured from the upwind roof edge and is greater than x_c . Wilson suggests that, if a roof-mounted stack is tall enough that the lower plume edge remains above zone II, contamination of

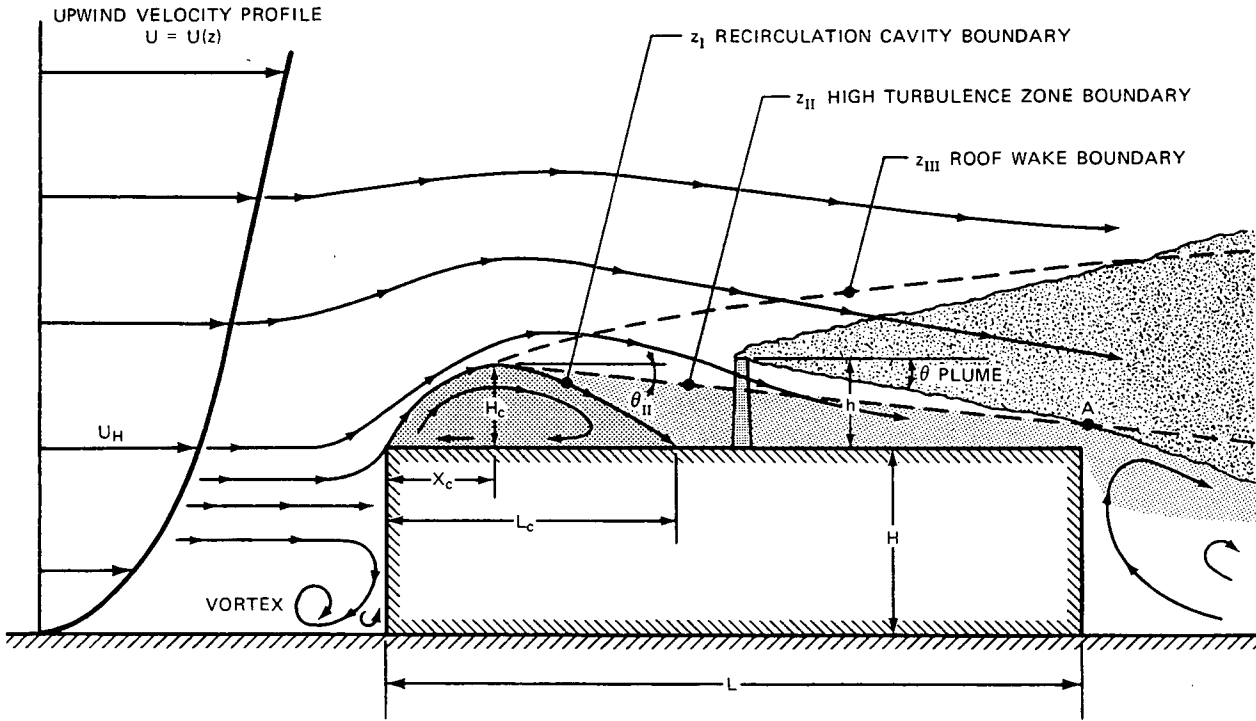


Fig. 3.3 Flow over center of a long flat building roof for wind perpendicular to the upwind face. [From D. J. Wilson, Flow Patterns Over Flat-Roofed Buildings and Application to Exhaust Stack Design, ASHRAE Trans., 85(Part 2): 284-295 (1979).]

the roof is unlikely, and if the plume clears the wake boundary as well, there is virtually no danger of contamination. Wilson recommends that a line of slope 0.2 be drawn in the upwind direction from a point on the zone II or zone III boundary (depending on the safety margin desired) immediately above the air intake or other critical receptor that is closest to the lee edge of the roof. The effective stack exit should then be above this line.

The wake cavity behind the structure is important because plumes caught in the cavity can be quickly mixed to the ground. Let x_r , y_r , and z_r be the length, width, and height of the wake cavity, respectively. Crosswind cavity dimensions y_r and z_r seldom exceed the building dimensions W and H by more than 50%. Hosker (1979, 1980) has developed the following empirical formulas for wake cavity length (x_r):

$$\frac{x_r}{H} = \frac{A(W/H)}{1 + B(W/H)} \quad (3.5)$$

where, for $L/H \leq 1$ or so,

$$A = -2.0 + 3.7 \left(\frac{L}{H}\right)^{-1/2}$$

$$B = -0.15 + 0.305 \left(\frac{L}{H}\right)^{-1/2} \quad (3.6a)$$

whereas for $L/H \geq 1$, where flow reattaches to the roof and sides,

$$\begin{aligned} A &= 1.75 \\ B &= 0.25 \end{aligned} \quad (3.6b)$$

Cavity extent is measured from the lee building face. For cubical buildings, these formulas predict that the wake cavity length (x_r) is about 2.5 times as great as the building height. The maximum wake cavity length ($\sim 10H$) is predicted for large W/H (i.e., two-dimensional buildings).

3-4 DIFFUSION CALCULATIONS AROUND BUILDINGS

The literature on diffusion around buildings is full of "rules of thumb" that are based on practical experience and wind-tunnel observations. In some cases these rules of thumb can be verified by physical

reasoning and theoretical derivations. The following sections are arbitrarily split into sources upwind of a building and sources near a building.

3-4.1 Isolated Sources Upwind of Buildings

If the source is a distance greater than $2H$ upstream of the building and its height (h_s) is greater than two-thirds the building height ($n_s > 2H/3$), the plume will rise over the building face. Parts of the plume at heights less than $2H/3$ will be caught in the downwash in the frontal eddy over the lower part of the building. Some of this material will be caught in the horseshoe vortex trailing off along the edge of the wake. If the flow reattaches to the building roof and sides, high concentrations may result at these points. If the building length (L) is small, the flow will not reattach, and the plume is deflected above the cavity. Any pollution caught in the wake cavity will mix thoroughly to the ground. The overall effect of the building is to increase the dispersion of the plume, although locally high ground-level concentrations may result owing to aerodynamic effects of the building.

Wilson and Netteville (1978) conclude that in this situation the most important effect of a building is to mix the plume concentrations between the ground and the roof. Thus the roof-level concentration should be held within limits. In design studies the stack height in a model can be varied so that the height of the maximum tolerable concentration isopleth, as calculated by a flat-terrain diffusion model, is higher than the maximum downwind building height.

For building clusters or out-of-the-ordinary building shapes, wind-tunnel and/or field tests are necessary for a realistic assessment of a site. Cagnetti (1975) shows how results for diffusion around a reactor complex vary strongly when there is a minor change in wind direction.

3-4.2 Sources Close to Buildings

In most cases vents and stacks are located on or near the building. Primary concerns are whether pollution is emitted directly into a cavity or recirculation zone, the magnitude of the concentration in these zones, and the deflection of streamlines and increase in dispersion for plumes outside these zones.

(a) **Vents.** As mentioned earlier, a vent located on the lower two-thirds of the upwind face will emit into the upwind eddy and be transported around the

sides, close to the ground, whereas a vent located higher up will emit into flow streaming over the building. If roof-vented vents are located in the separated areas near the leading edge of the roof and sides, as discussed above, ineffective ventilation can lead to high concentrations and recirculations. Halitsky (1963) and Wilson (1976) present wind-tunnel observations of concentration patterns resulting from various types of vent positions, building shapes, and efflux-to-wind-speed ratios (w_0/u). An example is given in Fig. 3.4, where the plotted concentration K is made dimensionless in the following way:

$$\text{Dimensionless } K = \frac{CAu}{Q} \quad (3.7)$$

where C = concentration ($\mu\text{g}/\text{m}^3$)

u = wind speed (m/sec)

Q = source strength ($\mu\text{g}/\text{sec}$)

A = convenient characteristic area (e.g., WH) for the building being studied (m^2)

The wind-tunnel experiments suggest that flush, low-velocity, roof vents give maximum values of K ranging from 10 to 100 at the roof surfaces. In the design of vent exhaust and intake systems, it may be wise to use a conservative value of 100 for K .

The effects of variations in efflux speed (w_0) and vent stack height (h_0) are shown in the experiments by Halitsky (1963) and Wilson (1976). Roof concentrations can be dramatically decreased by increasing the upward efflux speed and by installing relatively small stacks. If the ratio w_0/u is increased from 0.5 to 1.0, maximum roof concentration is reduced by a factor of 2 to 3. Wilson (1976) found that the upper bound on the ratio of concentration at distance x from the vent to the vent exit concentration was a function of wind speed (u), distance (x), effluent speed (w_0), and vent area (A_v):

$$\left[\frac{C(x)}{C(\text{exit})} \right]_{\text{upper bound}} \approx 9.1 \frac{w_0}{u} \frac{A_v}{x^2} \quad (3.8)$$

(b) **Stack Effective Height.** A major concern is to keep the plume away from the wake cavity, where it would be brought to the ground and recirculated in a region with low ventilation rates. This problem results if the plume is released too close to the building and/or at too low a speed w_0 . The familiar "2½ times rule" is often applied because experience has shown that there are few downwash problems if a stack whose height is at least 2.5 times as great as the height of the building is built. From the previous diagrams and discussion, it is clear that the wake

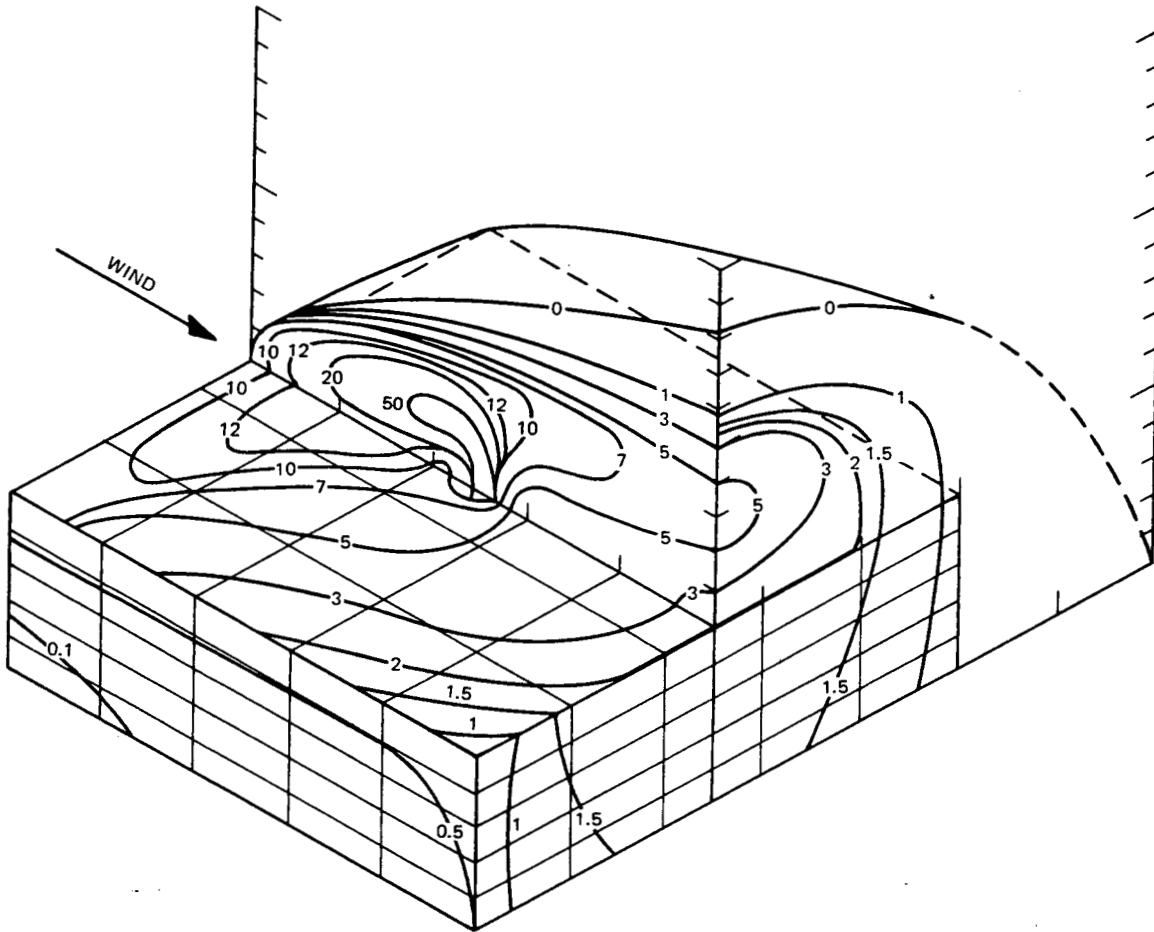


Fig. 3.4 Dimensionless concentration ($K = CAu/Q$) contours for centered flush roof vent on building where $L/H = W/H = 3.0$ and $w_0/u \approx 1.0$. [From J. Halitsky, *Gas Diffusion Near Buildings*, *ASHRAE Trans.*, 69: 476-477 (1963).]

cavity does not extend to this height, a fact obviously recognized over the years by “plume watchers.” In many cases the $2\frac{1}{2}$ times rule can be relaxed, and the pollutant concentrations can still be held within acceptable limits. Briggs (1973) has developed a straightforward method of determining the effective height of a plume near the wake cavity, as described in the next paragraph.

First, stack downwash is calculated by using Eq. 3.1. The effective stack height after downwash is h' , which equals the stack height (h_s) minus the downwash (h_d) (see Fig. 3.5). Next, let ζ be defined as the smaller of W and H . Then, if h' is greater than $H + 1.5 \zeta$, the plume is out of the wake, and the effective plume height (h_e) equals h' . Otherwise the plume is affected by the building.

For $h' > H + 1.5 \zeta$,

$$h_e = h' \quad (3.9)$$

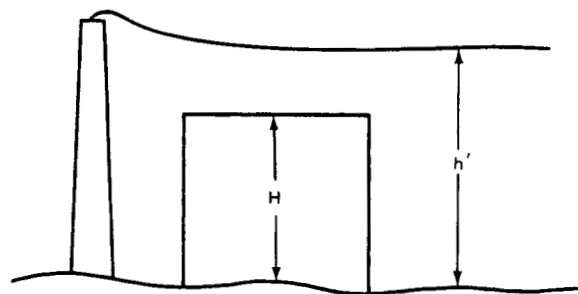


Fig. 3.5 Diagram of effective plume height in the case of downwash due to a nearby building.

For $h' < H + 1.5 \zeta$ and $h' > H$,

$$h_e = 2h' - (H + 1.5 \zeta) \quad (3.10)$$

For $h' < H$,

$$h_e = h' - 1.5 \zeta \quad (3.11)$$

Finally, the plume is assumed to be trapped in the cavity if the effective source height (h_e) calculated above is less than 0.5ζ . In this case the plume can be treated as a ground-level source with initial area ζ^2 .

On the basis of field observations of plumes released from a large vent from a reactor building, Johnson et al. (1975) developed the "split h" concept for evaluating effective plume height. They found that, for a particular reactor sample, for speed ratios w_0/u between 1 and 5, the plume would alternate between being in and out of the cavity. The percent of the time that the plume was in the cavity was given by

$$E = 2.58 - 1.58 \frac{w_0}{u} \quad \left(1 < \frac{w_0}{u} < 1.5\right) \quad (3.12)$$

$$E = 0.3 - 0.06 \frac{w_0}{u} \quad \left(1.5 < \frac{w_0}{u} < 5\right) \quad (3.13)$$

This result is probably highly site specific, however, depending on vent size, placement, and building geometry.

(c) Concentrations in and Downwind of Cavity. The dimensionless concentration ($K = CAu/Q$) in a wake cavity is generally found to be between 0.2 and 2.0 if we assume that the plume is nearly completely drawn into the cavity ($h_e < 0.5 \zeta$) (Barry, 1964; Meroney, 1979). Concentrations are relatively uniform from the lee side of the building throughout the cavity. Because of this rapid mixing, stack height usually makes little difference for plumes caught in a cavity. Because of this rapid mixing, release within the wake cavity of pollutants from ground-level or from low stacks makes little difference in the resulting concentrations. However, a taller stack of about the same height as the wake cavity may result in effluent being transported quite directly to the ground by the downward curving shear layer bounding the cavity. This is one instance where a tall stack may produce higher ground-level concentrations than a short one.

For plumes not entrained into building cavities ($h_e > \zeta/2$), the standard Gaussian plume formula (4.1) can be used to estimate concentrations. Usually wind speed (u) is defined at z equal to H . If a plume is entrained into the building cavity, modifications to the Gaussian plume formula for the centerline concentration due to a ground source are used:

$$C = \frac{Q}{(\pi\sigma_y\sigma_z + cWH)u} \quad (3.14)$$

The "constant" c is intuitively estimated by Gifford (1975) to be between 0.5 and 2, with the lower value agreeing fairly well with test results. The factor cWH represents the effective crosswind area of the building. Dispersion parameters σ_y and σ_z can be obtained by methods given in Chap. 4, although measurements suggest that σ_y and σ_z in wakes may need to be modified in the future. For example, the use of open-terrain σ_y and σ_z values leads to concentration decreasing in proportion to distance raised to the -1.3 to -1.6 power, depending on stability. Meroney and Yang (1971) and Huber and Snyder (1976) have found the power to be closer to -0.8 out to a distance of $50H$, which is presumably due to the dispersion inhibiting effects of a very persistent horseshoe vortex. In full-scale field studies (e.g., Dickson, Start, and Markee, 1969), the power has been found to be about -1.3 . The difference between the field and laboratory results may be due to mesoscale wind-direction fluctuations observed in the field but not present in the laboratory.

Problems

1. Assume that the vent in Fig. 3.4 is emitting toxic gases at a rate of 1 g/sec and that $w_0 = u = 1.0 \text{ m/sec}$. Estimate the maximum concentration on the building roof and on the downwind building face. The building is 10 m high and 30 m wide.

2. A stack 50 m high emitting 10 g of toxic gases per second is located just upwind of a 40-m cubical building. The stack diameter is 1 m and wind speed and initial plume effluent speed are 1 m/sec . The plume is nonbuoyant. Estimate the ground-level concentration on the plume axis at a downwind distance of 300 m .

3. Ms. McGraw is cooking cabbage on the third floor of a 30-m cubical apartment building. Her kitchen exhaust fan emits 5 g of cabbage gas per second to the outside, downwind side of the building. Wind speed is 2 m/sec . What concentration of cabbage gas is smelled by Ms. Jones while she hangs up her wash a distance of 30 m from that same side of the building?

4. For the situation in problem 3, what is the concentration on the plume centerline a distance of 1000 m from the building? Assume sunny conditions.

Gaussian Plume Model for Continuous Sources

4-1 WHY USE THE GAUSSIAN MODEL?

Other dispersion models, such as the K-model, the statistical model, and the similarity model, will be described in succeeding chapters. The Gaussian model is discussed first because it is still the basic workhorse for dispersion calculations, and it is the one most commonly used because

1. It produces results that agree with experimental data as well as any model.
2. It is fairly easy to perform mathematical operations on this equation.
3. It is appealing conceptually.
4. It is consistent with the random nature of turbulence.
5. It is a solution to the Fickian diffusion equation for constants K and u.
6. Other so-called theoretical formulas contain large amounts of empiricism in their final stages.
7. As a result of the above, it has found its way into most government guidebooks, thus acquiring a "blessed" status (Environmental Protection Agency, 1978).

4-2 FORM OF THE GAUSSIAN MODEL

The origin of the Gaussian model is found in work by Sutton (1932), Pasquill (1961, 1974), and Gifford (1961, 1968). Consider a continuous source of strength Q (in micrograms per second) at effective height (h) above the ground. Assume that the wind speed (u) is uniform. The concentration C (in micrograms per cubic meter) is then given by the formula:

$$\frac{C}{Q} = \frac{1}{2\pi\sigma_y\sigma_z u} e^{-y^2/2\sigma_y^2} \times [e^{-(z-h)^2/2\sigma_z^2} + e^{-(z+h)^2/2\sigma_z^2}] \quad (4.1)$$

The coordinate y refers to horizontal direction at right angles to the plume axis with y equal to zero on the axis. The coordinate z is height above ground, which for the time being is assumed to be flat and uniform. The parameters σ_y and σ_z are standard deviations of the distribution C in the y and z directions, respectively. The purpose of the last term is to account for reflection of the plume at the ground by assuming an image source at distance h beneath the ground surface. Figures 4.1 and 4.2 contain diagrams of the Gaussian plume. All variables are assumed to be averaged over a period of about 10 min. Corrections for different averaging times are given in Sec. 4.5. Averaging time should be chosen so that most of the turbulent eddies go through at least one cycle during that averaging time. Unfortunately averaging times in experiments are often dictated by other operational considerations, such as the duration of release of a tracer.

Newcomers to this field often ask, "What happens in the Gaussian equation when wind speed (u) goes to zero?" The standard reply is, "Calm winds are defined as u equal to 0.5 m/sec." The truth is that anemometers near the surface may register $u = 0$, but the winds in the planetary boundary layer very seldom stop entirely. There is nearly always a slight drift, and the seemingly facetious answer to the above question is based on considerable experience.

The effective height (h) can be estimated by using the techniques outlined in Chaps. 2 and 3. The remaining problem, then, is specification of the dispersion parameters σ_y and σ_z . These are given as

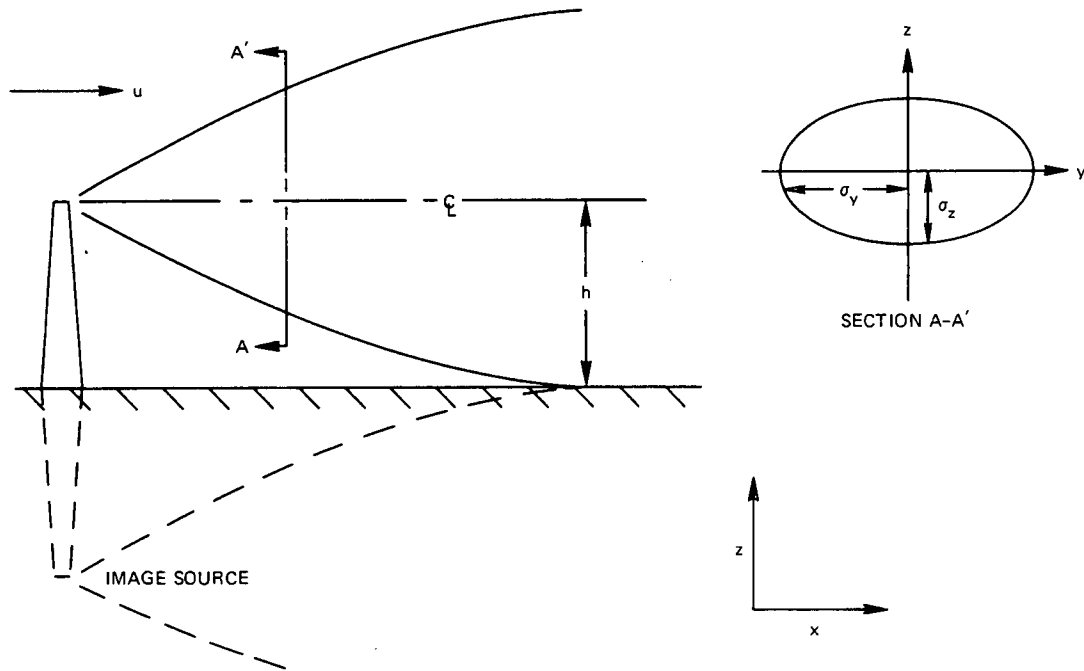


Fig. 4.1 Diagram of typical plume, illustrating concepts important in the Gaussian plume formula. Symbols: u is wind speed; h is effective source height; and σ_y and σ_z are standard deviations of crosswind concentration distributions.

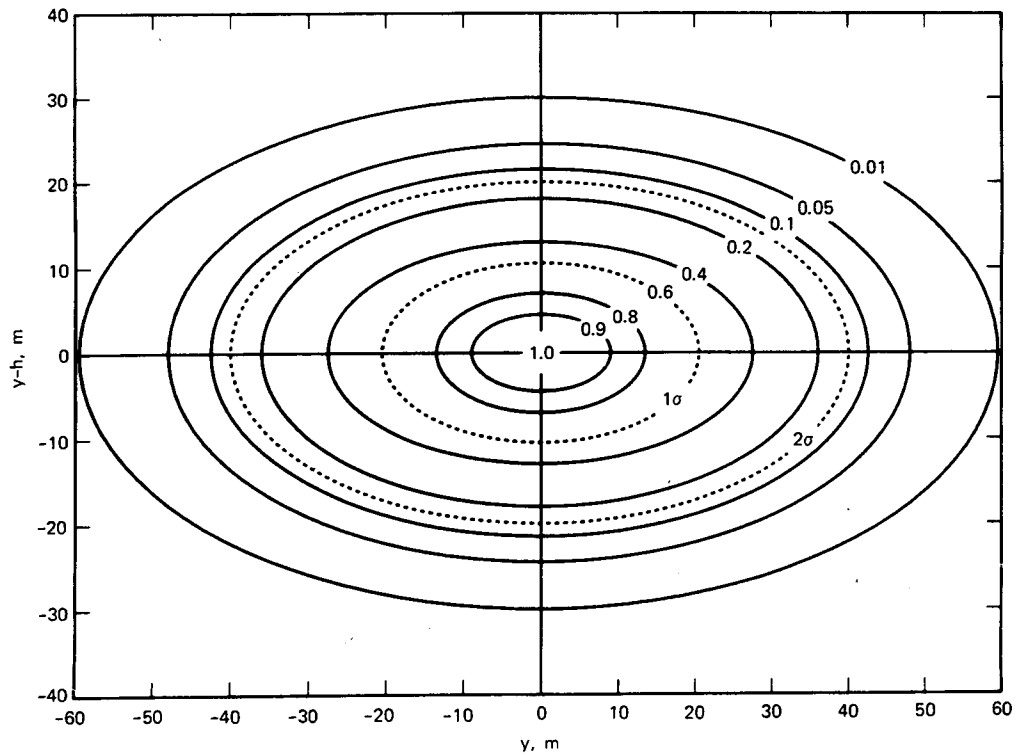


Fig. 4.2 Cross section through Gaussian plume with $\sigma_y = 20$ m, $\sigma_z = 10$ m, and centerline concentration of 1.0.

functions of downwind distance and stability and are based on a combination of experimental results and theory.

4-3 STABILITY CLASSIFICATION SCHEMES

For an estimate of σ_y or σ_z in the absence of research-grade turbulence measurements, the stability class must first be determined, preferably by a simple scheme based on inexpensive and easy measurements. The most widely used scheme was developed by Pasquill (1961) and was modified slightly by Turner (1967). Table 4.1 contains the criteria for Pasquill's six stability classes, which are based on five classes of surface wind speeds, three classes of daytime insolation, and two classes of nighttime cloudiness. In general, stability classes A through C represent unstable conditions, class D represents nearly neutral conditions, and classes E and F represent stable conditions. Some users have filled in the blank in Table 4.1 with a so-called "G" class, which they assert applies during light wind, stable conditions.

If turbulence measurements are available, it is preferable to estimate σ_y and σ_z by using σ_θ and σ_e , standard deviations of wind direction fluctuations in the horizontal and vertical directions, respectively. Early advocates of stability classification schemes based on σ_θ or σ_e were M. E. Smith (1951) and Cramer (1957). The Brookhaven National Laboratory (BNL) classes are defined by M. E. Smith (1951), using wind direction θ recorded over a 1-hr period, in the following manner:

- A: Fluctuations (peak to peak) of θ exceed 90° .
- B₁: Fluctuations of θ from 40 to 90° .
- B₂: Fluctuations of θ from 15 to 40° .
- C: Fluctuations of θ greater than 15° with strip chart showing an unbroken solid core in the trace.
- D: Trace in a line, short-term fluctuations in θ less than 15° .

Cramer's (1957) classes, which are based on observations of wind fluctuations at a height of 10 m, are defined in Table 4.2. Note that he distinguishes between two roughness types in the neutral class. The basic turbulence typing methods are compared in Table 4.3, as reproduced from a review article by Gifford (1976). The fact that these divisions and comparisons are arbitrary is important, and this system should not be considered perfect.

To further confuse the reader, the Tennessee Valley Authority (TVA) (Carpenter et al., 1971) and the Nuclear Regulatory Commission (NRC) use vertical temperature gradient (DT/Dz) to define stability

classes. This method does not explicitly consider the effects of wind speed on diffusion and consequently is not a sufficient method for all situations. It would be better to use Richardson's number (Ri) or the Monin-Obukhov length L to characterize stability since they are direct measures of atmospheric stability, which accounts for the effects of both mechanical mixing and buoyancy forces. Golder (1972) analyzed diffusion data to determine the graphical relation among roughness z_0 , the Monin-Obukhov length L , and the Pasquill class shown in Fig. 4.3. If two of these parameters are known, the other can be estimated from the figure.

The following recommendation was made by the American Meteorological Society Workshop on Stability Classification Schemes and Sigma Curves (Hanna et al., 1977):

... The following quantities are required to characterize σ_y and σ_z in the boundary layer:

1. Roughness length, z_0 , and friction velocity, u_* , as measures of the mechanical turbulence.
2. Mixing depth, z_i , and Monin-Obukhov length, L , or the heat flux H , as measures of the convective turbulence daytime.
3. Wind speed, u , and standard deviation of wind direction fluctuations, σ_θ (the wind vector is needed to specify the transport wind, and σ_θ is required to estimate σ_y , especially in stable conditions).

On a 61-m tower, all quantities but mixing depth (z_i) can be measured by standard instruments required by the Nuclear Regulatory Commission, and remote sounders that can measure z_i are available. Methods in Chap. 1 (Eqs. 1.37 to 1.53) can be used to extrapolate $\sigma_\theta \approx \sigma_v/u$ to plume height from a height of 10 m.

Despite the strong recommendation to use turbulence measurements to estimate diffusion, most people today still use the Pasquill letter classes because they have produced satisfactory results in most cases and because they are easy to use. However, the user must beware if he applies letter classes to problems outside the area of their derivation (e.g., complex terrain, distances greater than 10 km, effective release heights of above 100 m, and many other problems). For these problems, direct turbulence measurements or theoretical extrapolations are necessary.

4-4 CHOICE OF σ_y AND σ_z

4-4.1 Stability Class Method

Most published σ_y and σ_z curves as a function of downwind distance and stability are based on a few

Table 4.1 Meteorological Conditions Defining Pasquill Turbulence Types*

A: Extremely unstable conditions	D: Neutral conditions†	
B: Moderately unstable conditions	E: Slightly stable conditions	
C: Slightly unstable conditions	F: Moderately stable conditions	

Surface wind speed, m/sec	Daytime insolation			Nighttime conditions‡	
	Strong	Moderate	Slight	Thin overcast or > 3/8 low cloud	≤ 3/8 cloudiness
<2	A	A-B	B		
2	A-B	B	C	E	F
4	B	B-C	C	D	E
6	C	C-D	D	D	D
>6	C	D	D	D	D

*From F. A. Gifford, Turbulent Diffusion-Typing Schemes: A Review, *Nucl. Saf.*, 17(1): 71 (1976).

†Applicable to heavy overcast day or night.

‡The degree of cloudiness is defined as that fraction of the sky above the local apparent horizon that is covered by clouds.

Table 4.2 Cramer's Turbulence Classes*

Stability description	σ_θ , deg	σ_e , deg (at 10 m)
Extremely unstable	30	10
Near neutral (rough surface; trees, buildings)	15	5
Near neutral (very smooth grass)	6	2
Extremely stable	3	1

*From H. E. Cramer, A Practical Method for Estimating the Dispersal of Atmospheric Contaminants, in *Proceedings of the First National Conference on Applied Meteorology*, pp. C-33 to C-55, American Meteorological Society, Hartford, Conn., 1957.

Table 4.3 Relations Among Turbulence Typing Methods*

Stability description	Pasquill	Turner	BNL	σ_θ , deg (at 10 m)
Very unstable	A	1	A	25
Moderately unstable	B	2	B ₁	20
Slightly unstable	C	3	B ₂	15
Neutral	D	4	C	10
Slightly stable	E	6		5
Moderately stable	F	7	D	2.5

*From F. A. Gifford, Turbulent Diffusion-Typing Schemes: A Review, *Nucl. Saf.*, 17(1): 72 (1976).

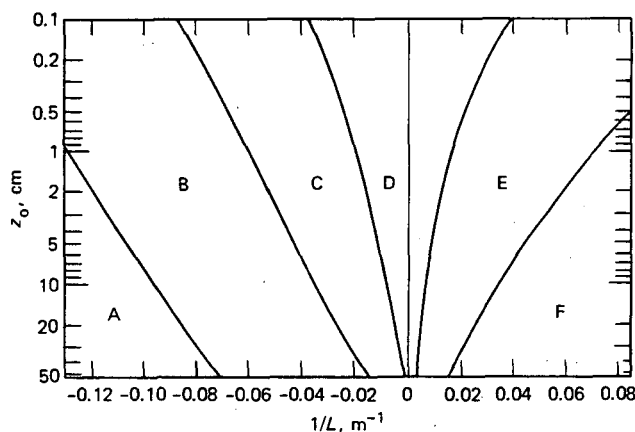


Fig. 4.3 Curves showing Pasquill's turbulence types as a function of the Monin-Obukhov stability length and the aerodynamic roughness length. A, extremely unstable conditions; B, moderately unstable conditions; C, slightly unstable conditions; D, neutral conditions (applicable to heavy overcast day or night); E, slightly stable conditions; F, moderately stable conditions. [From D. Golder, *Relations Among Stability Parameters in the Surface Layer*, *Boundary-Layer Meteorol.*, 3: 56 (1972).]

carefully performed diffusion experiments during the 1950's and 1960's. Project Prairie Grass (Haugen, 1959) is probably the most frequently quoted diffusion experiment. The terrain was uniform, releases were from near ground level, and concentration measurements were at downwind distances less than 1 km. These experiments resulted in Pasquill's (1961) curves, which were adapted by Gifford (1961, 1968, 1976) into the forms shown in Fig. 4.4. Note that, at distances beyond 1 km, the lines are dashed (i.e., a guess). They may work under certain ideal conditions at greater distances, but there is little basis in observations.

**Table 4.4 Brookhaven National Laboratory
Parameter Values in the Formulas
 $\sigma_y = ax^b$ and $\sigma_z = cx^d$**

Type	Parameter			
	a	b	c	d
B ₂	0.40	0.91	0.41	0.91
B ₁	0.36	0.86	0.33	0.86
C	0.32	0.78	0.22	0.78
D	0.31	0.71	0.06	0.71

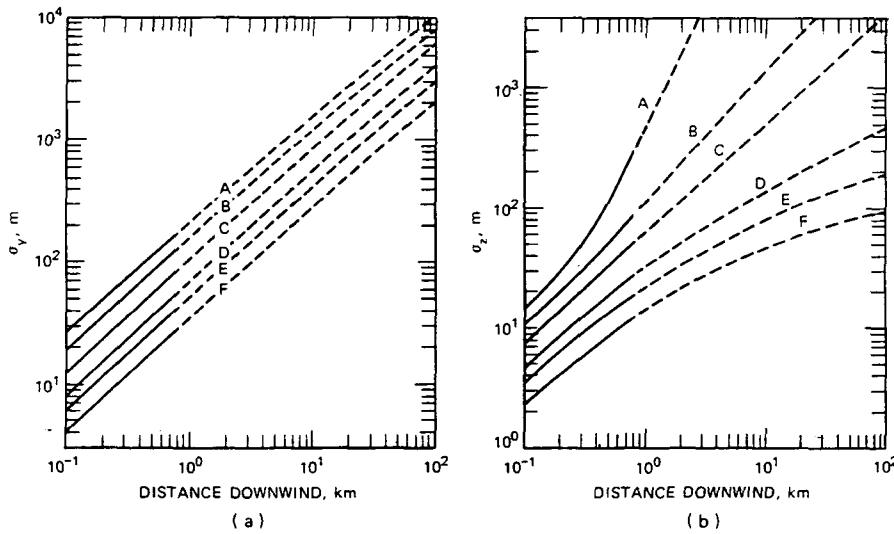


Fig. 4.4 Curves of σ_y and σ_z for turbulence types based on those reported by Pasquill (1961). [From F. A. Gifford, *Turbulent Diffusion-Typing Schemes: A Review*, *Nucl. Saf.*, 17(1): 71 (1976).]

Because calculators and computers are in such widespread use at present, most people would rather have a formula than a graph or table. Several researchers have worked out analytical power-law formulas for σ_y and σ_z . One of the early suggestions was by M. E. Smith (1968). He summarized the BNL formulas, which are based on hourly average measurements out to about 10 km of diffusion of a nonbuoyant plume released from a height of 108 m:

$$\sigma_y = ax^b \quad \sigma_z = cx^d \quad (x \text{ in meters}) \quad (4.2)$$

Values of the parameters a, b, c, and d are given in Table 4.4.

Briggs (1973) combined the Pasquill, BNL, and TVA curves (observations out to $x = 10$ km), using theoretical concepts regarding asymptotic limits of the formulas, to produce the widely used set of

formulas given in Table 4.5. Initial plume spread at all stabilities is proportional to x , the proportionality factor being σ_θ (in radians). At large distances, σ_y is proportional to $x^{1/2}$, as predicted by the Fickian and Taylor theories of diffusion. Note that σ_y and σ_z are independent of release height and roughness in these formulas. There are too few experimental data to support more complex formulations including these two variables.

The Prairie Grass experiments were carried out over terrain with roughness z_0 of 3 cm. F. B. Smith (1972) and Pasquill (1975, p. 19) have found that σ_z varies as z_0^p , where p lies in the range 0.10 to 0.25. A technique for incorporating Smith's (1972) recommendations into analytical forms for σ_z in each of the P-G categories was given by Hosker (1973). The larger values of the exponent p are applicable to shorter distances and rougher surfaces. Over rough

urban surfaces, especially under the influence of the nighttime urban heat island, the increased roughness should be taken into account. McElroy and Pooler's (1968) diffusion experiment in St. Louis was used by Briggs (1973) to develop the formulas given in Table 4.5. Other people make the assumption that urban σ_y and σ_z should be moved up one stability class (e.g., C to B) to account for increased dispersion over urban areas.

4-4.2 The σ_θ and σ_e Method

Much research concerning the best way to relate σ_y and σ_z to σ_θ and σ_e is being done. In perhaps 5 years the subject will reach a stage where definitive conclusions can be drawn. The recommendations in this section are based on the latest available research. The idea behind this research is to remove a layer of empiricism (the Pasquill-Gifford curves) from diffu-

Table 4.5 Formulas Recommended by Briggs (1973) for $\sigma_y(x)$ and $\sigma_z(x)$ ($10^2 < x < 10^4$ m)

Pasquill type	σ_y, m	σ_z, m
Open-Country Conditions		
A	$0.22x(1 + 0.0001x)^{-1/2}$	$0.20x$
B	$0.16x(1 + 0.0001x)^{-1/2}$	$0.12x$
C	$0.11x(1 + 0.0001x)^{-1/2}$	$0.08x(1 + 0.0002x)^{-1/2}$
D	$0.08x(1 + 0.0001x)^{-1/2}$	$0.06x(1 + 0.0015x)^{-1/2}$
E	$0.06x(1 + 0.0001x)^{-1/2}$	$0.03x(1 + 0.0003x)^{-1}$
F	$0.04x(1 + 0.0001x)^{-1/2}$	$0.016x(1 + 0.0003x)^{-1}$
Urban Conditions		
A-B	$0.32x(1 + 0.0004x)^{-1/2}$	$0.24x(1 + 0.001x)^{1/2}$
C	$0.22x(1 + 0.0004x)^{-1/2}$	$0.20x$
D	$0.16x(1 + 0.0004x)^{-1/2}$	$0.14x(1 + 0.0003x)^{-1/2}$
E-F	$0.11x(1 + 0.0004x)^{-1/2}$	$0.08x(1 + 0.00015x)^{-1/2}$

Recent diffusion experiments under clear, nearly calm nighttime conditions (so-called category G) suggest that horizontal diffusion is actually greater during these conditions than under conditions associated with category F (Sagendorf and Dickson, 1974) because the plume often meanders during G conditions, which results in σ_θ equal to 20° or more and relatively low hourly average ground concentrations at a given point. Van der Hoven (1976) analyzed several category G diffusion experiments and found that observed σ_y values corresponded to anything between categories A and F. Thus diffusion in terms of tabulated dispersion parameters is indeterminate when category G stability is found. Of course, diffusion can still be estimated on the basis of actual measurements of σ_θ .

With the use of stability classes in complex terrain situations, σ 's are also difficult to determine. The diffusion experiments summarized in Chap. 12 generally show that σ_y and σ_z in complex terrain are a factor of 2 to 10 greater than that predicted from the Pasquill curves. Again, measurements of σ_θ and σ_e are the best solution to this uncertainty.

sion calculations by developing a technique that relates diffusion directly to turbulence. Taylor's (1921) work suggests the formulas:

$$\sigma_y = \sigma_w t f_y \left(\frac{t}{T_y} \right) \quad (4.3)$$

$$\sigma_z = \sigma_w t f_z \left(\frac{t}{T_z} \right) \quad (4.4)$$

where f_y and f_z are universal functions and T_y and T_z are turbulence time scales in the y and z directions. The fact that averaging times for all variables are equal and that turbulence parameters are measured or estimated near the release height is implicit. Since diffusion calculations are generally made in practice for downwind distances (x) rather than times (t), the following forms of writing Eqs. 4.3 and 4.4 are desirable:

$$\sigma_y = \sigma_\theta x f_y \left(\frac{x}{uT_y} \right) \quad (4.5)$$

$$\sigma_z = \sigma_e x f_z \left(\frac{x}{uT_z} \right) \quad (4.6)$$

where it is assumed that $\sigma_\theta = \sigma_v/u$ and $\sigma_e = \sigma_w/u$. Once the universal functions f_y and f_z have been determined, then σ_y and σ_z are completely determined by observations of σ_θ and σ_e . Presumably T_y and T_z are similarity functions of z/z_0 , z_i/L , and Lf/u_* .

Pasquill (1976), Draxler (1976), Doran, Horst, and Nickola (1978), and Irwin (1979a) are among those actively investigating the best form for the universal functions f_y and f_z . Although Taylor's (1921) statistical diffusion equation (see Chap. 5, Sec. 5-2) can be used to derive a theoretical form for f_y and f_z , current data are scattered enough that simple empirical formulas are justified. For example, Pasquill (1976) gets good results by removing the dependence of f_y on the time scale T_y . Irwin (1979a) has derived the following approximations to Pasquill's empirical table:

$$f_y = (1 + 0.031 x^{0.46})^{-1} \quad (x \leq 10^4 \text{ m})$$

$$= 33x^{-1/2} \quad (x > 10^4 \text{ m}) \quad (4.7)$$

where x is in meters. This solution is diagrammed in Fig. 4.5. The approximation has the desirable property that $\sigma_y \propto x$ at small distances. At distances greater than about 10 km, mean wind direction shear in the planetary boundary layer may become important, and Pasquill (1976) suggests the rough rule: add to the σ_y^2 already derived the term $0.03 (\Delta\alpha)^2 x^2$, where $\Delta\alpha$ (in radians) is the change in wind direction over the plume depth.

The universal function f_z is more difficult to determine since there are fewer data on the vertical distribution of concentration. Furthermore, a Gaussian distribution in the vertical is found only as long as

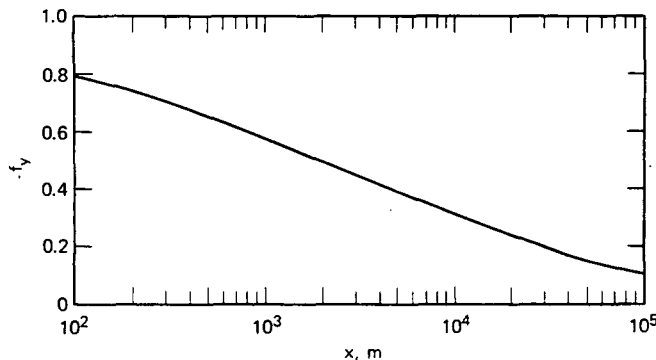


Fig. 4.5 $f_y = \sigma_y/(\sigma_\theta x)$ according to Eq. 4.7, which is Irwin's (1979a) attempt to fit Pasquill's (1979) table.

σ_z is less than the source height; otherwise reflection and absorption at the ground surface distort the plume. Of course, no matter what the plume shape is, σ_z can always be calculated as the standard deviation of the observed concentration distribution. Draxler (1976) plotted observed values of $f_z = \sigma_z/(\sigma_w t)$ as a function of time after release for several diffusion experiments. He divided the diffusion data into ground-level and elevated sources and suggested the following formula for ground-level sources for f_y (all stabilities) and f_z (stable and neutral):

$$f_y = f_z = [1 + 0.40(x/uT_y)]^{-1/2} \quad (4.8)$$

where T_i is assumed to equal $5 T_y$. Draxler presented a slightly different formula for elevated sources, but at all x the formulas agree within $\pm 20\%$, which is probably as good accuracy as we can hope for.

For unstable f_z , Irwin (1979a) plots observations of $\sigma_z/(\sigma_w t) = f_z$ vs. $t^* = w_* t/z_i$ for elevated and ground-level releases. These figures are reproduced here as Figs. 4.6 and 4.7, where the "best fit" curves are forced to obey the theoretical law $\sigma \propto t^{1/2}$ at large times. Unfortunately the data do not seem compelled to follow the same law. Values of the convective velocity scale (w_*) and the mixing depth (z_i) can be obtained from Eq. 1.43 and observations, respectively.

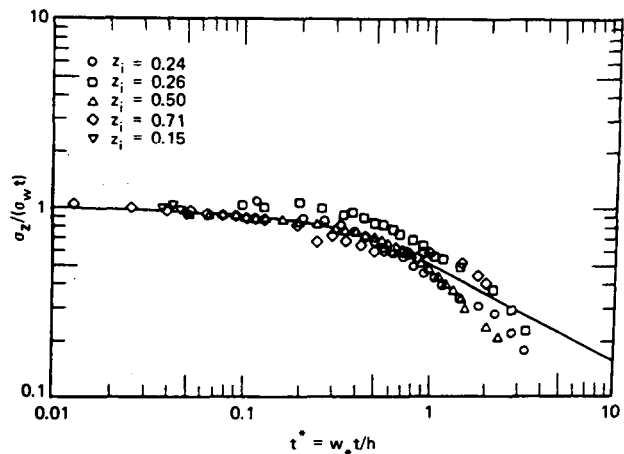


Fig. 4.6 Values of $\sigma_z/(\sigma_w t)$ vs. t^* for elevated releases (z_i) during unstable conditions. Release heights range from 0.15 to 0.71.

4-5 WIND-SPEED VARIATION WITH HEIGHT

The fact that the wind speed (u) appearing in the basic Gaussian plume formula (Eq. 4.1) should be an

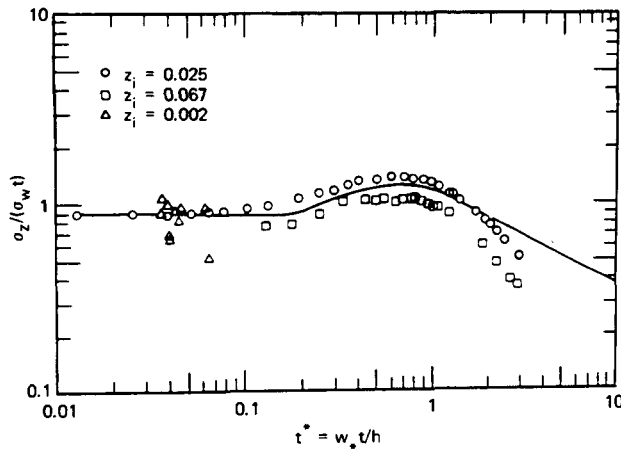


Fig. 4.7 Values of $\sigma_z/(\sigma_w t)$ vs. t^* for near-surface releases (z_i) during unstable conditions. Release heights range from 0.002 to 0.067.

average value over the plume depth is generally recognized. In practice, the wind speed at the effective release height (h) of the plume is used. Sometimes observations of this wind speed are available, but usually the wind speed must be estimated by using observations near the surface. The theoretical formulas (Eqs. 1.37 and 1.38) or a power-law formula can be used:

$$u = u_{10} \left(\frac{z}{10} \right)^p \quad (4.9)$$

where z is height in meters and u_{10} is the observed wind speed at a height of 10 m. This formula is used by several of the U. S. Environmental Protection Agency (EPA) models, with values of the parameter p estimated by Irwin (1979b) given in Table 4.6. The power law is less accurate than Eqs. 1.37 and 1.38

Table 4.6 Estimates of the Power (p) in Eq. 4.9 for Six Stability Classes and Two Roughnesses*

	Stability class					
	A	B	C	D	E	F
Urban p	0.15	0.15	0.20	0.25	0.40	0.60
Rural p	0.07	0.07	0.10	0.15	0.35	0.55

*Table is based on information by Irwin (1979b).

and should not be used at heights above 200 m (assume $u = u_{200}$ for $z > 200$ m), but it is an easy-to-use solution to the problem of wind variation with height.

4-6 MAXIMUM GROUND CONCENTRATION AND FUMIGATION

Because regulations are written in terms of maximum ground concentrations, it is informative to differentiate the Gaussian plume equation with respect to x and set the result equal to zero to determine the distance to the maximum concentration. When $\sigma_y \propto \sigma_z$, this occurs at the distance downwind where $2\sigma_z^2 = h^2$, where h is effective plume height (equal to $h_s + \Delta h$). The concentration at that distance is given by the formula:

$$C_{\max} = \frac{2Q}{\pi h^2 e u} \frac{\sigma_z}{\sigma_y} \quad (4.10)$$

Experience shows that this critical distance is a few tens of stack heights (h_s) downwind. There is a "critical" wind speed at which C_{\max} itself is a maximum if there is any plume rise at all. This phenomenon is called "high wind fumigation" and can persist for hours. The term "fumigation" in this context means a situation in which high concentrations are brought to the ground from an elevated plume. Equations 2.29 and 2.30 can be used to estimate the critical wind speed (u_c) and the distance (x_c) to the maximum concentration point. Equation 2.25 gives the plume rise (Δh) under those conditions. Concentration (C) can then be calculated from Eq. 4.9.

"Limited-mixing fumigation" occurs when upward diffusion or penetration of the plume is restricted by an inversion, below which strong mixing occurs. In Los Angeles, for example, a fairly persistent marine subsidence inversion exists at a height of about 500 m. If the inversion height is z_i and it is assumed that the vertical distribution of material in the plume is uniform from the ground to z_i , then the ground-level concentration is given by

$$C = \frac{Q}{(2\pi)^{1/2} u z_i \sigma_y} \quad (4.11)$$

Tennessee Valley Authority experience shows that limited-mixing fumigation more frequently gives the highest ground concentrations at their very tall stacks ($h_s > 100_m$), whereas high wind fumigation is more frequently critical at their shorter stacks.

This can be seen as follows: consider the ratio of the concentrations predicted by the two methods

$$\frac{C_{LM}}{C_{HW}} = \left(\frac{\pi}{2} \right)^{1/2} \frac{h^2 e}{2z_i \sigma_z} \quad (4.12)$$

If we assume that $h^2 = 2 \sigma_z^2$ at the maximum point, then Eq. 4.12 becomes

$$\frac{C_{LM}}{C_{HW}} \approx 2.4 \frac{h}{z_i} \quad (4.13)$$

If mixing height (z_i) is 500 m, then limited-mixing fumigation will be more important than high-wind fumigation when the effective plume height is greater than about 200 m.

4-7 AVERAGING TIMES AND PEAK-TO-MEAN CONCENTRATION RATIOS

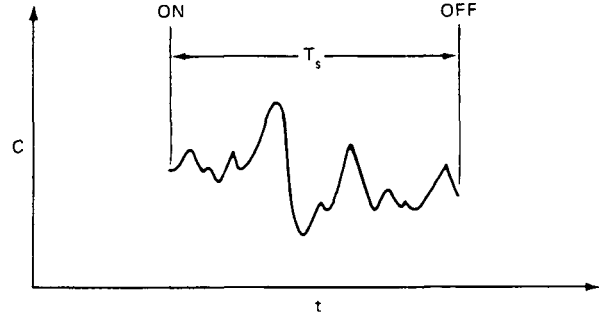
A measuring instrument must be turned on and off, and it always has some inertia that prevents it from responding to very rapid fluctuations. Also, so that the number of data points can be kept at a manageable level, groups of data are usually averaged together at certain intervals. The total period over which the instrument operates is called the sampling time, and the time imposed by instrument inertia and/or averaging is called the averaging time. These concepts are illustrated in the data records in Fig. 4.8.

The effect of finite sampling and averaging times is to remove very high and low frequency fluctuations from the data record, which would thus reduce the total variance. If the sampling time is T_s , then eddies with periods greater than T_s will not contribute to the calculated variance. Similarly, if the averaging time is T_a , then eddies with periods less than T_a will not contribute. Pasquill (1974) has expressed this analytically:

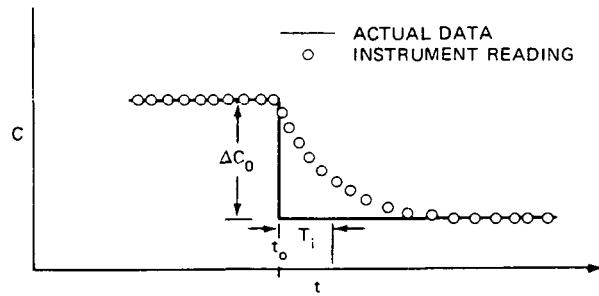
$$\sigma^2(T_s, T_a) = \sigma^2(\infty, 0) \int_0^\infty F(n) \frac{\sin^2 \pi n T_a}{(\pi n T_a)^2} \times \left[1 - \frac{\sin^2 \pi n T_s}{(\pi n T_s)^2} \right] dn \quad (4.14)$$

where $\sigma^2(T_s, T_a)$ is the variance for sampling time T_s and averaging time T_a and $F(n)$ is the spectrum function at frequency n .

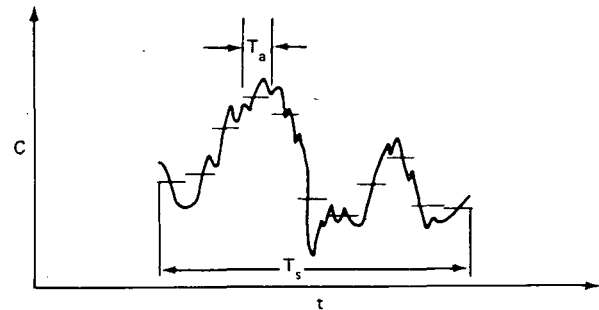
The diffusion parameters (σ_y and σ_z) are directly related to the standard deviations of the turbulent velocity fluctuations (σ_v and σ_w). As sampling time increases, intuition and Eq. 4.14 tell us that observed values of σ_v and σ_w , and hence σ_y and σ_z , increase. The exact level of increase is clearly a function of the spectrum $F(n)$ and the times T_s and T_a , and the analytical equation quickly becomes very compli-



(a) SAMPLING TIME (T_s) IS LENGTH OF TOTAL DATA RECORD



(b) INSTRUMENT TIME LAG (T_i) DEFINED BY $\Delta C/\Delta C_0 = e^{-(t-t_0)/T_i}$



(c) AVERAGING TIME (T_a)

Fig. 4.8 Illustration of sampling time (T_s) (a), instrument time lag (T_i) (b), and averaging time (T_a) (c).

cated. Furthermore, since the turbulent energy spectra of the y and z components are not necessarily the same, the increase of σ_y and σ_z with averaging time is not necessarily the same either. Gifford (1975) suggests accounting for the effects of sampling time through the empirical formula:

$$\frac{\sigma_{yd}}{\sigma_{ye}} = \left(\frac{T_{sd}}{T_{se}} \right)^q \quad (4.15)$$

where d and e represent two different cases, and q is in the range 0.25 to 0.3 for $1 \text{ hr} < T_{sd} < 100 \text{ hr}$ and equals approximately 0.2 for $3 \text{ min} < T_{sd} < 1 \text{ hr}$. The standard Pasquill-Gifford curves represent a sampling

time T_{se} of about 10 min. Thus σ_y for a sampling time of 1 hr equals $6^{0.2}$, or 1.43, times the σ_y found in Fig. 4.4. This is very close to an increase of one stability class interval.

An air-pollution concentration observation (C_a) involves an average over a period T_a . If the concentration record (as in Fig. 4.8c) has significant "energy" at periods greater than T_a , then the individual C 's are not very representative of the true mean (\bar{C}). Physically, this situation is caused by the plume meandering about, as in Fig. 4.9. As the narrow plume passes over a given point, the concentration is high for a brief time but then drops to a low value again as the plume meanders over to a new position. Gifford (1959a) stated that the ratio of peak-to-mean concentrations (P/M) is in the range from 1 to 5 for source and receptor at the same elevation. As effective plume height increases while the receptor remains at the ground, P/M increases, with values of 50 to 100 or greater near a 100-m stack. The ratio P/M decreases as distance from the source increases.

Gifford suggested that the P/M problem could be analyzed by assuming that there are two separate scales of diffusion, where the total diffusion σ^2 over a long period equals the sum of the diffusion \bar{y}^2 of the instantaneous plume due to small scales of turbulence plus a contribution D^2 due to meandering of the plume:

$$\sigma^2 = \bar{y}^2 + D^2 \quad (4.16)$$

This assumption leads to the following formula for the P/M :

$$\frac{P}{M} = \frac{\bar{y}^2 + D^2}{y^2} \exp \left[\frac{\bar{y}^2}{2(\bar{y}^2 + D^2)} + \frac{(z-h)^2}{2(\bar{y}^2 + D^2)} \right] \quad (4.17)$$

Unfortunately little is known about the behavior of either the large-scale component (D^2) or the small-scale component (\bar{y}^2).

4-8 SECTOR MODEL FOR LONG SAMPLING TIMES

Over a long period of time, such as days or months, the wind direction is likely to touch on all points of the compass. The horizontal crosswind distribution in the plume, usually represented by σ_y , will no longer be important since the wind-direction frequency distribution will be fairly smooth as we go around the compass. In this case the sector model can be used, where it is assumed that there is no horizontal crosswind variation in concentration within an angular sector equal to the resolution of the wind-direction data. For example, wind direction is commonly reported as N, NNE, NE, etc., giving rise to 16 sectors with width $22\frac{1}{2}^\circ$. The formula for ground-level concentration from a continuous-point source within sectors of arbitrary angular width $2\pi/n$ (in radians) is as follows:

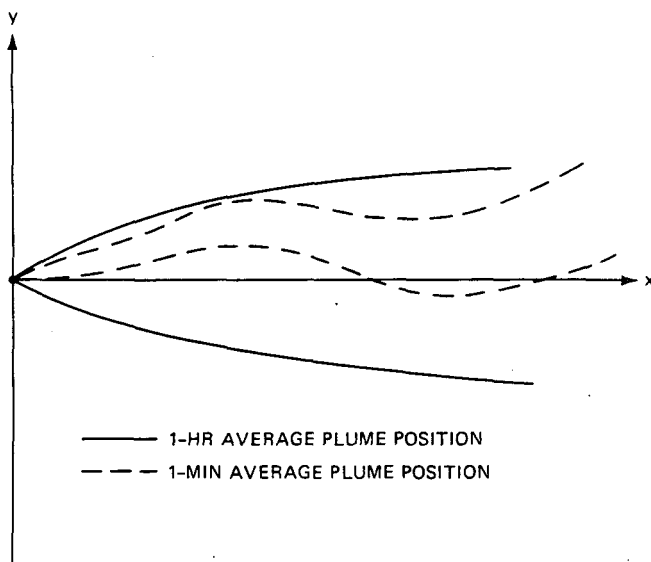


Fig. 4.9 Comparison of short- and long-term average plume position.

$$C = \left(\frac{2}{\pi}\right)^{1/2} \left(\frac{fQn}{2\pi\sigma_z u x}\right) e^{-h^2/2\sigma_z^2} \quad (4.18)$$

where f is the fraction of the time the wind blows toward that sector. Thus, given an annual wind rose, the distribution of annual average concentrations around a continuous source can be estimated.

Problems

1. Assume that the effective plume height is 100 m and that the continuous-source release rate is 10 g/sec. Stability is neutral, wind speed is 5 m/sec, σ_y is 10° , and σ_z is 5° . Calculate ground-level plume centerline concentration at a distance of 1 km from the source for the following σ methods: BNL, Briggs open country, Pasquill–Gifford–Turner figures, and Draxler (Eq. 4.8). Give the deviation of each answer from the average of the four.

2. Suppose that you are burning your trash after dark in your backyard. The fire has died down so that there is no plume rise, and assume no downwash or source effects. Source height is 1 m, wind speed at that height is 2 m/sec, stability class is F, and source strength of suspended particles is 1 g/sec. What concentration is your neighbor, sitting in his lawn chair on the plume centerline 100 m downwind, exposed to? How far must he move his chair sideways before the concentration decreases to 10 mg/m^3 ?

3. A big power plant releases 1000 g/sec of SO_2 . Effective source height is 200 m, wind speed at a height of 10 m is 6 m/sec, and it is cloudy. Plot the ground-level plume centerline concentration as a function of distance from $x = 0$ to $x = 20$ km.

4. Calculate maximum ground-level concentration and the downwind distance at which it occurs using both the “high-wind” and “limited mixing” formulas for the following conditions: $Q = 1000$ g/sec, $u(10 \text{ m}) = 4$ m/sec, sunny, $h = 250$ m, and $z_1 = 1000$ m.

Statistical Models of Diffusion from Continuous-Point Sources

5-1 INTRODUCTION

The statistical, similarity, and K theories of diffusion provide alternatives to the Gaussian plume model discussed in Chap. 4. These theories are discussed in Chaps. 5 to 8. The definition of statistical models used in this chapter is based on the fact that diffusive motions have a certain random or stochastic nature. Thus the path of an individual particle can be described by a statistical function. If particles are assumed to have no memory of their previous motions and if their chances of going left or right at any time are equal, then they will follow a "drunkard's walk" or "Monte Carlo" path. This simple discrete-step stochastic diffusion model is valid for molecular diffusion. Let n be steps downstream from the source and m be steps perpendicular to the axis (see Fig. 5.1). The particles flow downstream in the n direction at a constant rate and can diffuse only in the cross-stream direction. The probability of finding the particle at steps n, m is given by the formula

$$P(n, m) = \left(\frac{2}{\pi n}\right)^{1/2} \exp\left(-\frac{m^2}{2n}\right) \quad (5.1)$$

As n increases this solution approaches the familiar Gaussian or bell-shaped curve discussed in Chap. 4, with $\sigma^2 = n$. Since n is proportional to time, the result of a pure Monte Carlo diffusion model is $\sigma \propto t^{1/2}$.

5-2 TAYLOR'S THEOREM

The physical basis of the drunkard's walk or Monte Carlo method, i.e., noncorrelated motions, is

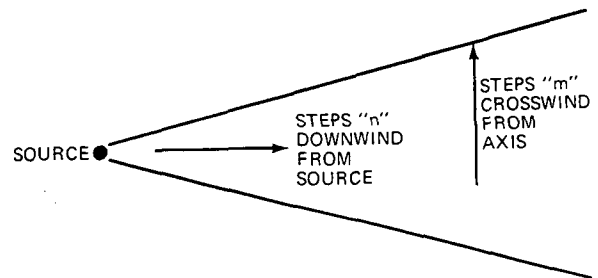


Fig. 5.1 Orientation of steps m and n in Monte Carlo problem.

not valid for atmospheric diffusion. In the boundary layer of the atmosphere at heights of 10 to 100 m during the daytime, the turbulent speed $v'(t)$ will be correlated with the speed $v'(t + \Delta t)$ for time lags Δt as great as several minutes. For very short time lags, on the order of 1 sec, the speeds $v'(t)$ and $v'(t + \Delta t)$ are nearly identical. An autocorrelation coefficient $R(\Delta t)$ is defined by the formula

$$R(\Delta t) = \frac{\overline{v'(t) v'(t + \Delta t)}}{\sigma_v^2} \quad (5.2)$$

where the bar indicates a time average. For small time lags, $R \rightarrow 1$, and for large time lags, $R \rightarrow 0$.

The speeds (v') discussed in this section refer to those felt by the particle or parcel as it moves. This system is called a Lagrangian system of motion. In contrast, the speeds felt by an anemometer fixed to a mast are called Eulerian. Relations between these two systems were discussed in Chap. 1, Sec. 1-7, and are further discussed in Sec. 5-5.

Taylor's (1921) theorem of diffusion from a continuous source begins with the assumption that y is the crosswind deviation from a fixed axis of a

typical particle due to eddy speed v' after a time t . The symbol $\overline{y^2}$ (equal to σ_y^2) indicates the mean square of a large number of values of y . Particles have been assumed to be released from a single point and travel paths illustrated in Fig. 5.2. Each particle is inertialess and follows the airflow exactly. Then the rate of change with time of σ_y^2 is given by

$$\begin{aligned} \frac{d\sigma_y^2}{dt} &= \frac{d\overline{y^2}}{dt} = 2\overline{y} \frac{dy}{dt} = 2\overline{yv'} \\ &= 2 \int_0^t \overline{v'(t)v'(t+t')} dt' \end{aligned} \quad (5.3)$$

If the turbulence is homogeneous (does not vary in space) and stationary (does not vary in time), then

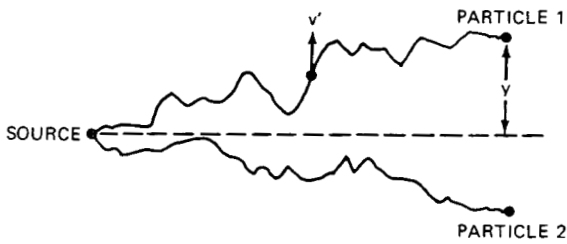


Fig. 5.2 Trajectories followed by two typical particles.

Eq. 5.2 can be substituted into Eq. 5.3 to yield, upon integration,

$$\sigma_y^2 = 2\sigma_v^2 \int_0^t \int_0^{t'} R(t') dt' dt \quad (5.4)$$

This is usually referred to as Taylor's equation.

We can use simple approximations to determine the behavior of σ_y^2 at small and large times.

As $t \rightarrow 0$,

$$\begin{aligned} R(t) &\rightarrow 1 \quad \text{and} \quad \sigma_y^2 \approx \sigma_v^2 t^2 \\ \text{or} \quad \sigma_y &\propto t \end{aligned} \quad (5.5)$$

As $t \rightarrow \infty$,

$$\int_0^{t'} R(t') dt' = T$$

where T is a constant known as the "time scale," and

$$\sigma_y^2 \approx 2\sigma_v^2 Tt \quad \text{or} \quad \sigma_y \propto t^{1/2} \quad (5.6)$$

Thus, as travel time for a continuous plume increases, the rate of diffusion decreases. Particle motions are at first linear because the particles "remember" their initial velocity. However, when such travel times are reached that the particles no longer remember their

initial motions, the problem reduces to a Monte Carlo problem, and $\sigma_y \propto t^{1/2}$.

A simple exponential form

$$R(t) = \exp\left(-\frac{t}{T}\right) \quad (5.7)$$

has often proved to be a useful approximation to the autocorrelation. The integration of Eq. 5.4 with the use of this form for $R(t)$ results in the solution

$$\sigma_y^2(t) = 2\sigma_v^2 T^2 \left[\frac{t}{T} - 1 + \exp\left(-\frac{t}{T}\right) \right] \quad (5.8)$$

which is plotted in Fig. 5.3. It is interesting to note that the asymptotic lines $\sigma_y^2 = \sigma_v^2 t^2$ and $\sigma_y^2 = 2\sigma_v^2 Tt$ meet roughly at a time equal to twice the time scale T .

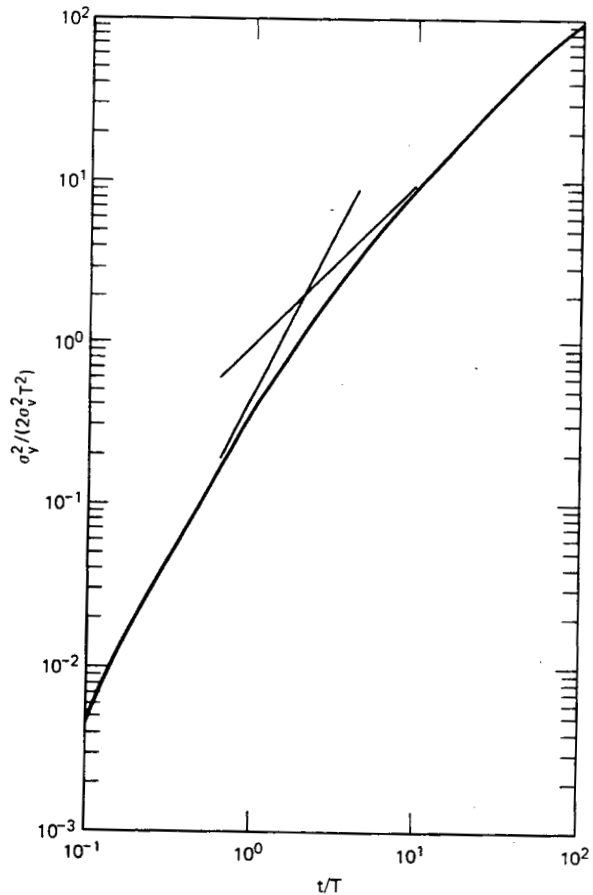


Fig. 5.3 Analytical solution (Eq. 5.8) to Taylor's equation with the assumption that $R(t) = \exp(-t/T)$. Asymptotic solutions for small and large times are also shown.

Equation 5.8 can be used to derive a theoretical form for the function f_y discussed in Sec. 4-4.2:

$$f_y\left(\frac{t}{T}\right) = \frac{\sigma_y}{\sigma_v t} = (2)^{\frac{1}{2}} \frac{T}{t} \left[\frac{t}{T} - 1 + \exp\left(-\frac{t}{T}\right) \right]^{\frac{1}{2}} \quad (5.9)$$

This formula for f_y (in which it is assumed that $t = x/u$ and $u = 5$ m/sec and $T = 50$ sec) is compared with Pasquill's (1976) curve in Fig. 5.4. There is good agreement in the midrange, where f_y is approximately 0.5 and x is approximately 1 km, but formula 5.9 slightly overpredicts at small x and slightly underpredicts at large x when compared with Pasquill's curve.

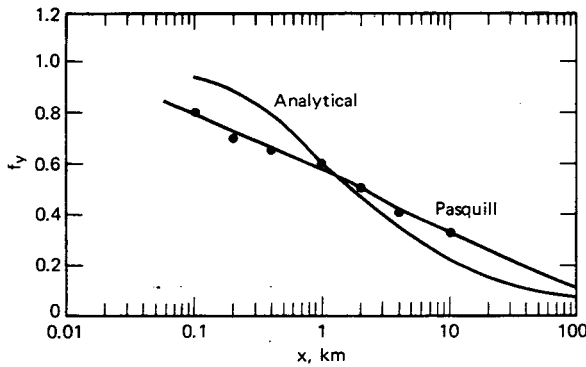


Fig. 5.4 Comparison of Pasquill's empirical suggestion for $f(x)$ with the analytical solution (Eq. 5.9) to Taylor's equation with the assumption that $t = x/u$ and $u = 5$ m/sec and $T = 50$ sec.

Doran, Horst, and Nickola (1978) and Draxler (1976) define a different time scale (T_i) as the time at which the function f_y drops to 0.5. Equation 5.9 can be used to show that $T_i \approx 7T$, where T is the Lagrangian time scale. Of course, any user of Taylor's equation must realize the strict physical assumptions made in its derivation. Since turbulence is assumed to be stationary and homogeneous, the theory cannot be expected to be strictly valid in shear zones, such as the near-surface layer of the atmosphere.

Sutton (1953) solved Taylor's equation (5.4) by using the following assumed form for R :

$$R(t) = \left(\frac{\nu}{\nu + \sigma_v^2 t} \right)^n \quad (0 < n < 1) \quad (5.10)$$

where ν is viscosity. It develops that

$$\begin{aligned} \sigma_y^2 &= \frac{2\nu^n}{(1-n)(2-n)\sigma_v^2} (\sigma_v^2 t)^{2-n} \\ &= \frac{1}{2} C_y^2 (ut)^{2-n} \end{aligned} \quad (5.11)$$

The factor n is determined from

$$\frac{u_1}{u_2} = \left(\frac{z_1}{z_2} \right)^{n/(2-n)} \quad (5.12)$$

This method was used extensively in the 1950's but eventually got so complicated by empirical factors that it was replaced by the simpler Pasquill-Gifford method.

5-3 INFLUENCE OF EDDY SIZE ON σ

According to the results of Taylor's theory derived above, the rate of change of σ_y with time is a decreasing function of time of travel for continuous plumes. We can guess intuitively that the influence of small eddies decreases as the plume grows since small oscillations of particles deep within the plume do not contribute to "diffusion" of the plume as a whole. Instead, eddies with diameters roughly equal to and larger than σ cause most of the diffusion. This result can be shown analytically since the autocorrelation coefficient [$R(t)$] and the energy spectrum [$F(n)$] are known to be Fourier transforms of each other. The variable $nF(n)$ is proportional to the amount of turbulent energy carried by eddies of frequency n . (The frequency n of an eddy equals the inverse of its period; n increases as eddy size decreases.)

Without going through the details of the mathematics, we can rewrite Taylor's equation (5.4) as:

$$\sigma_y^2 = \sigma_v^2 t^2 \int_0^\infty F(n) \frac{\sin^2(\pi n t)}{(\pi n t)^2} dn \quad (5.13)$$

Sampling time (T_s) is assumed to be much greater than travel time (t); thus the plume is assured of being continuous instead of instantaneous. The term $\sin^2(\pi n t)/(\pi n t)^2$ is unity for large eddies with frequencies less than roughly $1/t$ and drops to zero for small eddies with frequencies greater than roughly $1/t$. In other words, this term is a filter that passes only low frequency eddies, and, as travel time increases, fewer and fewer eddies are passed by this filter; hence $\sigma_y \propto t$ for small t and $\sigma_y \propto t^{1/2}$ for large t .

There is a low frequency cutoff imposed by the finite sampling time, T_s . This cutoff is accounted for by multiplying inside the integral (5.13) by $[1 - \sin^2$

$(\pi n T_s)/(\pi n T_s)^2]$ (see Eq. 4.14). We can conclude that continuous-source diffusion is influenced only by eddies with periods ranging roughly between the travel time and the sampling time. Pasquill (1974) points out that these results are equivalent to the simple equation:

$$\sigma_y^2 = \sigma_v^2 (T_s/\beta, t/\beta)^2 \quad (5.14)$$

where β is the ratio of Lagrangian to Eulerian time scales, which has been observed to average about four. The terms in the parentheses imply that σ_v^2 is sampled by a fixed anemometer over a total time T_s/β , where consecutive averages over a time t/β are taken within that sampling period before σ_v^2 is computed. The concept of sampling and averaging time has been illustrated in Fig. 4.8. Thus for constant T_s the effective turbulent energy σ_v^2 will decrease as travel time increases. With Eq. 5.14, diffusion can be calculated by using basic wind-speed observations, which makes this equation a very practical but so far underused model.

Doran, Horst, and Nickola (1978) assume a standard form for the spectrum $F(n)$ for stable and unstable conditions and integrate Eqs. 4.14 and 5.13, which thus accounts for the effects of averaging time t and sampling time T_s on σ_y^2 . They find that larger values of $\sigma_y/(\sigma_\theta x)$ are associated with longer averaging time and sampling time. However, because of the scatter in the results of diffusion experiments, the improvement over simpler models for $\sigma_y/(\sigma_\theta x)$ (e.g., Fig. 5.4) is difficult to see.

5-4 LAGRANGIAN-EULERIAN RELATIONS

Small elements of pollutant gases or inertialess particles follow the airflow exactly. Intuitively, velocities measured by parcels following the airflow (*Lagrangian*) are more slowly varying than those measured by a fixed anemometer (*Eulerian*). The problem is that we must use fixed anemometer observations to estimate diffusion, which requires that relations between Eulerian and Lagrangian turbulence be developed. The spectrum $F(n)$ in Eq. 5.13 and the autocorrelation $R(t)$ in Taylor's equation (5.4) are Lagrangian parameters.

If σ_v^2 is known, the $nR_L(t)$ σ_v^2 can be estimated (see Eq. 5.4) from $d^2 \sigma_y^2/dt^2$. However, second derivatives of field observations are very difficult to compute accurately. A more common method of comparison of Lagrangian and Eulerian turbulence is

to calculate $R_L(t)$ and $R_E(t)$ by using concurrent observations from free-floating balloons and fixed anemometers. Gifford (1955) and Hay and Pasquill (1959) suggested that Lagrangian and Eulerian spectra and autocorrelograms were similar in shape but displaced from each other by a factor β . Figure 5.5 illustrates this similarity concept, which can be written analytically;

$$n F_L(n) = \beta n F_E(\beta n) \quad (5.15)$$

$$R_L(\beta t) = R_E(t) \quad (5.16)$$

where β can be formally defined as the ratio of the Lagrangian to the Eulerian time scale:

$$\beta = \frac{T_L}{T_E} \quad (5.17)$$

A simple method of evaluating β is to consider the circular eddy in Chap. 1, Sec. 1-6, which gave the result that β was inversely proportional to turbulence intensity [$\beta = 0.5/i = 0.5/(\sigma_v/u)$]. Pasquill (1974) suggests that, on the average, in the planetary boundary layer, β equals 4 for neutral conditions, $\beta \rightarrow 10$ as

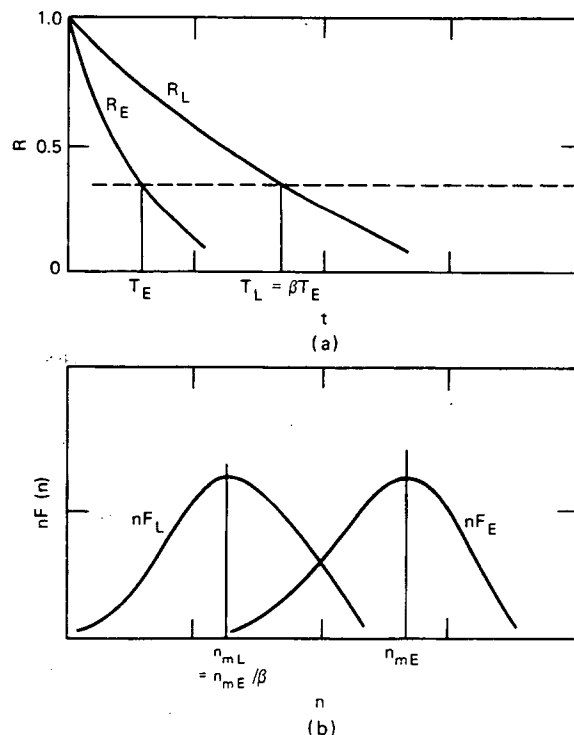


Fig. 5.5 Eulerian (R_E) and Lagrangian (R_L) autocorrelograms (a) and spectra (b), which are assumed to have similar shapes but time scales that are different by a factor β .

stability increases, and $\beta \rightarrow 1$ as stability decreases. There is much scatter in observations of β .

5-5 MONTE CARLO PARTICLE TRAJECTORY MODELS OF DIFFUSION

Thousands of particle trajectories can be easily calculated by today's high-speed computers, and the statistics (e.g., σ_y) of the particle distribution after a certain time can be estimated. This is potentially a powerful technique for the evaluation of diffusion in nonuniform and nonstationary wind and turbulence fields. In practice, time steps Δt of a few seconds are used in the computer model, and the following equation is assumed:

$$x(t) = x(t - \Delta t) + u \Delta t \quad (5.18)$$

where the total speed, u , is the sum of a mean and a turbulent component,

$$u = \bar{u} + u' \quad (5.19)$$

The turbulent component is the sum of a correlated component and a random or Monte Carlo component:

$$u'(t) = u'(t - \Delta t) R(\Delta t) + u'' \quad (5.20)$$

where the random component u'' is assumed to have a Gaussian distribution with zero mean and variance $\sigma_{u''}^2$ given by

$$\sigma_{u''}^2 = \sigma_{u'}^2 [1 - R^2(\Delta t)] \quad (5.21)$$

This relation is necessary to conserve energy $\sigma_{u'}^2$ from one time step to the next. The autocorrelation coefficient $R(\Delta t)$ is a Lagrangian variable.

The turbulent energy $\sigma_{u'}^2$ can be estimated from boundary-layer equations, such as 1.42 to 1.53. Any form for $R(\Delta t)$ can be used, but the simplest is $R(\Delta t) = \exp(-\Delta t/T_L)$. Thus the Lagrangian time scale must be estimated before Eq. 5.20 can be used. We use the formula

$$T_L = \beta T_E = \beta \frac{\lambda_{mE}}{5u} \quad (5.22)$$

where λ_{mE} is the wavelength of peak energy in the Eulerian spectrum, as given by Eqs. 1.57 and 1.58 for the three velocity components. The fraction ($1/5$)

comes from the fact that the spectrum for an assumed autocorrelagram of the form $\exp(-\Delta t/T_E)$ has peak energy at a period of about $5T_E$. Then, if we substitute Eq. 1.65 (with $i = \sigma_{u'}/u$) in Eq. 5.22, the time scale (T_L) becomes

$$T_L = \frac{0.1\lambda_{mE}}{\sigma_{u'}} \quad (5.23)$$

Typical time scales (T_L) for a convective boundary layer of depth 1000 m and sampling times of about 1 hr are on the order of 100 sec.

The advantage of this technique is that diffusion calculations are related directly to basic turbulence characteristics. The calculated σ_y values agree exactly with the analytical solution to Taylor's equation (see Eq. 5.8) when mean winds and turbulence are assumed to be stationary and homogeneous. In these applications the particles are released from the same point, and the initial turbulent velocity is chosen randomly from a Gaussian distribution with zero mean and variance $\sigma_{u'}^2$.

Reid (1979) applied this technique to estimate vertical dispersion from a ground-level source and was able to satisfactorily simulate observed distributions in the Prairie Grass diffusion experiments. In that case strong vertical shears of mean wind speed were present. This Monte-Carlo-type method will be most applicable to difficult situations, such as sea breezes or complex terrain, in which the Gaussian plume model does not apply.

Problems

1. Assume that $R(t') = 1 - |t'|/T$ for $|t'|/T \leq 1$ and $R(t') = 0$ for $|t'|/T > 1$. Find an analytic formula for σ_y^2 with Taylor's equation.

2. A continuous release of neutrally buoyant material is made at a rate of 1 g/sec from a height of 100 m. Lagrangian time scales T in the y and z directions are 50 and 10 sec, respectively. Wind speed is 5 m/sec. Calculate the centerline concentration after a travel time of 30 sec.

3. In the daytime $\beta \approx 2$. A plume is sampled over a period of 10 min, and averages of 10 sec are made within that period. What sampling and averaging times should be used in calculating σ_v^2 so that the equation $\sigma_y^2 = \sigma_v^2 t^2$ is valid?

4. Show that Eq. 5.22 follows from Eq. 5.21. Hint: square both sides of Eq. 5.21 and average by using Reynolds' averaging conventions.

Puff Diffusion

6-1 INTRODUCTION

Possibly the most confusing aspect of atmospheric diffusion is the difference between plume and puff diffusion. Plume diffusion formulas apply to so-called continuous plumes, where the release and sampling times are long compared with the travel time from source to receptor. On the other hand, puff or relative diffusion formulas apply to so-called instantaneous sources, where the release time or sampling time is short compared with the travel time. These definitions lead to a dilemma when the release time is roughly equal to the sampling and travel times, as shown in Fig. 6.1. In this case a combination of the two techniques may be necessary.

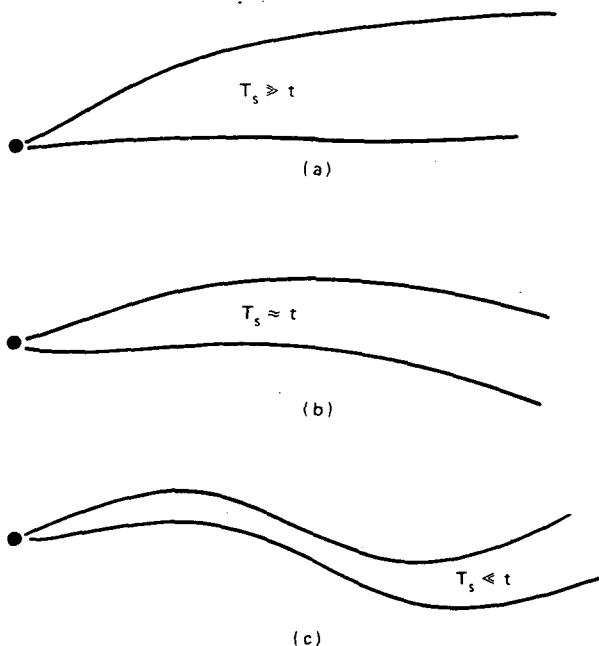


Fig. 6.1 Plume shapes relative to sampling time (T_s) and travel time (t). (a) Continuous-source plume ($T_s \gg t$). (b) Continuous or instantaneous plume ($T_s \approx t$). (c) Instantaneous plume ($T_s \ll t$).

Puff or relative diffusion parameters (σ) appropriate for the instantaneous plumes in Fig. 6.1(c) have been measured in very few field experiments. Consequently questionable situations arise in which some model developers use Pasquill-Gifford continuous plume σ 's for puffs. In this chapter several theoretical approaches for estimating puff σ 's are outlined, and a few comparisons with data are made.

6-2 STATISTICAL APPROACH

In the Taylor statistical approach to diffusion from continuous plumes covered in Chap. 5, the trajectories of single particles relative to a fixed axis were discussed. However, for puff diffusion, no fixed axis can be defined, and the motion of one particle relative to another must be studied. For this reason puff diffusion is often called relative diffusion. Batchelor (1950) writes an equation analogous to Taylor's equation:

$$\overline{y^2} = y_0^2 + 2 \int_0^T \int_0^{t'} \overline{\delta v(t) \delta v(t + t_1)} dt_1 dt' \quad (6.1)$$

where y_0 is the initial separation of two particles and δv is their relative velocity (i.e., the difference between the velocities of the particles, $\delta v = v_2 - v_1$). However, very little is known about the correlation term $\overline{\delta v(t) \delta v(t + t_1)}$.

Smith and Hay (1961) expand on Batchelor's analysis and assume an exponential correlogram with length scale l to derive an equation for the growth of a puff:

$$\frac{d\sigma}{dx} = 2\beta i^2 \int_0^\infty \frac{n^2}{(1+n^2)^2} \left[\frac{1 - e^{-r^2 n^2}}{nr} \right] dn \quad (6.2)$$

where $i = \sigma_v/u$ is the intensity of turbulence, $r = \sigma/l$, and $n = \kappa l$ (κ is wave number). The weighting function (in brackets) is, in effect, a filter function analogous to that used in the statistical theory for

continuous plumes. This filter function tells us that eddies with sizes roughly equal to the size of the puff or cluster are most important for the growth of the puff. In contrast, eddies with sizes much less or much greater than the size of the puff contribute little to the puff diffusion. The filter can be thought of as a window that passes eddy sizes between roughly $\sigma/2$ and 5σ . The argument for the lack of contribution from small eddies is the same for plume and puff diffusion: small eddies move particles inside the plume or puff with little influence on diffusion. Large eddies merely transport a puff bodily. On the other hand, large eddies can contribute to the diffusion of a plume from a fixed axis. This situation is simply summarized in Table 6.1.

Table 6.1 Influence of Eddy Sizes on Puff and Plume Diffusion

Diffusion type	Size range of eddies contributing to diffusion
Plume	Only eddies with sizes greater than u times travel time and less than u times sampling time
Puff	Only eddies with sizes close to the puff size (\pm factor of 3)

Once the standard deviation (σ) of the distribution of material in a puff is known, the concentration (C) of material can be calculated by the Gaussian formula:

$$C = \frac{Q_p}{(2\pi)^{1/2} \sigma^3} e^{-r^2/2\sigma^2} \quad (6.3)$$

where Q_p represents emissions (in mass per second) and diffusion is assumed to be isotropic (i.e., the same in all directions). The variable r is the radial distance from the puff center. Richardson (1926) recognized the dependence of puff diffusion on puff dimension when he used empirical data at many scales to derive an expression for the effective eddy diffusivity for puffs:

$$K = 0.2\sigma^{4/3} \quad (6.4)$$

where K has units of square meters per second and σ has units of meters.

The main result of the difference between plume and puff diffusion is that there is a region in which puff growth is greater than plume growth. This occurs when the puff is growing through sizes within the inertial subrange of the energy spectrum, where the spectral energy is rapidly increasing as eddy size increases. A precise formulation of this effect is better given by similarity theory.

6-3 SIMILARITY APPROACH

Batchelor (1952) isolated the basic physical parameters involved in puff diffusion and used them to derive similarity formulas. For example, he reasoned that at short times, when the puff dimensions were at scales within the inertial subrange, the rate of diffusion of the puff ($d\sigma^2/dt$) was a function of the eddy dissipation rate (ϵ), the time after release (t), and the initial size of the puff (σ_0):

$$\frac{d\sigma^2}{dt} \propto t(\epsilon\sigma_0)^{2/3} \quad (6.5)$$

or

$$\sigma^2 = \sigma_0^2 + c_1 t^2 (\epsilon\sigma_0)^{2/3} \quad (6.6)$$

In practice, this diffusion law applies for only a few seconds. At longer times, when the puff has forgotten its initial size, the following similarity law is valid:

$$\frac{d\sigma^2}{dt} \propto \epsilon t^2 \quad (6.7)$$

or

$$\sigma^2 = c_2 \epsilon t^3 \quad (6.8)$$

The constant c_2 has been evaluated from a few experiments and is generally thought to be of order unity. Most experiments yield the relation $0.5 < c_2 < 2$.

At still longer times, when the puff dimensions are at scales larger than the eddy sizes in the inertial subrange, the rate of puff diffusion becomes equal to the rate of plume diffusion.

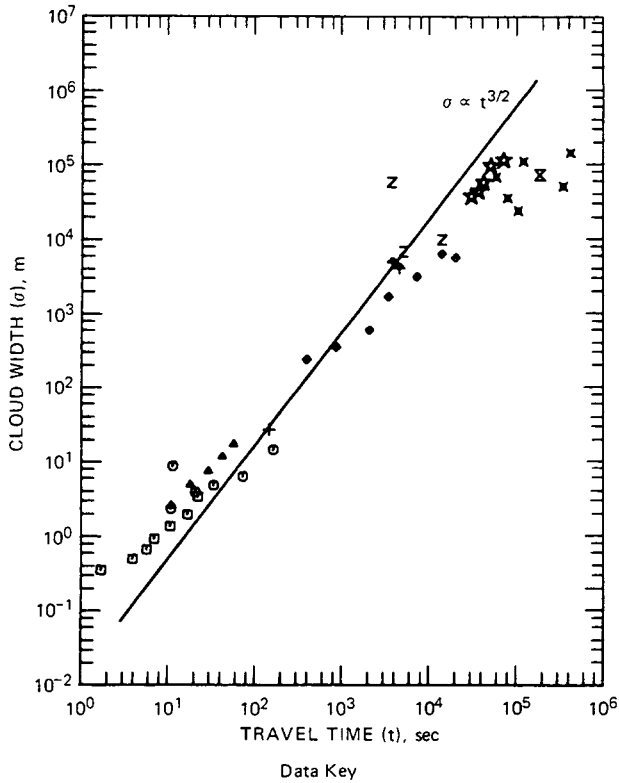
$$\lim_{t \rightarrow \infty} \sigma_{\text{puff}}^2 = \sigma_{\text{plume}}^2 \quad (6.9)$$

Using these formulas, we can summarize the differences between puff and plume diffusion (Table 6.2).

Table 6.2 Comparison of Puff and Plume Diffusion

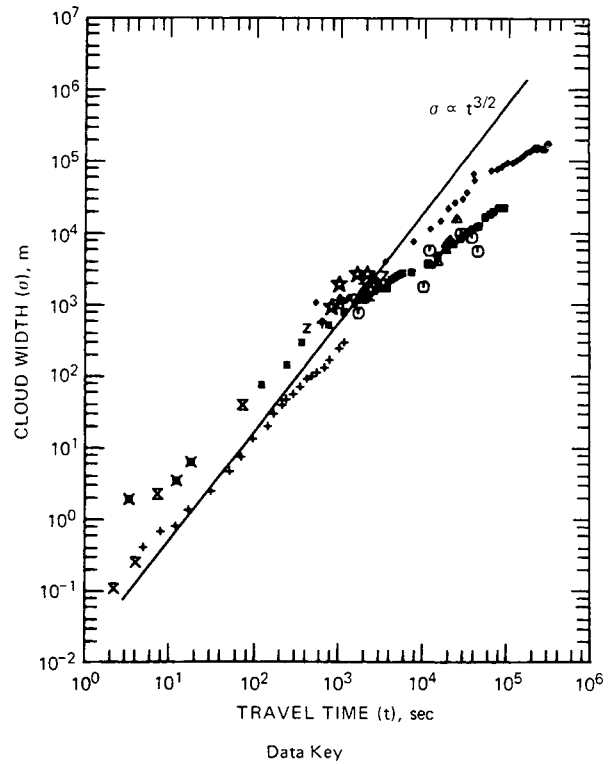
	Short times		Long times	
Puff	$\sigma \propto t$	(very short t)	$\sigma \propto t^{1/2}$	($t > T_L$)
	$\sigma \propto t^{3/2}$	(intermediate)		
Plume	$\sigma \propto t$	($t < T_L$)	$\sigma \propto t^{1/2}$	($t > T_L$)

The $\sigma \propto t^{3/2}$ regime does show up in puff diffusion observations, as shown in Figs. 6.2 and 6.3 (Gifford, 1977). These data include radioactive clouds, tetroon



- Data Key
- Frenkiel and Katz (1956)
 - Seneca (1955)
 - ▲ Smith and Hay (1961)
 - + Högström (1964)
 - ◆ Pack and Angell (1963)
 - ◆ Crozier and Seely (1955)
 - Z Braham, Seely, and Crozier (1952)
 - ✕ Machta et al. (1957)
 - ✕ Heffter (1965)
 - ★ Crawford (1966)

Fig. 6.2 Ten tropospheric experiments on relative diffusion. [From F. A. Gifford, *Tropospheric Relative Diffusion Observations, J. Appl. Meteorol.*, 16: 312 (1977).]



- Data Key
- Angell et al. (1971)
 - Peterson (1968) Outbound
 - ▲ Peterson (1968) Inbound
 - + Byzova et al. (1970)
 - ◆ Randerson (1972)
 - ◆ Davies (1959)
 - ✕ Edinger (1952)
 - Z Kao and Wendell (1968)
 - ✕ Roberts (1923)
 - ✕ Kazanski and Monin (1957)
 - ★ Smith and Hefferman (1956)
 - Hanna (1975)

Fig. 6.3 Twelve tropospheric experiments on relative diffusion. [From F. A. Gifford, *Tropospheric Relative Diffusion Observations, J. Appl. Meteorol.*, 16: 312 (1977).]

pairs, photographs of plumes, artillery bursts, and soap bubbles. Typically a $t^{3/2}$ law is valid over part of the range of most experiments, although a $t^{1.0}$ law seems to give the best agreement over the largest part of the figure. The figures show that the $\sigma \propto t^{3/2}$ region is not often present at large times owing to the presence of mesoscale and synoptic scale eddies (high and low pressure systems).

In an attempt to develop a theory for σ_y that fits both puff and plume observations, Gifford (1981) began with the statistical equation (5.20), $v'(t) = v'(t - \Delta t) R(\Delta t) + v''$. Here the lateral component (v') is used instead of the component u' . He recognized that this is a form of Langevin's equation:

$$\frac{dv'}{dt} + \beta v'(t) = \eta(t) \quad (6.10)$$

where η is a random acceleration and β^{-1} equals the Lagrangian turbulence time scale T_{Lv} . A solution to Eq. 6.10 is as follows:

$$\begin{aligned} \frac{\sigma_y^2}{2 K_y t} = & \frac{t}{T_{Lv}} - (1 - e^{-t/T_{Lv}}) \\ & - 0.5 \left(1 - \frac{v_0^2 T_{Lv}}{K_y} \right) (1 - e^{-t/T_{Lv}})^2 \end{aligned} \quad (6.11)$$

where the eddy diffusivity (K_y) applies to the entire flow, i.e., it is strictly a large-scale quantity, and v_0 is the initial velocity at the source. If Eq. 6.11 is averaged over all possible initial velocities (v_0), then Taylor's solution (Eq. 5.8) for diffusion from a continuous source is obtained. For fixed v_0 , however, the above solution applies to instantaneous (puff) diffusion at small times. As time increases, the solution approaches the Fickian equation, $\sigma_y^2 = 2 K_y t$.

Equation 6.11 was compared by Gifford (1981) with the field observations in Figs. 6.2 and 6.3, assuming that $K = 5 \times 10^4 \text{ m}^2/\text{sec}$, $v_0 = 0.15 \text{ m/sec}$, and $T_{Lv} = 10^4 \text{ sec}$. The resulting curve provided a good fit to the observations for all travel times.

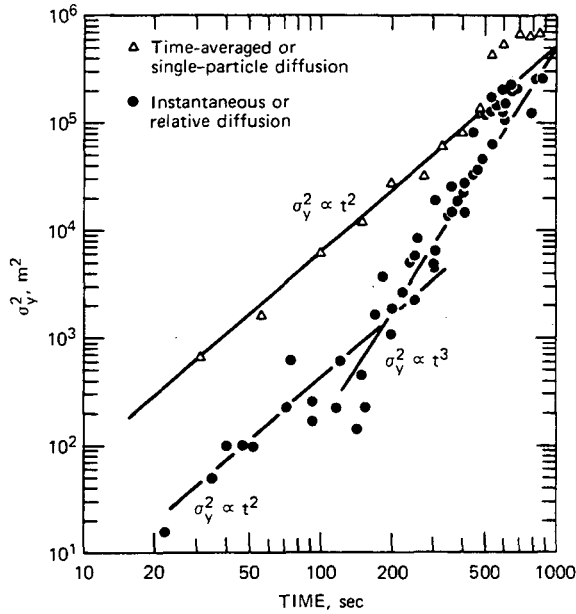


Fig. 6.4 Chart of σ_y^2 vs. time for instantaneous and time-averaged plumes. (From C. J. Nappo, *Relative and Single Particle Diffusion Estimates Determined from Smoke Plume Photographs*, in *Proceedings of the Fourth Symposium on Turbulence, Diffusion, and Air Pollution*, Jan. 15-19, 1979, American Meteorological Society, 1979.)

6.4 APPLICATIONS

We have a few theories for puff diffusion and a data set that is several orders of magnitude smaller than the data set for plume diffusion. There is no ordering of the σ curves by stability in Figs. 6.2 and 6.3. It is no wonder, then, that many applied models for puff diffusion slip back and use plume σ 's.

We recommend using Batchelor's formula,

$$\sigma_y^2 = \epsilon t^3$$

for puff travel times that are less than 10^4 sec. The eddy dissipation rate should be evaluated locally at first and then at a height midway in the boundary layer as σ approaches $0.3z_i$. Equation 1.42 and the equations in Chap. 1, Sec. 1.5 can be used to calculate ϵ . For travel times greater than 10^4 sec, the constant c_3 in the formula $\sigma_y = c_3 t$ should be fitted so that $c_3 = \epsilon^{1/2} (10^4 \text{ sec})^{1/2}$; i.e., the two curves intersect at $t = 10^4$ sec. A similar procedure is used for σ_z except that $\sigma_z = 0.3z$ for all times after σ_z first attains that value.

A photograph of a continuous plume yields information about puff diffusion since the sampling time is essentially zero. The results of an experiment by Nappo (1979) are shown in Fig. 6.4. Four

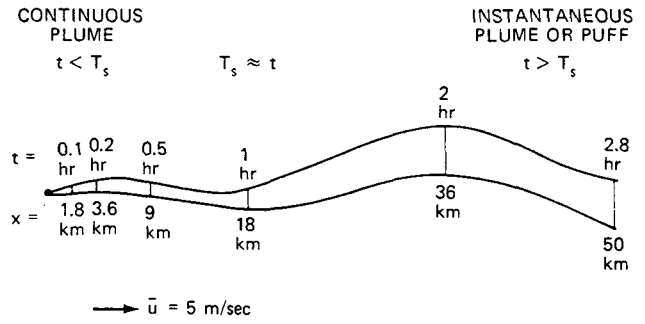


Fig. 6.5 Diagram of plume sampled by an aircraft for 1 hr ($T_s = 1$ hr) at the downwind distances indicated. When travel time (t) is less than T_s , the observed distribution indicates a continuous plume. When t is greater than T_s , the observed distribution indicates an instantaneous plume or puff.

photographs taken by a U-2 aircraft of a large oil fog plume are first analyzed individually and then used to form a composite plume. As shown, σ is proportional to $t^{3/2}$ for the individual photographs (puff diffusion), as predicted by our theory.

Figure 6.5 illustrates another case in which the results of a single experiment can provide information on puff diffusion, plume diffusion, and a combination of the two. Suppose a long power-plant plume is sampled by several aircraft over a period of 1 hr. Each aircraft flies through cross sections of the plume at a given distance downwind for the whole hour. The wind speed is 5 m/sec. During a travel time that is equal to the sampling time, the plume covers a distance of 18 km. Thus, for downwind distances (x) less than about 10 km, the aircraft observations yield information about continuous plume diffusion. For x greater than about 30 km, the aircraft observations are related more to puff diffusion. Most photographs and aircraft observations of plumes at great distances ($x > 50$ or 100 km) are useful only in that they give us information on puff diffusion.

Problems

1. The following table contains a variety of travel times and sampling times for a continuous plume. In

Sampling time	Travel time			
	0.1 sec	10 sec	10 min	10 hr
2 sec				
1 min				
30 min				
2 hr				
2 days				

the boxes write either "puff" or "plume," depending on which kind of diffusion analysis is appropriate.

2. With the use of Fig. 6.2 and Richardson's formula, plot a graph of K_y vs. travel time over the range of travel times from 1 sec to 10^7 sec.

3. Suppose a puff of 100 dandelion seeds is suddenly released from the top of a 100-m-high tower. Assume that $\epsilon = u_*^3/0.4z$ and $u_* = 0.2$ m/sec. Calculate the density of dandelion seeds in the center of the puff after a travel time of 100 sec. Assume $c_2 = 1.0$.

4. Assume you are conducting a field experiment in which a long power-plant plume is being sampled by lidar on an aircraft. You take only a 5-sec traverse at each downwind distance, with distances greater than 1 km from the power plant. Wind speed is 3 m/sec. Are you measuring plume or puff diffusion? Suppose you take several traverses over a time period of 20 min at each downwind distance and average the results. At what distance from the power plant does the meaning of your measurement change from plume to puff?

Similarity Models of Diffusion

7-1 INTRODUCTION

Useful models of diffusion are often possible to derive if the important variables and governing parameters for a problem are known. Such models are called similarity models because they imply "similar" behavior of the atmosphere from one place or time to another if we assume that certain parameters, such as z_i/L or z/z_0 , are held constant. The techniques that lead to similarity models are sometimes called dimensional analysis.

The first step in developing a similarity model is to isolate all the variables and parameters that apply to a problem. In general, if there are n variables and parameters (a_1, a_2, \dots, a_n) of m different units (e.g., grams and seconds), then $n - m$ dimensionless independent numbers can be formed. For example, consider the wind speed in an unstable surface layer. We have the parameters u (in meters per second), u_* (in meters per second), z (in meters), z_0 (in meters), and L (in meters) and can conclude that $5 - 2 = 3$ independent dimensionless numbers can be formed:

$$\frac{u}{u_*} = f(z/z_0, z/L)$$

which we know from Chap. 1 is a solution to the problem.

If $n - m$ equals 1, then we know the solution to the problem to within a constant factor. This is how Briggs arrived at some of his plume-rise predictions in Chap. 2. For example, plume rise Δh (m) in a calm, stable environment is a function of initial plume buoyancy flux F_0 (m^4/sec^3) and environmental stability s (sec^{-2}). Therefore $n - m = 3 - 2 = 1$, and we can write the universal similarity formula $\Delta h = C_1 F_0^{1/4} s^{-3/8}$. The powers $1/4$ and $-3/8$ are necessary to make the units correct, and the constant C_1 can be determined by plotting observations of Δh vs. $F_0^{1/4} s^{-3/8}$. This formula is found to be valid for plume rises Δh ranging from centimeters to kilometers.

In Chap. 6 we showed how similarity theory could be satisfactorily applied to the diffusion of a puff in the inertial subrange, where the important variables and parameters are σ , ϵ , and t .

In this chapter the discussion is restricted to the diffusion of continuous plumes released near the ground in the surface boundary layer. Detailed derivations of this theory are given by Gifford (1968, pp. 88-90), Pasquill (1974, pp. 116-123), Monin and Yaglom (1971, Chap. 5), and Horst (1979).

7-2 DIFFUSION OF CONTINUOUS PLUMES IN THE SURFACE LAYER

7-2.1 Neutral Conditions

In the first example neutral conditions are assumed. As a result, the stability parameter z/L does not enter the problem. In our search for important governing parameters, we look for parameters that are constant in the surface layer ($0 < z \lesssim 50$ m). The friction velocity u_* is one such parameter, and it is known to be an important scaling velocity for the wind profile. Several people independently postulated the equation

$$\frac{d\bar{z}}{dt} = cu_* \quad (7.1)$$

where \bar{z} is the mean height at time t after release of particles released continuously from some point near the ground. This equation can be converted from $d\bar{z}/dt$ to $d\bar{z}/d\bar{x}$ by dividing by the wind speed. However, the wind speed transporting the plume is effective at height $a\bar{z}$. Pasquill recommended, on theoretical grounds, that $c = 0.4$ and $a = 0.56$. Horst (1979) recommends $a = 0.63$ in neutral conditions, with a between 0.5 and 0.6 in unstable conditions

and 0.8 to 0.9 in stable conditions. With the use of $u = (u_*/0.4) \ln(z/z_0)$, Eq. 7.1 can be written in the form

$$\frac{d\bar{z}}{d\bar{x}} = \frac{0.16}{\ln(\bar{z}/z_0)} \quad (7.2)$$

which can be integrated, by using $\bar{z} = z_0$ at $\bar{x} = 0$, with $a = 0.56$, to give the solution

$$\frac{\bar{x}}{z_0} = 6.25 \left(\frac{\bar{z}}{z_0} \ln \frac{\bar{z}}{z_0} - 1.58 \frac{\bar{z}}{z_0} + 1.58 \right) \quad (7.3)$$

This solution is plotted in Fig. 7.1.

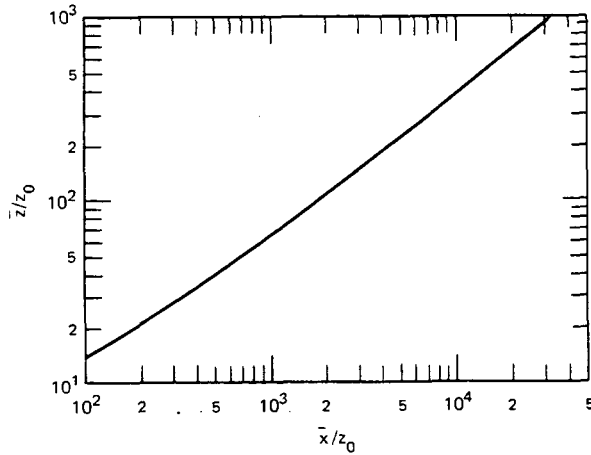


Fig. 7.1 Solution to Eq. 7.3 for the variation of mean cloud height (\bar{z}/z_0) with distance downwind (\bar{x}/z_0) for ground-level sources in a neutral boundary layer.

The only information this analysis gives is the mean height of the plume. It does not tell anything about the vertical distribution of material in the plume, which is not necessarily Gaussian because of the nearness of the ground and the strong wind shear. Several observations of crosswind-integrated concentration C' in the surface layer due to continuous releases are summarized by Horst (1979), who found that the following equation is valid:

$$\frac{C'(\bar{x}, z)}{C'(\bar{x}, 0)} = \exp \left[- \left(\frac{z}{b\bar{z}} \right)^r \right] \quad (7.4)$$

The factor b equals $\Gamma(1/r)/\Gamma(2/r)$, where Γ is the gamma function (which is partially tabulated in Table 8.1). The Gaussian distribution value $r = 2$ (which gives $b = 1.77$) is an overestimate except for fairly stable conditions, the value $r = 1.5$ (which gives $b = 1.52$) is valid for nearly neutral conditions, and r

is less than 1.5 for unstable conditions. The concentration is not very sensitive to the value of a used in Eq. 7.2.

One final equation is needed to obtain concentration predictions with this technique. We are dealing here with crosswind-integrated concentrations: $C'(x, z) = \int_{-\infty}^{\infty} C(x, y, z) dy$. Then the mass continuity condition is given by the equation

$$\int_0^{\infty} u(z) C'(x, z) dz = Q \quad (7.5)$$

where Q is the continuous-source strength. By substituting Eq. 7.4 into Eq. 7.5, we get the solution under neutral conditions for the variation of crosswind-integrated ground-level concentration with downwind distance,

$$C'(x, 0) = \frac{(0.4Q/u_*z_0)}{\int_1^{\infty} \ln(z/z_0) \exp[-(z/b\bar{z})^r] d(z/z_0)} \quad (7.6)$$

which must be solved numerically. (An analytical solution for the integral is available if $r = 2$.) Horst (1979) gives a graphical solution that can be approximated by the simple power-law formula:

$$\frac{u_*z_0 C'(x, 0)}{0.4Q} = 2.4 \left(\frac{x}{z_0} \right)^{-0.96} \quad (7.7)$$

This formula is within 10% of his curve for dimensionless distances x/z_0 ranging from 10^2 to 10^7 .

Before these equations are applied out to x/z_0 equal to 10^7 , they should be checked to determine if the mean plume height (\bar{z}) is still within the surface layer. Remember that we are assuming that friction velocity (u_*) is constant and that the wind profile is logarithmic, assumptions that are valid only for \bar{z} less than about 50 or 100 m. For typical z_0 values, this will limit downwind distance \bar{x} to just a few kilometers. Also, a ground-level source has been assumed.

7.2.2 Nonneutral or Adiabatic Conditions

In nonneutral or adiabatic conditions, Eq. 7.1 must be rewritten to include a dependence on the stability parameter (z/L):

$$\frac{d\bar{z}}{dt} = cu_* f(z/L) \quad (7.8)$$

Chaudhry and Meroney (1973) assume that

$$f(z/L) = \phi_h^{-1}(z/L) \quad (7.9)$$

where ϕ_h is the dimensionless temperature gradient given by Eq. 1.36:

$$\begin{aligned} \phi_h(z/L) &= 0.74 \left(1 - 9 \frac{z}{L}\right)^{-1/2} && \text{(unstable)} \\ &= 0.74 + 5 \frac{z}{L} && \text{(stable)} \end{aligned}$$

This result follows from their assumptions that $f(z/L)$ is similar to the stability-dependent term in the eddy diffusivity formula ($K = 0.4u_*z/\phi$) and that the eddy diffusivity for pollutant equals the eddy conductivity for heat.

As in Sec. 7-2.1, the dependence on time in Eq. 7.8 is converted to a dependence on downwind distance x through the relation: $d\bar{x}/dt = u(a\bar{z})$. However, the wind-speed function, as given by Eq. 1.37, is more complicated than in the neutral calculation. The procedures used in the last section give the following equation for the crosswind-integrated surface concentration:

$$C'(x,0) = \frac{Q/z_0}{\int_1^\infty u(z/z_0, z/L) \exp[-(z/b\bar{z})^r] d(z/z_0)} \quad (7.10)$$

Fortunately Horst (1979) has already solved this equation on the computer for 15 values of z_0/L ranging from -10^{-2} to 10^{-2} , yielding the graph of normalized C' given in Fig. 7.2. He assumed that the

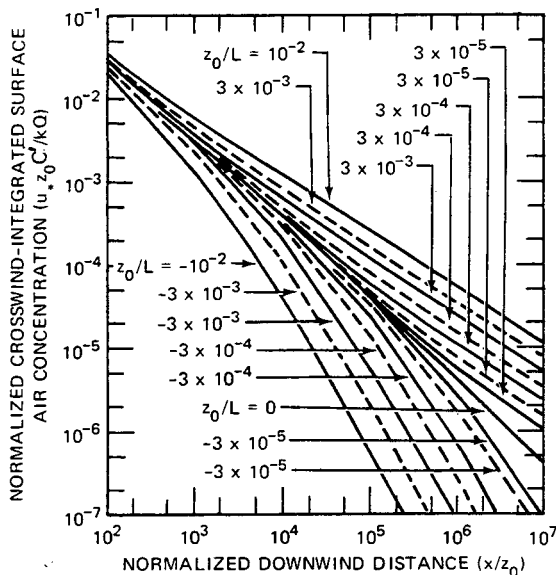


Fig. 7.2 Predicted crosswind-integrated concentration at ground level as a function of downwind distance for various stability conditions. [From T. W. Horst, Lagrangian Similarity Modeling of Vertical Diffusion from a Ground Level Source, *J. Appl. Meteorol.*, 18: 734 (1979).]

vertical distribution parameter (r) equaled 1.5 for all stabilities. The following simple empirical formulas provide a satisfactory fit (\pm factor of 2) to the most stable and unstable curves:

At $z_0/L = 10^{-2}$

$$\frac{u_* z_0 C'(x,0)}{0.4Q} = 0.75 \left(\frac{x}{z_0}\right)^{-0.69} \quad (7.11)$$

At $z_0/L = -10^{-2}$

$$\frac{u_* z_0 C'(x,0)}{0.4Q} = 35 \left(\frac{x}{z_0}\right)^{-1.54} \quad (7.12)$$

Horst tested his predictions by using observations of crosswind-integrated ground concentration from the Prairie Grass diffusion experiment (Barad, 1958) and an experiment at Idaho Falls (Isplitzer and Dumbauld, 1963). He found good agreement for all stabilities at distances x/z_0 out to 2×10^5 .

The concentrations (C') calculated above refer to crosswind-integrated values. The actual point concentrations at the ground [$C(x,y)$] at a crosswind distance y from the plume axis can be calculated from Eq. 7.7 or 7.10 or from Fig. 7.2 by the following conversion:

$$C(\bar{x},y,0) = \frac{C'(\bar{x},0)}{(2\pi)^{1/2} \sigma_y} \exp\left(-\frac{y^2}{2\sigma_y^2}\right) \quad (7.13)$$

The dispersion parameter (σ_y) can be obtained through standard techniques outlined in Chap. 4. In fact, the published Pasquill-Gifford σ_y curves were based on concentration measurements taken at ground level for emissions at ground level.

7-3 DIFFUSION IN THE FULL DEPTH OF THE DAYTIME PLANETARY BOUNDARY LAYER

Other basic theories of diffusion owe their existence to the similarity approach. A good example of this is the problem of diffusion in the full depth of the daytime planetary boundary layer. Recent experiments in Minnesota and England show that important scaling parameters for this problem are the mixing depth (z_i) and the convective velocity scale (w_*), which is defined by Eq. 1.41:

$$w_* = \left(\frac{g w' T_0' z_i}{T}\right)^{1/2} = \left(-\frac{z_i}{0.4L}\right)^{1/2} u_*$$

We can postulate the similarity formula

$$\frac{\sigma_y}{z_i} = \frac{C_2 w_* t}{z_i} \quad (7.14)$$

and find that this formula is indeed valid, with $C_2 = 0.56$, for times less than the Lagrangian time scale. The Lagrangian time scale (T_{Lv}) is given by another similarity formula:

$$T_{Lv} = 0.15 \frac{z_i}{\sigma_v} \quad (7.15)$$

where σ_v is a function of z_i/L and w_* . In general, we find that any distance variable (l) and speed variable (s) in the daytime planetary boundary layer are described by the similarity formulas

$$\frac{l}{z_i} = f(tw_*/z_i, z_i/L, z/z_i, z_i/z_0) \quad (7.16)$$

$$\frac{s}{w_*} = g(tw_*/z_i, z_i/L, z/z_i, z_i/z_0) \quad (7.17)$$

where f and g are universal functions.

Lamb (1979) has used the turbulence fields from Deardorff's (1974) numerical model of the daytime planetary boundary layer to calculate the maximum concentration expected from effective release heights (z_r) greater than about $0.025z_i$. The calculated maximum ground-level concentration (C_{max}) and the distance (x_{max}) at which it occurs are given by the formulas

$$C_{max}(x, 0, 0) \approx 1.2 \frac{Q}{z_r z_i u} \quad (7.18)$$

$$x_{max} \approx 2z_r \frac{u}{w_*} \quad (7.19)$$

The result in Eq. 7.18 implies that $C_{max} \propto z_r^{-1}$, which is in disagreement with the prediction of the Gaussian model (given by Eq. 4.9) that $C_{max} \propto z_r^{-2}$. Observation of fumigation in daytime conditions is not detailed enough to permit selection of one model over another.

Problems

1. With the use of the same coefficient C_1 as that derived on Earth, would you expect the plume-rise equation $\Delta h = C_1 F_0^{1/4} s^{-3/8}$ to be valid on Mars? Why?

2. What is the ground-level crosswind-integrated concentration during neutral conditions at a distance of 200 m from the source for roughness (z_0) equal to 1 cm, friction velocity (u_*) equal to 0.5 m/sec, and surface source strength (Q) equal to 10 g/sec? Calculate the concentration on the plume axis assuming $\bar{\sigma}_\theta = 0.1$ radian.

3. Assume that the roughness length equals 0.3 cm. There is a continuous source of strength of 5 g/sec. What is the ratio of the ground-level crosswind-integrated concentration for L equal to 10 m to the ground-level crosswind-integrated concentration for L equal to -10 m at a downwind distance of 300 m? How do plume axis concentrations compare with those made by using the standard Gaussian formula? (Assume same σ_y for both methods.)

4. The mean height (\bar{z}) can be calculated for the standard Pasquill-Gifford-Turner Gaussian plume model (half of area of Gaussian curve is within 0.67σ) for a surface-level source with full reflection. Calculate the variation with x of \bar{z} for neutral conditions for the Gaussian model and compare it with Fig. 7.1 for $z_0 = 1$ cm. How far apart are the two \bar{z} estimates at $x = 100$ m?

Gradient Transport (K) Models

8-1 THE BASIC GRADIENT TRANSPORT MODEL

Chapter 1, Sec. 1-4, gives a derivation of the continuity equation for a substance (C), where turbulent fluxes of C are assumed to be proportional to the mean gradient of C:

$$\overline{-w'C'} = K_z \frac{\partial C}{\partial z} \quad (8.1)$$

The basic gradient transport model can be written:

$$\begin{aligned} \frac{\partial C}{\partial t} + u \frac{\partial C}{\partial x} + v \frac{\partial C}{\partial y} + w \frac{\partial C}{\partial z} = S + \frac{\partial}{\partial x} K_x \frac{\partial C}{\partial x} \\ + \frac{\partial}{\partial y} K_y \frac{\partial C}{\partial y} + \frac{\partial}{\partial z} K_z \frac{\partial C}{\partial z} \end{aligned} \quad (8.2)$$

So-called cross-diagonal terms, such as $\partial/\partial x (K_{xy} \partial C/\partial y)$, are not included here, because they are usually insignificant.

It is important to point out that certain time and space scales are implicit in the diffusion equation. The mean wind components (u, v, and w) and mean concentration (C) represent averages over a time scale (T_a) and space scale (x_a). Velocity fluctuations with time and space scales less than these values are considered turbulence and are implicitly included in the K coefficients. However, as shown in Chap. 5, the rate of diffusion of a plume depends on the plume size. This statement contradicts the diffusion equation, which uses constant K's. We can conclude that the diffusion equation is valid only if the size of the plume is greater than the size of the dominant turbulent eddies so that all of the turbulence implicit in K is taking part in the diffusion.

Point sources and the diffusion equation are therefore compatible for vertical diffusion when the source is near the ground, where turbulent eddies are

sure to have scales less than the thickness of the plume. For greater point release heights (e.g., tall stacks), the diffusion equation should not be used until the pollutant of interest is spread out over several hundred meters.

8-2 ANALYTICAL SOLUTIONS

Equation 8.2 is impossible to solve analytically for completely general functional forms for the diffusivities K and wind speeds u, v, and w. Before the days of computers, it was a popular exercise to solve this equation for specific forms for K and u. Carslaw and Jaeger (1959), Pasquill (1974, pp. 108-116), and Sutton (1953) give further details. Many of these cases are highly instructive.

8-2.1 One-Dimensional Equation, Time-Dependent, Constant K, No Wind, Instantaneous Area Source

Consider a simplified form of Eq. 8.2:

$$\frac{\partial C}{\partial t} = K \frac{\partial^2 C}{\partial x^2} \quad (8.3)$$

That concentration (C) varies only with time and distance (x) and that diffusivity (K) is a constant are assumed. Boundary conditions are

$$C \rightarrow 0 \text{ as } t \rightarrow \infty, \text{ all } x$$

$$C \rightarrow 0 \text{ as } t \rightarrow 0, \text{ all } x \text{ except } x = 0$$

$$\int_{-\infty}^{\infty} C \, dx = Q'$$

where Q' is the instantaneous area source strength (mass per unit area). Thus this problem simulates an

instantaneous emission from a very large plane surface. The solution is

$$C = \frac{Q'}{(4\pi Kt)^{1/2}} \exp\left(-\frac{x^2}{4Kt}\right) \quad (8.4)$$

which has Gaussian form with the standard deviation of the distribution (σ) given by the equation

$$\sigma = (2Kt)^{1/2} \quad (8.5)$$

This type of diffusion (constant K) is called Fickian diffusion. The implied relation between σ and K is often used by researchers to estimate the diffusivity (K) from the observed diffusion parameter (σ). However, a quick look at the assumptions made to derive this result tells us that it is likely to be questionable because diffusivity (K) is seldom a constant in space and time.

Note that the $\sigma \propto t^{1/2}$ dependence in Eq. 8.5 is the same as the functional dependence given by Eq. 5.6, the solution to Taylor's statistical diffusion equation at large times. An assumption important for both solutions is that the cloud of pollutants is larger than the space scales of the turbulent eddies. The following relation can be obtained by equating Eqs. 5.6 and 8.5

$$K = \sigma_v^2 T \quad (8.6)$$

where T is the Lagrangian time scale. This equation, like Eq. 8.5, has often been used to estimate the Lagrangian time scale. Again, caution is advisable in applying any of these formulas which are derived under highly restrictive assumptions.

8-2.2 Three Dimensions, Time-Dependent, Constant K, No Wind, Instantaneous Point Source

The solution in Sec. 8-2.1 is simple to expand to three dimensions, which implies diffusion of a puff from an instantaneous point source [$Q_{ip}(\text{mass})$] in an environment with no mean wind. The diffusivity is assumed constant in any given direction but can be different for different directions. The basic equation and boundary conditions are

$$\frac{\partial C}{\partial t} = K_x \frac{\partial^2 C}{\partial x^2} + K_y \frac{\partial^2 C}{\partial y^2} + K_z \frac{\partial^2 C}{\partial z^2} \quad (8.7)$$

$$C \rightarrow 0 \text{ as } t \rightarrow \infty, \text{ all } x, y, z$$

$$C \rightarrow 0 \text{ as } t \rightarrow 0, \text{ all } x, y, z \text{ except } x = 0, y = 0, z = 0$$

$$\int_{-\infty}^{\infty} \int_{-\infty}^{\infty} \int_{-\infty}^{\infty} C \, dx \, dy \, dz = Q_{ip}$$

The solution is

$$C = \frac{Q_{ip}}{(4\pi t)^{3/2} (K_x K_y K_z)^{1/2}} \times \exp\left[-\frac{1}{4t} \left(\frac{x^2}{K_x} + \frac{y^2}{K_y} + \frac{z^2}{K_z}\right)\right] \quad (8.8)$$

This solution, like Eq. 8.4, is Gaussian with standard deviations

$$\begin{aligned} \sigma_x &= (2K_x t)^{1/2} \\ \sigma_y &= (2K_y t)^{1/2} \\ \sigma_z &= (2K_z t)^{1/2} \end{aligned} \quad (8.9)$$

This type of diffusion is also known as Fickian diffusion.

8-2.3 Two-Dimensional, Time-Independent, Variable u and K, Continuous Ground-Level Line Source

Diffusion from an infinite crosswind continuous source is described by the following simplification of Eq. 8.2:

$$u \frac{\partial C}{\partial x} = \frac{\partial(K_z \frac{\partial C}{\partial z})}{\partial z} \quad (8.10)$$

with boundary conditions

$$C \rightarrow 0 \text{ as } x, z \rightarrow \infty$$

$$C \rightarrow \infty \text{ as } x = z \rightarrow 0$$

$$K_z \frac{\partial C}{\partial z} \rightarrow 0 \text{ as } z \rightarrow 0 \text{ and } x > 0$$

$$\int_0^{\infty} uC \, dz = Q_l, x > 0$$

where Q_l (in mass per unit length divided by unit time) is the continuous-line source strength. The third boundary condition ensures that there is no flux of material into the lower boundary (i.e., ground).

Much work has been done on obtaining analytical solutions to this equation for specified functional forms for K_z and u . These solutions should be applied to ground-level sources only, for which eddy sizes are generally less than plume size. Roberts (1923) gave the correct solution for the conditions

$$K_z = K_1 \left(\frac{z}{z_1}\right)^n \quad (8.11)$$

$$u = u_1 \left(\frac{z}{z_1}\right)^m \quad (8.12)$$

The generalized solution is

$$C(x,z) = \frac{Q_I z_1^m (m-n+2)}{2u_1 \Gamma(s)} \left[\frac{u_1}{(m-n+2)^2 z_1^{m-n} K_1 x} \right]^s \times \exp \left[\frac{u_1 z^{m-n+2}}{z_1^{m-n} (m-n+2)^2 K_1 x} \right] \quad (8.13)$$

where $s = (m+1)/(m-n+2)$ and Γ is the gamma function (e.g., Abramowitz and Stegun, 1964, Chap. 6). Representative values of m , n , s , and $\Gamma(s)$ are listed in Table 8.1. The first nine values of $\Gamma(s)$ in

Table 8.1 Gamma Function for Typical Values of s^*

m	n	s	$\Gamma(s)$
0.9	0.1	0.679	1.33
0.8	0.2	0.692	1.31
0.7	0.3	0.708	1.29
0.6	0.4	0.727	1.26
0.5	0.5	0.750	1.23
0.4	0.6	0.778	1.19
0.3	0.7	0.813	1.15
0.2	0.8	0.857	1.11
0.1	0.9	0.917	1.06
0	0	0.5	1.77

*First nine rows assume $m = 1 - n$; last row assumes constant K and u .

Table 8.1 are calculated by using the conjugate power law, $m = 1 - n$, which arises from the surface-boundary-layer relation

$$u_*^2 = K \frac{\partial u}{\partial z} \quad (8.14)$$

Since the stress u_*^2 is constant in the surface boundary layer, it is required that $m = 1 - n$ if $K \propto z^n$ and $u \propto z^m$.

For the simple case of constant u and K ($n = m = 0$; the last column in Table 8.1), the solution is Gaussian:

$$C = \frac{Q_I}{1.23u_1} \left(\frac{u_1}{4K_1 x} \right)^{1/2} \exp \left(-\frac{u_1 z^2}{4K_1 x} \right) \quad (8.15)$$

Note that, if we assume $t \equiv x/u_1$, the standard deviation of the distribution is

$$\sigma = \left(\frac{2K_1 x}{u_1} \right)^{1/2} = (2Kt)^{1/2} \quad (8.16)$$

which is the same result as that obtained for the instantaneous area source in Sec. 8-2.1.

Pasquill (1974) gives references for further analytical solutions under the conditions $u = \text{constant}$ and

$$K \propto (h-z)^a \quad (0 < z < h)$$

$$K \propto z(h-z) \quad (0 < z < h)$$

$$K \propto z \quad (0 < z < h/2)$$

$$K \propto (h-z) \quad (h/2 < z < h)$$

8-2.4 Three-Dimensional, Time-Independent, Constant u and K , Continuous-Point Source at Ground Level

For continuous-point sources at ground level, we can assume that $u \partial C / \partial x \gg \partial(K_x \partial C / \partial x) / \partial x$; i.e., advection dominates diffusion in the downwind direction. The basic equation is then

$$u \frac{\partial C}{\partial x} = \frac{\partial(K_y \partial C / \partial y)}{\partial y} + \frac{\partial(K_z \partial C / \partial z)}{\partial z} \quad (8.17)$$

$$C \rightarrow 0 \text{ as } x, y, z \rightarrow \infty$$

$$C \rightarrow \infty \text{ as } x, y, z \rightarrow 0$$

$$K_z \frac{\partial C}{\partial z} \rightarrow 0 \text{ as } z \rightarrow 0 \text{ and } x, y > 0$$

$$\int_0^\infty \int_{-\infty}^\infty uC \, dy \, dz = Q, \, z > 0$$

where Q is continuous-point-source strength (mass per time). The approximate solution for u and $K_y = K_z$ equal to constants is

$$C = \frac{Q}{4\pi K_x} \exp \left[-\frac{y^2}{4K(x/u)} - \frac{z^2}{4K(x/u)} \right] \quad (8.18)$$

The problem with this solution is that axial concentration drops off as x^{-1} , whereas observations show that $x^{-1.75}$ is more accurate. The reason for this error is the assumption of constant K , which results in a failure of the diffusion equation to account for rapid diffusion at small times, where we know that σ should be proportional to x . However, the constant K diffusion equation can give us only $\sigma \propto x^{1/2}$.

The only situations for which the solutions described above are accurate are a continuous ground-level line source and a continuous or instantaneous ground-level area source. Here the diffusion scale is always greater than the turbulence scale. These methods are also valid at times or distances downwind beyond which the diffusion scale is larger than the Lagrangian time or distance scale. However,

these techniques should not be used for such situations as local diffusion of a neutrally buoyant effluent from a tall smokestack.

8-3 NUMERICAL SOLUTIONS OF THE DIFFUSION EQUATION

Analytical solutions to the diffusion equation are interesting but are limited in applicability by restrictions on K and u . Furthermore, because of physical limitations, the models should not be applied to elevated point sources. As a result, analytical solutions are no longer widely used. This is in great contrast to computer solutions of this equation, which are very common. Time and space variability in K and u can be handled by carrying a large number of grid points in the computer. Major problems are numerical instabilities and the fact that our knowledge of the distribution of K and u is not up to the potential of the computer.

8-3.1 Numerical Instabilities

Computer solutions are obtained by stepping forward in time or in space. If a random error introduced at some point will amplify indefinitely with each succeeding time or space step, then the solution is said to be numerically unstable. An analysis of Eq. 8.3 shows this:

$$\frac{\partial C}{\partial t} = K \frac{\partial^2 C}{\partial x^2}$$

An explicit finite difference approximation to this equation is

$$C_{i+1,j} - C_{i,j} = \left(K \frac{\Delta t}{\Delta x^2} \right) \times (C_{i,j+1} - 2C_{i,j} + C_{i,j-1}) \quad (8.19)$$

where i is the current time position and j is the current space position (see Fig. 8.1). By writing C in complex form, it can be shown that this solution is numerically stable only if the following condition is met:

$$K \frac{\Delta t}{\Delta x^2} < \frac{1}{2} \quad (8.20)$$

Thus, if the diffusivity (K) is $10 \text{ m}^2/\text{sec}$ (typical daytime boundary layer) and the grid distance (Δx) is 100 m , then the time step (Δt) must be less than 500 sec , or about 8 min . If a time step of 1 hr were

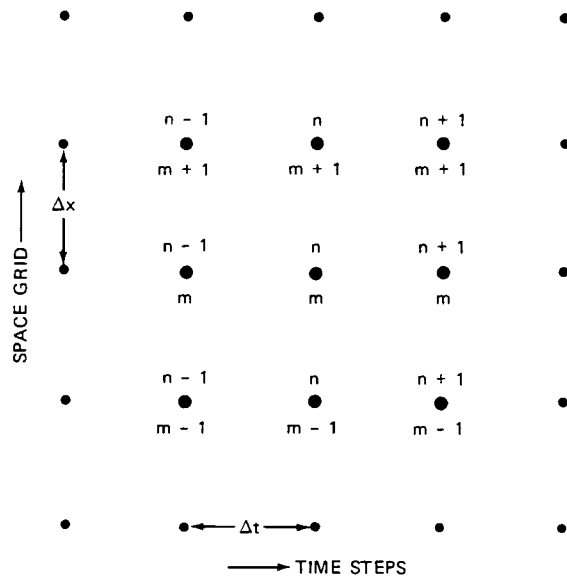


Fig. 8.1 Illustration of numbering system for finite differencing grid.

used in this problem, the numerical solution would “blow up.”

This restriction on Δt can be somewhat relaxed by using more accurate finite difference schemes. Even if the solution is stable, however, there still is some undesirable “diffusion” that appears solely due to the finite difference method. The advection term ($u \partial C / \partial x$) in Eq. 8.2 is especially noted for its contribution to numerical diffusion. A standard technique for studying the diffusive characteristics of a finite difference scheme is to begin with a cosine-shaped hill and then advect it around the edge of a circle by using the equation

$$\frac{\partial C}{\partial t} + u \frac{\partial C}{\partial x} + v \frac{\partial C}{\partial y} = 0 \quad (8.21)$$

The solutions for six different finite difference techniques studied by Long and Pepper (1976) are plotted in Fig. 8.2. In each case the hill is advected once around the circle. The second moment, cubic spline, and Chapeau function do not distort the hill too much. However, numerical diffusion significantly distorts the hill in the donor cell, fully implicit, and Crank–Nicolson schemes. If these schemes were used to solve the diffusion equation, it would be difficult to know if the calculated diffusion was real or numerical.

Other techniques can be used to get around the problem of numerical diffusion. The second-moment scheme devised by Egan and Mahoney (1972) belongs

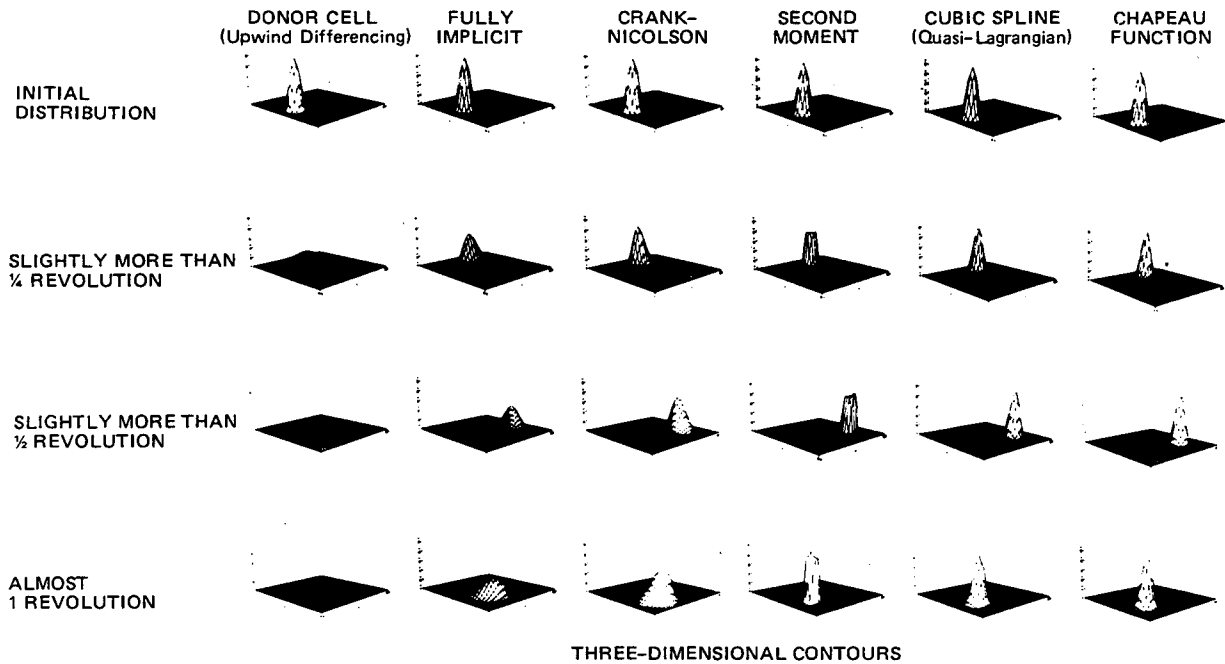


Fig. 8.2 Application of six types of numerical schemes to solve the advection equation (8.21). The initial cosine hill is at the top of each series. The next three figures are the distributions resulting from applications of the numerical schemes to advection in a circle around the plane. (Adapted from Long and Pepper, 1976.)

to this class and was evaluated in the paper by Long and Pepper (1976). Spectral approximations suggested by Prahm and Christensen (1977) are useful but are too complicated to describe here. The Particle-in-Cell (PIC) method (Lange, 1978) is sometimes used, where an effective velocity equal to the actual velocity minus $(K/C) \partial C/\partial y$ is used to transport particles.

It is sobering to think that none of the very extensive work described in this section has anything to do with the *physics* of the diffusion problem. The purpose of this work is solely to speed up the computer calculations and to make them more true to the physical equation.

8-3.2 Specifying the Vertical Diffusivity

In most applications of the gradient transport or diffusion equation at scales less than 10 km, the horizontal diffusivity (K_y) is neglected, but the variation of the vertical diffusivity (K_z) must be known. In addition, the vertical variation of the wind speed must be input to the model. As a result, in the comparison of the Gaussian and the gradient transport models, the question reduces to the relative accuracy of two empirical parameters, σ_z and K_z . At this point, K_z is probably less well known than σ_z at

heights above about $0.1z_i$. The old adage that you cannot get something for nothing applies to the diffusion modeling business also. The gradient transport model may be physically attractive, but it encounters problems when the time comes to specify K_z .

The eddy diffusivity coefficient can be assumed to equal the eddy conductivity coefficient (K_h). In the lowest 50 to 100 m of the atmosphere ($z \lesssim 0.1z_i$), formulas by Businger et al. (1971) (Eqs. 1.36 and 1.39) can be used:

$$K_z = 0.35 \frac{u_* z}{\phi_h(z/L)}$$

$$\phi_h(z/L) = 0.74 \left(1 - 9 \frac{z}{L}\right)^{-1/2} \quad (\text{unstable})$$

$$= 0.74 + 5 \frac{z}{L} \quad (\text{stable})$$

Note that Businger et al. prefer to use 0.35 for von Kármán's constant (k). During daytime conditions and at heights between about $0.1z_i$ and $0.7z_i$, K_z can be assumed constant, with a value equal to its value at $0.1z_i$. Above $0.7z_i$, K_z probably decreases linearly to a small value at the mixing height z_i . This type of behavior was reported by Crane, Panofsky, and

Zeman (1977), who calculated K_z from observed vertical pollutant fluxes $w'C'$ and gradients $\partial C/\partial z$ over Los Angeles during the daytime. At night K_z is quite uncertain above heights of about 50 to 100 m but probably has some small residual value, say $0.1 \text{ m}^2/\text{sec}$.

The coefficient K_z used by Smith (1972) is based on a suggestion by Hanna (1968) (Eq. 1.63):

$$K_z = 0.15\sigma_w\lambda_m$$

where λ_m is the wavelength of peak energy in the w spectrum. The parameters σ_w and λ_m can be calculated for all stability conditions by using Eqs. 1.42 to 1.47, 1.57, 1.59, and 1.82.

In Smith's analysis, he solves the diffusion equation and then extracts σ_z from the calculated concentration distributions. The goal of this work is to devise a revision to the Pasquill-Gifford σ_z curves, where σ_z is dependent on surface roughness as well as on stability.

Other researchers use different formulas for K_z , but common characteristics of these formulas are a linear variation near the ground, a constant value at mid-mixing depth, and a decrease as the top of the mixing layer is approached. For example, Shir (1973) recommends the formula

$$K_z = 0.4u_*ze^{-4fz/u_*} \quad (8.22)$$

which is based on a theoretical analysis of the neutral boundary layer. The depth of the neutral boundary layer is about $0.25 u_*/f$, where f is the Coriolis parameter. Equation 8.22 is plotted in dimensionless form in Fig. 8.3.

8.4 HIGHER ORDER CLOSURE

The derivation of the gradient transport equation in Chap. 1, Sec. 1-4, used assumptions of the form

$$C = \bar{C} + C'$$

This results in the appearance of second-order unknown terms like $\overline{w'C'}$ and $\overline{v'C'}$ in the continuity equation. So that the system can be closed (i.e., reduce the number of unknowns to equal the number of equations), these terms are eliminated by making hypotheses like

$$\overline{w'C'} = K_z \frac{\partial \bar{C}}{\partial z}$$

Now the mean value C is the only unknown in the equation since the diffusivity K_z is assumed to be

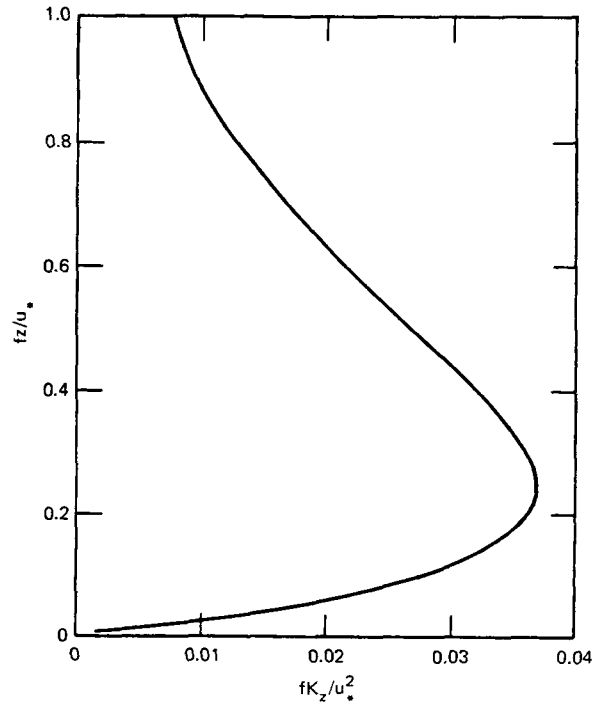


Fig. 8.3 Dimensionless plot of Shir's (1973) formulation for K_z .

known. This method of solution is known as "first order closure." However, this closure assumption is not always valid; for example, at the top of the mixing layer is an upward flux of heat against a positive temperature gradient. Also, as just shown, the diffusivity K_z is highly variable and is not well known in the upper half of the mixing layer.

We can eliminate some of these problems (and generate some new problems) by invoking a higher order closure. Consider the z component of Eq. 1.16,

$$\frac{\partial C}{\partial t} + w \frac{\partial C}{\partial z} = B + S \quad (8.23)$$

Substitute $w = \bar{w} + w'$ and $C = \bar{C} + C'$ into this equation, and use the continuity equation to convert $w \partial C/\partial z$ to $\partial wC/\partial z$. Then, multiplying the equation by w' and averaging yields

$$\frac{\partial}{\partial t} \overline{w'C'} + \frac{\partial}{\partial z} \overline{C w' w'} + \frac{\partial}{\partial z} \overline{w w' C'} + \frac{\partial}{\partial z} \overline{w' w' C'} = \bar{B} + \bar{S} \quad (8.24)$$

We now have an extra equation, for $w'C'$, and a new third-order term: $\overline{w' w' C'}$. At this step second-order

closure is introduced to reduce the number of knowns to the same value as the number of equations.

$$\overline{w'w'C'} = \sigma_w \Lambda \frac{\partial \overline{w'C'}}{\partial z} \quad (8.25)$$

In this expression Λ is an (unknown) length scale. This same procedure could be followed to generate methods of third-order, fourth-order, or whatever-order closure you desire. With each new order a new unrestricted term on the plus side is gained, but there is a longer, more-complicated, string of governing equations on the negative side.

At first sight the introduction of the new length scale Λ appears to be a problem. It turns out, however, that Λ in the second-order scheme is not as variable as K in the first-order scheme. Donaldson's (1973) review of second-order closure models gives methods of estimating Λ . He shows that these models give predictions of boundary-layer winds and turbulence which are in good agreement with observations. However, at this point second-order closure models are useful for basic research only and have not made their way into the field of applied diffusion modeling. They usually consume large amounts of computer core and time.

Problems

1. The wind is blowing from the west at 5.0 m/sec at a height of 5 m perpendicular to a highway with carbon monoxide emissions of $1.0 \text{ g m}^{-1} \text{ sec}^{-1}$. The power law parameter for the wind profile is 0.1, and the diffusivity K_z has a value of $1.0 \text{ m}^2/\text{sec}$ at a height of 5 m. Plot the variation of ground-level concentration with downwind distance from the highway for $x = 5 \text{ m}$ to $x = 200 \text{ m}$. At a height of 20 m, at what downwind distance does the maximum concentration occur?

2. In a numerical model for bomb-debris transport in the upper atmosphere, K_y equals $10^6 \text{ m}^2/\text{sec}$, and the grid distance Δx is 200 km. What is the range of time steps that can be used to ensure numerical stability? Assume that a simple explicit finite difference scheme is being used.

3. Plot the variation of K_z with height up to 100 m by using (1) Businger's formula and (2) Smith's formula. Assume that $L = -100 \text{ m}$ and $z_i = 1000 \text{ m}$.

4. Plot the variation of K_z with height up to 1000 m by using (1) Smith's formula and (2) Shir's formula. Assume that $L = 50 \text{ m}$, $z_i = 1200 \text{ m}$, $u_* = 0.5 \text{ m/sec}$, and $f = 10^{-4} \text{ s}^{-1}$.

Urban Diffusion Models

9-1 IMPORTANCE OF EMISSIONS

An urban area contains thousands, or even millions, of individual sources that range from small sources, such as incinerators, to large sources, such as power plants. The application of a diffusion model to each of these sources is impractical, even if the assumption can usually be made that the contributions of individual sources to the total concentration at a point are additive. Consequently we combine most of the small sources into larger area sources of strength, Q_a (mass per unit time per unit area), and assume that emissions from the ground surface are uniform over that particular area. An example of average annual area source emissions for SO_2 in Frankfurt, West Germany, is given in Fig. 9.1, where a square grid (4 by 4 km) is used. Most area source-emission inventories are given on square grids, although often the grid size may vary over the urban area.

Diffusion from the largest point sources can be calculated individually, and the resulting concentrations at a receptor point can be added to the contribution from area sources. The number of point sources treated this way is usually between 10 and 100. Some pollutants, such as carbon monoxide, have very few point sources, whereas others, such as SO_2 , are mostly emitted from point sources. An accurate emissions inventory is essential for successful urban diffusion modeling. This inventory includes a knowledge of the seasonal, weekly, and diurnal variations of emissions. If emissions are not known within a factor of 2, then the diffusion model has that error imposed on it even before it starts working.

9-2 BOX MODEL

The assumption that emissions in an urban area are constant over a distance Δx , which runs roughly

from one edge of the urban area to the other, is often useful. The pollutant is then assumed to be uniformly mixed in a layer of depth z_i between the ground and the mixing height. The wind speed (u) is assumed constant within the layer (see Fig. 9.2). An additional assumption can be made that the mixing depth is increasing with time ($\partial z_i / \partial t$), as it does in the morning. The concentrations upwind of the city and above the mixing height are C_b and C_a , respectively. Then the continuity equation for this volume is:

$$\Delta x z_i \frac{\partial C}{\partial t} = \Delta x Q_a + u z_i (C_b - C) + \Delta x \frac{\partial z_i}{\partial t} (C_a - C) \quad (9.1)$$

Change in C with time = source + change due to horizontal advection + change due to mixing layer growth and vertical advection

Some simplifications are possible. If conditions are steady state ($\partial C / \partial t = \partial z_i / \partial t = 0$) and the background concentration (C_b) is zero, then the solution is simply

$$C = \frac{\Delta x Q_a}{z_i u} \quad (9.2)$$

This is the well-known box model solution.

Lettau (1970) defines the equilibrium box model concentration given by Eq. 9.2 as C^* and defines a scaling time $\Delta x / u$ as the flushing time required for the air to pass completely over the urban area. Define a nondimensional time $t^* = tu / \Delta x$. Then, if C_b and C_a can be neglected, Lettau's (1970) simplification of Eq. 9.1 can be written:

$$\frac{\partial C}{\partial t^*} = C^* - C \quad (9.3)$$

which has the solution:

$$C = C^* + (C_0 - C^*) e^{-t^*} \quad (9.4)$$

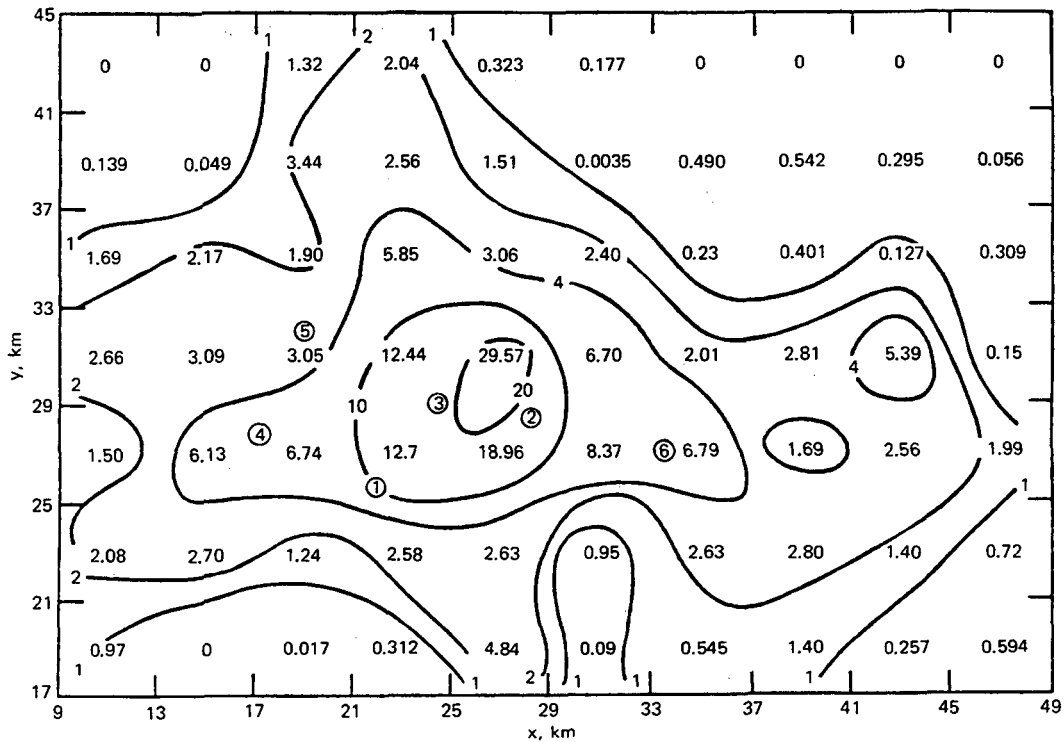


Fig. 9.1 Average annual SO₂ area source emissions (in milligrams per square meter per second) for Frankfurt, W. Germany (Hanna and Gifford, 1977). Emissions are printed in the center of the 4 by 4-km grid squares, and isopleths based on these values are drawn. Monitoring station locations are circled.

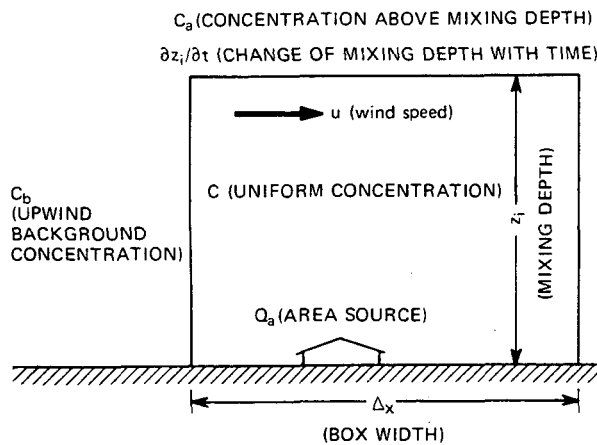


Fig. 9.2 Parameters in box model.

where C_0 is the initial value of concentration. As time (t^*) increases, the concentration (C) in this equation approaches the equilibrium concentration (C^*) given by Eq. 9.2.

Venkatram (1978) points out that, if the source term Q_a suddenly drops to zero in Eq. 9.4, the concentration appears to decrease exponentially, dropping to $0.37 C_0$ after one flushing time $\Delta x/u$ has elapsed, because of the assumption of rapid mixing

and resulting uniform concentration in the box model. Realistically, however, as clean air enters the urban area, the pollutant is swept out; so, after $\Delta x/u$, there should be virtually no pollutant material left in the box. Venkatram suggests instead a "slug model" that gives the following solution for the situation where emissions are suddenly shut off:

$$\frac{C}{C_0} = (1 - t^*) \quad (9.5)$$

However, it should be recognized that a fundamental assumption of the box model is that there are no extreme changes occurring, such as the situation suggested by Venkatram.

The box model is often used as a screening model, where, for example, a government agency might wish to identify a few substances in a long list of toxic chemical emissions that should be singled out for special attention. In many cases, though, the box model has been used as the basic workhorse in a diffusion study, and it has been found to perform quite well. An example of this is the application of a photochemical box model to ozone air quality in Houston, Tex., by Demerjian and Schere (1979). They use Eq. 9.1 and retain the final term relating to

changes due to vertical advection. Ozone is often trapped above the inversion layer over urban areas at night and is mixed down to the surface by the growing mixing layer the next morning. Their application requires a 32-km grid size. The most complicated part of the model is the 36-step chemical kinetic mechanism. They find that predicted hourly concentrations of hydrocarbons, carbon monoxide, NO_x, and ozone are within a factor of 2 of observed concentrations. They had an advantage here that might not be available at other locations in that detailed emission estimates were made as part of an Environmental Protection Agency study in Houston.

9-3 THE ATMOSPHERIC TURBULENCE AND DIFFUSION LABORATORY MODEL

The Atmospheric Turbulence and Diffusion Laboratory (ATDL) urban diffusion model described by Hanna (1971, 1973) and Gifford and Hanna (1973) is essentially a box model with the height of the top lid proportional to the vertical dispersion parameter [$\sigma_z(\Delta x)$] rather than to the mixing depth (z_i). For grid distances (Δx) less than about 10 km, $\sigma_z(\Delta x)$ is significantly less than z_i , which is typically 500 to 1000 m. This model uses the integral form of the Gaussian plume model and treats an area source as an infinite array of infinitesimal point sources of strength $Q_a(x,y)$. The concentration C at point $x = 0$, $y = 0$, $z = 0$ is given by an integration over the upwind half plane (Gifford, 1970):

$$C = \int_0^\infty \int_{-\infty}^\infty \left[\frac{Q_a}{\pi u \sigma_y \sigma_z} \exp\left(-\frac{y^2}{2\sigma_y^2}\right) \right] dy dx \quad (9.6)$$

where sources are assumed to be at ground level. Gifford's (1959b) "narrow plume hypothesis" permits the elimination of the y dependence in Eq. 9.6. As shown in Fig. 9.3, a typical plume that subtends an angle of only 10° to 20° crosses lines of constant Q_a in such a way that little accuracy is lost by assuming that Q_a is a function only of x . In this case Eq. 9.6 becomes

$$C = \int_0^\infty \left[(2/\pi)^{1/2} \frac{Q_a}{u \sigma_z} \right] dx \quad (9.7)$$

This can be written in the form

$$C = (2/\pi)^{1/2} \frac{\Delta x \bar{Q}}{u \bar{\sigma}_z} \quad (9.8)$$

which is equivalent to the equilibrium solution (Eq. 9.2) to the box model.

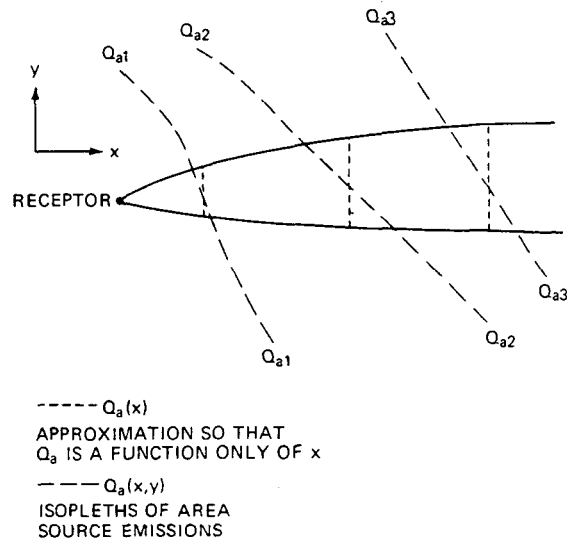


Fig. 9.3 Illustration of narrow plume hypothesis. For most purposes, emissions can be considered a function only of distance x .

Next, the solution must be written in a form consistent with the typical square grid that is used to present urban emissions data. Consider Fig. 9.4, in which the receptor point is located in the center of grid square "0" and upwind grid squares are denoted by subscripts 1, 2, 3, . . . N. The grid size is Δx . The solution is obtained by piecewise integration:

$$C = \frac{(2/\pi)^{1/2}}{u} \left(\int_0^{\Delta x/2} \frac{Q_{a0}}{\sigma_z} dx + \int_{\Delta x/2}^{3\Delta x/2} \frac{Q_{a1}}{\sigma_z} dx + \dots \right) \quad (9.9)$$

We assume that σ_z has the form

$$\sigma_z = ax^b \quad (9.10)$$

Parameters a and b , suggested by Smith (1968), are listed in Table 9.1. The source strength within each grid square is assumed to be constant.

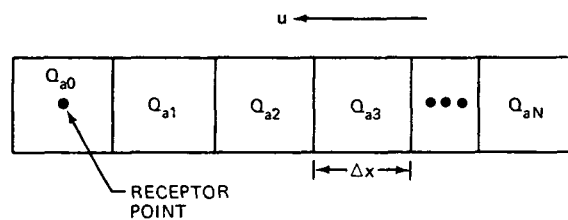


Fig. 9.4 Area source grid pattern assumed in the derivation of Eq. 9.11.

Table 9.1 Parameters a and b in Eq. 9.10

Meteorological conditions	Parameter	
	a	b
Very unstable	0.40	0.91
Unstable	0.33	0.86
Neutral	0.22	0.80
Estimated Pasquill D	0.15	0.75
Stable	0.06	0.71

Smith's (1968) parameters are assumed to apply to both urban and rural regions. The solution is then:

$$C = \frac{(2/\pi)^{1/2} (\Delta x/2)^{1-b}}{ua(1-b)} \left\{ Q_{a0} + \sum_{i=1}^n Q_{ai} [(2i+1)^{1-b} - (2i-1)^{1-b}] \right\} \quad (9.11)$$

Values of the coefficients in the summation term for several values of b and i are given in Table 9.2.

Table 9.2 Values of Summation Term $[(2i+1)^{1-b} - (2i-1)^{1-b}]$ in Eq. 9.11 for Various Stabilities and i Values

i	Stability				
	Very unstable	Unstable	Neutral	Pasquill's D	Stable
1	0.10	0.17	0.25	0.32	0.38
2	0.05	0.09	0.14	0.18	0.22
3	0.04	0.06	0.10	0.13	0.16
4	0.03	0.05	0.08	0.11	0.13
5	0.02	0.04	0.06	0.09	0.11
6	0.01	0.03	0.05	0.08	0.10

Generally, N is the number of grid blocks necessary to reach the upwind edge of the urban area. Equation 9.11 is most valid for time periods of about 1 hr, for which the σ_z values in Table 9.1 apply, and the wind direction and speed are fairly uniform ($\pm 20^\circ$, $\pm 30\%$).

Extension to longer averaging times is made by solving Eq. 9.11 for a variety of wind directions and then weighting each result by the frequency with which the wind blows from that direction. When the wind direction crosses emissions grid squares obliquely, as in Fig. 9.5, an arbitrary scheme must be devised for including the squares in Eq. 9.11. Also, Δx must be multiplied by $1/\cos \Delta\theta$, where $\Delta\theta$ is the departure of the wind direction from north to south or east to west directions ($0 < \Delta\theta < 45^\circ$). A computer program for these computations, which includes provisions for point sources, is given in a report by

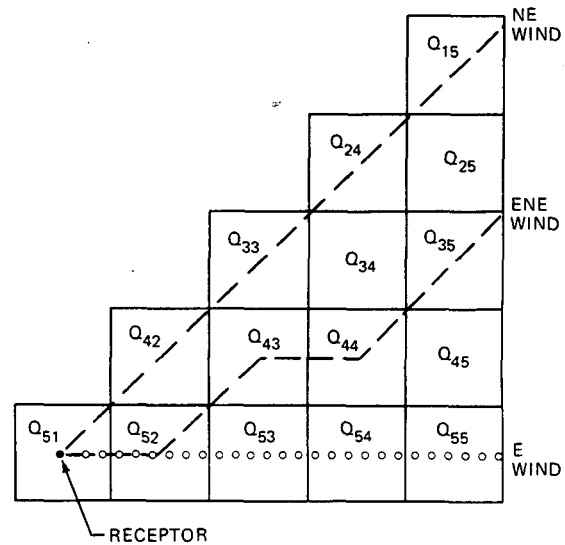


Fig. 9.5 Method of accounting for area source emissions when the wind direction is at an angle to the grid squares.

Hanna (1973). The Gaussian plume model is used for point sources in this program.

After this technique had been applied to several urban areas, it was noticed that the calculated concentration (C) at any receptor was usually proportional to the emissions Q_{a0} in the grid square in which the receptor was located. The reason for this is that the distribution of emissions is usually quite smooth and the coefficients of the upwind Q_{ai} terms in Eq. 9.11 are quite small. For most applications, it is sufficient to use the simple ATDL model, which is obtained by approximating the various source strengths Q_{ai} by Q_{a0} in Eq. 9.11:

$$C = A \frac{Q_{a0}}{u} = (2/\pi)^{1/2} \frac{[\Delta x(2N+1)/2]^{1-b} Q_{a0}}{a(1-b)u} \quad (9.12)$$

The dimensionless parameter A is evaluated in Table 9.3 for several values of $\Delta x(2N+1)/2$ (distance to edge of city) and stabilities. Approximate values for A for unstable, average annual (class D), and stable conditions are 60, 200, and 600, respectively. Slightly different estimates of A might be made if Briggs's proposed formulas for σ_y and σ_z in an urban region (Table 4.8) were used in the derivation following Eq. 9.9. Gifford and Hanna (1973) verified the annual value of 200, using suspended particle data from several U. S. cities, and Hanna (1978) verified the variation with stability, using carbon monoxide data from several cities. SO_2 observations are best

Table 9.3 Evaluation of A in Eq. 9.12 for Various City Sizes and Stabilities

City radius $\Delta x(2N + 1)/2, m$	Stability			Pasquill's	
	Very unstable	Unstable	Neutral	D	Stable
5000	48	57	100	180	545
10000	51	63	115	213	667
20000	54	69	132	258	814

simulated if the parameter A predicted above is divided by four, presumably to account for the fact that most SO₂ sources are elevated. On the other hand, carbon monoxide observations in most cities are best simulated if the parameter A is multiplied by three, presumably to account for the placement of carbon monoxide monitors near busy streets. However, A is calculated to equal about 200 (its value in Table 9.3) from data from the St. Louis Regional Air Pollution Study where monitoring stations are placed away from busy streets in schoolyards and parks. In any case, the model described in this section ideally predicts concentrations over a broad area.

9.4 STREET CANYON AND HIGHWAY SUBMODELS

The box model and the ATDL model can give the average carbon monoxide concentration over a broad area (say 10 by 10 km). In a street canyon or adjacent to a highway in an urban area, there is an additional contribution to the concentration from local sources. In this case the total concentration C is the sum of a spatially averaged C_a and a local ΔC₁ component:

$$C = C_a + \Delta C_1 \quad (9.13)$$

Johnson et al. (1976) outline methods of estimating ΔC₁. Consider the street canyon in Fig. 9.6, where the important variables are defined. If the wind is more or less normal to the street, the equations for the concentration ΔC₁ in the street canyon are:

Lee side,

$$\Delta C_1 = \frac{0.1KNS^{-0.75}}{(u + 0.5)[(x^2 + z^2)^{1/2} + 2]} \quad (9.14)$$

Windward side,

$$\Delta C_1 = \frac{0.1KNS^{-0.75}}{W(u + 0.5)} \quad (9.15)$$

where ΔC = carbon monoxide concentration (ppm)
 N = traffic flow (vehicles/hr)
 S = average vehicle speed (miles/hr)
 u = wind speed at roof level (m/sec)
 W = street width (m)
 x and y = horizontal distance and height (both m) of the receptor point relative to the traffic lane, respectively
 K = dimensionless "best fit" constant

The data suggest that K ≈ 7. For wind directions nearly parallel to the street,

$$\Delta C_1 = \frac{1}{2} [\Delta C_1(\text{windward}) + \Delta C_1(\text{lee})] \quad (9.16)$$

Equations 9.14 and 9.15 are subject to some revision since the average emission rate (e.g., grams of carbon monoxide per vehicle mile) changes with the vehicle vintage and type of mixture, which would thus modify the numerator (source term) of both expressions.

The excess concentration ΔC₁ contributed by a major highway in an urban area is important for perhaps 200 or 300 m downwind of the highway. Many highway diffusion models are referenced by Johnson et al. (1976), but most are based on the Gaussian model for an infinite line source:

$$C_1 = \left(\frac{2}{\pi}\right)^{1/2} \frac{Q_l \exp(-H^2/2\sigma_z^2)}{u\sigma_z \sin \phi} \quad (9.17)$$

where Q_l is line source strength (in mass per unit time per unit length), H is the effective height of emissions (probably 2 or 3 m), and φ is the angle between the

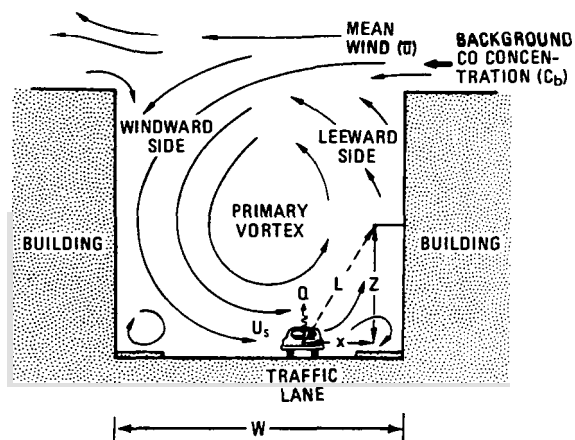


Fig. 9.6 Schematic of cross-street air circulation in a street canyon. [From W. B. Johnson, R. C. Sklarew, and D. B. Turner, Urban Air Quality Simulation Modeling, in Air Pollution, Vol. 1, 3rd ed., Chap. 10, p. 530, A. G. Stern (Ed.), Academic Press, New York, 1977.]

wind direction and the highway. An initial value of σ_z (e.g., 2 or 3 m) is assumed to account for the turbulent wake behind moving vehicles. If d is the perpendicular distance from the highway, then the distance x to be used in evaluating σ_z is $d/\sin \phi$.

9-5 COMPUTERIZED K MODELS FOR URBAN DIFFUSION

In Chap. 8, K diffusion models were discussed. The basic equation was given as well as various techniques for estimating K. Most of the applications of K models to urban diffusion described below took place in the mid-1970's. Anyone interested in using any of these models should consult the original reference since the models and their input and output are too complex to cover fully in this brief summary.

9-5.1 An Urban Diffusion Model That Also Predicts Winds and Temperatures

Pandolfo and Jacobs (1973) applied their K model to estimate carbon monoxide concentrations in Los Angeles. The model was originally developed for studying the dynamics of the three-dimensional planetary boundary layer and includes radiative exchange processes. Basic dependent variables are wind velocity and temperature. The diffusion equation was easy to add to the list of governing equations since the pollutant concentration has little feedback to the other equations. The model accounts for sloping terrain through the continuity equation.

With all the sophistication of this model, it is surprising that the carbon monoxide predictions made by this model are no better correlated with observations ($R = 0.6$ to 0.8) than predictions made by other models that did not include weather variables. The explanation is apparently that the other models used the most recent observed winds and temperatures at each stage, which are more accurate than the weather predictions of the Pandolfo and Jacobs (1973) model. There seems to be a paradox: to run a complex model, we need good observations of initial and boundary data from a network of instruments. However, if these instruments are in place and operating, there is often no longer a need for the complex model.

9-5.2 Trajectory Models

In a trajectory model, a box with dimensions of 1 to 5 km is allowed to move with the observed wind,

which picks up pollutants emitted by the areas it passes over. Vertical diffusion takes place by means of a vertical K_z coefficient. Eschenroeder, Martinez, and Nordsieck (1972) developed a model of this type for application to photochemical pollution in Los Angeles. The advantage of the trajectory model is that calculations must be made for only those few trajectories which end at the monitoring stations.

9-5.3 Grid Models with Winds Prescribed

Several models use a fixed grid and assume that all meteorological parameters are known. Generally observed wind speeds at specific stations are interpolated to the grid points by means of a $1/r^2$ weighting scheme. Only a few models (e.g., MacCracken and Grant, 1976) adjust the wind field so that mass continuity is preserved.

Vertical K_z profiles are usually linear up to a height of about 100 m in these models. Above this height K_z is assumed constant and sometimes decreases near the top of the mixed layer (see Fig. 8.3). Models by Reynolds and Roth (1973) and by Shir and Shieh (1974) are typical of this group. Horizontal diffusion can often be neglected for area sources, but in some models it is handled by specifying a constant K_y .

Plumes from point sources cannot be resolved at scales less than the grid distance and are usually arbitrarily assigned to various grid squares on the basis of the length of the trajectory over the grid square. Pollutants whose major source is tall stacks cannot be accurately modeled at small scales by grid models.

9-6 ENVIRONMENTAL PROTECTION AGENCY MODELS

A set of diffusion models recommended by the U. S. Environmental Protection Agency is available on magnetic tape from the National Technical Information Service, U. S. Department of Commerce, Springfield, VA 22161. Eleven models are in this "UNAMAP" system; all are based on the Gaussian formula described in Chap. 4. The latest urban model (RAM) uses the ATDL formulations for area sources derived in Sec. 9-3. The cast of models in this system is continually being updated as new models are developed and evaluated. For example, plans have been made to include a model for urban reactive pollutants in the near future. Turner (1979) gives a detailed review of the status of the UNAMAP models as of May 1979. The appendix to his paper is reproduced in this chapter as Table 9.4, which very

briefly describes each model and gives references to users' guides. The models are all state of the art and are quite satisfactory. Some are conservative; i.e., the predicted concentrations are probably higher than the actual concentrations.

9-7 MODEL EVALUATION

Most urban diffusion models yield correlations between hourly values of observed and predicted concentrations at a given station of about 0.6 to 0.8. This result seems to be independent of the number of statements in the computer program. Good results depend mainly on good knowledge of emissions and wind velocities.

Hayes (1979) and Nappo (1974) discussed several methods that can be used to evaluate models. These include:

Bias evaluation: Ratio of mean predicted concentration to mean observed concentration.

Error analysis: The mean square of the differences between predicted and observed concentrations is calculated.

Time correlation: Correlation between observed and predicted concentration distributions with time at a given station.

Space correlation: Correlation between observed and predicted concentration distributions across a monitoring network at a given time.

Peak analysis: Comparisons of magnitudes and locations of peak observed and predicted concentrations from point sources are made.

Distribution functions: Observed and predicted cumulative distribution functions are compared to see if they are significantly different.

The types of results obtained from some of these techniques are illustrated in Fig. 9.7. A small bias in an urban diffusion model can be corrected merely by "adjusting" the model by using monitoring data. Of course, if there is a large bias, the modeler should look carefully for fundamental errors in his physical assumptions or computer program.

Time and space correlations are useful, but we should realize that correlation coefficients can mask many strange variations in the data. For example, assume that the observed concentrations at nine monitoring stations are all 100 mg/m³, and the observed concentration at a tenth station is 1000 mg/m³. If the model predicts 100 mg/m³ at the first

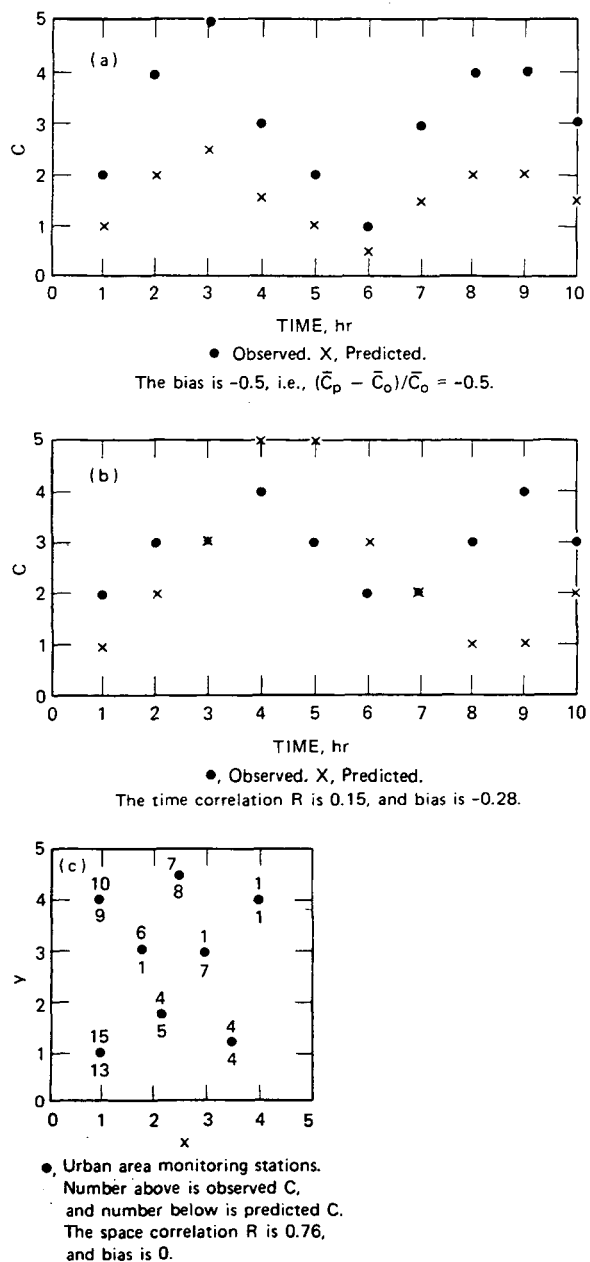


Fig. 9.7 Illustration of (a) bias, (b) time correlation, and (c) space correlation.

nine stations and 105 mg/m³ at the final station, the correlation R will be a perfect 1.0. Consider an urban area with ten observing stations, all reporting concentrations between 80 and 120 mg/m³. The model may do very well predicting the mean concentrations, with values between 80 and 120 mg/m³, also. However, there may be a very low correlation coefficient. In this case the model is unfairly given a low rating by the spatial correlation method. A combination of evaluation methods is best, including a subjective judgment by an experienced modeler.

Table 9.4 Abstracts of Models in UNAMAP (Version 3)*

APRAC: Stanford Research Institute's urban carbon monoxide model. Computes hourly averages for any urban location. Requires an extensive traffic inventory for the city of interest. Requirements and technical details are documented in:

User's Manual for the APRAC-1A Urban Diffusion Model Computer Program (NTIS† accession number PB-213-091).

Additional information is available on APRAC from:

A Practical, Multipurpose Urban Diffusion Model for Carbon Monoxide (NTIS accession number PB-196-003).

Field Study for Initial Evaluation of an Urban Diffusion Model for Carbon Monoxide (NTIS accession number PB-203-469).

Evaluation of the APRAC-1A Urban Diffusion Model for Carbon Monoxide (NTIS accession number PB-210-813).

Dabberdt, Walter F., F. L. Ludwig, and Warren B. Johnson, Jr., 1973, *Validation and Applications of An Urban Diffusion Model for Vehicular Pollutants*, *Atmos. Environ.*, 7: 603-618.

Johnson, W. B., F. L. Ludwig, W. F. Dabberdt, and R. J. Allen, 1973, *An Urban Diffusion Simulation Model for Carbon Monoxide*, *J. Air Pollut. Control Assoc.*, 23 (6): 490-498.

CDM: The Climatological Dispersion Model determines long-term (seasonal or annual) quasi-stable pollutant concentrations at any ground-level receptor using average emission rates from point and area sources and a joint frequency distribution of wind direction, wind speed, and stability for the same period.

Busse, A. D., and J. R. Zimmerman, 1973, *User's Guide for the Climatological Dispersion Model*, U. S. Environmental Protection Agency, Research Triangle Park, NC, Environmental Monitoring Series, EPA-R4-73-024, 131 pp. (NTIS accession number PB-227-346).

HIWAY: Computes the hourly concentrations of non-reactive pollutants downwind of roadways. It is applicable for uniform wind conditions and level terrain. Although best suited for at-grade highways, it can also be applied to depressed highways (cut sections).

Zimmerman, J. R., and R. S. Thompson, 1975, *User's Guide for HIWAY: A Highway Air Pollution Model*, U. S. Environmental Protection Agency, Research Triangle Park, NC, Environmental Monitoring Series, EPA-650/4-74-008, 59 pp. (NTIS accession number PB-239-944).

Three Point

Source Models: The three following point source models use Briggs plume rise methods and Pasquill-Gifford dispersion methods as given in EPA's AP-26, *Workbook of Atmospheric Dispersion Estimates*, to estimate hourly concentrations for stable pollutants.

PTMAX: Performs an analysis of the maximum short-term concentrations from a single point source as a function of stability and wind speed. The final plume height is used for each computation.

PTDIS: Estimates short-term concentrations directly downwind of a point source at distances specified by the user. The effect of limiting vertical dispersion by a mixing height can be included, and gradual plume rise to the point of final rise is also considered. An option allows the calculation of isopleth half-widths for specific concentrations at each downwind distance.

PTMTP: Estimates for a number of arbitrarily located receptor points at or above ground level, the concentration from a number of point sources. Plume rise is determined for each source. Downwind and crosswind distances are determined for each source-receptor pair. Concentrations at a receptor from various sources are assumed additive. Hourly meteorological data are used; both hourly concentrations and averages over any averaging time from 1 to 24 hours can be obtained.

Turner, D. B., and A. D. Busse, 1973, *Users' Guide to the Interactive Versions of Three Point Source Dispersion Programs: PTMAX, PTDIS, and PTMTP*, Preliminary Draft, Meteorology Laboratory, U. S. Environmental Protection Agency, Research Triangle Park, NC.

- CDMQC: This algorithm is the Climatological Dispersion Model (CDM) altered to provide implementation: of calibration, of individual point and area source contribution lists, and of averaging time transformations. The basic algorithms to calculate pollutant concentrations used in the CDM have not been modified, and results obtained using CDM may be reproduced using the CDMQC.
Brubaker, Kenneth L., Polly Brown, and Richard R. Cirillo, 1977, *Addendum to User's Guide for Climatological Dispersion Model*, prepared by Argonne National Laboratory for the U. S. Environmental Protection Agency, Research Triangle Park, NC, EPA-450/3-77-015 (NTIS accession number PB-274-040).
- CRSTER: This algorithm estimates ground-level concentrations resulting from up to 19 colocated elevated stack emissions for an entire year and prints out the highest and second-highest 1-hour, 3-hour, and 24-hour concentrations as well as the annual mean concentrations at a set of 180 receptors (5 distances by 36 azimuths). The algorithm is based on a modified form of the steady-state Gaussian plume equation which uses empirical dispersion coefficients and includes adjustments for plume rise and limited mixing. Terrain adjustments are made as long as the surrounding terrain is physically lower than the lowest stack height input. Pollutant concentrations for each averaging time are computed for discrete, non-overlapping time periods (no running averages are computed) using measured hourly values of wind speed and direction, and estimated hourly values of atmospheric stability and mixing height.
U. S. Environmental Protection Agency, Research Triangle Park, NC, Monitoring and Data Analysis Division, 1977, *User's Manual for Single-Source (CRSTER) Model*, EPA-450/2-77-013 (NTIS accession number PB-271-360).
- PAL: Point, Area, Line source algorithm. This short-term Gaussian steady-state algorithm estimates concentrations of stable pollutants from point, area, and line sources. Computations from area sources include effects of the edge of the source. Line source computations can include effects from a variable emission rate along the source. The algorithm is not intended for application to entire urban areas but for smaller scale analysis of such sources as shopping centers, airports, and single plants. Hourly concentrations are estimated, and average concentrations from 1 hour to 24 hours can be obtained.
Petersen, William B., 1978, *User's Guide for PAL—A Gaussian-Plume Algorithm for Point, Area, and Line Sources*, U. S. Environmental Protection Agency, Research Triangle Park, NC, Environmental Monitoring Series EPA-600/4-78-013 (NTIS accession number PB-281-306).
- VALLEY: This algorithm is a steady-state, univariate Gaussian plume dispersion algorithm designed for estimating either 24-hour or annual concentrations resulting from emissions from up to 50 (total) point and area sources. Calculations of ground-level pollutant concentrations are made for each frequency designed in an array defined by six stabilities, 16 wind directions, and six wind speeds for 112 program-designed receptor sites on a radial grid of variable scale. Empirical dispersion coefficients are used and includes adjustments for plume rise and limited mixing. Plume height is adjusted according to terrain elevations and stability classes.
Burt, Edward W., 1977, *VALLEY Model User's Guide*, U. S. Environmental Protection Agency, Research Triangle Park, NC, EPA-450/2-77-018 (NTIS accession number PB-274-054).
- RAM: Gaussian-Plume Multiple-Source Air Quality Algorithm. This short-term Gaussian steady-state algorithm estimates concentrations of stable pollutants from urban point and area sources. Hourly meteorological data are used. Hourly concentrations and averages over a number of hours can be estimated. Briggs plume rise is used. Pasquill-Gifford dispersion equations with dispersion parameters thought to be valid for urban areas are used. Concentrations from area sources are determined using the method of Hanna; that is, sources directly upwind are considered representative of area source emissions affecting the receptor. Special features include determination of receptor locations downwind of significant sources and determination of locations of uniformly spaced receptors to ensure good area coverage with a minimum number of receptors.
Turner, D. Bruce, and Joan Hrenko Novak, 1978, *User's Guide for RAM*. Vol. I, Algorithm Description and Use, EPA-600/8-78-016a (NTIS accession number PB-294-791). Vol. II, Data Preparation and Listings, EPA-600/8-78-016b (NTIS accession number PB-294-792), U. S. Environmental Protection Agency, Research Triangle Park, NC.

*From D. B. Turner, Atmospheric Dispersion Modeling: A Critical Review, *J. Air Pollut. Control Assoc.*, 29: 518-519 (1979).

†NTIS, National Technical Information Service, U. S. Department of Commerce, Springfield, VA 22161.

Problems

1. If the initial concentration in an urban area is zero and the sources are suddenly turned on, how many "flushing times" will pass before the concentration equals 95% of its equilibrium value.

2. What is the concentration in the receptor block of Fig. 9.4 if Pasquill's D stability class is valid, wind speed (u) is 2 m/sec, and grid size (Δx) is 5 km?

$$(1) Q_{a0} = 10, Q_{a1} = 5, Q_{a2} = 20, Q_{a3} = 2 \\ \text{mg m}^{-2} \text{ sec}^{-1}$$

$$(2) Q_{a0} = 1, Q_{a1} = 20, Q_{a2} = 20, Q_{a3} = 10 \\ \text{mg m}^{-2} \text{ sec}^{-1}$$

(3) Compare the solutions in (1) with the answers you get from Eq. 9.12. Assume that there are no sources beyond square 3.

3. What is the concentration at receptor 5 in Fig. 9.1 for east winds with a speed of 3 m/sec and D stability class?

4. Motown, USA, has a street 20 m wide with 500 vehicles/hr driving on it at a speed of 20 miles/hr. Wind speed at roof top is 5 m/sec and wind direction is perpendicular to the street. Background or area source concentration of carbon monoxide is 4 ppm. What is the added concentration on the windward side of the street?

Removal Mechanisms

10-1 INTRODUCTION

Most air pollution is eventually removed from the atmosphere, either by transport to vegetation, soil, or water or by chemical transformation to another compound. For example, SO_2 is removed by all these mechanisms and has a half-life in the atmosphere of a few hours or days, depending on rain intensity and relative humidity, other chemicals in the air, and surface characteristics. On the other hand, about half of all the CO_2 we put into the atmosphere remains there. The difference between the atmospheric half-lives of SO_2 and CO_2 is due to their reactivity with substances in the air and at the ground surface.

Methods of transport to vegetation, soil, or water include dry deposition and precipitation scavenging. Despite extensive field and laboratory experiments and detailed theoretical calculations, there is much uncertainty connected with fundamental parameters, such as the dry deposition velocity.

10-2 DRY DEPOSITION

10-2.1 Gravitational Settling

Particles with radii greater than about $5 \mu\text{m}$ have significant gravitational settling speeds. Stokes' law for the terminal settling speed (v_t) is valid for particles with radii less than 10 to $30 \mu\text{m}$, depending on particle density:

$$v_t = \frac{2r^2 g \rho_p}{9\mu} \quad (10.1)$$

where ρ_p is particle density and μ is the dynamic viscosity of air ($1.8 \times 10^{-4} \text{ g sec}^{-1} \text{ cm}^{-1}$). For particles with larger radii, Stokes' law must be modified somewhat, and the graphical solution given

by Van der Hoven (1968) for spherical particles with densities of 5 g/cm^3 is plotted for sea-level situations in Fig. 10.1. Settling speeds for particles with different densities (ρ_p) can be approximated by multiplying the speed in the figure by $[\rho_p/(5 \text{ g/cm}^3)]$. The settling speed of nonspherical particles can be calculated by dividing the speed of the equivalent spherical particle [equivalent radius $r_e = (3V_p/4\pi)^{1/3}$, V_p = particle volume] by a dynamical shape factor α . Typical shape factors are shown in Table 10.1 (Chamberlain, 1975).

Van der Hoven (1968) suggests that, when v_t is greater than 100 cm/sec (radius $r \gtrsim 100 \mu\text{m}$), the particles are falling through the turbulence so fast that diffusion is no longer important. In this case particle trajectories are calculated by a straight-

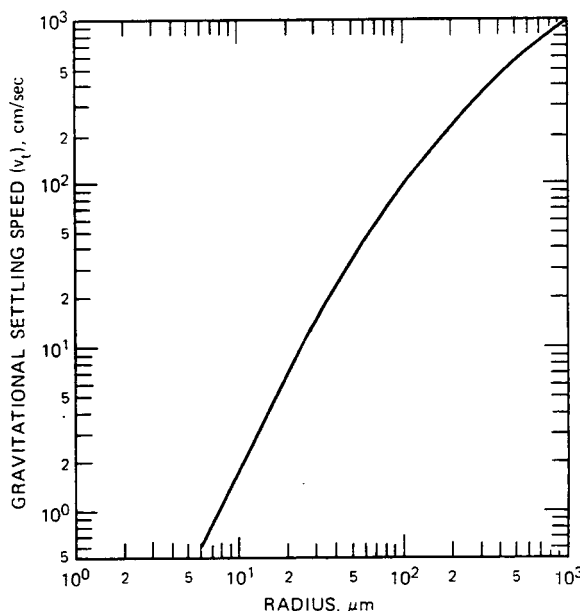


Fig. 10.1 Gravitational settling speeds for particles with densities of 5 g/cm^3 near the earth's surface. (Adapted from Van der Hoven, 1968, p. 203.)

Table 10.1 Dynamical Shape Factor α^*

Shape†	Ratio of axes	$\alpha‡$
Ellipsoid	4	1.28
Cylinder	1	1.06
Cylinder	2	1.14
Cylinder	3	1.24
Cylinder	4	1.32
Two spheres touching	2	1.10
Two spheres touching	2	1.17
Three spheres touching		
As triangle		1.20
In line	3	1.34
In line	3	1.40
Four spheres touching		
In line	4	1.58
In line	4	1.56

*From A. C. Chamberlain, *The Movement of Particles in Plant Communities*, in *Vegetation and the Atmosphere*, Vol. 1, Chap. 5, p. 157, J. L. Monteith (Ed.), Academic Press, London, 1975.

†In all cases preferential motion is perpendicular to long axes.

‡Ratio of terminal velocity of equivalent sphere to that of particle.

forward ballistics approach that is based on the wind speed and the gravitational settling speed.

For a v_t of less than 100 cm/sec (radius $r \lesssim 100 \mu\text{m}$), the particles are assumed to be dispersed by turbulence in the same way as particles having no inertia. A plume model is used, but $h_g = xv_g/u$ is substituted for effective plume height (h) to account for gravitational settling. This model, called the "tilted plume model," is illustrated in Fig. 10.2. Deposition of particles with $5 \text{ cm/sec} \lesssim v_t \lesssim 100 \text{ cm/sec}$ at the ground at any position x, y is given by the expression

$$\omega = v_t C(x,y,0) \quad (10.2)$$

where ω is the deposition rate in mass per unit area per unit time. In a Gaussian model of this situation, roughly half of the material is deposited by a distance hu/v_t , where the particle plume centerline strikes the

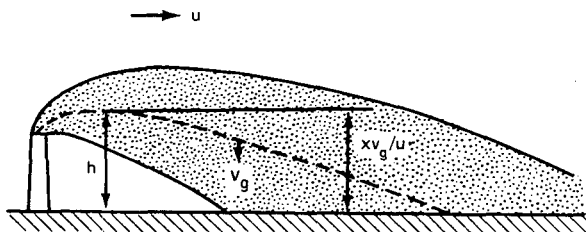


Fig. 10.2 Tilted plume model. The plume axis drops with speed v_g .

ground. Thus, for h equal to 100 m, u equal to 5 m/sec, and $20\text{-}\mu\text{m}$ -diameter particles with densities of 5 g/cm^3 ($v_t = 6 \text{ cm/sec}$), about half of the material is deposited within a distance of 8.3 km.

10-2.2 Deposition of Gases and of Particles with Radii Less Than About $10 \mu\text{m}$

Very small particles and gases are also deposited on surfaces as a result of turbulent diffusion and Brownian motion. Chemical absorption, impaction, photosynthesis, and other biological, chemical, and physical processes cause the material to be retained at the surface. In this case a deposition velocity (v_d) can be defined as an empirical function of the observed deposition rate (ω) and concentration near the surface (C_0):

$$v_d = \frac{\omega}{C_0} \quad (10.3)$$

The height at which C_0 is measured is typically about 1 m. Once v_d is known for a given set of conditions, the formula $\omega = v_d C_0$ can be used to predict dry deposition of gases and small particles, where C_0 would be obtained from some appropriate diffusion model.

Many methods of incorporating dry deposition into existing effluent dispersion models are available [see Hosker (1980) for a survey]. Even the relatively simple Gaussian plume model has been adjusted for dry removal by at least four techniques. The most common, and one of the easiest to use, is the so-called "source depletion" model, in which the apparent strength of the source is allowed to vary with downwind distance to account for the diminishing amount of material remaining aloft. The rate of change of Q with distance is

$$\begin{aligned} \frac{\partial Q}{\partial x} &= - \int_{-\infty}^{\infty} \omega(x,y) dy \\ &= - \left(\frac{2}{\pi}\right)^{1/2} \frac{v_d Q}{u \sigma_z} e^{-h^2/2\sigma_z^2} \end{aligned} \quad (10.4)$$

which leads to

$$\frac{Q(x)}{Q(0)} = \left[\exp \int_0^x \frac{dz}{\sigma_z \exp(h^2/2\sigma_z^2)} \right]^{-(2/\pi)^{1/2} (v_d/u)} \quad (10.5)$$

Graphical solutions to this equation with the use of standard Pasquill-Gifford curves for σ_z are given by Van der Hoven (1968). The resulting $Q(x)$ is then

sed instead of the usual fixed-source strength (Q) in the Gaussian plume equation (Eq. 4.1). Table 10.2 uses Van der Hoven's graphs to estimate the downwind distance at which 50% of the plume is depleted or a wind speed (u) of 1.0 m/sec and a deposition speed (v_d) of 0.01 m/sec. Because of the $\exp(h^2/2\sigma_z^2)$ term in Eq. 10.5, the distance for 50% depletion in Table 10.2 is not always a continuously decreasing function of stability for any given source height. This model implicitly assumes that depletion occurs over the whole depth of the plume rather than at the surface; the plume's vertical profile is therefore invariant with distance.

Table 10.2 Distance in Kilometers at Which 50% of Q Is Depleted by Dry Deposition as a Function of Pasquill's Stability Class and Source Height*

Pasquill's class	Source height, m			
	0	10	50	100
A and B	>10			
C	1.8	18	43	60
D	0.4	3.5	8.6	19
E	0.15	2.2	8.3	17
F	0.10	2.0	10.0	28

* $u = 1.0$ m/sec; $v_d = 0.01$ m/sec.

The "partial reflection" model, summarized by Overcamp (1976), is a somewhat different approach. In this instance the "image" term (involving $z + h$) in Eq. 4.1 is preceded by a reflection coefficient (α), which is thus a fraction of the strength of the real source. This coefficient is determined by setting the deposition flux equal to the difference in fluxes from the real and image terms. The plume is also allowed to "tilt" to incorporate gravitational settling of large particles at terminal speed (v_t):

$$C = \frac{Q}{2\pi\sigma_y\sigma_z u} \exp\left(-\frac{y^2}{2\sigma_y^2}\right) \left(\exp\left\{-\frac{[z - h + (v_t x/u)]^2}{2\sigma_z^2}\right\} + \alpha(x_G) \exp\left\{-\frac{[z + h - (v_t x/u)]^2}{2\sigma_z^2}\right\} \right) \quad (10.6)$$

The reflection coefficient [$\alpha(x_G)$] can be computed by solving an implicit relation for x_G

$$\left[h - \frac{v_t x_G}{u} \right] \frac{\sigma_z(x)}{\sigma_z(x_G)} = z + h - \frac{v_t x}{u} \quad (10.7)$$

and the following equation for $\alpha(x)$:

$$\alpha(x) = 1 - \frac{2v_d}{v_t + v_d + (uh - v_t x) \sigma_z^{-1} (d\sigma_z/dx)} \quad (10.8)$$

In this model dry deposition removes material from the lower portions of the plume, which therefore begins to show a non-Gaussian vertical concentration distribution. In unstable conditions, because of rapid mixing within the plume, the results from Eqs. 10.5 and 10.6 are not very different; in stable conditions, however, the flux to the surface estimated by using Eq. 10.6 will be significantly smaller than Eq. 10.5 would suggest, especially far downwind.

Horst (1979) has compared the results of various deposition models. He concluded that, close to the source, the partial reflection model is the easiest to use and is fairly accurate. Far downwind, however, the source depletion model performed better than the partial reflection model. He then suggested a modified version of the source depletion model which permits the plume vertical profile to vary with distance. Field data to validate any dry deposition model are largely unavailable or inadequate (Sehmel, 1980). The model is selected mostly on the basis of the physical plausibility of the model's assumptions and predictions.

A knowledge of the dry deposition velocity (v_d) is necessary to operate any deposition model. Both measured and theoretical estimates of v_d are commonly used (Sehmel, 1980). Some theoretical models of deposition assume the deposition process is analogous to electrical current flow across resistances. In effect, the deposition speed (v_d) is inversely proportional to the sum of an aerodynamic resistance to turbulent mass transfer (r_a), a resistance to transfer across the surface boundary layer (r_b), and a resistance to transfer into the surface (r_s). In principle, then, deposition speed should be a function of roughness length, friction velocity, and many other surface parameters. Wind-tunnel data show clearly the dependence on roughness length and friction velocity. However, field measurements of deposition speeds contain much scatter and do not always agree with theories or with measurements in controlled laboratory environments. The values of v_d recommended in this chapter are based on reviews of field data by McMahon and Denison (1979) and Sehmel (1980). Original references are given in their reviews. We arbitrarily assume that the field measurements are more reliable than theoretical estimates.

Figure 10.3 shows measured deposition speeds for particles to grass. For particles larger than about $1 \mu\text{m}$, turbulent diffusion and gravitational settling are the dominant processes, whereas, for particles smaller than $0.1 \mu\text{m}$, Brownian diffusion becomes increasingly important. Theory and laboratory data

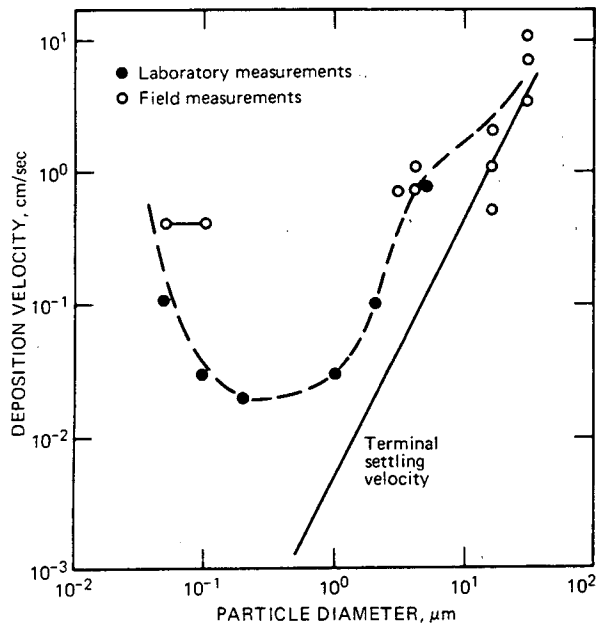


Fig. 10.3 Laboratory and field measurements of deposition speeds of particles to grass. [From T. A. McMahon and P. J. Denison, *Empirical Atmospheric Deposition Parameters—A Survey*, *Atmos. Environ.*, 13: 1000 (1979); by permission of Pergamon Press, Ltd.]

indicate a minimum in v_d for particles between 0.1 and 1 μm in diameter; the exact value for v_d is predicted to depend on such things as particle density, friction velocity (u_*), and surface roughness (z_0). Figure 10.4 shows typical calculated values. However, the scatter and sparsity of the field data preclude a vigorous validation of the expected behavior of v_d , although the general trends seem to be verified. The inaccuracies of the data suggest that, in any particular model calculation, a range (often orders of magnitude) of possible v_d values should be used rather than a single estimate, such as the average. This will place upper and lower bounds on the computed deposition results, which is really all the accuracy that can be expected with the present state of the art. A few special cases in which the deposition rate is dramatically enhanced are known. For example, the deposition of particles to a forest canopy is about 2 to 16 times as great as that over open terrain, whereas mosses give rise to an order-of-magnitude increase in v_d . Special caution is warranted for unusual types of ground cover.

Many measurements of v_d for gases have been reported by McMahon and Denison (1979) and Sehmel (1980). Biological and chemical activity play key roles in gaseous deposition and may, in fact, provide the rate-limiting steps for deposition and uptake. For example, relatively inert gases, such as

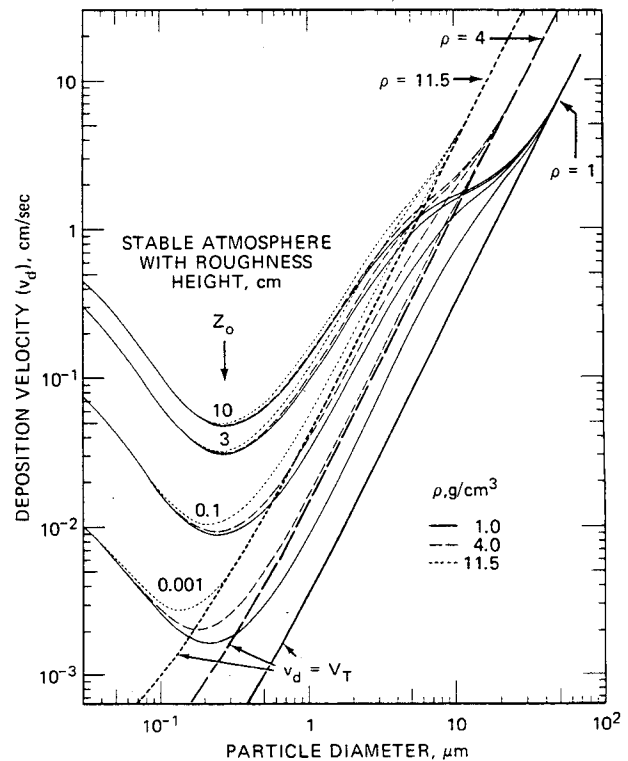


Fig. 10.4 Predicted deposition velocities at 1 m for $u_* = 50$ cm/sec and particle densities of 1, 4, and 11.5 g/cm^3 . [From G. A. Sehmel, *Particle and Gas Dry Deposition: A Review*, *Atmos. Environ.*, 14: 1002 (1980); by permission of Pergamon Press, Ltd.]

carbon monoxide, typically have nearly negligible deposition speeds, 10^{-3} to 10^{-4} cm/sec. If the gas is biologically or chemically active, however, the measured deposition speed is likely to be on the order of 0.5 to 3 cm/sec. For example, SO_2 deposition speeds for various surface types are summarized in Table 10.3 [McMahon and Denison (1979)]. The v_d for SO_2 in forests is not significantly enhanced over that for grasses or crops. A dependence on wind speed cannot be discerned from the available data. During the night or the winter, when stomata are closed, v_d is about a factor of 2 to 5 less than during summer days.

The deposition speed of other reactive gases is similar to that of SO_2 . I_2 is deposited at an average speed (v_d) of 1.5 cm/sec, and it has relatively little scatter. Ozone is deposited at a speed (v_d) ranging from 0.02 to 1.4 cm/sec, with an average speed of 0.5 cm/sec. The lowest ozone deposition speeds were observed over water and snow ($v_d \approx 0.1$ cm/sec). Also, the ozone deposition speed for neutral conditions appears to be twice as large as that for unstable conditions. Many other experimental factors influenced the results, such as reference height, roughness, surface conditions, etc., but the data do not

Table 10.3 SO₂ Deposition Rates*

Surface	v _d , cm/sec	Comment
Short grass	0.5	0.1 m in height
Medium crop	0.7	1.0 m in height
Calcareous soil	0.8	Wet or dry
Acid soil	0.4	Dry
Acid soil	0.6	Wet
Dry snow	0.1	If wet, behaves like water
Water	0.7	
Countryside	0.8	
Cities	0.7	Based on London data only

*From T. A. McMahon and P. J. Denison, Empirical Atmospheric Deposition Parameters—A Survey, *Atmos. Environ.*, 13: 575 (1979); by permission of Pergamon Press, Ltd.

permit any quantitative conclusions regarding these factors.

10-3 WET DEPOSITION

The theoretical treatment of wet deposition is often divided into rainout (within cloud scavenging) and washout (below cloud scavenging). In practical applications the two processes are generally lumped together since they can be modeled similarly [see the reviews by Hosker (1980) or Slinn (1981)].

There are also two methods of modeling this problem. In the first the concentration (C) is assumed to decrease exponentially with time:

$$C(t) = C(0) e^{-\Lambda t} \quad (10.9)$$

where Λ is the so-called scavenging coefficient (time⁻¹) and t is time since precipitation began. The precipitation-induced flux of effluent to the ground is given by

$$F_{\text{wet}} = \int_0^{Z_w} \Lambda C dz \quad (10.10a)$$

where Z_w is the depth of the wetted plume layer. For rain falling completely through a Gaussian plume,

$$F_{\text{wet}} = \frac{\Lambda Q}{(2\pi)^{1/2} \sigma_y u} \exp\left(-\frac{y^2}{2\sigma_y^2}\right) \quad (10.10b)$$

The method is, strictly speaking, applicable only to particles of a single size (monodisperse) and to highly reactive gases, which are *irreversibly* captured by the precipitation. Furthermore, the derivation of Eq. 10.9 involves the assumption that the scavenging coefficient is independent of both space and time. In modeling practice, however, Λ is often allowed to

vary with position to account for changes in precipitation (and hence in scavenging rate) over the region of interest. The scavenging coefficient method *cannot* be applied directly to aerosols with a *range* of diameters (polydisperse) unless an empirical value of Λ is available for particles of that type and size. In particular, a scavenging coefficient cannot be applied for an "average" particle whose size is equal to the geometric mean of the particle size range; the scavenging rate will be too small by more than an order of magnitude. Methods of estimating scavenging coefficients for polydisperse aerosols have been summarized by Dana and Hales (1976). The scavenging coefficient method is also *not* applicable to gases which are not highly reactive or which are merely soluble in water since it is essential in such cases to account for the possible desorption of gases from droplets as they fall from regions of high effluent concentration (e.g., an elevated plume) toward the ground (Hales, 1972). Soluble gases are discussed in reports by Hales et al. (1973) and Slinn (1974). Slinn has found that close to the source the shape of a Gaussian plume is unaltered by the wet removal process but the concentration diminishes exponentially with distance. Far from the source, the plume is "washed down" or "tilted" from its initial height by an amount dependent on the precipitation rate, droplet size, gas chemistry, wind speed, and distance downwind. The vertical dispersion parameter is also enhanced by an amount strongly dependent on droplet size.

Other methods of modeling wet removal use the so-called washouts ratio (W_r). Let k_0 and C_0 be the concentration of effluent in the precipitation (e.g., raindrops) and in the air, respectively, at some reference height; both quantities are measured in unit of mass per volume. Then

$$W_r \equiv \frac{k_0}{C_0} \quad (10.11a)$$

Other definitions are widely used (e.g., McMahon and Denison, 1979); let k'_0 be the effluent concentration in the precipitation in terms of mass (e.g., micrograms per gram of H₂O). In this case the washout ratio is written as

$$W' \equiv \frac{\rho_a k'_0}{C_0} \quad (10.11b)$$

where ρ_a is the density of air ($\sim 1.2 \times 10^{-3}$ g/cm³). The dimensionless ratios are related by

$$W' = \frac{\rho_a}{\rho_w} W_r \quad (10.11c)$$

where ρ_w is the density of water (1 g/cm^3). Thus W_r is almost 1000 times as large as W' ; since both definitions (Eqs. 10.11a and 10.11b) are common in the literature, the user must be careful. In the following discussion, W_r is used for convenience.

The flux of effluent to the surface as a result of the precipitation is just

$$F_{\text{wet}} = k_0 J_0 \quad (10.12)$$

where J_0 is the equivalent rainfall rate in, for example, millimeters per hour. If W_r is known and the concentration in air (C_0) can be measured or estimated from a plume model, then

$$F_{\text{wet}} = C_0 W_r J_0 \quad (10.13)$$

The washout ratio can also be used to define a wet deposition velocity by analogy to the dry:

$$v_w \equiv \frac{F_{\text{wet}}}{C_0} = W_r J_0 \quad (10.14)$$

This can then be used like v_d to develop models for the wet scavenging process. An analysis (summarized by Hosker, 1980) of the microphysics of the wet scavenging process yields an approximate relation between the scavenging rate and the washout ratio:

$$\Lambda \approx \frac{W_r J_0}{Z_w} \quad (10.15)$$

where Z_w is the depth of the wetted plume layer. Hence the washout ratio can also be used in exponential decay models of wet plume depletion (Eq. 10.9).

The scavenging coefficient (Λ) is theoretically a function of droplet size spectrum, physical and chemical characteristics of the particle or gas, and precipitation rate. McMahon and Denison (1979) report 20 field experiments in which Λ was measured for particles which gave Λ a median value of $1.5 \times 10^{-4} \text{ sec}^{-1}$ and a range from $0.4 \times 10^{-5} \text{ sec}^{-1}$ to $3 \times 10^{-3} \text{ sec}^{-1}$. They found washout and rainout coefficients to be nearly equal but did not find systematic differences in Λ as particle size or rain characteristics changed. Their median value of Λ for SO_2 is about $2 \times 10^{-5} \text{ sec}^{-1}$, and one laboratory experiment showed that $\Lambda = 17 \times 10^{-5} J_0^{0.6}$, where J_0 is rainfall (in millimeters per hour). A value of Λ ranging from 10^{-5} to 10^{-4} sec^{-1} implies a half-life for wet removal processes ranging from about 2 hr to 1 day. The use of scavenging coefficients for wet removal modeling is probably best regarded as an order-of-magnitude estimation procedure. This is particularly true if empirical values of Λ are unavailable or inappropriate for the conditions at hand; thus

theoretical estimates of Λ must be used. The procedure is most useful for single episodic events, where the available theory does permit some adjustment for the peculiarities of individual storms.

There are many field observations of washout ratio (W_r) which can be determined by measuring pollutant concentrations in air and in rainwater. The washout ratio has been observed to decrease with precipitation amount during any given experiment, presumably because the pollutant cloud becomes more dilute. On the average, W_r decreases by a factor of 2 for each order-of-magnitude increase in rainfall. Over half of the washout ratios (W_r) reported by McMahon and Denison (1979) are in the range from 3×10^5 to 10^6 with a median of about 6×10^5 . There may be some variation with pollutant type, although the ranges in observed W_r for different pollutants generally overlap each other and no statistically significant differences can be proven. Washout ratios are probably best suited to long-term estimates, in which the variability induced by single storm events is integrated out.

10.4 CHEMICAL REMOVAL

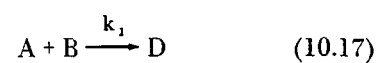
Primary pollutants are those which are emitted directly into the atmosphere, such as SO_2 , CO , and NO_2 . Secondary pollutants are those which are created through chemical reactions involving the primary pollutants. For example, sulfates form when SO_2 is oxidized, or ozone is formed when a mixture consisting of NO_2 , NO , and reactive hydrocarbons is subjected to sunlight.

Often an exponential chemical decay rate is assumed with time constant T_c :

$$\frac{C(t)}{C(0)} = e^{-t/T_c} \quad (10.16)$$

The conversion from SO_2 to sulfate is often treated as an exponential process, but there is much debate over the proper value for the time constant (T_c). The reaction rate depends on humidity and the presence of catalysts, and thus T_c has been measured to range from an hour to several days. A typical value of T_c used in long-range transport models is about 4 days.

Chemical removal can also be studied by using the kinetic equations. For example, assume that the following two chemical kinetic equations are valid:



where k_1 and k_2 are rate constants (concentration⁻¹ time⁻¹). Then the rate of change of concentration of substance D due to chemical reactions is given by the equation

$$\frac{dC_D}{dt} = k_1 C_A C_B - k_2 C_D C_E \quad (10.19)$$

This term should be added to the right-hand side of the continuity equation (8.2) for substance D. Equation 10.19 is often used in the analysis of photochemical smog. The set of chemical kinetic equations for photochemical smog is in a continual state of development; a recent model (Falls and Seinfeld, 1978) uses 55 equations. A rough schematic diagram of smog formation is given in Fig. 10.5. Primary emissions consist of hydrocarbons, NO, and some NO₂. Sunlight ($h\nu$, i.e., energy of a photon from sunlight) results in the formation of free radicals and the ultimate production of the problem pollutants ozone (O₃) and peroxyacetylnitrate (PAN).

10-5 REMOVAL PROCESSES IN THE BOX MODEL

Chapter 9, Sec. 9.2, presented the box model, in which concentration (C) is assumed to be uniform across a region of along-wind width (Δx) and depth (z_i). Removal processes in this model can be accounted for by using the models developed in previous sections:

$$\text{Dry deposition removal} = -v_d C \Delta x$$

$$\text{Precipitation scavenging} = -\Lambda C \Delta x z_i$$

$$\text{Chemical removal} = -(C/T_c) \Delta x z_i$$

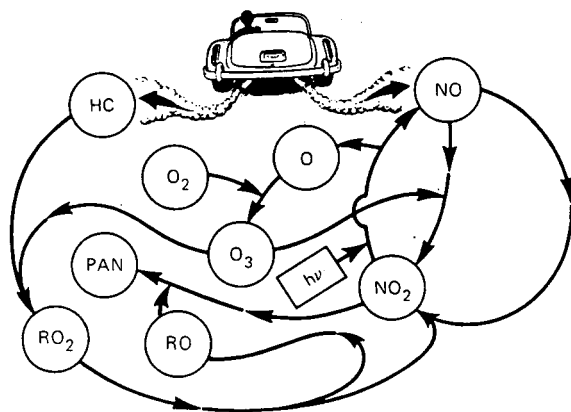


Fig. 10.5 Simplified diagram of photochemical smog reactions. $h\nu$ is the energy of a photon (from sunlight), and R is a free radical.

If a steady state and no upwind background are assumed, the continuity equation for this box becomes

$$\begin{aligned} \Delta x Q_a - \underset{\text{Source}}{uz_i C} - \underset{\text{Advec-}}{v_d C \Delta x} - \underset{\text{Dry de-}}{\text{position}}{\Lambda C \Delta x z_i} - \underset{\text{loss}}{(C/T_c) \Delta x z_i} = 0 \end{aligned} \quad (10.20)$$

The solution is:

$$C = \frac{Q_a (\Delta x / uz_i)}{\{1 + [(v_d / z_i) + \Lambda + (1/T_c)] (\Delta x / u)\}} \quad (10.21)$$

The numerator of Eq. 10.21 ($Q_a \Delta x / uz_i$) is the steady-state box-model solution in the absence of removal processes. The terms in the denominator all act to decrease the concentration. Realizing that $\Delta x / u$ is the flushing time for the box, we can then think of all these correction terms as the ratio of the flushing time to the characteristic removal time scale for that process. The smaller the removal time scale, the greater the ratio and the smaller the concentration (C). Typical values of the parameters in this equation are

$$\begin{aligned} v_d = 0.01 \text{ m/sec} \quad \Lambda = 10^{-4} \text{ sec}^{-1} \quad T_c = 10^4 \text{ sec} \\ \Delta x = 2 \times 10^4 \text{ m} \quad u = 5 \text{ m/sec} \quad z_i = 500 \text{ m} \end{aligned}$$

These parameters might be used for urban SO₂ pollution on a rainy day. The denominator in the equation for this set of parameters is thus 1.88, which implies that the concentration is almost 50% less than that given by the simple box model with no removal processes.

Problems

1. Particles with radii of 50 μm and densities of 5 g/cm^3 are released at a rate of 1 g/sec in a nonbuoyant plume from a stack 100 m high. What is the deposition rate on the plume axis at a distance of 100 m from the stack for D stability and wind speed of 5 m/sec ?

2. For the situation in problem 1, what fraction of the original effluent is still remaining airborne?

3. The area source strength of SO₂ in an urban region of width 30 km is 10 $\text{mg m}^{-2} \text{ sec}^{-1}$. Mixing depth is 1 km, and wind speed is 3 m/sec . What would the concentration be (a) in the absence of any removal process, (b) assuming only dry deposition, (c) assuming only wet deposition, (d) assuming only chemical removal, and (e) assuming that all three removal mechanisms are acting?

Cooling Tower Plumes and Drift Deposition

11-1 INTRODUCTION

More and more cooling towers are being constructed today to conserve water and prevent the discharge of heated water to streams, lakes, and estuaries. Hot water from the industrial process drips over wooden or plastic barriers in a cooling tower and evaporates into the air that passes through the tower. As a result, about 540 calories of heat are lost for each gram of water evaporated. Cooling towers can be tall (~150 m tall and 30 m in radius) natural-draft towers (Fig. 11.1), in which vertical motions are induced by density differences, or short (~20 m tall and 5 m in radius) mechanical-draft towers (Fig. 11.2), in which vertical motions are forced by large fans. Vertical velocities of about 5 m/sec are observed in natural-draft towers and about 10 m/sec in mechanical-draft towers. Temperature and moisture differences between the plume and the environment are about the same in both types of towers, about 20°C and 0.03 g/g, respectively. The plume is saturated when it leaves the tower, and liquid water concentrations are about 0.001 g/g.

Heat and moisture fluxes from cooling towers at large power plants can cause fog or cloud formation and at times can induce additional precipitation. Another potential problem is drift deposition, in which circulating cooling water with drop sizes ranging from 50 to 1000 μm is carried out of the tower and may be deposited on nearby structures and vegetation. These drops generally contain salts, fungicides, and pesticides, which may harm the surfaces they strike. A comprehensive review of atmospheric effects of cooling tower plumes is given by Hanna (1981).

11-2 PLUME RISE FROM COOLING TOWERS

About 80% of the total energy leaving a cooling tower is latent heat, which can influence plume rise

only if water vapor is condensed. The important parameters are listed in Fig. 11.3, which is a schematic drawing of a cooling tower plume. The influence of latent heat on plume rise is shown by the psychrometric chart of Fig. 11.4. The curved line is a plot of saturated specific humidity (q_s) vs. temperature. Initial plume and environmental temperature (T) and specific humidity (q) are indicated by points p and e , respectively. By simple mixing of plume and environmental air, the mixture T and q would follow the straight line to any point l . However, the plume would then be supersaturated and would have to condense water and warm itself to point l' . At this point the amount of latent heat released is proportional to the liquid water in the plume (q_L), or the difference on the diagram between q_1 and q_1' (about 0.002 g/g in this case).

The ratio of latent heat released to initial latent heat flux is

$$r = \frac{Vq_L}{V_0(q_{p0} - q_{e0})} \quad (11.1)$$

where V and V_0 are the current and initial volume fluxes, respectively. The ratio of volume fluxes (V/V_0) can be approximated by $(T_{p0} - T_e)/(T_{l'} - T_e)$. Therefore, at point l' , the fraction r is

$$r = \frac{q_L}{(q_{p0} - q_{e0})} \frac{(T_{p0} - T_e)}{(T_{l'} - T_e)} = \frac{0.002 (33^\circ)}{0.028 (16^\circ)} = 0.15 \quad (11.2)$$

Only 15% of the initial latent heat flux is released at point l . If this exercise were carried out at the other points along the curved line between points e and p in the figure, r would have a maximum of about 20%. At a typical cooling tower with 80% latent heat and 20% sensible heat, the initial sensible heat flux (F_0) would be no more than doubled owing to latent heat release. Since plume rise is proportional to $F_0^{1/2}$, the release of latent heat would increase plume rise by no

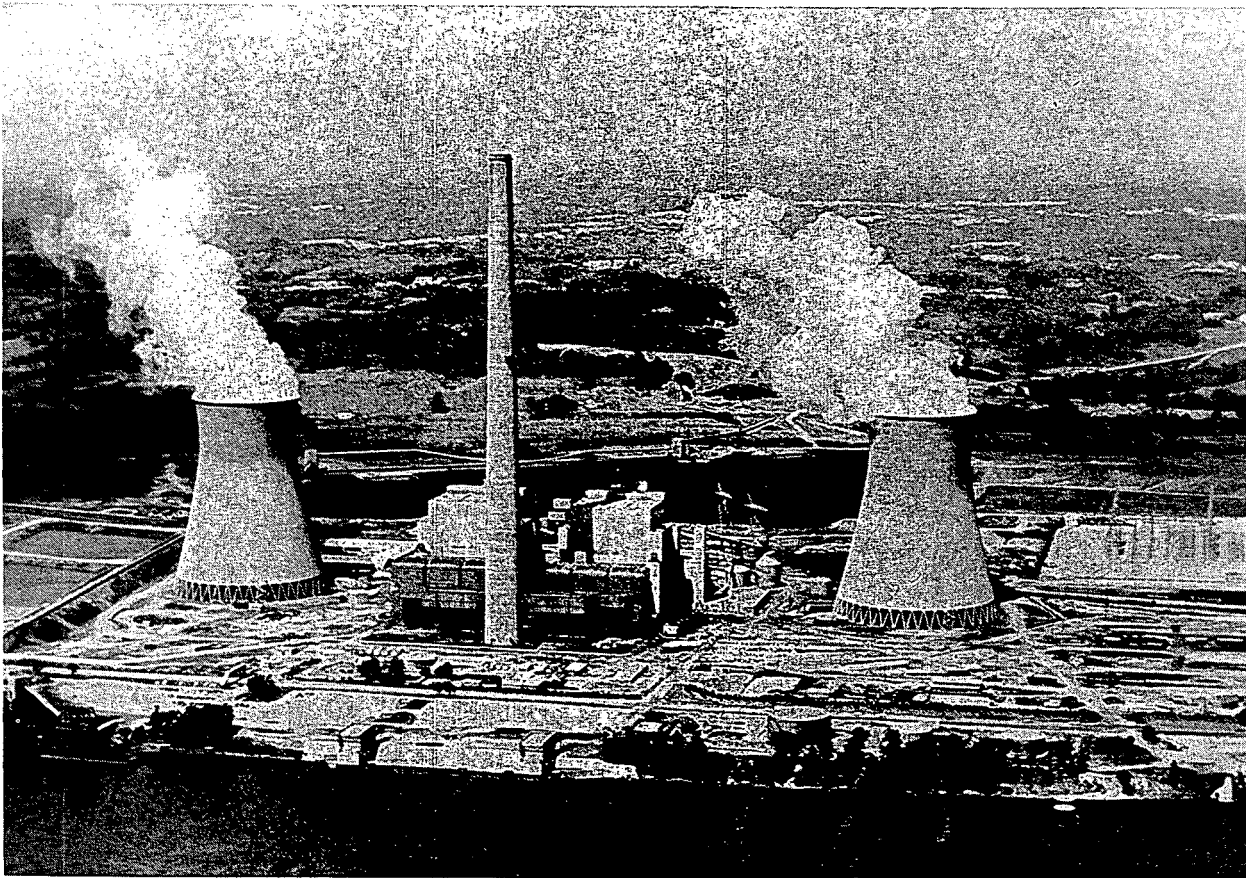


Fig. 11.1 Typical natural-draft cooling towers. (Photograph courtesy of M. Kramer, Meteorological Evaluation Services, Inc.)

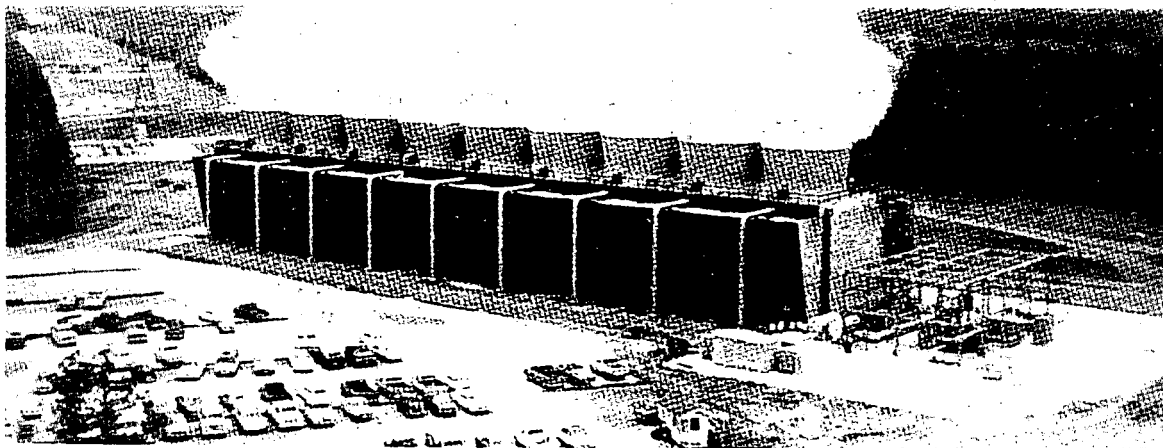


Fig. 11.2 Typical mechanical-draft cooling tower. (Photograph courtesy of J. Holmberg, The Marley Cooling Tower Company.)

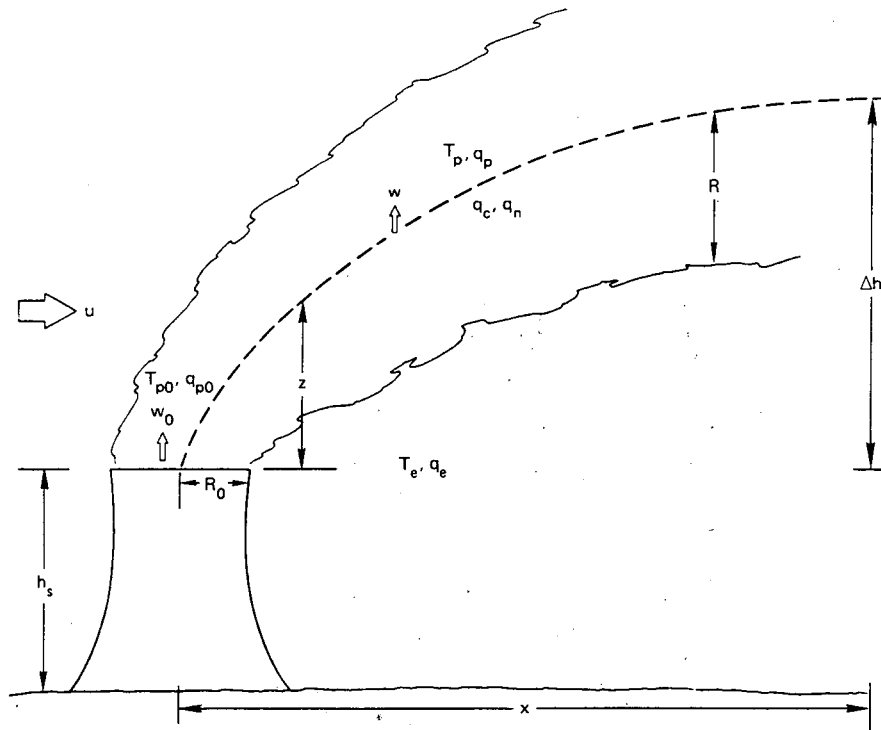


Fig. 11.3 Parameters important for cooling plume analysis.

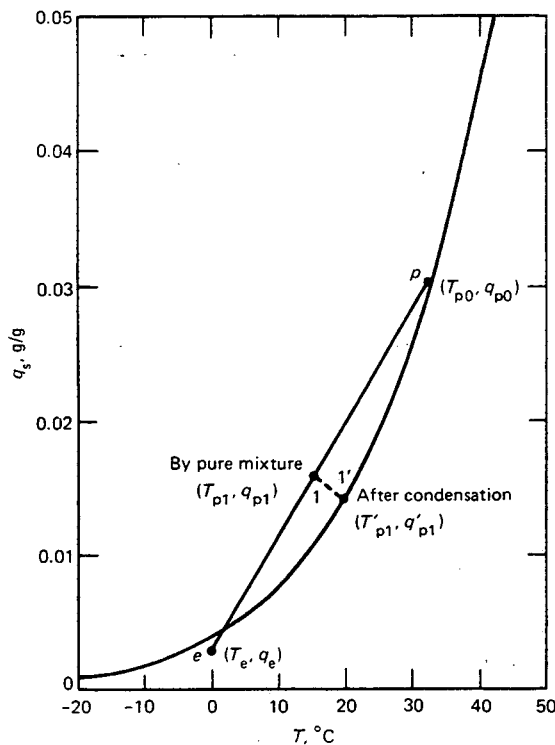


Fig. 11.4 Psychrometric chart. Curved line is the variation of saturation specific humidity with temperature. As an illustration, equal parts of plume (p) and environment (e) air are assumed to mix.

more than about 30%. Since this increase is probably within the errors of measurement, the formulas for dry plume rise in Chap. 2 are recommended for calculating cooling tower plume rise. At any rate the dry formulas would always predict less plume rise and therefore would be "conservative." As shown by experience, the bent-over plume-rise formula should be used for wind speeds greater than 1 m/sec, and the calm plume-rise formula should be used for wind speeds less than 1 m/sec.

11-2.1 Visible Plume Dimensions

The plume trajectory near the source can be calculated by using the formulas in Chap. 2, Sec. 2-3. The initial flux of moisture [$V_0(q_{p0} + q_{L0})$] and the variation with height of the saturation deficit flux [$V(q_s - q_e)$] must be known to predict the dimensions of the visible plume. The term q_{L0} is the initial specific humidity of liquid water in the plume and is often assumed to equal 0.001 g/g. The parameter q_s is the saturation specific humidity of the environment. The plume will be condensed when the following condition is satisfied.

$$V_0(q_{p0} + q_{L0}) \geq V(q_s - q_e) \quad (\text{condensation}) \quad (11.3)$$

Chapter 2, Sec. 2-2.1, shows that the effective radius (R_m) of the momentum plume is about 1.5 times the effective radius (R_t) of the thermal plume. Meyer et al. (1974) have found that observed visible plume lengths are best simulated if the effective moisture plume radius (R_w) is assumed to be about 0.71 times the effective thermal plume radius. Thus the momentum flux ratio (V/V_0) at height z can be estimated by the formulas (Hanna, 1976):

$$\frac{V}{V_0} = \left[1 + 0.28 \frac{z}{R_0} \left(\frac{u}{w_0} \right)^{1/2} \right]^2 \quad (\text{windy}) \quad (11.4)$$

$$\frac{V}{V_0} = \left(1 + 0.11 \frac{z}{R_0} \right)^2 \quad (\text{calm}) \quad (11.5)$$

For calm plumes, Eqs. 11.3 and 11.5 can be combined to give the height (z_l) of the visible plume:

$$z_l = 9R_0 \left[\left(\frac{q_{p0} + q_{L0}}{q_s - q_e} \right)^{1/2} - 1 \right] \quad (\text{calm}) \quad (11.6)$$

For bent-over plumes, Eqs. 11.3 and 11.4 and the equation $z = 1.6F_0^{1/2}u^{-1}x^{3/2}$ can be used to predict the height (z_l) and length (x_l) of the visible plume:

$$z_l = 3.6R_0 \left(\frac{w_0}{u} \right)^{1/2} \left[\left(\frac{q_{p0} + q_{L0}}{q_s - q_e} \right)^{1/2} - 1 \right] \quad (\text{windy}) \quad (11.7)$$

$$x_l = 3.4 \frac{R_0^{3/2} u^{3/4} w_0^{3/4}}{F_0^{1/2}} \left[\left(\frac{q_{p0} + q_{L0}}{q_s - q_e} \right)^{1/2} - 1 \right]^{3/2} \quad (\text{windy}) \quad (11.8)$$

Since ambient variables, such as q_e , q_s , and u , are assumed to be constant with height in this method, use of the method is limited to visible plume heights less than about 100 m.

11-2.2 Numerical Approach for Deep Visible Plumes

When the variables q_e , q_s , and u change with height, models that use differential equations must be used to follow the plume. Visible plume dimensions, cloud-water concentration, cloud formation, and rainout can be predicted. Several models are available to the interested reader (e.g., Wigley and Slawson, 1971; Hanna, 1976, 1981; Weil, 1974; Koenig, Murray, and Tag, 1978). In general, these models are a marriage of plume-rise and cloud-growth models and include the following equations, expressed in words.

Entrainment assumptions:

$$\partial R / \partial z = \dots \quad (11.9)$$

Equation of motion (w , + possibly u):

$$\frac{\partial w}{\partial z} = \text{buoyancy force} - \text{entrainment} - \text{drag due to water drops} \quad (11.10)$$

First law of thermodynamics:

$$\frac{\partial T_p}{\partial z} = \text{dry adiabatic change} + \text{latent heat release} - \text{entrainment} \quad (11.11)$$

Equation for saturated q_{ps} as a function of temperature and pressure:

$$\text{Clausius - Clapeyron or any one of a number of empirical equations} \quad (11.12)$$

Equation for variation in water vapor:

$$\begin{aligned} \frac{\partial q_p}{\partial z} &= - \text{entrainment (if unsaturated)} \\ &= \frac{\partial q_{ps}}{\partial z} \text{ (if saturated)} \end{aligned} \quad (11.13)$$

Equation for cloud water q_c change:

$$\frac{\partial q_c}{\partial z} = \text{condensation} - \text{conversion and coalescence to rainwater} - \text{entrainment} \quad (11.14)$$

Equation for rainwater q_h change:

$$\frac{\partial q_h}{\partial z} = \text{conversion and coalescence from cloud water} - \text{rainout} - \text{entrainment} \quad (11.15)$$

The cloud-physics parameterizations of Kessler (1969) can be used in the last two equations for cloud water and rainwater.

An interesting problem that can be studied with the above model is the question of whether dry cooling towers are more likely to cause cloud formation than wet cooling towers. In a dry tower, heat exchange is accomplished in a manner similar to that in an automobile radiator. Koenig, Murray, and Tag (1978) found that the plumes and clouds from dry towers were much larger than those from wet towers for the same total (latent + sensible) heat flux.

The reason for the difference is that the latent heat from the wet towers is not all available, whereas the sensible heat from the dry towers is immediately available. The model by Koenig (1979) has also been used to simulate snowfall from wet cooling tower plumes, a phenomenon that has been observed on isolated occasions (e.g., Otts, 1976).

11-3 DRIFT DEPOSITION

Drift is circulating water drops that escape from the cooling tower. Since the circulating water contains impurities, drift should be minimized. Highly efficient drift eliminators, such as sinusoidal baffles, which deflect and capture drift drops, can reduce drift loss to a small fraction (<0.002%) of the circulating water rate. As a result, environmental effects of drift deposition on ground surfaces and vegetation are observed to be minimal except in the immediate vicinity (<200 m) of mechanical-draft cooling towers.

Drift deposition is calculated in much the same way as the dry deposition of particles because of gravitational settling (see Chap. 10, Sec. 10-2.1). For drops with radii less than about 100 μm , the plume of drops is assumed to disperse in a Gaussian manner but the axis of the drop plume is assumed to settle with terminal speed (v_t) with respect to the gaseous plume. The drift deposition flux is given by

$$\omega = v_t C(x,y,0) \quad (11.16)$$

where $C(x,y,0)$ is the ground concentration of droplets. Generally, this calculation is made for drops in a specified size range. A typical drift drop-size distribution is given in Table 11.1, which indicates that 84.5% of the drift mass is in drops with diameters less than 200 μm . A plume calculation would be made for each of the nine drop-size classes with diameters less than 200 μm . Terminal speed [v_t (cm/sec)] for

diameters [D (cm)] can be estimated by using the following equations (after Engelmann, 1968):

$$\begin{aligned} v_t &= 3.02 \times 10^5 D^2 && (D < 0.0093 \text{ cm}) \\ &= 6816 \times D^{1.177} && (0.0093 < D < 0.068 \text{ cm}) \\ &= 2155 \times D^{0.746} && (0.068 < D < 0.26 \text{ cm}) \\ &= 1077 \times D^{0.224} && (0.26 \text{ cm} < D) \end{aligned} \quad (11.17)$$

Water deposition calculations are more difficult than particle deposition calculations because the water drops will shrink owing to evaporation if relative humidity is less than 100%. A drop may evaporate completely before it hits the ground, and the very small particle remaining will not have sufficient settling speed to fall through the turbulence. Thus, for relative humidities less than 100%, the change in mass (m) of the drop due to evaporation must be accounted for (Mason, 1971):

$$\frac{dm}{dt} = -\pi\delta(q_d - q_e)D\rho\text{Sh} \quad (11.18)$$

where δ = diffusion coefficient of water vapor ($\sim 0.24 \text{ cm}^2/\text{sec}$)

q_d = specific humidity at drop surface

ρ = air density, g/cm^3

ν = kinematic viscosity of air ($\sim 0.15 \text{ cm}^2/\text{sec}$)

$Re = Dv_t/\nu$ (droplet Reynolds number)

$\text{Sh} = [2 + 0.552 Re^{1/2}/(\delta/\nu)^{1/2}]$ (Sherwood number)

The difference ($q_d - q_e$) can also be estimated by using a formula from Mason (1971):

$$\frac{q_d - q_e}{q_e} = \frac{\{1 + i(M_0/M_s)[m_s/(m - m_s)]\}^{-1} - \text{RH}}{\text{RH} + [L^2\delta\text{MSh}\rho q_e/(R_g T^2 k_t \text{Nu})]} \quad (11.19)$$

where $R_g = 8.32 \times 10^7 \text{ ergs mole}^{-1} \text{ }^\circ\text{K}^{-1}$

RH = relative humidity (on scale of 0 to 1)

m_s = mass of solute, g

Table 11.1 Drop-Size Distribution at Mouth of Chalk Point Tower*

Drop diameter range, μm	Percent of total mass	Drop diameter range, μm	Percent of total mass	Drop diameter range, μm	Percent of total mass	Drop diameter range, μm	Percent of total mass
10-30	13.8	150-180	3.8	350-400	0.9	800-900	0.8
30-50	28.8	180-210	3.0	400-450	0.7	900-1000	0.7
50-70	13.4	210-240	2.3	450-500	0.6	1000-1100	0.6
70-90	8.9	240-270	1.7	500-600	1.0	1100-1200	0.4
90-110	6.2	270-300	1.3	600-700	1.0	1200-1300	0.1
110-130	4.2	300-350	1.4	700-800	0.9	1300-1400	0.1
130-150	3.4						

*From Environmental Systems Corporation, *Cooling Tower Drift Dye Tracer Experiment*, PPSP-CPCTP, 1977.

M_s = molecular weight of solute, g/mole
 M_0 = molecular weight of water, g/mole
 i = van't Hoff's factor (~ 2 for sea salt)
 $Nu = 2 + 0.552 Re^{1/2} (\nu/k_t)^{1/3}$
 k_t = thermal diffusivity of air = $0.24 \text{ cm}^2 \text{ sec}^{-1}$ at 0°C

In these formulas the drop temperature is assumed to equal the ambient wet-bulb temperature. Probably the most satisfactory way to solve the evaporation problem is by means of a numerical solution in time, where a new drop size and settling speed are calculated from the above equations at each time step.

For large drops with diameters greater than $200 \mu\text{m}$, deposition is calculated by a ballistic trajectory. Owing to these larger drops, maximum drift deposition is usually observed at distances less than 1 or 2 km from the cooling tower. The smaller drops carry a larger fraction of the drift-water mass, but their deposition is spread over a much larger area. Trajectory calculations are generally made for about 10 to 20 drop sizes, which represent the drop-size class boundaries or midpoints from such data as those in Table 11.1.

Drops are assumed to be initially distributed uniformly over the plume cross section. The plume centerline (z_c) is calculated as shown in Chap. 2, Sec. 2-3, and the bottom of the vapor plume (z_b) is given by the relation

$$z_b = z_c - R_w \quad (11.20)$$

The vapor plume radius is found from

$$R_w = R_0 + 0.28z_c \quad (11.21)$$

Consider drift drops of diameter D settling with speed v_g in the plume. Since the interior of the plume is probably saturated, evaporation need not be considered. A scheme for calculating the fraction f_i of drops that "break away" or settle out of the plume in distance interval Δx is shown in Fig. 11.5. The fraction f_i is estimated by using the equation

$$f_i = \frac{v_g (\Delta x_i / u)}{2R_w} \quad (11.22)$$

which is the ratio of the distance the drops fall in the interval Δx_i to the plume diameter at that distance.

At each downwind distance interval Δx_i , the fraction f_i of drops that break away will be different for each of the ten or twenty drop-size classes. After breakaway, the drops may evaporate in the ambient air. Equations 11.18 and 11.19 are used to estimate drop evaporation and changes in settling speed. For

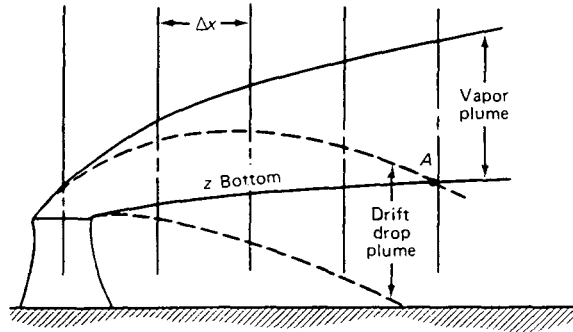


Fig. 11.5 Outline of a cooling tower vapor plume and a drift drop plume (for drops in a narrow size range). By point A, all drift drops in this size range have dropped out of the plume. In any interval Δx , a fraction $[v_g (\Delta x / u) / 2R]$ of the drops breaks away.

each drop size and breakaway point, there is a unique distance (x) from the cooling tower at which the drop is calculated to strike the ground. Thus the drops in a size range leaving the plume in the distance range x to $x + \Delta x_i$ will strike the ground between distances x_a and x_b . They are spread over a crosswind distance equal to θx , where θ is the plume angle (shown in Fig. 11.6), which can be estimated from observed σ_θ

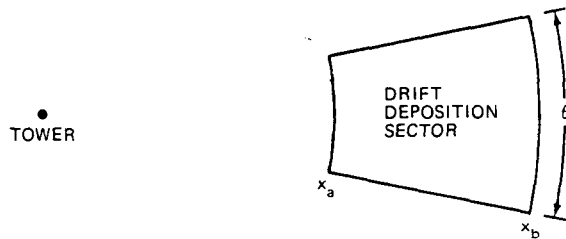


Fig. 11.6 Sector in which drops in a given size range, breaking away from the plume at a certain distance, will be deposited on the ground.

or from Pasquill-Gifford σ_y values. A typical value of θ is 10° to 20° . Then the drift deposition flux (ω_{ij}) for the mass (M_j) of drops in that size range leaving the plume in the interval (Δx_i) is given by

$$\omega_{ij} = \frac{M_j f_i}{\theta (x_b^2 - x_a^2)} \quad (11.23)$$

The total drift deposition pattern is obtained by summing Eq. 11.23 over all drop-size classes and all breakaway intervals.

Policastro, Dunn, and Breig (1978) have compared the predictions of several drift deposition models against some limited observations from Chalk Point and have shown that there are six or seven

models that are roughly equal. Accuracies are probably within a factor of 2 to 5. With all the possibilities for error, such as the breakaway and evaporation calculations, it is easy to see why drift deposition models can never be highly accurate.

Problems

1. A single typical natural-draft cooling tower is located in a valley. Environmental temperature, wind speed, and relative humidity are 20°C , 5 m/sec, and 50%, respectively. What is the flux of water from this tower (in g/sec)? Assuming that the tower effluent fills up the valley, which is 10 km wide and 1 km deep, what would be the flux of water from the tower necessary to saturate the environment? What is the ratio of the actual tower flux to the flux necessary to saturate the environment?
2. Environmental temperature is 25°C and relative humidity is 70%. Calculate the saturation deficit. A natural-draft cooling tower has a radius of 40 m and an initial temperature of 45°C . The plume is saturated but contains no liquid water. What will be the visible plume height in a calm environment?
3. A drift drop has a diameter of $50\ \mu\text{m}$. The difference between the specific humidity at the drop surface and the environmental specific humidity is 0.002 g/g. What is the rate of change of mass (m) of the drop as a result of evaporation?
4. Calculate the gravitational settling speed for water drops with diameters of 40, 200, and $1400\ \mu\text{m}$. Suppose these drops were released from a plume at a height of 300 m in a wind speed of 5 m/sec. At what distance from the release point would each drop strike the ground?

Air-Pollution Meteorology in Complex Terrain

12-1 INTRODUCTION

In the past decade air-pollution meteorology in complex terrain has emerged as a top issue. Part of the reason for this is that many new power plants and other industries are being built in the mountainous western part of the United States. Furthermore, many eastern industries are located near hills and ridges, and recent regulations require that pollutant concentrations be calculated at the surface of these terrain obstacles. Interest is also inspired by the requirement to calculate the impact of sources on distant national parks and forest preserves.

Complex terrain influences the trajectory and the diffusion of a plume. Does the plume strike a ridge, or is it deflected above the ridge? What methods should be used to estimate diffusion? Field data necessary to answer these questions are seriously lacking. A few good field programs are now under way by the Environmental Protection Agency, the U. S. Department of Energy, and the Electric Power Research Institute. The techniques described in this chapter provide guidance for estimating diffusion in complex terrain.

12-2 METEOROLOGY

Even though it is possible that high-pollutant concentrations may occur in complex terrain (e.g., where plumes intercept hillsides), several physical processes are acting that tend to lower concentrations. The first of these is the tendency of wind to favor the "grain" of the terrain; it rarely goes across it. Many field studies show the validity of this statement: Figure 12.1 is a topographic map of the Widows Creek Steam Plant area in northeastern Alabama, where the major terrain obstacle is a linear 250-m terrain step. Figure 12.2 is a wind-rose diagram for meteorological stations in the valley and on the mountain (Hanna, 1980b). The wind on the mountain blows with nearly the same frequency from all directions, but the wind in the valley is strongly

channeled up or down the valley, which reduces the probability of plume impingement on the mountain-side.

Another favorable meteorological effect in complex terrain is the enhancement of turbulence due to eddies that are set up by air passing over and around terrain obstacles. Panofsky, Egolf, and Lipschutz (1978) found that, for a meteorological tower 500 m downwind of a ridge, the standard deviation of wind-direction fluctuations (σ_θ) was increased by a factor of 2.5. Hanna (1980b) found that σ_θ was increased by a factor of 1.6 during neutral conditions when the wind direction was perpendicular to the valley (Fig. 12.1). The tower was located 2 to 10 km from the ridges to the northwest and southwest in Fig. 12.1. More detailed observations of σ_θ were made at a network of eleven towers in the Geysers, Calif., geothermal area. The terrain consists of randomly oriented 1000-m mountains and ridges. For the eleven stations, Hanna (1980c) calculated the median hourly σ_θ values from 5 days of observations at a height of 10 m. These σ_θ values are plotted against the hour of the day in Fig. 12.3, which shows that nighttime σ_θ values are about 20° to 26° and daytime values are about 30° to 35°. Over flat terrain nighttime σ_θ values are predicted to be only 5° or less (see Tables 4.2 and 4.3). With extreme stabilities, meandering may cause occasional high values of σ_θ . However, in the Geysers, σ_θ is consistently high for all stable conditions, which leads us to the conclusion that terrain obstacles cause an enhancement of σ_θ . This conclusion is further confirmed by the data in Fig. 12.4, in which σ_θ is plotted against wind speed for nighttime runs at a given station. At low wind speeds, corresponding to the largest static stability $[(g/T) \partial\theta/\partial z]$ at night, σ_θ is a maximum as a result of these terrain effects.

Of course, complex terrain also causes changes in surface-layer wind speed and direction which adversely affect pollutant concentrations. Pollutants emitted near the ground into the nighttime drainage

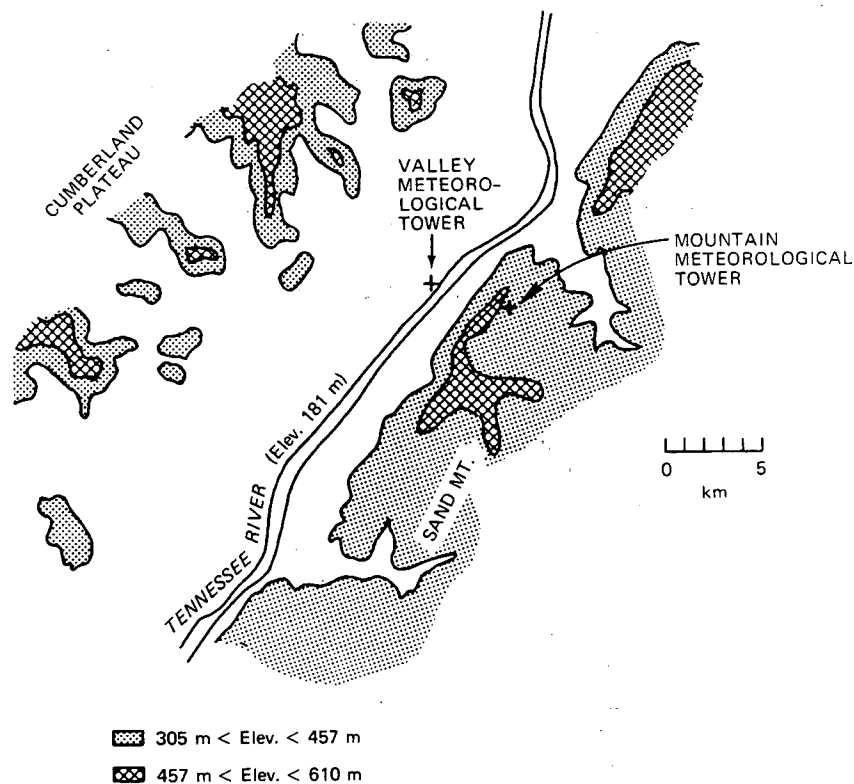


Fig. 12.1 Topographic map of area within 10 km of Widows Creek Steam Plant. Meteorological station locations are given.

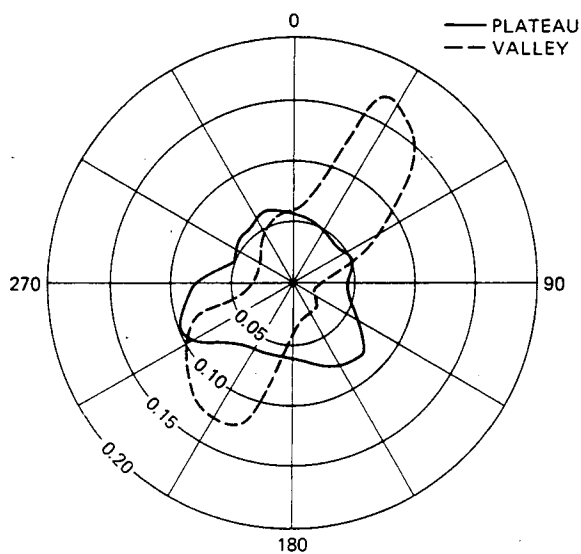


Fig. 12.2 Annual (1977) wind rose for valley and plateau meteorological stations (61-m level) at Widows Creek. Numbers are frequency per 22½° sector.

layer over sloping terrain may follow the drainage flow downhill toward population centers. The thickness (h) of the drainage layer on a simple slope is suggested by Briggs (1979) to be given by the formulas:

$$h = 0.05 \times \sin \beta \quad (\beta > 20^\circ) \quad (12.1)$$

$$h = 0.037 \times \beta^{2/3} \quad (\beta < 20^\circ) \quad (12.2)$$

where x is the distance along the slope from the top of the slope and β is the slope angle in radians. For an angle of 20° and a distance of 500 m, the thickness (h) is about 9 m. Briggs (1979) used energy conservation principles to arrive at the following formula for the characteristic wind speed in the drainage layer:

$$u = 2.15(\sin \beta)^{2/3}(Hx)^{1/3} \quad (12.3)$$

where H is the downward sensible heat flux (in units of m^2/sec^3), which is given by

$$H = -g \frac{w'T'}{T} \quad (12.4)$$

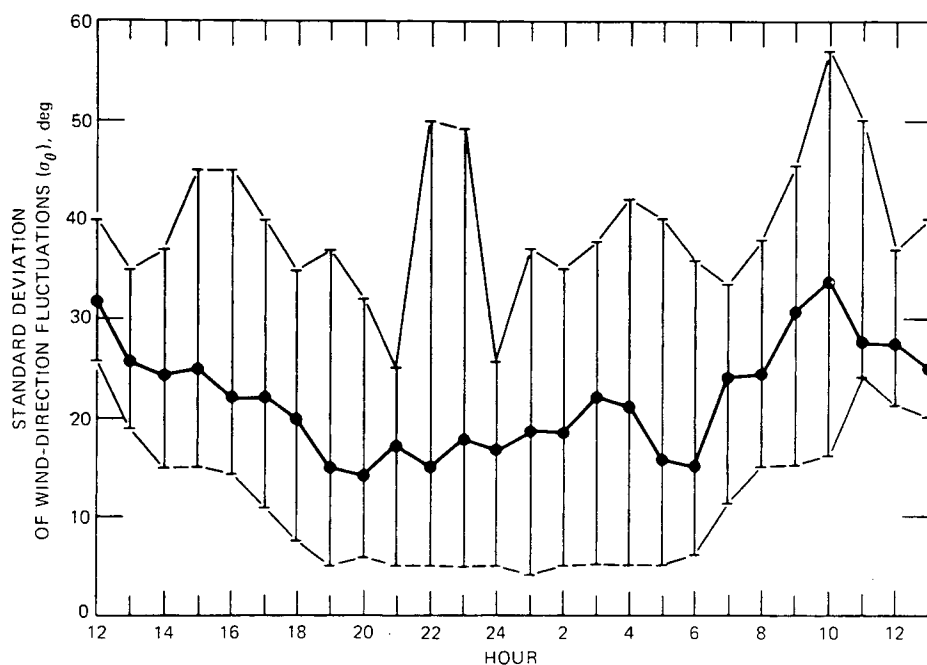


Fig. 12.3 Diurnal variation of σ_θ at a height of 10 m for 11 meteorological towers in complex terrain at the Geysers geothermal area. Hourly σ_θ values for 5 days were averaged together for each of 11 stations. The highest, median, and lowest of the 11 σ_θ values at each hour are plotted.

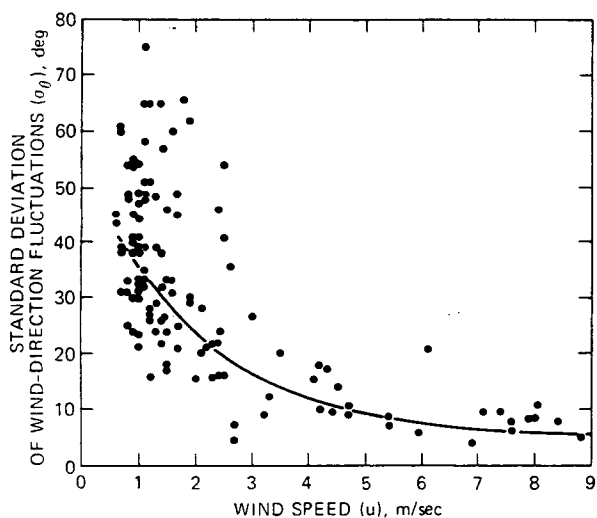


Fig. 12.4 Hourly average σ_θ vs. wind speed for nighttime (2100 to 0600) data from five observation-nights at the Geysers geothermal area. This station is located about halfway down a 1000-m-elevation ridge.

For typical values, H can be of the order of $0.001 \text{ m}^2/\text{sec}^3$ on a clear night. If $\beta = 27^\circ$ and $x = 1 \text{ km}$, then $u = 1.8 \text{ m/sec}$, which is a value of wind speed often observed in drainage layers. Drainage from the ideal slopes considered in the above derivation usually rises to converge into a narrower valley, which gives

a deeper drainage "river." An example of typical air trajectories in a valley is shown in Fig. 12.5, which is also taken from the results of the Geysers experiment (Nappo et al., 1980). This drainage flow has a depth of 50 to 100 m and a speed of 2 to 3 m/sec and is about 2 to 3 km downhill from the ridgetops. A few kilometers farther down the valley, where it broadens out and the slope decreases, the drainage pool is observed to be about 200 m deep with a speed of about 1 m/sec.

Numerical or physical models can be used to estimate wind flow over complex terrain. Most of the work before 1975 has been reported by Egan (1975). Numerical models in use are all "research-grade," and much developmental work needs to be done. The biggest need is for field data, which would aid in the development and testing of such models. In numerical models, it is difficult to obtain the necessary detail (small grid size) while still retaining a large enough domain size to cover the area of interest. For simple two-dimensional hills, the potential flow theory appears to give good results.

Physical models of flow over complex terrain have been reviewed by Hosker (1980), who points out that the most obvious effects occur when the flow is stratified. Blocking, lee waves, rotors, and wake formation are some of the more interesting

phenomena that have been observed. The stability parameter most often used to classify this work is the internal Froude number:

$$F_H \equiv \frac{U}{NH} \quad (12.5)$$

where U is the free-stream wind speed, H is the hill height, and N is the Brunt-Väisälä frequency (in rads/sec):

$$N \equiv \left(\frac{g}{T} \frac{\partial \theta}{\partial z} \right)^{1/2} \quad (12.6)$$

where θ is the potential temperature and N is the natural frequency of oscillation of an air parcel

displaced slightly in a stable atmosphere. For $F_H \leq 1$, motions tend to be limited to horizontal planes; i.e., plumes will impact the surface and try to go around hills rather than over them (Hunt, Snyder, and Lawson, 1978). For $F_H > 1$, the airflow is likely to be over the top of the hill.

12-3 DIFFUSION CALCULATIONS

As Pasquill (1974) suggests, observations of wind flow and turbulence parameters, if available, should be used to calculate diffusion. However, in most real

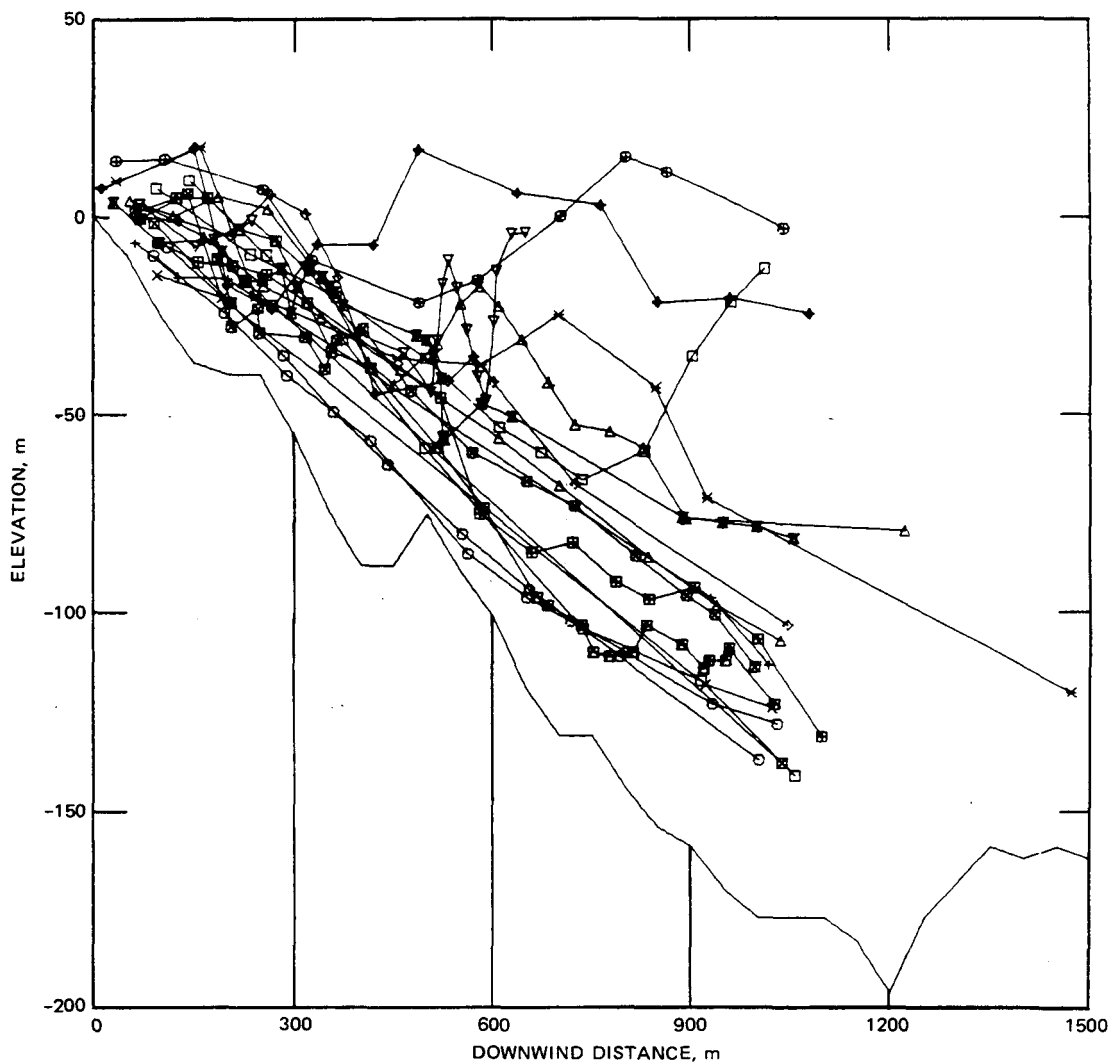


Fig. 12.5 Composite view of nighttime neutral pilot balloon trajectories down Anderson Creek canyon in the Geysers geothermal area. The solid line beneath all the trajectories is the underlying terrain elevation. Presumably the top of the drainage flow is marked by the point at which the trajectories pop up out of the flow. (From C. J. Nappo, S. R. Hanna, and H. F. Snodgrass, *Drainage Wind Observations Using Neutral-Lift Balloons*, in *Second Joint Conference on Applications of Air Pollution Meteorology*, p. 496, American Meteorological Society, Boston, Mass., 1980.)

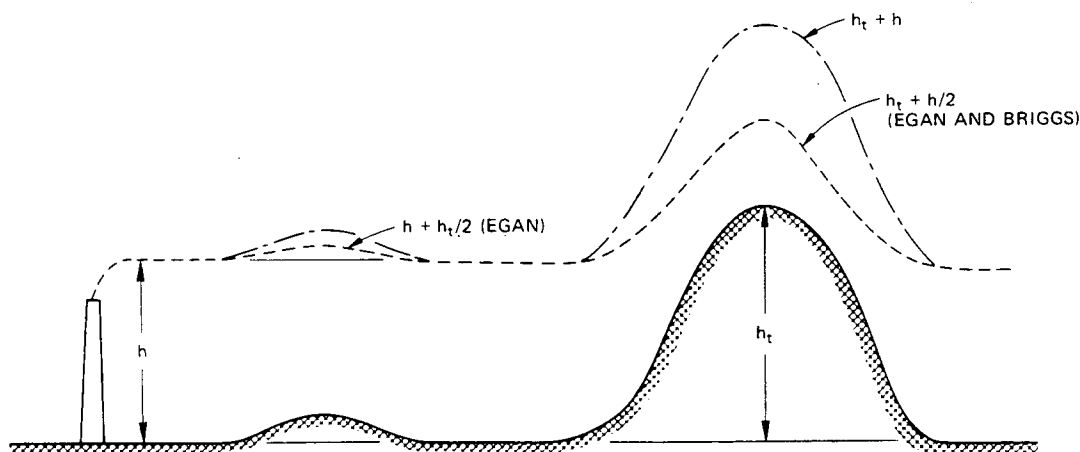


Fig. 12.6 Illustration of plume height assumptions in Briggs (1973) (—) and Egan (1975) (---) models for neutral and unstable conditions. The line $h_t + h$ is also shown.

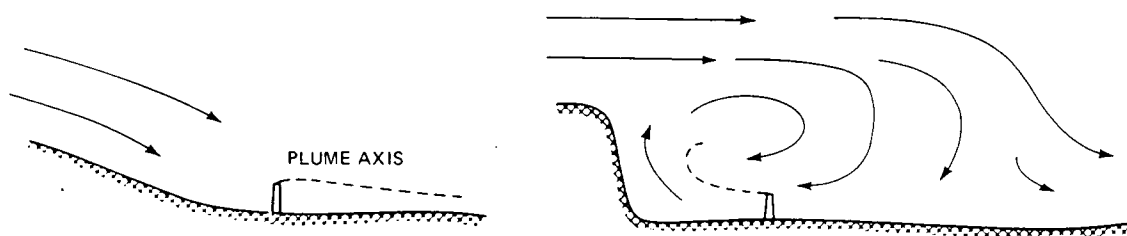


Fig. 12.7 Effect of upwind terrain on plume trajectories for gentle slopes and abrupt ridges.

situations we do not have the luxury of such detailed observations. In this case the empirical methods, which are based on models developed by Briggs (1973) and Egan (1975, 1979), described in the following paragraphs can be used to estimate diffusion from elevated point sources.

First, will a plume impact on a terrain obstacle, or will it ride up over the obstacle? If a terrain rise is downwind of a source in neutral and unstable conditions (Pasquill-Gifford classes A-B-C-D; or $F_H > 1$), the plume tends to ride up the slope while losing part of its effective stack height (h) relative to the ground. In this case Briggs (1973) suggests that h should be reduced by the terrain height (h_t) or $h/2$, whichever is the smallest reduction. Terrain height (h_t) is measured from the base of the source stack. This concept is illustrated in Fig. 12.6. The $h/2$ correction for high terrain is based on potential flow theory and wind-tunnel experiments, as mentioned in Sec. 12-2. Egan's (1975) model is the same as that of Briggs except that Egan suggests a reduction of $h_t/2$ rather than h_t for terrain heights less than half the effective plume height. Thus the assumption by Egan would give slightly lower ground-level concentrations at the surface of small hills than that by Briggs. In

stable conditions (Pasquill-Gifford classes E-F; or $F_H < 1$), both modelers assume that the plume maintains a constant elevation; thus the effective plume height (h) is reduced by terrain height (h_t). If the terrain height is greater than the effective plume height, the plume may impinge on it in E or F conditions.

If there is a terrain rise upwind of the source and the average slope of the rise above the source exceeds 2%, downwash may be induced by the air flowing down over the terrain drop. For steep hills, it is possible to get a "cavity" effect, i.e., a counter-rotating eddy. The cavity would extend three to ten hill heights downwind, which would possibly cause downwash and fumigation of a plume in this region. Figure 12.7 illustrates these effects. For more precise estimates of concentration distributions in this case, wind-tunnel or water-channel modeling of the situation should be done since the trajectories depend heavily on details of the topography.

Chapter 4 shows that an image source can be used in the Gaussian plume model to account for "reflection" from the ground surface. However, Egan et al. (1979) point out that this assumption leads to an abrupt factor of 2 increase in axial plume concentra-

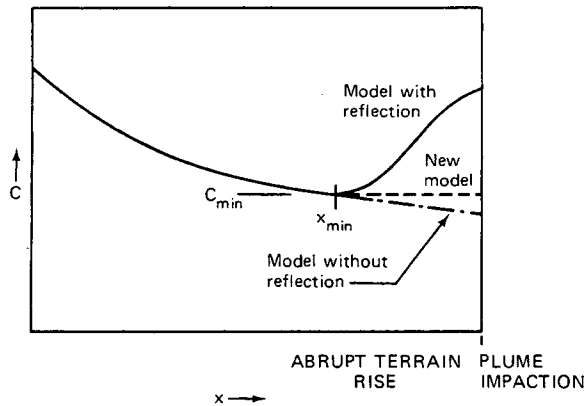


Fig. 12.8 Axial concentration variation with downwind distance as an abrupt terrain rise is approached. —, Gaussian model with reflection. - · -, Gaussian model without reflection. - - -, recommended curve.

tion from plumes impinging on steep terrain in stable (E-F; $F_H < 1$) conditions. Therefore his model has the requirement that axial plume concentration can never increase with downwind distance (see Fig. 12.8). For this model to be applied, the solid curve in the figure must first be calculated so that the minimum concentrations (C_{min}) at point x_{min} can be determined. From point x_{min} to the point at which the plume strikes the terrain, the axial concentration is assumed to equal C_{min} .

The analysis of σ_θ observations in complex terrain at the Geysers geothermal site described in Sec. 12-2 showed that σ_θ was close to what would be expected over flat terrain during the day; however, owing to terrain effects, it was enhanced during the night. In fact, nighttime σ_θ does not fall much below the "neutral" value. This result is consistent with the few limited diffusion experiments that have been conducted in complex terrain and supports the assumption by Egan et al. (1979) that stable classes E and F should be shifted to neutral class D when selecting σ_y and σ_z . Knowledge of the site (e.g., valley width) should be used to modify σ_y if necessary. During neutral and unstable conditions, flat-terrain σ_y and σ_z curves can be used.

Diffusion in valleys is limited when the valley width (W) equals roughly $2\sigma_y$. At night elevated plumes could fill up the valley horizontally with very little vertical diffusion (see Fig. 12.9). The highest concentration experienced by the valley walls would be given by

$$C = \left(\frac{2}{\pi}\right)^{1/2} \frac{Q}{\sigma_z u W} \quad (12.7)$$

In the morning, "break-up fumigation" brings the pollutant to the valley floor when the stable layer is eroded from below by the heating of the ground. The average concentration in this case is

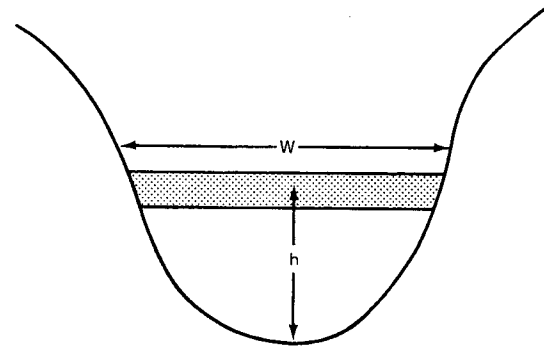


Fig. 12.9 Schematic view of an elevated plume mixed across a valley of width W during stable conditions.

$$C = \frac{Q}{uhW} \quad (12.8)$$

where all variables are nighttime values.

Problems

1. A highway follows a constant elevation contour along the side and very near the top of a two-dimensional slope with an angle of 10° . Carbon monoxide emissions are $0.1 \text{ g sec}^{-1} \text{ m}^{-1}$. Assume night conditions with a drainage wind of 1 m/sec. If the carbon monoxide mixes uniformly within the drainage layer, what is the carbon monoxide concentration a distance of 200 m, 500 m, and 1000 m down the slope from the highway?

2. Consider an isothermal atmosphere with a wind speed of 5 m/sec flowing over a hill of height 200 m. Calculate the internal Froude number. What will happen to a plume heading toward the hill?

3. With the use of Briggs's criteria, fill in the following table. Assume neutral conditions.

Plume rise above level terrain (h), m	Hill height (h_t), m	Predicted height of plume above hill
200	10	
10	9.9	
100	200	
500	1000	
0	100	

4. Assume that an elevated point-source plume will impact a steep mesa during very stable conditions. The source strength is 10 g/sec and the wind speed is 4 m/sec. Calculate the centerline concentration at the point the plume impacts the mesa a distance of 5 km from the source.

Long-Range Transport and Diffusion

13-1 INTRODUCTION

Long-range transport and diffusion calculations have been important for the nuclear industry since the 1940's because of the dangers of bomb tests. However, during the past decade the problems of long-range transport of sulfur and nitrogen compounds from power plants and smog from urban areas have become increasingly important. Sulfur from distant sources reacts with water in the atmosphere to form acid rain, which can cause serious environmental damage in such remote areas as the Adirondack Mountains of New York and the lakes of Scandinavia. These effects are difficult and expensive to monitor, although a few large programs are under way by the Organization for Economic Cooperation and Development in Europe and the U. S. Department of Energy, U. S. Environmental Protection Agency, and Electric Power Research Institute in the United States. Several recent review papers exist on this subject, including those by Bass (1980) and Eliassen (1980).

Numerous models are available, and some of these models are described in this chapter. However, as yet there is no definitive model for long-range transport and diffusion. There are simply too many missing pieces of information, such as σ_y or K_y coefficients, at these scales. Since the Pasquill-Gifford σ_y and σ_z curves are defined only to downwind distances of about 10 km, "long range" is defined in this chapter as any downwind distance greater than about 10 km. At these distances wind speed and direction shears and time and space variation in wind velocity become important.

13-2 MODELING CONCEPTS

In practice, winds are always averaged over a certain period, such as an hour. Turbulent diffusion is then defined as the diffusion contributed by turbulent eddies with time scales less than the averaging

time, in this case, roughly 1 hr. In the diffusion equation,

$$\frac{\partial C}{\partial t} + u \frac{\partial C}{\partial x} + v \frac{\partial C}{\partial y} = \frac{\partial}{\partial x} K_x \frac{\partial C}{\partial x} + \frac{\partial}{\partial y} K_y \frac{\partial C}{\partial y} + \frac{\partial}{\partial z} K_z \frac{\partial C}{\partial z} \quad (13.1)$$

the turbulence contribution appears on the right-hand side. As the average wind field changes from hour to hour, the effect is felt in the advection terms $u \partial C / \partial x$ and $v \partial C / \partial y$ on the left-hand side, which also contribute to variations in concentration C . If we assume an averaging period of 1 day rather than 1 hr for the wind speed, then hour-to-hour variations should be parameterized as turbulence on the right side of Eq. 13.1. Thus turbulent diffusivities K_x , K_y , and K_z or dispersion parameters σ_x , σ_y , and σ_z are increasing functions of averaging time.

So-called "puff" models claim to handle both small-scale diffusion and large-scale meander (see, for example, Heffter, 1980; Bass et al., 1979; Johnson, Wolf, and Mancuso, 1978; Wendell et al., 1976). Figure 13.1 shows how a plume is represented by a

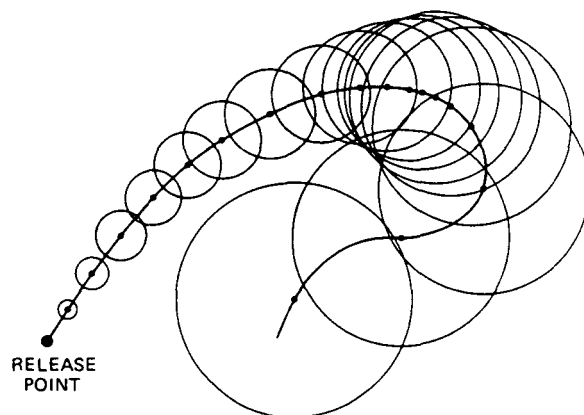


Fig. 13.1 Simulation of a plume by a series of puffs released at equal time intervals. It is assumed that $\sigma \propto t$.

series of puffs. Puff release frequency is adjusted so that there is roughly the amount of puff overlap shown on the figure. A wind field is needed, which would be based on radiosonde stations (spacing, ~300 km), surface stations (spacing, ~50 km), or a mesoscale research grid (spacing, ~20 km) of meteorological towers. In models such as Sherman's (1978), the continuity equation is used to adjust the wind field so that it is mass consistent. The mixing depth must also be known since all models confine the pollutants to the mixed layer. Transport wind velocity seems to be defined differently by each model; e.g., it equals 0.75 times the 850-mb wind in the model by Johnson, Wolf, and Mancuso (1978) and equals the concentration-weighted wind in the model by Heffter (1980). The observed winds must be interpolated into other regions, generally using a $1/(\text{distance})^2$ weighting, although some models use an additional weighting factor involving wind direction. This situation is depicted schematically in Fig. 13.2.

Diffusion of the puff is handled quite crudely. The first tenuous assumption is that puff diffusion is similar to plume diffusion, which is known to be wrong theoretically (see Chap. 6) but is still useful in applied models. Nevertheless, there is no information available on the spread of puffs at long range in the mixed layer, and it is necessary to fall back on plume σ 's. Wendell et al. (1976) have extrapolated the Pasquill-Gifford curves for σ_y and σ_z (Fig. 4.4) to great distances—a procedure not recommended by Pasquill or Gifford. The Heffter (1980) model uses the simple expression $\sigma_y = 0.5t$ (σ_y in meters and t in seconds) for all situations. Fay and Rosenzweig (1980) and Johnson, Wolf, and Mancuso (1978) assume that the Fickian law, $\sigma_y^2 = 2Kt$, is valid, with

$K = 10^4 \text{ m}^2 \text{ sec}^{-1}$. It is found that σ_y is not too crucial for the calculation of pollutant concentrations averaged over a day or longer since total diffusion is dominated by meander for large averaging times. For these large averaging times, it is sufficient to know the wind-direction frequency distribution in 22 $\frac{1}{2}$ -degree sectors. Sheih (1977) and Draxler (1979a) specify K_z profiles to handle vertical diffusion. At short distances this is important for elevated sources; however, at long distances ($>100 \text{ km}$) the plume can be assumed to fill up the mixed layer uniformly (Johnson, Wolf, and Mancuso, 1978). Draxler's (1979a) K_z assumptions are listed in Table 13.1.

Table 13.1 Draxler's Suggested Relation Between K_z and Stability Class

[Below 100 m, $K_z(z) = (z/100 \text{ m})K_z(100 \text{ m})$]

Stability class	$K_z, \text{m}^2/\text{sec}$
A	160
B	100
C	70
D	15
E	5.0
F	1.5
G	0.13

On the other hand, removal is quite important since the half-lives for dry deposition, wet deposition, and chemical transformations of chemicals, such as SO_2 , are typically on the order of a few days. Here again, however, crude assumptions, such as $v_d = 1 \text{ cm/sec}$ for SO_2 and $v_d = 0.1 \text{ cm/sec}$ for sulfates, are made by most investigators. The conversion of SO_2 to sulfate is generally assumed to take place at a rate of about 1%/hr. Wet removal rate is assumed to be proportional to rainfall rate raised to some power; e.g., Smith and Hunt (1978) use λ (fraction removed per second) = $10^{-4} R^{1/2}$, where R is rainfall rate (in mm/hr). For a moderate rain of 4 mm/hr, wet removal takes place at a rate of 72%/hr. A slightly different formula is used by Johnson, Wolf, and Mancuso (1978), with $\lambda = 0.6 \times 10^{-4} R$. When it is raining, wet removal is quite effective; however, over a long time period, wet and dry removal are equally effective.

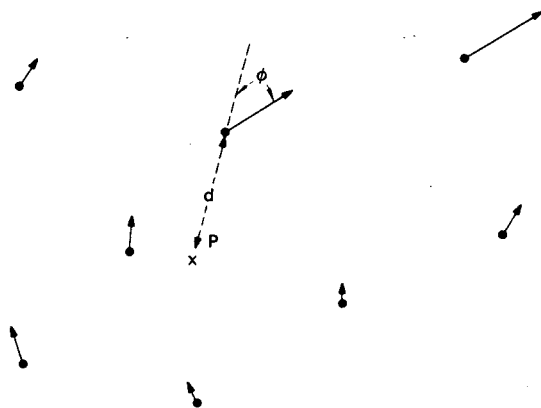


Fig. 13.2 Example of wind vectors observed at eight surface stations, which must be used to estimate the wind vector at point P. Most models weight each observation by $1/d^2$. The models by Draxler (1979b) and Heffter (1980) weight, in addition, each observation by $1-0.5 |\sin \phi|$.

Recommendations for the parameters discussed above are as follows:

$$\sigma_y = 0.5t \quad (\sigma_y \text{ in m and } t \text{ in sec}) \quad (13.2)$$

$$K_z \quad (\text{use Table 13.1}) \quad (13.3)$$

$$v_d (\text{SO}_2) = 1.0 \text{ cm/sec} \quad (13.4)$$

$$v_d (\text{SO}_4^{-2}) = 0.1 \text{ cm/sec} \quad (13.5)$$

$$\text{SO}_2 \rightarrow \text{SO}_4^{-2} \text{ conversion rate} = 0.01 \text{ hr}^{-1} \quad (13.6)$$

$$\lambda = 10^{-4} R^{1/2} \quad (\lambda \text{ in fraction sec}^{-1} \text{ and } R \text{ in mm/hr}) \quad (13.7)$$

Wind velocity: Use observed profiles, weighted by concentration distribution with height. Interpolate between stations using $1/r^2$ weighting (13.8)

With so many uncertain adjustable parameters, the matching of predicted and observed concentration patterns becomes quite easy. In these applications, however, the model is not truly validated since validation requires testing of the model with an independent data set.

13-3 APPLICATION TO AN INERT TRACER

Some of the problems encountered with long-range transport and diffusion models for sulfur are due to uncertainties in dry deposition, wet deposition, and chemical transformations. The testing of models by using inert tracers, such as ^{85}Kr , a gas that is released routinely from nuclear installations, or man-made inert tracers, such as SF_6 or heavy methanes, is useful. For these tracers, the observed concentration patterns are due solely to winds and turbulence. Draxler (1979b) describes an application of his model to the Savannah River Laboratory (SRL) area; the locations of rawinsonde stations, surface stations, towers, release site, and a 90-km sampling arc are shown in Fig. 13.3. In addition to routine releases of ^{85}Kr , two tracers, SF_6 and heavy methane ($^{13}\text{CH}_4$), were released from a 62-m stack over a 4-hr period.

The model simulates the pollutant plume by a series of puffs, whose trajectories are computed by hourly advection segments. First, the rawinsonde profile from the station nearest the segment starting point is used to estimate the average layer wind (\bar{V}_A) weighted by the concentration:

$$\bar{V}_A = \frac{\sum_i^n C_i V_i}{\sum_i C_i} \quad (13.9)$$

where n is the number of levels up to the mixing height. Mixing height is determined by following the maximum surface temperature up dry adiabatically

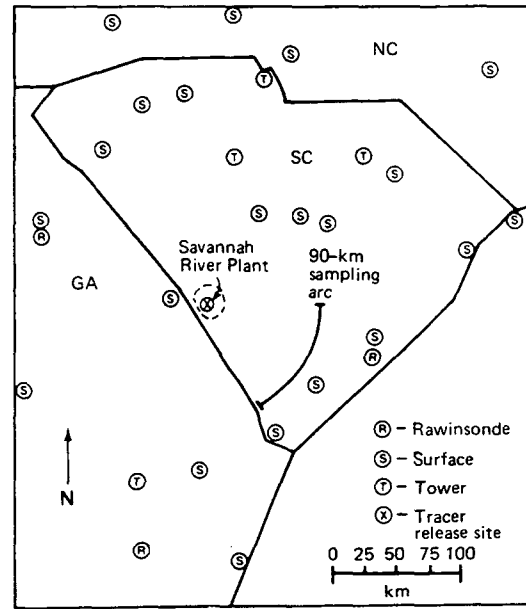


Fig. 13.3 The Savannah River experiment sampling arc and meteorological data locations. [From R. R. Draxler, Modeling the Results of Two Recent Mesoscale Dispersion Experiments, *Atmos. Environ.*, 13: 1526 (1979).]

until it intercepts the 1200 GMT sounding. The relations between the magnitude and direction of the surface wind (V_s), and average layer wind (\bar{V}_A) are determined and are arbitrarily assumed to apply at all stations on the network. The advantage of using surface winds is that they report hourly, in contrast to rawinsondes, which report at 12-hr intervals. For example, this analysis may show that $V_s/|\bar{V}_A| = 0.5$ and that the direction of V_s is 20° to the left of the direction of \bar{V}_A . Next, a surface wind at the segment starting point is calculated by using a d^{-2} distance weighting and a direction weighting (α_s) given by

$$\alpha_s = 1 - 0.5 |\sin \phi_s| \quad (13.10)$$

where ϕ_s is the angle between the wind direction and the line from the station to the segment starting point. Only angles with magnitudes of 90° or less are considered. Finally, a transport wind is determined by using the calculated surface wind and the relations developed at the rawinsonde station.

Vertical diffusion is calculated from the one-dimensional diffusion equation by using a vertical diffusivity equal to $7 \text{ m}^2/\text{sec}$ at a height of 100 m. This is the value Draxler was assuming for neutral conditions before he prepared the revised Table 13.1. Horizontal diffusion is given by $\sigma_y(m) = 0.5t$ (sec). Concentration contributions from each puff that passes a receptor during the sampling period are summed, and an average concentration is calculated.

Observed and predicted SF₆ concentrations on the 90-km sampling arc are plotted in Fig. 13.4. Draxler has "adjusted" K_z to a value of 30 m²/sec so that the maximum predicted concentration agrees with the observation. Neutral stability conditions (Pasquill-Gifford) prevailed during this experiment, but a value of K_z equal to 7 m²/sec produced a peak concentration that was much too high. The figure shows that the predicted plume is displaced about 20 km from the observed peak, which indicates a wind-direction error of about 10° to 15°. This error is not surprising since the input wind observations are given only to the nearest 10°. However, the net result is a poor correlation between observed and predicted concentrations at fixed points. We can conclude that the model did fairly well in estimating the crosswind concentration distribution but erred slightly in estimating plume direction.

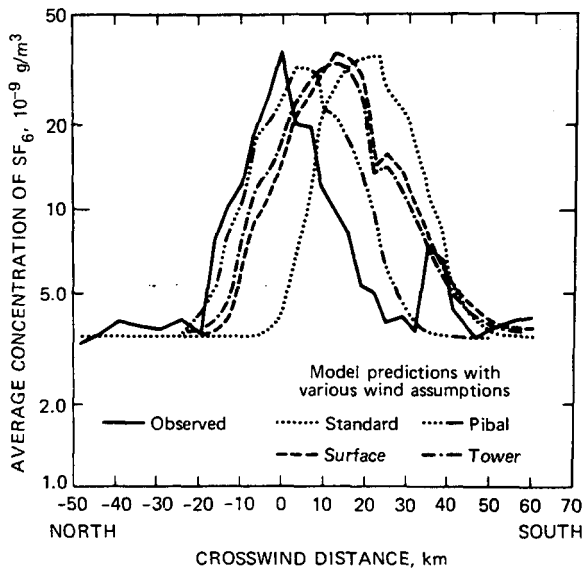


Fig. 13.4 Observed and predicted SF₆ concentration on the 90-km sampling arc at Savannah River. [From R. R. Draxler, Modeling the Results of Two Recent Mesoscale Dispersion Experiments, *Atmos. Environ.*, 13: 1528 (1979).]

Problems

1. Assume mixing depths z_i of 500 m, 1000 m, and 2000 m. For each of these mixing depths, estimate the distance downwind at which $\sigma_z = 0.3 z_i$ for stability classes A, B, C, D, E, and F (use Briggs's σ formulas).

2. What is the difference between σ_y used by Heffter (1980) and that used by Fay and Rosenzweig (1980) at downwind distances of 5 km, 10 km, 50 km, 100 km, 500 km, and 1000 km? Assume wind speed is 5 m/sec.

3. Crudely estimate the fraction of SO₂ remaining in an air mass after it has crossed the Atlantic Ocean from New York to London. Assume typical wind speeds and rainfall frequencies. Explain all your assumptions.

4. A segment starting point in a trajectory calculation is at $x = 0, y = 0$. Ten stations with the following coordinates are reporting the following wind velocities:

Station	x (east), km	x (north), km	Speed, m/sec	Direction, degrees
1	-3.0	-1.0	8.0	190
2	-5.0	2.0	10.0	180
3	-2.0	5.0	11.0	230
4	0.5	2.0	9.0	200
5	2.0	9.0	3.0	280
6	6.0	6.0	2.0	300
7	6.0	2.0	5.0	330
8	3.0	-1.0	6.0	320
9	1.0	-2.0	5.0	270
10	2.0	-4.0	4.0	290

Calculate the interpolated speed at the segment starting point by using

1. $1/d^2$ weighting.
2. $1/d^2$ and direction weighting.

References

- Abramowitz, M., and I. A. Stegun (Eds.), 1964, *Handbook of Mathematical Functions*, National Bureau of Standards Applied Math Ser. #55, GPO.
- Angeli, J. K., P. W. Allen, and E. A. Jessup, 1971, Mesoscale Relative Diffusion Estimates from Tetron Flights, *J. Appl. Meteorol.*, 10: 43-46.
- Barad, M. L. (Ed.), 1958, *Project Prairie Grass: A Field Program in Diffusion*, Geophysical Research Papers, No. 59, Vols. I and II, Report AFCRC-TR-58-235, Air Force Cambridge Research Center.
- Barry, P. J., 1964, *Estimation of Downwind Concentration of Airborne Effluents Discharged in the Neighborhood of Buildings*, Report AECL-2043, Atomic Energy of Canada, Ltd., Chalk River, Ontario.
- Bass, A., 1980; Modeling Long Range Transport and Diffusion, in *Proceedings of 2nd Joint Conference on Applications of Air Pollution Meteorology*, New Orleans, La., Mar. 24-27, 1980, American Meteorological Society, Boston, Mass.
- , C. W. Benkley, J. S. Scire, and C. S. Morris, 1979, *Development of Mesoscale Air Quality Simulation Models*. Vol. I. Comparative Sensitivity Studies of Puff, Plume and Grid Models for Long-Distance Dispersion Modeling, Report EPA-600/7-79-XX, Environmental Protection Agency.
- Batchelor, G. K., 1950, Application of the Similarity Theory of Turbulence to Atmospheric Diffusion, *Q. J. R. Meteorol. Soc.*, 76(328): 133-146.
- , 1952, Diffusion in a Field of Homogeneous Turbulence. II. The Relative Motion of Particles, *Proc. Cambridge Philos. Soc.*, 48: 345-362.
- Braham, R. B., B. K. Seely, and W. D. Crozier, 1952, A Technique for Tagging and Tracing Air Parcels, *Trans. Am. Geophys. Union*, 33: 825-833.
- Briggs, G. A., 1973, *Diffusion Estimation for Small Emissions*, ATDL Contribution File No. 79, Atmospheric Turbulence and Diffusion Laboratory.
- , 1974, Plume Rise from Multiple Sources, in *Cooling Tower Environment—1974*, ERDA Symposium Series, College Park, Md., Mar. 4-6, 1974, Steven R. Hanna and Jerry Pell (Coordinators), pp. 161-179, CONF-740302, NTIS.
- , 1975, Plume Rise Predictions, in *Lectures on Air Pollution and Environmental Impact Analyses*, Workshop Proceedings, Boston, Mass., Sept. 29-Oct. 3, 1975, pp. 59-111, American Meteorological Society, Boston, Mass.
- , 1979, *Analytic Modeling of Drainage Flows*, ATDL Report 79/22, Atmospheric Turbulence and Diffusion Laboratory.
- , 1981, Plume Rise and Buoyancy Effects, in *Atmospheric Science and Power Production*, Darryl Randerson (Ed.), DOE Report DOE/TIC-27601, in press.
- Businger, J. A., J. C. Wyngaard, Y. Izumi, and E. F. Bradley, 1971, Flux-Profile Relationships in the Atmosphere Surface Layer, *J. Atmos. Sci.*, 28: 181-189.
- Byzova, N. L., Ye. K. Garger, and V. N. Ivanov, 1970, Experimental Estimation of the Lagrangian Time Scale of Turbulence, *Izv. Atmos. Oceanic Phys.*, 6: 315-320.
- Cagnetti, P., 1975, Downwind Concentrations of an Airborne Tracer Released in the Neighborhood of a Building, *Atmos. Environ.*, 9(8): 739-747.
- Carpenter, S. B., F. W. Thomas, and F. E. Gartrell, 1968, *Full-Scale Study of Plume Rise at Large Electric Generating Stations*, Tennessee Valley Authority, Muscle Shoals, Ala.
- , T. L. Montgomery, J. M. Leavitt, W. C. Colbaugh, and F. W. Thomas, 1971, Principal Plume Dispersion Models, TVA Power Plants, *J. Air Pollut. Control Assoc.*, 21: 491-495.
- Carlsaw, H. S., and J. C. Jaeger, 1959, *Conduction of Heat in Solids*, 2nd ed., Oxford University Press, London.
- Caughey, S. J., J. C. Wyngaard, and J. C. Kaimal, 1979, Turbulence in the Evolving Stable Layer, *J. Atmos. Sci.*, 36: 1041-1052.

- Chamberlain, A. C., 1975, The Movement of Particles in Plant Communities, in *Vegetation and the Atmosphere*, Vol. 1, Chap. 5, pp. 155-203, J. L. Monteith (Ed.), Academic Press, London.
- Chaudhry, F. H., and R. N. Meroney, 1973, Similarity Theory of Diffusion and the Observed Vertical Spread in the Diabatic Surface Layer, *Boundary-Layer Meteorol.*, 3: 405-415.
- Cramer, H. E., 1957, A Practical Method for Estimating the Dispersal of Atmospheric Contaminants, in *Proceedings of the First National Conference on Applied Meteorology*, Sec. C, pp. C-33-C-35, American Meteorological Society, Hartford, Conn.
- Crane, G., H. A. Panofsky, and O. Zeman, 1977, A Model for Dispersion from Area Sources in Convective Turbulence, *Atmos. Environ.*, 11: 893-900.
- Crawford, T. V., 1966, *Predicting and Sampling Nuclear Clouds from the Viewpoint of Diffusion Theory*, USAEC Report UCRL-14983, University of California, Lawrence Radiation Laboratory.
- Crozier, W. D., and B. K. Seely, 1955, Concentration Distributions in Aerosol Plumes Three to Twenty-Two Miles from a Point Source, *Trans. Am. Geophys. Union*, 36: 42-52.
- Dana, M. T., and J. M. Hales, 1976, Statistical Aspects of the Washout of Polydisperse Aerosols, *Atmos. Environ.*, 10: 45-50.
- Davies, R. W., 1959, Large-Scale Diffusion from an Oil Fire, in *Advances in Geophysics*, Vol. 6, pp. 413-414, F. N. Frenkiel and P. A. Sheppard (Eds.), Academic Press, New York.
- Deardorff, J. W., 1970, A Three Dimensional Numerical Investigation of the Idealized Planetary Boundary Layer, *J. Geophys. Fluid Dyn.*, 1: 377-410.
- , 1974, A Three Dimensional Numerical Study of the Height and Mean Structure of a Heated Planetary Boundary Layer, *Boundary-Layer Meteorol.*, 1: 81-106.
- Demerjian, K. L., and K. L. Schere, 1979, Applications of a Photochemical Box Model for O₃ Air Quality in Houston, Texas, in *Proceedings of Specialty Conference on Ozone/Oxidants: Interactions with the Total Environment*, Environmental Protection Agency, Research Triangle Park, N. C.
- Dickson, C. R., G. E. Start, and E. H. Markee, Jr., 1969, Aerodynamic Effects of the EBR-II Reactor Complex on Effluent Concentration, *Nucl. Saf.*, 10: 228-242.
- Donaldson, C. DuP., 1973, Atmospheric Turbulence and the Dispersal of Atmospheric Pollutants, in *AMS Workshop on Micrometeorology*, pp. 313-390, D. A. Haugen (Ed.), Science Press, Princeton, N. J.
- Doran, J. C., T. W. Horst, and P. W. Nickola, 1978, Variations in Measured Values of Lateral Diffusion Parameters, *J. Appl. Meteorol.*, 17(6): 825-831.
- Draxler, R. R., 1976, Determination of Atmospheric Diffusion Parameters, *Atmos. Environ.*, 10: 99-105.
- , 1979a, Estimating Vertical Diffusion from Routine Meteorological Tower Measurements, *Atmos. Environ.*, 13: 1559-1564.
- , 1979b, Modeling the Results of Two Recent Mesoscale Dispersion Experiments, *Atmos. Environ.*, 13: 1523-1533.
- Edinger, J. G., 1952, *A Technique for Measuring the Detailed Structure of Atmospheric Flow*, Geophysics Research Papers, No. 19, Air Force Cambridge Research Laboratories, Geophysics Research Directorate, Cambridge, Mass.
- Egan, B. A., 1975, Turbulent Diffusion in Complex Terrain, in *Lectures on Air Pollution and Environmental Impact Analyses*, pp. 112-135, D. Haugen (Ed.), American Meteorological Society, Boston, Mass.
- , R. D'Errico, and C. Vaudo, 1979, Estimating Air Quality Levels in Regions of High Terrain Under Stable Atmospheric Conditions, *Preprints, Fourth Symposium on Turbulence, Diffusion, and Air Pollution*, Am. Meteorol. Society, Boston, Mass.
- , and J. Mahoney, 1972, Numerical Modeling of Advection and Diffusion of Urban Area Source Pollutants, *J. Appl. Meteorol.*, 11: 312-322.
- Ekman, V. W., 1902, On jordrotationens inverkan på vindströmmar i nafvet, *Nytt. Mag. För Naturv.*, 40: 37-63.
- Eliassen, A., 1980, A Review of Long-Range Transport Modeling, *J. Appl. Meteorol.*, 19: 231-240.
- Engelmann, R. J., 1968, The Calculation of Precipitation Scavenging, in *Meteorology and Atomic Energy—1968*, pp. 208-221, D. H. Slade (Ed.), USAEC Report TID-24190, U. S. Atomic Energy Commission, NTIS.
- Environmental Protection Agency, 1978, *Guideline on Air Quality Models*, OAQPS Guideline Series No. 1.2-080, Report EPA-45012-78-027, Office of Air Quality Planning and Standards, Research Triangle Park, N. C.
- Environmental Systems Corporation, 1977, *Cooling Tower Drift Dye Tracer Experiment*, Report PPSP-CPCTP, Environmental Systems Corporation, Knoxville, Tenn.
- Eschenroeder, A. Q., J. R. Martinez, and R. A. Nordsieck, 1972, *Evaluation of a Diffusion Model for Photochemical Smog Simulation*, Final Re-

- port, Contract No. 68-02-0336 by General Research Corporation, Santa Barbara, Calif., for Environmental Protection Agency.
- Falls, A. H., and J. H. Seinfeld, 1978, Continued Development of a Kinetic Mechanism for Photochemical Smog, *Environ. Sci. Technol.*, 12: 1398-1405.
- Fay, J. A., M. Escudier, and D. P. Hoult, 1969, *A Correlation of Field Observations of Plume Rise*, Fluid Mechanics Laboratory Publication No. 69-4, Massachusetts Institute of Technology.
- , and J. J. Rosenzweig, 1980, An Analytical Diffusion Model for Long Distance Transport of Air Pollutants, *Atmos. Environ.*, 14: 355-366.
- Frenkiel, F. N., and I. Katz, 1956, Studies of Small-Scale Turbulent Diffusion in the Atmosphere, *J. Meteorol.*, 13: 388-394.
- Gifford, F. A., Jr., 1955, A Simultaneous Lagrangian-Eulerian Turbulence Experiment, *Monthly Weather Rev.*, 83: 293-301.
- , 1959a, Statistical Properties of a Fluctuating Plume Dispersion Model, in *Advances in Geophysics*, Vol. 6, pp. 117-138, F. N. Frenkiel and P. A. Sheppard (Eds.), Academic Press, New York.
- , 1959b, Computation of Pollution from Several Sources, *Int. J. Air Water Pollut.*, 2: 109-110.
- , 1961, Use of Routine Meteorological Observations for Estimating Atmospheric Dispersion, *Nucl. Saf.*, 2(4): 47-57.
- , 1968, An Outline of Theories of Diffusion in the Lower Layers of the Atmosphere, in *Meteorology and Atomic Energy—1968*, pp. 66-116, D. H. Slade (Ed.), USAEC Report TID-24190, U. S. Atomic Energy Commission, NTIS.
- , 1970, Atmospheric Diffusion in an Urban Area, in *Proceedings of 2nd Congress of the International Radiation Protection Association*, Brighton, England, May 3-8, 1970, W. Englund (Ed.), Air Pollution Control Association.
- , 1975, Atmospheric Dispersion Models for Environmental Pollution Applications, in *Lectures on Air Pollution and Environment Impact Analyses*, Boston, Mass., Sept. 29-Oct. 3, 1975, pp. 35-58, American Meteorological Society, Boston, Mass.
- , 1976, Turbulent Diffusion Typing Schemes—A Review, *Nucl. Saf.*, 17: 68-86.
- , 1977, Tropospheric Relative Diffusion Observation, *J. Appl. Meteorol.*, 16: 311-313.
- , 1981, *Horizontal Diffusion in the Atmosphere: A Lagrangian-Dynamical Theory*, DOE Report LA-8667-MS, Los Alamos Scientific Laboratory, NTIS.
- , and S. R. Hanna, 1973, Modeling Urban Air Pollution, *Atmos. Environ.*, 7: 131-136.
- Golder, D., 1972, Relations Among Stability Parameters in the Surface Layer, *Boundary-Layer Meteorol.*, 3: 47-58.
- Halitsky, J., 1963, Gas Diffusion near Buildings, *ASHRAE Trans.*, 69: 464-485.
- Hanna, S. R., 1968, A Method of Estimating Vertical Eddy Transport in the Planetary Boundary Layer Using Characteristics of the Vertical Velocity Spectrum, *J. Atmos. Sci.*, 25: 1026.
- , 1971, A Simple Method of Calculating Dispersion from Urban Area Sources, *J. Air Pollut. Control Assoc.*, 21: 774-777.
- , 1973, Description of ATDL Computer Model for Dispersion from Multiple Sources, in *Industrial Air Pollution Control*, pp. 23-32, Ann Arbor Science Publishers, Ann Arbor, Mich.
- , 1974, Meteorological Effects of the Mechanical Draft Cooling Towers of the Oak Ridge Gaseous Diffusion Plant, in *Cooling Tower Environment—1974*, ERDA Symposium Series, College Park, Md., Mar. 4-6, 1974, Steven R. Hanna and Jerry Pell (Coordinators), pp. 291-306, CONF-740302, NTIS.
- , 1975, Relative Diffusion of Tetroon Pairs During Convective Conditions, paper presented at *First Conference on Regional and Mesoscale Modeling, Analysis and Prediction*, Las Vegas, Nev., American Meteorological Society, Boston, Mass.
- , 1976, Predicted and Observed Cooling Tower Plume Rise and Visible Plume Length at the John E. Amos Power Plant, *Atmos. Environ.*, 10: 1043-1052.
- , 1978, Diurnal Variations of the Stability Factor in the Simple ATDL Urban Dispersion Model, *J. Air Pollut. Control Assoc.*, 28: 147-150.
- , 1980a, *User's Guide for ATCOOL Cooling Tower Plume Model*, Report ERLTM-ARL-80, Environmental Science Services Administration, Air Resources Laboratory.
- , 1980b, Measured σ_y and σ_θ in Complex Terrain near the TVA Widows Creek, Alabama, Steam Plant, *Atmos. Environ.*, 14: 401.
- , 1980c, Diurnal Variation of Horizontal Wind Direction Fluctuations σ_θ in Complex Terrain at Geysers, Calif., *Boundary-Layer Meteorol.*, 58: 1305-1309.
- , 1981, Atmospheric Effects of Energy Production, in *Atmospheric Science and Power Production*, Darryl Randerson (Ed.), DOE Report DOE/TIC-27601, in press.
- , and F. A. Gifford, 1977, Application of the ATDL Sample Urban Dispersion Model to Frank-

- furt, West Germany, in *Proceedings of Seventh NATO/CCMS Meeting*, Louvaine le Neuf, Belgium, ATDL Contribution No. 77/17, Atmospheric Turbulence and Diffusion Laboratory.
- , G. A. Briggs, J. Deardorff, B. A. Egan, F. A. Gifford, and F. Pasquill, 1977, Summary of Recommendations made by the AMS Workshop on Stability Classification Schemes and Sigma Curves, *Bull. Am. Meteorol. Soc.*, 58: 1305-1309.
- Haugen, D. A. (Ed.), 1959, *Project Prairie Grass: A Field Program in Diffusion*, Geophysical Research Papers, No. 59, Vol. III, Report AFCRC-TR-58-235, Air Force Cambridge Research Center.
- Hay, J. S., and F. Pasquill, 1959, Diffusion from a Continuous Source in Relation to the Spectrum and Scale of Turbulence, in *Advances in Geophysics*, Vol. 6, pp. 345-365, F. N. Frenkiel and P. A. Sheppard (Eds.), Academic Press, New York.
- Hayes, S. R., 1979, *Performance Measures and Standard for Air Quality Simulation Models*, Report EF78-93R2, Environmental Protection Agency.
- Heffter, J. L., 1965, The Variation of Horizontal Diffusion Parameters with Time for Travel Periods of One Hour or Longer, *J. Appl. Meteorol.*, 4(1): 153-156.
- , 1980, *Air Resources Laboratories Atmospheric Transport and Dispersion Model (ARL-ATAD)*, Report ERLTM-ARL-81, National Oceanic and Atmospheric Administration, Air Resources Laboratory.
- Högström, U., 1964, An Experimental Study on Atmospheric Diffusion, *Tellus*, 16(2): 205-251.
- Holzworth, G., 1972, *Mixing Depths, Wind Speed, and Potential for Urban Air Pollution Throughout the Contiguous United States*, Environmental Protection Agency Publication No. AP-101.
- Horst, T. W., 1977, A Surface Depletion Model for Deposition from a Gaussian Plume, *Atmos. Environ.*, 11: 41-46.
- , 1979, Lagrangian Similarity Modeling of Vertical Diffusion from a Ground Level Source, *J. Appl. Meteorol.*, 18: 733-740.
- Hosker, R. P., Jr., 1979, Empirical Estimation of Wake Cavity Size Behind Block-Type Structures, in preprints of *Fourth Symposium on Turbulence, Diffusion, and Air Pollution*, Reno, Nev., Jan. 15-18, 1979, pp. 603-609, American Meteorological Society, Boston, Mass.
- , 1980, Practical Application of Air Pollution Deposition Models—Current Status, Data Requirements, and Research Needs, in *Proceedings of the International Conference on Air Pollutants and Their Effects on the Terrestrial Ecosystem*, Banff, Alberta, Canada, May 10-17, 1980, S. V. Krupa and A. H. Legge (Eds.), John Wiley & Sons, New York.
- , 1981, Flow and Diffusion Near Obstacles, in *Atmospheric Science and Power Production*, Darryl Randerson, (Ed.), DOE Report DOE/TIC-27601, in press.
- Huber, A. H., and W. H. Snyder, 1976, Building Wake Effects on Short Stack Effluents, in preprints of *Third Symposium on Atmospheric Turbulence, Diffusion, and Air Quality*, Raleigh, N. C., Oct. 19-22, 1976, pp. 235-242, American Meteorological Society, Boston, Mass.
- Hunt, J. C. R., W. H. Snyder, and R. E. Lawson, Jr., 1978, Flow Structure and Turbulent Diffusion Around a Three-Dimensional Hill, Fluid Modeling Study on Effects of Stratification. Part I. Flow Structure, DOE Report EPA-600/4-78-041, Environmental Protection Agency.
- Irwin, J. S., 1979a, Estimating Plume Dispersion—A Recommended Generalized Scheme, in preprints of *Fourth Symposium on Turbulence, Diffusion, and Air Pollution*, Reno, Nev., Jan. 15-18, 1979, pp. 62-69, American Meteorological Society, Boston, Mass.
- , 1979b, A Theoretical Variation of the Wind Profile Power Law Exponent as a Function of Surface Roughness and Stability, *Atmos. Environ.*, 13: 191-194.
- Isitzer, N. F., and R. K. Dumbauld, 1963, Atmospheric Diffusion-Deposition Studies over Flat Terrain, *Int. J. Air Water Pollut.*, 7(11-12): 999-1022.
- Johnson, W. B., E. Shelar, R. E. Ruff, H. B. Singh, and L. Salas, 1975, *Gas Tracer Study of Roof-Vent Effluent Diffusion at Millstone Nuclear Power Station*, Atomic Industrial Forum Report AIF/NESP-007b, Stanford Research Institute, Palo Alto, Calif.
- , R. C. Sklarew, and D. B. Turner, 1976, Urban Air Quality Simulation Modeling, in *Air Pollution*, 3rd ed., Vol. 1, Chap. 10, pp. 503-562, A. C. Stern (Ed.), Academic Press, New York.
- , D. E. Wolf, and R. L. Mancuso, 1978, Long Term Regional Patterns and Transfrontier Exchanges of Airborne Sulfur Pollution in Europe, *Atmos. Environ.*, 12: 511-527.
- Kaimal, J. S., et al., 1977, Turbulence Structure in the Convective Boundary Layer, *J. Atmos. Sci.*, 33: 2152-2169.

- Kao, S. K., and L. L. Wendell, 1968, Some Characteristics of Relative Particle Dispersion in the Atmosphere's Boundary Layer, *Atmos. Environ.*, 2: 397-407.
- Kazanski, A. B., and A. S. Monin, 1957, The Form of Smoke Jets, *Izv. Atmos. Oceanic Phys.*, 8: 1020-1033.
- Kessler, E., 1969, On the Distribution and Continuity of Water Substance in Atmospheric Circulations, *Meteorol. Monogr.*, 10.
- Koenig, L. R., 1979, *Anomalous Cloudiness and Precipitation Caused by Industrial Heat Rejection*, Report R-2465-DOE, The Rand Corporation.
- , F. W. Murray, and P. M. Tag, 1978, Differences in Atmospheric Convection Caused by Waste Energy Rejected in the Forms of Sensible and Latent Heats, *Atmos. Environ.*, 12: 1013-1020.
- Lamb, R. G., 1979, The Effects of Release Height on Material Dispersion in the Convective Planetary Boundary Layer, in *Fourth Symposium on Turbulence, Diffusion, and Air Pollution*, Reno, Nev., Jan. 15-19, 1979, pp. 27-33, American Meteorological Society, Boston, Mass.
- Lange, R., 1978, ADPIC—A Three Dimensional Particle-In-Cell Model for the Dispersal of Atmospheric Pollutants and Its Comparison to Regional Tracer Studies, *J. Appl. Meteorol.*, 17: 320-329.
- Lettau, H., 1970, Physical and Meteorological Basis for Mathematical Models of Urban Diffusion, in *Proceedings of Symposium on Multiple Source Urban Diffusion Models*, Air Pollution Control Official Publication No. AP 86, Environmental Protection Agency.
- Long, P. E., and D. W. Pepper, 1976, A Comparison of Six Numerical Schemes for Calculating the Advection of Atmospheric Pollution, in *Proceedings of the Third Symposium on Atmospheric Turbulence, Diffusion, and Air Quality*, Raleigh, N. C., Oct. 19-22, 1976, pp. 181-186, American Meteorological Society, Boston, Mass.
- MacCracken, M. C., and K. E. Grant, 1975, Livermore Regional Air Quality Model (LIRAQ-1), in *American Meteorological Society Conference on Regional and Mesoscale Modeling, Analysis, and Prediction*, Las Vegas, May 6-9, 1975, American Meteorological Society, Boston, Mass.
- McElroy, J. L., and F. Pooler, 1968, *St. Louis Dispersion Study*, Report AP-53, U. S. Public Health Service, National Air Pollution Control Administration.
- McMahon, T. A., and P. J. Denison, 1979, Empirical Atmospheric Deposition Parameters—A Survey, *Atmos. Environ.*, 13: 571-585.
- Machta, L., H. L. Hamilton, Jr., L. F. Hubert, R. J. List, and K. M. Nagler, 1957, Airborne Measurements of Atomic Debris, *J. Meteorol.*, 14(2): 165-175.
- Mason, B. J., 1971, *The Physics of Clouds*, Clarendon Press, Oxford, England.
- Meroney, R. N., 1979, Turbulent Diffusion near Buildings, in *Engineering Meteorology*, E. J. Plate (Ed.) (to be published).
- , and B. T. Yang, 1971, *Wind-Tunnel Study on Gaseous Mixing Due to Various Stack Heights and Injection Rates Above an Isolated Structure*, Report CER71-72RNM-BTY16, Colorado State University, Fluid Dynamics and Diffusion Laboratory.
- Meyer, J. H., T. W. Eagles, L. C. Kohlenstein, J. A. Kagan, and W. D. Stanbro, 1974, Mechanical Draft Cooling Tower Plume Behavior: Measurements, Models, Predictions, in *Cooling Tower Environment—1974*, ERDA Symposium Series, College Park, Md., Mar. 4-6, 1974, Steven R. Hanna and Jerry Pell (Coordinators), pp. 307-352, CONF-740302, NTIS.
- Monin, A. S., and A. M. Obukhov, 1953, Dimensionless Characteristics of Turbulence in the Layer of Atmosphere near the Ground, *Dokl. Akad. Nauk SSSR*, 93: 257-267.
- , and A. M. Yaglom, 1971, *Statistical Fluid Mechanics, Mechanics of Turbulence*, Vol. I, J. Lumley (Ed.), The MIT Press, Cambridge, Mass.
- Moore, D. J., 1974, Observed and Calculated Magnitudes and Distances of Maximum Ground Level Concentration of Gaseous Effluent Material Downwind of a Tall Stack, *Adv. Geophys.*, 18B: 201-221.
- Nappo, C. J., 1974, A Method for Evaluating the Accuracy of Air Pollution Prediction Models, in *Proceedings of the Symposium on Atmospheric Diffusion and Air Pollution*, Santa Barbara, Calif., Sept. 9-13, 1974, pp. 325-329, American Meteorological Society, Boston, Mass.
- , 1979, Relative and Single Particle Diffusion Estimates Determined from Smoke Plume Photographs, in *Fourth Symposium on Turbulence, Diffusion, and Air Pollution*, Reno, Nev., Jan. 15-19, 1979, pp. 45-47, American Meteorological Society, Boston, Mass.
- , S. R. Hanna, and H. F. Snodgrass, 1980, Drainage Wind Observations Using Neutral-Lift Balloons, in *Proceedings of 2nd Joint Conference on Applications of Air Pollution Meteorology*, New Orleans, La., Mar. 24-27, 1980, pp. 495-498, American Meteorological Society, Boston, Mass.

- Ott, R. E., 1976, *Locally Heavy Snow Downwind from Cooling Tower*, NOAA Tech. Memo. NWS ER-72, National Oceanic and Atmospheric Administration.
- Overcamp, T. J., 1976, A General Gaussian Diffusion-Deposition Model for Elevated Point Sources, *J. Appl. Meteorol.*, 15: 1167-1171.
- Pack, D. H., and J. K. Angell, 1963, A Preliminary Study of Air Trajectories in the Los Angeles Basin Derived from Tetron Flights, *Mon. Weather Rev.*, 91: 583-604.
- Pandolfo, J. P., and C. A. Jacobs, 1973, *Tests of an Urban Meteorological Pollutant Model Using CO Validation Data in the Los Angeles Metropolitan Area*. Vol. I. CEM Report 490a, Contribution 68-02-0223, prepared by The Center for the Environment and Man, Inc., for the Environmental Protection Agency.
- Panofsky, H. A., H. Tennekes, D. H. Lenschow, and J. C. Wyngaard, 1977, The Characteristics of Turbulent Velocity Components in the Surface Layer Under Convective Conditions, *Boundary-Layer Meteorol.*, 11: 355-361.
- , C. A. Egolf, and R. Lipschutz, 1978, On Characteristics of Wind Direction Fluctuations in the Surface Layer, *Boundary-Layer Meteorol.*, 15: 439-446.
- Pasquill, F., 1961, The Estimation of the Dispersion of Windborne Material, *Meteorol. Mag.*, 90: 33-49.
- , 1974, *Atmospheric Diffusion*, 2nd ed., John Wiley & Sons, New York.
- , 1975, The Dispersion of Materials in the Atmospheric Boundary Layer. The Basis for Generalization, in *Lectures on Air Pollution and Environmental Impact Analyses*, pp. 1-34, American Meteorological Society, Boston, Mass.
- , 1976, *Atmospheric Dispersion Parameters in Gaussian Plume Modeling: Part II. Possible Requirements for Change in the Turner Workbook Values*, Report EPA-600/4-760306, U. S. Environmental Protection Agency.
- Paulson, C. A., 1970, The Mathematical Representation on Wind Speed and Temperature Profiles in the Unstable Atmospheric Surface Layer, *J. Appl. Meteorol.*, 9: 857-861.
- Peterson, K. R., 1968, Continuous Point-Source Plume Behavior out to 160 Miles, *J. Appl. Meteorol.*, 7: 217-226.
- Policastro, A. J., W. E. Dunn, and M. Breig, 1978, Evaluation of Theory and Performance of Salt Drift Deposition Models for Natural Draft Cooling Towers, in *Proceedings of the 2nd AIAA/ASME Thermophysics and Heat Transfer Conference*, Palo Alto, Calif., May 24-28, 1978, American Institute of Aeronautics and Astronautics, New York.
- Prahn, L. P., and O. Christensen, 1977, Long Range Transport of Pollutants Simulated by a 2D Pseudospectral Dispersion Model, *J. Appl. Meteorol.*, 16: 896-910.
- Randerson, D., 1972, Temporal Changes in Horizontal Diffusion Parameters of a Single Nuclear Debris Cloud, *J. Appl. Meteorol.*, 11: 670-673.
- Reid, J. D., 1979, Markov Chain Simulations of Vertical Dispersion in the Neutral Surface Layer for Surface and Elevated Releases, *Boundary-Layer Meteorol.*, 16: 3-22.
- Reynolds, S. D., and P. M. Roth, 1973, Mathematical Modeling of Photochemical Air Pollution. Pt. 1. Formulation of the Model, *Atmos. Environ.*, 7: 1022-1061.
- Richardson, L. F., 1926, Atmospheric Diffusion Shown on a Distance-Neighbour Graph, *Proc. R. Soc. (London), Ser. A*, 110: 709.
- Roberts, O. F. T., 1923, The Theoretical Scattering of Smoke in a Turbulent Atmosphere, *Proc. R. Soc. (London), Ser. A*, 104: 640-654.
- Sagendorf, J., and C. R. Dickson, 1974, *Diffusion Under Low Wind Speed and Inversion Conditions*, Technical Memorandum 52, National Oceanic and Atmospheric Administration, Environmental Research Laboratories, Air Resources Laboratory.
- Schmel, G. A., 1980, Particle and Gas Dry Deposition: A Review, *Atmos. Environ.*, 14: 983-1012.
- Seneca, J., 1955, Mesures de diffusivité turbulente sur des flocons de fumée, *J. Sci. Meteorol.*, 7: 221-225.
- Sheih, C. M., 1974, Application for a Statistical Trajectory Model to the Simulation of Sulfur Pollution over Northeastern United States, *Atmos. Environ.*, 11: 173-178.
- Sherman, C. A., 1978, A Mass Consistent Model for Wind Fields over Complex Terrain, *J. Appl. Meteorol.*, 17: 312-319.
- Shir, C. C., 1973, A Preliminary Numerical Study of Atmospheric Turbulent Flows in the Idealized Planetary Boundary Layer, *J. Atmos. Sci.*, 30: 1327-1339.
- , and L. J. Shieh, 1974, A Generalized Urban Air Pollution Model and Its Application to the Study of SO₂ Distributions in the St. Louis Metropolitan Area, *J. Appl. Meteorol.*, 13: 185-204.
- Simon, C., and W. Proudfit, 1967, Some Observations of Plume Rise and Plume Concentration Distributed over N.Y.C., Paper 67-83 of the *60th Annual Meeting of the Air Pollution Control Association*, Cleveland, Ohio, June 11-16, 1967, Air Pollution Control Association.

- Slinn, W. G. N., 1974, The Redistribution of a Gas Plume Caused by Reversible Washout, *Atmos. Environ.*, 8: 233-239.
- Smith, E. J., and K. J. Hefferman, 1956, The Decay of the Ice-Nucleating Properties of Silver Iodide Released from a Mountain Top, *Q. J. R. Meteorol. Soc.*, 82: 301-309.
- Smith, F. B., 1967, The Eulerian-Lagrangian Time Scale Relationship in One-Dimensional Turbulence, in *Proceedings of the U. S. Atomic Energy Commission Meteorological Information Meeting*, Chalk River, Ontario, Canada, Sept. 11-15, 1967, CONF-670931.
- , 1972, A Scheme for Estimating the Vertical Dispersion of a Plume from a Source near Ground Level, in *Proceedings of the Third Meeting of the Expert Panel on Air Pollution Modeling*, Report NATO-CCMS-14, North Atlantic Treaty Organization, Brussels.
- , and J. S. Hay, 1961, The Expansion of Clusters of Particles in the Atmosphere, *Q. J. R. Meteorol. Soc.*, 87(371): 82-101.
- , and R. D. Hunt, 1978, Meteorological Aspects of the Transport of Pollution over Long Distances, *Atmos. Environ.*, 12: 461-477.
- Smith, M. E., 1951, The Forecasting of Micrometeorological Variables, *Meteorol. Monogr.*, 4: 50-55.
- , 1968, *Recommended Guide for the Prediction of the Dispersion of Airborne Effluents*, 1st ed., American Society of Mechanical Engineers, New York.
- Sutton, O. G., 1932, A Theory of Eddy Diffusion in the Atmosphere, *Proc. R. Soc. (London)*, Ser. A, 135: 143.
- , 1953, *Micrometeorology*, McGraw-Hill Book Company, New York.
- Taylor, G. I., 1921, Diffusion by Continuous Movements, *Proc. London Math. Soc.*, 20: 196.
- , 1948, *Dynamics of a Mass of Hot Gas Rising in Air*, USAEC Report MDDC-919 (LADC-276), Los Alamos Scientific Laboratory, NTIS.
- Turner, D. B., 1967, *Workbook of Atmospheric Dispersion Estimates*, Public Health Service, Publication 999-AP-26, Robert A. Taft Sanitary Engineering Center, Cincinnati, Ohio.
- , 1979, Atmospheric Dispersion Modeling: A Critical Review, *J. Air Pollut. Control Assoc.*, 29: 502-519.
- U. S. Department of Commerce, 1968, Environmental Data Service, *Climate Atlas of the United States*.
- Van der Hoven, I., 1968, Deposition of Particles and Gases, in *Meteorology and Atomic Energy—1968*, pp. 202-207, D. Slade (Ed.), USAEC Report TID-24190, U. S. Atomic Energy Commission, NTIS.
- , 1976, A Survey of Field Measurements of Atmospheric Diffusion Under Low Wind Speed, Inversion Conditions, *Nucl. Saf.*, 17(2): 223-230.
- Venkatram, A., 1978, An Examination of Box Models for Air Quality Simulation, *Atmos. Environ.*, 12: 2243-2250.
- Weil, J., 1974, The Rise of Moist Buoyant Plumes, *J. Appl. Meteorol.*, 13: 435-443.
- Wendell, L. L., D. C. Powell, and R. L. Drake, 1976, A Regional Scale Model for Computing Deposition and Ground Level Air Concentration of SO₂ and Sulfates from Elevated and Ground Sources, in preprint Volume, *Third Symposium on Atmospheric Turbulence, Diffusion, and Air Quality*, Raleigh, N. C., Oct. 19-22, 1976, pp. 318-324, American Meteorological Society, Boston, Mass.
- Wigley, T. M. L., and P. R. Slawson, 1971, On the Condensation of Buoyant, Moist, Bent-Over Plumes, *J. Appl. Meteorol.*, 10: 259-263.
- Wilson, D. J., 1976, *Contamination of Building Air Intakes from Nearby Vents*, University of Alberta Department of Mechanical Engineering Report No. 1, University of Alberta, Edmonton, Alberta, Canada.
- , 1979, Flow Patterns over Flat-Roofed Buildings and Application to Exhaust Stack Design, *ASHRAE Trans.*, 85(2): 284-295.
- , and D. D. J. Netteville, 1978, Interaction of a Roof-Level Plume with a Downwind Building, *Atmos. Environ.*, 12(5): 1051-1059.
- Wyngaard, J. C., 1975, Modeling the Planetary Boundary Layer. Extension to the Stable Case, *Boundary-Layer Meteorol.*, 9: 441-460.
- , O. R. Cote, and K. S. Rao, 1974, Modeling the Atmospheric Boundary Layer, *Adv. Geophys.*, 18A: 193-211.

Author Index

- Abramowitz, M. (Ed.), 52
Allen, P. W., 43
Angell, J. K., 43
- Barad, M. L. (Ed.), 48
Barry, P. J., 24
Bass, A., 87
Batchelor, G. K., 41, 42
Benkley, C. W. (cited as Bass et al.), 87
Bradley, E. F. (cited as Businger et al.), 7, 54
Braham, R. B., 43
Breig, M., 79
Briggs, G. A., 11, 14, 16, 17, 19, 29, 30, 82, 85
Briggs, G. A. (cited as Hanna et al.), 27
Businger, J. A., 7, 54
Byzova, N. L., 43
- Cagnetti, P., 22
Carpenter, S. B., 17, 27
Carslaw, H. S., 50
Caughey, S. J., 8
Chamberlain, A. C., 67
Chaudhry, F. H., 47
Christensen, O., 54
Colbaugh, W. C. (cited as Carpenter et al.), 27
Cote, O. R. (cited as Wyngaard et al.), 7
Cramer, H. E., 27, 28
Crane, G., 54
Crawford, T. V., 43
Crozier, W. D., 43
- Dana, M. T., 71
Davies, R. W., 43
Deardorff, J. W., 7, 49
Deardorff, J. W. (cited as Hanna et al.), 27
Demerjian, K. L., 58
D'Errico, D., 85
Denison, P. J., 69, 70
Dickson, C. R., 24, 30
Donaldson, C., 5, 50
Doran, J. C., 31, 38, 39
Drake, R. L., 47
Draxler, R. R., 31, 38, 88, 89
Dumbauld, R. K., 48
Dunn, W. E., 79
- Eagles, T. W. (cited as Meyer et al.), 77
Edinger, J. G., 43
Egan, B. A., 53, 83, 85
Egan, B. A. (cited as Hanna et al.), 27
Egolf, C. A., 81
Ekman, V. W., 53
Eliassen, A., 87
Engelmann, R. J., 78
Environmental Protection Agency, 25
Environmental Systems Corporation, 78
Eschenroeder, A. Q., 62
Escudier, M., 14
- Falls, A. H., 73
Fay, J. A., 14, 88
Frenkiel, F. N., 43
- Garger, Ye. K., 43
Gartrell, F. E. (cited as Carpenter et al.), 17, 27
Gifford, F. A., 24, 25, 27, 29, 33, 34, 39, 42, 43, 46, 58, 59, 60
Gifford, F. A. (cited as Hanna et al.), 27
Golder, D., 27
Grant, K. E., 62
- Hales, J. M., 71
Halitsky, J., 22, 23
Hamilton, H. L., Jr. (cited as Machta et al.), 43
Hanna, S. R., 17, 27, 43, 55, 58, 59, 60, 74, 77, 81, 83, 84
Haugen, D. A. (Ed.), 29
Hay, J. S., 39, 41, 43
Hayes, S. R., 63
Hefferman, K. J., 43
Heffter, J. L., 43, 87
Högström, U., 43
Holzworth, G., 6
Horst, T. W., 31, 38, 39, 46, 47, 48, 69
Hosker, R. P., Jr., 19, 21, 29, 68, 71, 72, 83
Hoult, D. P., 14
Huber, A. H., 24
Hubert, L. F. (cited as Machta et al.), 43
Hunt, J. C. R., 84
Hunt, R. D., 88
- Irwin, J. S., 7, 31, 32
Islitzer, N. F., 48
Ivanov, V. N., 43
Izumi, Y. (cited as Businger et al.), 7, 54
- Jacobs, C. A., 62
Jaeger, J. C., 50
Jessup, E. A., 43
Johnson, W. B., 24, 61, 87
- Kagan, J. A. (cited as Meyer et al.), 77
Kaimal, J. S., 7, 8
Kao, S. K., 43
Katz, I., 43
Kazanski, A. B., 43
Kessler, E., 77
Koenig, L. R., 77, 78
Kohlenstein, L. C. (cited as Meyer et al.), 77
- Lamb, R. G., 49
Lange, R., 54
Lawson, R. E., Jr., 84
Leavitt, J. M. (cited as Carpenter et al.), 27
Lenschow, D. H. (cited as Panofsky et al.), 7, 54
Lettau, H., 57
Lipschutz, R., 81
List, R. J. (cited as Machta et al.), 43
Long, P. E., 54
- MacCracken, M. C., 62
McElroy, J. L., 30
McMahon, T. A., 69, 70
Machta, L., 43
Mahoney, J., 53
Mancuso, R. L., 87
Markee, E. H., 24
Martinez, J. R., 62
Mason, B. J., 78
Meroney, R. N., 24, 47
Meyer, J. H., 77
Monin, A. S., 6, 43, 46
Montgomery, T. L. (cited as Carpenter et al.), 27
Moore, D. J., 17
Morris, C. S. (cited as Bass et al.), 87
Murray, F. W., 77

- Nagler, K. M. (cited as Machta et al.), 43
 Nappo, C. J., 44, 63, 83, 84
 Netterville, D. D. J., 22
 Nickola, P. W., 31, 38, 39
 Nordsieck, R. A., 62
- Obukhov, A., 6
 Otts, R. E., 78
 Overcamp, T. J., 69
- Pack, D. H., 43
 Pandolfo, J. P., 62
 Panofsky, H. A., 7, 54, 81
 Pasquill, F., 9, 10, 25, 27, 29, 31, 33, 38, 39, 46, 50, 52, 84
 Pasquill, F. (cited as Hanna et al.), 27
 Paulson, C. A., 7
 Pepper, D. W., 54
 Peterson, K. R., 43
 Policastro, A. J., 79
 Pooler, F., 30
 Powell, D. C., 87
 Prahm, L. P., 54
 Proudfit, W., 15
- Randerson, D., 43
 Rao, K. S. (cited as Wyngaard et al.), 7
 Reid, J. D., 10, 40
 Reynolds, S. D., 62
 Richardson, L. F., 42
 Roberts, O. F. T., 43, 51
- Rosenzweig, J. J., 88
 Roth, P. M., 62
 Ruff, R. E. (cited as Johnson et al.), 24
- Sagendorff, J., 30
 Salas, L. (cited as Johnson et al.), 24
 Schere, K. L., 58
 Scire, J. S. (cited as Bass et al.), 87
 Seely, B. K., 43
 Sehmel, G. A., 69, 70
 Seinfeld, J. H., 73
 Seneca, J., 43
 Sheih, C. M., 62, 88
 Shelar, E. (cited as Johnson et al.), 24
 Sherman, C. A., 88
 Shir, C. C., 55, 62
 Simon, C., 15
 Singh, H. B. (cited as Johnson et al.), 24
 Sklarew, R. C., 61
 Slawson, P. R., 77
 Slinn, W. G. N., 71
 Smith, E. J., 43
 Smith, F. B., 29, 41, 52, 88
 Smith, M. E., 27, 29, 59, 60
 Snodgrass, H. F., 83, 84
 Snyder, W. H., 24, 84
 Stanbro, W. B. (cited as Meyer et al.), 77
 Start, G. E., 24
 Stegan, I. A. (Ed.), 52
 Sutton, G., 25, 38, 50
- Tag, P. M., 77
 Taylor, G. I., 12, 30, 36
- Tennekes, H. (cited as Panofsky et al.), 7, 54
 Thomas, F. W., 17, 27
 Thomas, F. W. (cited as Carpenter et al.), 27
 Turner, D. B., 27, 61, 62, 64, 65
- U. S. Department of Commerce, 2
- Van der Hoven, I., 30, 67
 Vaudo, C., 85
 Venkatram, A., 58
- Weil, J., 77
 Wendell, L. L., 43, 87
 Wigley, T. M. L., 77
 Wilson, D. J., 20, 21, 22
 Wolf, D. E., 87
 Wolf, M. A., 71
 Wyngaard, J. C., 7, 8, 54
 Wyngaard, J. C. (cited as Businger et al.), 7, 54
 Wyngaard, J. C. (cited as Panofsky et al.), 7, 54
- Yaglom, A. M., 46
 Yang, B. T., 24
- Zeman, O., 55

Subject Index

- Acid rain, 87
- Adiabatic temperature gradient, 2, 3, 12
- Air trajectories in a valley, 81-84
- Airflow around obstacles, 19-24
- APRAC model, 64
- Area sources
 - continuous, 57-66
 - instantaneous, 50, 51
- Atmospheric Turbulence and Diffusion Laboratory (ATDL) model for urban diffusion, 59-61
- Averaging time
 - effect on regional scale turbulence, 87
 - effect on σ_y and σ_z , 25, 27
- Ballistic trajectory of drift drop, 79
- Bent-over plume
 - buoyancy conservation equation, 13
 - entrainment velocity, 12
 - momentum conservation equation, 13
 - rise in stable environment, 14
 - trajectory near source, 13, 14
 - volume flux, 11
- β , 9, 10, 39, 40
- Bias, 63
- Box model
 - diffusion from area sources, 57-59
 - removal processes, 73
- Breakaway mechanism for drift drops, 79
- Breakup model for plume rise, 17
- Brookhaven National Laboratory, 27, 28
- Brownian diffusion, 69
- Brunt-Väisälä frequency, 4, 12, 14, 84
- Buildings, diffusion around, 19-24
- Buoyancy flux of plume, 11
- Carbon monoxide
 - area source model, 61
 - deposition speed, 70
 - street canyon model, 61-62
- Cavity, building, 19-24
- CDM model, 64
- CDMQC model, 65
- Chemical kinetic equations, 72-73
- Chemical removal, 72-73, 88, 89
- Chemical transformation rate,
 - SO₂-sulfate, 73, 88, 89
- Closure assumption for plume rise, 12
- Cloud microphysics, 77
- Complex terrain air-pollution meteorology, 30, 81-86
- Computers, 40, 53-54
- Concentration in cavity, 24
- Conjugate power law, 52
- Continuity equation, 5
- Continuous sources, 25-40, 46-49
- Convective scaling velocity (w_*), 7, 32, 48
- Conversion from SO₂ to sulfate, 73, 88, 89
- Cooling towers, 17, 74-80
- Coriolis force, 2, 5, 6, 55
- Correlation coefficient, 8, 36-40, 63
- Critical wind speed for maximum C,
 - 17, 22
- Crosswind-integrated concentration,
 - 47, 48
- CRSTER model, 65
- Deposition rate
 - of gases, 68
 - of SO₂ and sulfate, 88
- Deposition speed (v_d), 68-70
- Diffusion
 - around obstacles, 19-24
 - calm conditions, 25
 - daytime PBL, similarity theory, 48, 49
 - Gaussian model, 25-35
 - puff, 41-45, 51
 - similarity models, 46-49
 - statistical models, 36-40
 - surface layer, similarity theory, 46-48
 - urban, 57-66
- Diffusion equation, 5, 50-56
 - analytical solutions, 50-53
 - long range, 87
 - numerical solutions, 53-56
 - urban areas, 62
- Diffusivity coefficient, 5-7
 - large scale (K_1), 42, 88
 - vertical (K_2), 51, 54, 55, 88
- Dimensional analysis, 42, 46-49
- Distribution functions, 63
- Downwash, 19, 23
 - induced by terrain, 85
- Drainage flow, 81-84
- Drift deposition, 78-80
- Dry cooling towers, 77-78
- Dry deposition, 67-71, 88
- Eddy conductivity, 7, 54
- Eddy diffusivity, 5, 7, 42, 54, 55
- Eddy dissipation rate, 8, 16, 42, 44
- Eddy energy spectra, 8, 9, 41, 42
- Eddy viscosity, 5, 6
- Effective radius of momentum,
 - temperature, and moisture plume, 77
- Effective stack height, 11, 19, 22, 85
- Ekman spiral, 5
- Emissions, importance of, 57
- Entrainment in rising plume, 12, 13, 77
- Environmental Protection Agency (EPA) models, 62
- Equation of motion, 2, 77
- Equation of state, 1
- Error analysis, 63
- Eulerian turbulence, 9
- Evaluation of models, 63
- Exponential chemical decay rate, 72, 73
- Fickian diffusion equation, 25, 51, 88
- Filter function for spectrum, 6, 38
- Finite difference approximations, 53, 54
- First law of thermodynamics, 2, 77
- Flushing time, 57
- Frankfurt, West Germany, 57
- Friction velocity, 6, 16, 17, 46, 54
- Froude number, 84
- Fumigation, 17, 32, 33, 86
- Gamma function, 52
- Gaussian distribution of turbulent speeds, 40
- Gaussian formula
 - plume, 24-35
 - puff, 42
- General circulation, 1, 2
- Geostrophic wind speed, 2, 6
- Geysers, Calif., 81, 84
- Gradient transport models, 50-56
- Gravitational settling, 67-68
- Hadley cells, 1
- Half-life of SO₂, 67
- Higher order closure, 55, 56
- Highway models, 61, 64
- HIWAY model, 64
- Hydrostatic equation, 1

- Inertial subrange influence on puff diffusion, 42
 Instantaneous plume snapshot, 44
 Instantaneous source, 41-45, 51
 Intensity of turbulence, 41
 Inversion, 3, 14-16
- Jet stream, 2
- K coefficients, 5-7, 50-56, 62, 88
 Krypton 85, 89, 90
- Lagrangian-Eulerian relations, 9, 10, 40
 Lagrangian time scale, 37-40, 43, 49, 51
 Lagrangian turbulence, 9
 Langevin's equation, 43
 Lapse rates, 3, 12
 Latent heat, 3, 74
 Line source, 51
 Long-range transport and diffusion, 87-90
 Los Angeles model for CO, 62
- Mass change of drift drops, 78
 Maximum ground-level concentration, 11, 17, 22-24, 32, 33
 Mean plume height (\bar{z}), 46-48
 Mechanical-draft cooling towers, 74
 Mesoscale eddies, 43
 Mixing layer height (z_i), 6-8, 27, 31, 48, 55
 Mixing ratio, 3
 Model evaluation, 63
 Models, EPA, 64, 65
 Moist adiabatic temperature gradient, 3
 Momentum flux, turbulent, to ground, 6
 Momentum flux of plume, 11, 12
 Monin-Obukhov length (L), 6, 27, 47-49, 54
 Monte Carlo model, 36-40
 Multiple sources, plume rise, 17
- Narrow plume hypothesis, 59
 National Climatic Center, 2
 Natural-draft cooling tower, 74
 Neutral lapse rate, 3
 Neutral plume rise, 16
 Neutral profiles of σ_u , σ_v , and σ_w , 8
 Nuclear Regulatory Commission, 27
 Numerical cooling tower plume models, 77
 Numerical instabilities, 53
- PAL model, 65
 Partial reflection model, 69
 Particle-in-cell method, 54
 Particle trajectory model, 40
 Peak analysis for model evaluation, 63
 Peak-to-mean concentration ratio, 33, 34
 Performance measures, 63
 Photochemical box model, 58
 Photochemical smog, chemical description, 73
- Physical models of flow over complex terrain, 83, 84
 Planetary boundary layer, 4-6
 Plume, bent-over (*see* Bent-over plume)
 Plume impaction on terrain, 84
 Plume meander, 30, 34
 Plume penetration of elevated inversion, 14, 15
 Plume rise
 from cooling towers, 74, 76
 determined by ambient turbulence, 15-17
 general, 11-18, 46
 limited by ambient stability, 14
 multiple sources, 17
 trajectory near source, 13, 14
 Potential temperature, 3
 Prairie Grass experiment, 29, 40, 48
 Primary pollutants, 72
 Psychrometric chart, 74, 76
 PTDIS model, 64
 PTMAX model, 64
 PTMTP model, 64
 Puff diffusion, 41-45, 51
 Puff models of long-range diffusion, 87, 88
- Rainfall effect on deposition, 71, 72
 RAM model, 65
 Ravenswood power plant, 15
 Recirculation zones, 19-21
 Regional Air Pollution Study (St. Louis), 61
 Release time, 41
 Removal mechanisms, 67-73
 Resistance analogy for deposition, 69
 Reynolds averaging, 5
 Richardson number, 4, 7, 27
 Roughness length, 6, 29
- Sampling time, 33, 38, 39, 41
 Saturation deficit, 76, 77
 Savannah River Laboratory experiment, 89, 90
 Scavenging coefficient, 71-73
 Screening model, 58
 Second-order closure, 5, 55, 56
 Secondary pollutants, 72
 Sector model, 34
 σ_e , 30, 31
 σ_θ , 8, 30, 31, 39, 81-83
 σ_u profiles in PBL, 8
 σ_v profiles in PBL, 8
 σ_v use in statistical models, 36-40
 σ_w profiles in PBL, 8
 σ_y
 from diffusion equation, 52
 in Gaussian equation, 25-33
 for long-range diffusion, 88
 peak to mean, 33, 34
 puff, 41-45
 from σ_θ method, 27-31
 stability class method, 27-30
 statistical models, 36-40
- σ_z
 in Gaussian equation, 25-35
 from σ_e method, 28, 31
 stability class method, 27-30
 Similarity theory
 for diffusion, 46-49
 for spectra, 8
 for wind and temperature profiles, 6, 7
 Snowfall from cooling tower plume, 78
 SO₂ deposition speeds, 71, 88
 Source depletion model, 68
 Source effects on airflow and diffusion, 19-24
 Sources close to building, 22
 Sources upwind of building, 22
 Spectra, 8, 38, 39
 Split-H concept, 24
 Stability
 classification schemes, 27, 85, 86
 general definition, 3
 limits to plume rise, 14
 term s, 12-14
 Stable lapse rate, 3
 Stable profiles of σ_u , σ_v , and σ_w , 8
 Stack aerodynamic effect, 19
 Statistical models, 36-40
 Stokes's law, 67
 Street canyon model, 61
 Surface buoyancy flux, 6, 16, 17
- Taylor entrainment assumption, 12, 13
 Taylor's statistical theory, 36-38, 41, 51
 Temperature gradient
 as indicator of stability class, 27
 in surface layer, 7
 Tennessee Valley Authority, 27, 29
 Terminal speed of water drops, 78
 Tilted plume model, 68
 Time scale of turbulence, 9, 30, 37-40
 Top-hat model, 11, 12
 Trajectory models
 for long-range transport, 87-90
 for urban diffusion, 62
 Travel time, 36-41
 Turbulence
 fluxes, 4, 5, 50, 55
 influence on plume rise, 15, 16
 intensity, 8
 velocity fluctuations σ_u , σ_v , and σ_w , 8
- UNAMAP models, 62, 64-65
 Unstable lapse rate, 3
 Unstable profiles of σ_u , σ_v , and σ_w , 8
 Urban diffusion, 30, 57-66
- Valley limited diffusion, 86
 VALLEY model, 65
 Vents, diffusion from, 22-24
 Vertical diffusivity, 54, 55

102 ATMOSPHERIC DIFFUSION

Vertical distribution of concentration,
47, 48

Vertical plume

buoyancy conservation equation, 12
entrainment velocity, 12
momentum conservation equation, 13
rise in stable environment, 14
trajectory near source, 13
volume flux, 11

Virtual source, 14, 17

Visible plume dimensions for cooling
tower, 76-77

Volume flux of plume, 11, 12
von Kármán's constant, 6

Wake cavity, 20-24

Washout ratio, 71, 72

Wavelength of maximum energy, 8

Weighting scheme for winds, 88, 90

Wet deposition, 71, 72

Wet removal of sulfur, 88

Widows Creek Steam Plant, 81, 82

Wind direction shear, 5, 6

Wind profile in surface layer, 6, 7

Wind-speed power law, 32

Wind-tunnel experiments, 19-22

DISCLAIMER

This book was prepared as an account of work sponsored by an agency of the United States Government. Neither the United States Government nor any agency thereof, nor any of their employees, makes any warranty, express or implied, or assumes any legal liability or responsibility for the accuracy, completeness, or usefulness of any information, apparatus, product, or process disclosed, or represents that its use would not infringe privately owned rights. Reference herein to any specific commercial product, process, or service by trade name, trademark, manufacturer, or otherwise, does not necessarily constitute or imply its endorsement, recommendation, or favoring by the United States Government or any agency thereof. The views and opinions of authors expressed herein do not necessarily state or reflect those of the United States Government or any agency thereof.